Université d'Ottawa · University of Ottawa

Optical Cross-Connects: Architecture and System Perspective

by

Yongdong Jin, B.Eng., M.Sc.

A thesis submitted to
the School of Graduate Studies and Research
in partial fulfillment of the requirements for the degree of

Doctor of Philosophy

in Electrical Engineering

Ottawa-Carleton Institute for Electrical and Computer Engineering

School of Information Technology and Engineering
Faculty of Engineering
University of Ottawa
Ottawa, Ontario, Canada

0-612-26125-5

Abstract

This thesis focuses on the architecture and system perspective of optical cross-connect systems using semiconductor optical amplifiers. The work includes architecture study, system performance analysis, simulation, and experimental investigations.

Optical cross-connects are promising for future large capacity switching systems and cross-connect systems in high-speed transport networks. To construct large capacity cross-connect systems using presently available technologies, multi-dimensional optical cross-connects are explored. A novel architecture using wavelength-division and space-division multiplexing techniques is proposed, where the wavelengths of WDM are effectively reused and the size of space switches is dramatically reduced. Conceptual designs are presented to show the feasibility of its implementation. As for the system performance, homo-wavelength crosstalk from space switches is identified as a main degradation factor. The performance is further investigated with Gaussian approximation of signal-crosstalk beat noise for a reasonably large size (64×64) cross-connect as a high-speed switching core. It is shown that a 64×64 cross-connect can be constructed with 4-wavelengths WDM and 16×16 space switches using presently available technology. Also, a 4×4 optical cross-connect based on the proposed architecture was experimentally demonstrated.

Performance degradation due to homo-wavelength crosstalk in multi-wavelength optical networks using dynamic wavelength routing is addressed. Enhanced crosstalk degradation due to ASE noise of optical amplifiers is identified for the first time.

Mechanisms and classification of homo-wavelength crosstalk are further investigated comprehensively. To analyze homo-wavelength crosstalk implications on system performance, a theoretical model based on moment generating functions (MGF) is presented. Further, the saddlepoint approximation is employed to evaluate the power penalty with the MGF of the received signal. The evaluation results justify the estimation of the required crosstalk ratio calculated with the Gaussian approximation for a large

number of crosstalk channels ($N > 4$). Several experiments were carried out in order to verify the theoretical analysis and study the effect of wavelength alignment between the signal and the crosstalk. A good agreement is achieved between the analysis and experiments. The wavelength range for generating homo-wavelength beat noise is found around 0.05 nm for a 1 Gb/s directly-modulated signal.

As primary optical switching components in the proposed cross-connect system, semiconductor optical amplifiers (SOAs) are investigated in various aspects. The available SOAs are tested and characterized for switching application. They perform very well in terms of polarization insensitivity and contrast ratio. As for system applications of SOAs, an input dynamic range of SOAs is studied experimentally and further simulated numerically. An input dynamic range can be over 20 dB for a single-stage SOA system and over 10 dB for a three-stage SOA system at 1 Gb/s. The simulation shows a signal bit rate can be up to 20 Gb/s with a reasonable input dynamic range. By using a wide optical bandwidth of SOAs, we propose to construct bi-directional cross-connects using semiconductor optical amplifiers. The feasibility of bi-directional cross-connection using SOAs is confirmed experimentally at a bit rate of 1 Gb/s. The maximum input power, however, is limited due to the cross-gain modulation, particularly for multi-stage SOA systems.

Acknowledgments

I wish first to express my sincere gratitude to my academic supervisor Dr. Mohsen Kavehrad for his scientific guidance, encouragement, financial and moral support during the course of my program. I would like to thank the member of my supervisory committee Dr. J. Chrostowski and Dr. M. El-Tanany for their helpful recommendations.

I would like to thank Mr. Ernst Munter of Nortel Technologies for his valuable suggestion, stimulating discussion, and help at the early stage of the research of my thesis.

I am very grateful to Dr. J. Chrostowski of the National Research Council of Canada for his suggestion for my experiments and great help and guidance during my research at NRC. I am also grateful to Dr. P. Myslinski of NCR for his help and discussion during my experiments. Also, I would like to thank Mr. T. Devenyi and Mr. D. Nguyen of Oprel Technology for packaging components for my experiments, and Mr. A. Dufour and R. Misner of NRC for their excellent technical assistance.

I wish to thank all professors, colleagues and friends at the Department of Electrical Engineering, University of Ottawa, for the good academic atmosphere and the encouragement during the period of my studies. Special thanks goes to Dr. Q. Jiang for his help and discussion during my research.

I am very grateful for the love, support and patience provided by my family during the many hours spent in my Ph.D. program. In particular I would like to dedicate this thesis to my beloved wife, Xiaoyin and daughter, Yixin, who have been and continue to be a constant source for inspiration in all that I do. Special thanks is to my parents and parents-in-law for their many-years, constant encouragement and support for my education.

This research was financially supported by the Telecommunication Research Institute of Ontario (TRIO), Photonic Networks and Systems Thrust, and partially supported by the Optical Processing and Computing Consortium of Canada (OPCOM).

Table of Contents

List of Figures

List of Tables

1. Introduction

1.1 Motivation

A significant trend in today's telecommunications makes the network bandwidth so demanding. This is, the introduction of broadband integrated service digital networks (B-ISDN) [1]. B-ISDN is designed as an information infrastructure to integrate all telecommunication services in one common network so as to reduce the cost of construction, operation and maintenance by avoiding use of one network for each service. Asynchronous transform mode (ATM) [2] has been adopted as the standard multiplexing technique for B-ISDN. With ATM, information from each service is broken into many ATM cells (53 bytes) and then statistically multiplexed with information from other services. ATM switches are used in the network to switch ATM cells to their destinations where ATM cells are recombined into the original information. Successful implementation of future B-ISDN will strongly depend on the optical technologies in two respects: ultra-high capacity transport networks and very large ATM switching systems.

Optical fibers as a kind of information medium have achieved great success with their very low loss, low dispersion, and ultra-wide bandwidth (~25 THz). Operation cost of long-distance carriers has been dramatically reduced since high-speed digital optical fiber transmission systems based on the SONET/SDH (Synchronous Optical NETwork /Synchronous Digital Hierarchy) [3] standard were introduced. To accommodate continuously increasing demand for bandwidth and flexibility, the networks are being enhanced by deploying more fibers, adding more wavelength channels or increasing the bit rate of each channel, and meanwhile by upgrading the switching size, throughput and functionality.

In addition to the application of optical technologies in transmission, photonics will also play an important role in telecommunication switching. By using photonics, the electronic bottlenecks, such as clock skew, waveform distortion due to electromagnetic induction and *R-C* time constants of circuits, and limit of interconnection, could be avoided in broadband high-capacity switching systems [4, 5]. Due to lack of effective optical logic functional devices, the best high-capacity switching approach would be an effective combination of photonics and electronics. Therefore, photonic switching will be first successfully used for optical cross-connection and interconnection within broadband switching systems [6, 7, 8].

According to the applications, optical cross-connects can be classified into two main categories: one is for optical networking in which optical cross-connects are used to set optical paths such as wavelength paths in WDM networks [9, 10]. Using optical cross-connects, optical networks can be very flexible to respond to traffic changes and to recover networks from a disaster. Another application is for switching or digital cross-connect systems in which an optical cross-connect is used as a high-speed switching core [6, 7]. In high-speed optical transport networks, such as SONET OC-192 (10 Gb/s), optical cross-connects can be more efficient to handle large traffics than electronic ones. As an internal switching core, the optical cross-connect can significantly benefit ATM switches to reduce their complexity. Optical cross-connects can have a very-high internal line rate (say 10 Gb/s) without any electronic bottlenecks, and provide signal format transparency. In addition to the above applications, optical cross-connects are also very desirable to interconnect super-computers or high-performance parallel computers.

There are four kinds of optical division techniques which can be used for optical cross-connections: wavelength division multiplexing (WDM), space division multiplexing (SDM), time division multiplexing (TDM), and code division multiplexing (CDM). The first two division multiplexing techniques have the potential to be transparent to signal formats and bit rates, while the last two techniques only work for specific signal formats. The size and capacity of cross connects based on a single one of these techniques are very limited due to technological constraints. Multi-dimensional (division multiplexing) optical cross-connects are exploited to take advantage of each different technique to increase the connectivity and relieve technological constraints on the components.

We were motivated to exploit multi-dimensional techniques for optical cross-connect systems with existing technologies and to investigate associated problems which would limit the system performance. From the review of optical cross-connect architectures and related technologies in the next chapter, we can see that the combination of wavelength division and space division techniques can be a very promising approach to construct high-capacity optical cross-connect systems. Our research efforts have been concentrated on the following aspects of optical cross-connect systems:

1. Effective cross-connect architecture for ultra-high speed switching cores employing wavelength division and space division techniques and its system performance;
2. Crosstalk impact on the performance of cross-connect systems with wavelength reuse, particularly degradation due to homo-wavelength crosstalk;
3. Switching applications of semiconductor optical amplifiers in cross-connect systems, and their transmission performance.

1.2 Contributions

The contributions of the thesis are listed as follows:

1. We proposed a new optical cross-connect architecture using wavelength-division and space-division techniques. Wavelengths are effectively reused and the size of space switches is dramatically reduced. The architecture was reported in [11, 12].
2. The system performance was analyzed as the proposed cross-connect is used as a high-speed switching core. The main factors degrading the performance were identified. Required crosstalk ratio of space switches were calculated for a 64×64 cross-connect at a line rate of 10 Gb/s. The analysis and results were reported in [13, 14].
3. We experimentally demonstrated a 4×4 optical cross-connect based on the proposed architecture in terms of switching functions with available components.
4. We evaluated the performance degradation due to homo-wavelength crosstalk in multi-wavelength optical networks employing dynamic wavelength routing. It was identified that the impact on performance is intensified by the ASE noise. The results were reported in [15].

5. We further carried out theoretical analysis of the performance implications of homo-wavelength crosstalk. The moment generating function (MGF) with the saddlepoint approximation is used to accurately evaluate the power penalty. Also, the crosstalk impact was investigated, experimentally. We showed a good agreement between the calculated and experimental results.

6. Optical switching systems employing semiconductor optical amplifiers were simulated and experimentally investigated. Dynamic range of input signals versus injection currents and signal bit rates were investigated. Simulation results are in a good agreement with the experimental results.

7. We carried out, for the first time, a bi-directional cross-connection experiment. It shows the feasibility of constructing bi-directional cross-connects using SOAs. The results were reported in [16].

1.3 Outline of the Thesis

The rest of the thesis is organized as follows:

In Chapter 2, we present a review of the development of optical networking and switching. Optical cross-connect architectures and enabling technologies are discussed in detail. Optical cross-connect architectures based on different multiplexing techniques are discussed. We underline the cross-connect applications of WDM and SDM and their combination because of the potential for providing signal transparent paths. We also review enabling devices for realizing WDM and SDM-based optical cross-connects.

In Chapter 3, we present a novel optical cross-connect architecture based on WDM and SDM. Conceptual designs for its implementation are discussed. In Chapter 4, we analyze the system performance of the proposed optical cross-connect as a high-speed switching core. Main factors limiting the system performance are identified. The bit error rate and power penalty are evaluated numerically for a 64×64 cross-connect system. To further prove the switching functions, an experimental demonstration of a 4×4 optical cross-connect is presented in Chapter 5.

In Chapter 6, we investigate the performance degradation due to homo-wavelength crosstalk in multi-wavelength optical networks using dynamic wavelength routers. Impact of homo-wavelength crosstalk on the system performance is further studied analytically and experimentally in Chapter 7. The saddlepoint approximation method for BER evaluation is described in detail. Calculated results are compared with those from the experiment.

In Chapter 8, we briefly introduce the fundamentals of semiconductor optical amplifiers. Gain and noise characteristics are described in detail. Test results for available semiconductor optical amplifiers are also presented. In Chapter 9 we first present transmission experiments on SOA-based systems. Then we discuss the simulation model and results. Main discussions are concentrated on the input dynamic range of SOA-based switching systems. In Chapter 10, we report our experimental study of a WDM-based bi-directional cross-connect system using semiconductor optical amplifiers.

Finally, in Chapter 11 we summarize our research and present our suggestions for future work.

2. Overview of Optical Cross-Connect Architectures and Technologies

2.1 Introduction

An efficient application of photonics in switching would be infrequent and relatively slow switching of ultra-high bit-rate signals. Switching should be controlled by electronics and has not to be synchronized to the bit streams being switched. This optical switching system is a cross-connect system. There are two applications where optical cross-connects are likely to be used in telecommunication switching systems: cross-connects for SONET transport networks and internal cross-connects within large ATM switches [6, 7].

In the following sections, we will first discuss the development of optical networks, particularly optical transport networks and multi-wavelength optical networks, and optical (photonic) switching. It will be pointed out where and how optical cross-connects can play their roles. Then, we review optical cross-connect architectures for multi-wavelength optical networks and for switching cores. Multi-dimensional optical cross-connects are underlined for their potential applications in the future. Enabling technologies for optical cross-connects are then discussed in order to understand their strengths and limitations.

2.2 Development of Optical Networks and Photonic Switching

2.2.1 Optical Transport Networks

An entire telecommunication network can be divided into two components [17, 18]: a transport network and a service network. The transport network is responsible for moving information among geographically remote users and equipment locations such as central exchanges, and relaying packets through switching nodes. The service network may consist of many different sub-networks, each of which is dedicated to a specific service. Obviously, the service network is service-dependent. In contrast, the transport network should be capable to support many different services simultaneously.

The present realization of the optical transport network is based on high-speed optical transmission and advanced digital transport technologies. A digital transport node can be a SONET digital cross-connect or add/drop multiplexer or an ATM cross-connect depending on the multiplexing modes used in the network. It has been shown that the use of ATM to create virtual paths can simplify the cross-connect node architecture and reduce the cost of the node and transmission, but require a high-capacity ATM cross-connect system with a high-speed line interface (say 2.5 Gb/s) [18].

With the rapid increase in broadband services, the transport capability of the existing transport networks will become very limited in the near future. Optical technologies have been recognized to be critical to greatly enhance the capacity and flexibility of the optical transport network. Two possible approaches are highlighted here: One is using optical cross-connects or photonic switches to enhance existing electronic digital cross-connect systems. This would be a more smooth approach to considerably increase the transport capacity as ultra-high speed SONET (≥ 10 Gb/s) transmission systems are deployed. Optical cross-connects are used as switching cores for ultra-high speed SONET digital cross-connects or ATM cross-connects. Photonic packet switches may also be directly used for ATM cross-connects. Although optical-to-electrical (E/O) and electrical-to-optical (O/E) interfaces might be applied at the input and output ports, most of the problems encountered in high-speed electronic switching systems will be avoided. It should be noted that, an electronic digital cross-connect system (DCS) may also be included in this optical transport node to complement the optical cross-connect in order to accomplish some grooming and sorting functions. This is considered as the first likely application of photonic switching [4, 7].

Another future-proof approach is introducing an optical path layer in the transport network hierarchy by using WDM [19, 20]. This kind of optical network is often referred to as a multi-wavelength optical network. The basic idea is using different optical wavelengths through wavelength routing to create service-independent optical paths. Some possible architectures for these networks will be briefly discussed in the next section. The main benefits using the optical path layer include: transmission capacity enhancement with effective use of the optical fiber bandwidth, simplification and throughput increases of cross-connect nodes, flexible service provisioning, and a complete all-optical platform for various transmission applications including analog transmission.

2.2.2 Multi-wavelength Networks

Multi-wavelength networks have been studied extensively last few years[9, 21, 22, 23]. They can be classified into two categories: *broadcast-and-select* networks, and *wavelength routing* networks. Each of these can be further classified into *single-hop* and *multihop* networks [10].

In a broadcast-and-select network, the optical signal from each network node is broadcast to all the nodes in the network. The desired signal is extracted from all the signals at the receiver. To access a node, either tunable filters or tunable lasers or both are utilized at the transmitters or receivers. In packet-switched networks, the tuning speed of the transmitters or receivers must be fast enough so that the wavelength can be tuned between successive packets. To support efficient packet switching along with a large number of network nodes with the single-hop approach, we must have either lasers or filters tuning rapidly over a wide wavelength range with a high selectivity. The limitations on tuning speed and range, say of component tunability, is a problem. Before rapidly and widely tunable devices become available, single-hop broadcast-and-select networks are only suitable to circuit-switched or small-size high-speed packet switched networks. To realize a packet-switched single-hop broadcast-and-select network, an efficient media-access control (MAC) protocol is required to coordinate the transmission between various network nodes. Many MAC protocols have been proposed and their performance has been compared in [10, 24] with respect to processing requirements, transmitting schemes, network throughput, synchronization, and available number of channels.

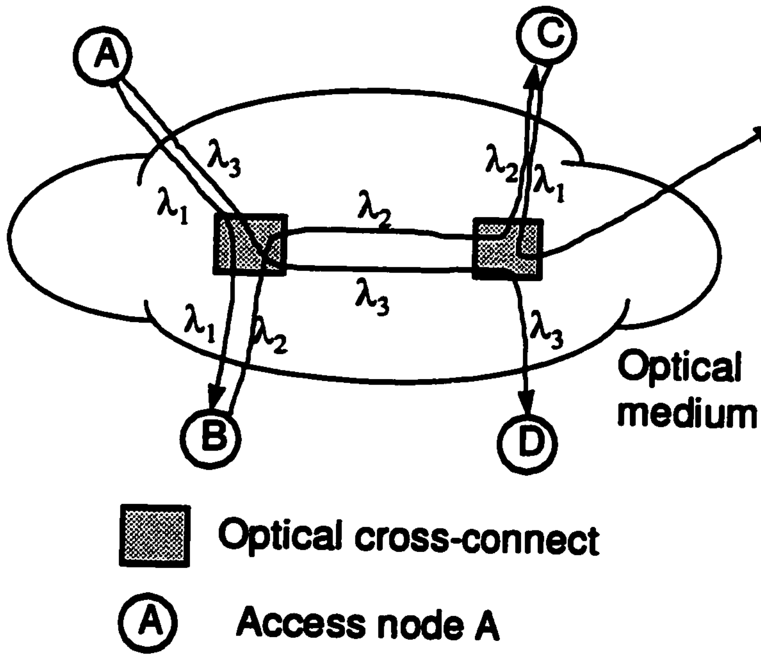

Figure 2.1: Multi-wavelength routing network.

Several problems are associated with broadcast-and-select networks. The first is a lack of wavelength reuse. There are at least as many wavelengths as the number of nodes in a broadcast-and-select network unless there is time-, space- or code-division multiplexing on a wavelength. As pointed out above, the wavelength tunability will ultimately limit the size of these networks. Another problem in the networks is the inherent splitting loss. Unlike an electrical signal, to broadcast an optical signal to all the nodes, the optical power has to be distributed to all the nodes. Each node receives only a small fraction of the transmitted power. Although optical amplifiers can be used to improve the power budget, the inherent splitting loss in a large broadcast-and-select network is still a main problem. From networking point of view, lack of scalability of the broadcast-and-select networks limits their use to optical LANs or MANs. It is hard to have a star-based WAN with thousands of users.

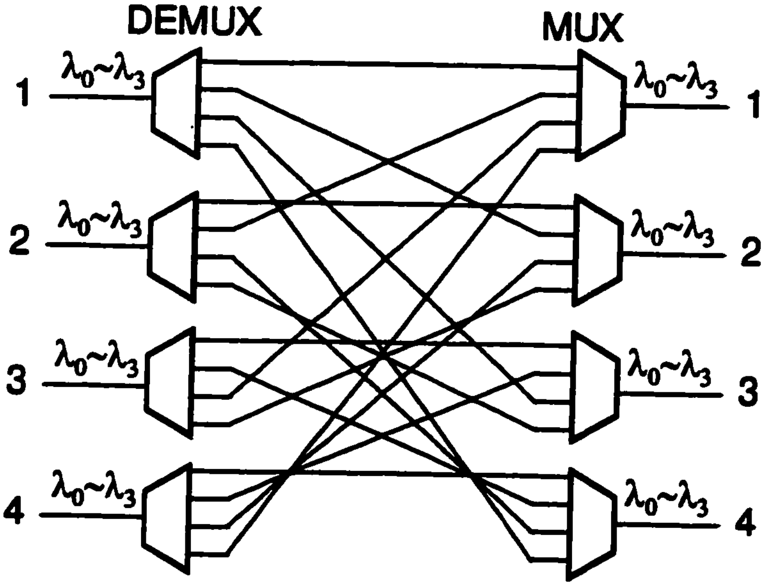

(a)

	Output			
Input	λ_0	λ_1	λ_2	λ_3
	λ_1	λ_0	λ_3	λ_2
	λ_2	λ_3	λ_0	λ_1
	λ_3	λ_2	λ_1	λ_0

(b)

Figure 2.2: (a) Architecture of a static optical routing node. (b) wavelength routing matrix.

Wavelength routing networks have the potential of avoiding the three aforementioned problems in broadcast-and-select networks. In a wavelength routing network, there are many access nodes which send and receive signals, and some WDM cross-connects which set interconnections between access nodes. At any time, each connection between a pair of access nodes is carried by a certain wavelength. As long as the path of any two connections do not overlap, they can be on the same wavelength. This results in a tremendous reduction in the number of required wavelengths for network interconnections. Figure 2.1 shows an architecture of multi-wavelength routing networks and illustrates how the wavelengths can be reused. With specific topologies, the number of wavelengths required to support one connection per node with an acceptable blocking probability can be very reasonable [10]. However, with arbitrary topologies, in a non-reconfigurable routing network with N nodes, at least $\sqrt{N}$ wavelengths are required to support one connection per node without any blocking [25]. With ideal components, a path between a source and a destination can be loss-free since there is no inherent splitting loss. However, amplifiers may still be required to overcome excess losses in the routing nodes and the fiber links.

A routing node is primarily a WDM cross-connect which is either static or dynamic. Figure 2.2 shows the structure of a 4×4 static WDM cross-connect [26, 27]. At each input port, we have four incoming wavelengths which are spatially separated by using a wavelength demultiplexer. The internal connections are made so that different wavelengths from different input ports can be multiplexed into a single output fiber. It should be noted that the internal interconnection can be in many patterns [27] provided there is no same wavelength going to an output port. This static wavelength routing can meet the need of networks well when traffic distribution among the nodes is uniform.

With non-uniform traffic among access nodes, it is very desirable to dynamically change the wavelength routing patterns in order to respond to traffic changes. To dynamically route wavelengths, we can introduce space switches in optical routing nodes, as shown in Figure 2.3 [10, 27]. After demultiplexed, the signals at the same wavelength from different input ports are sent to a $(N+1)\times(N+1)$ space switch where the signal channels are switched according to present traffic patterns. Then, signals from different space switches are multiplexed into an output fiber. The introduction of space switches in optical routing nodes invites homo-wavelength crosstalk [28, 29] which is accumulated through routing as the signal travels. Two mechanisms can make the homo-wavelength crosstalk be a very serious degrading factor to the end-to-end transmission performance.

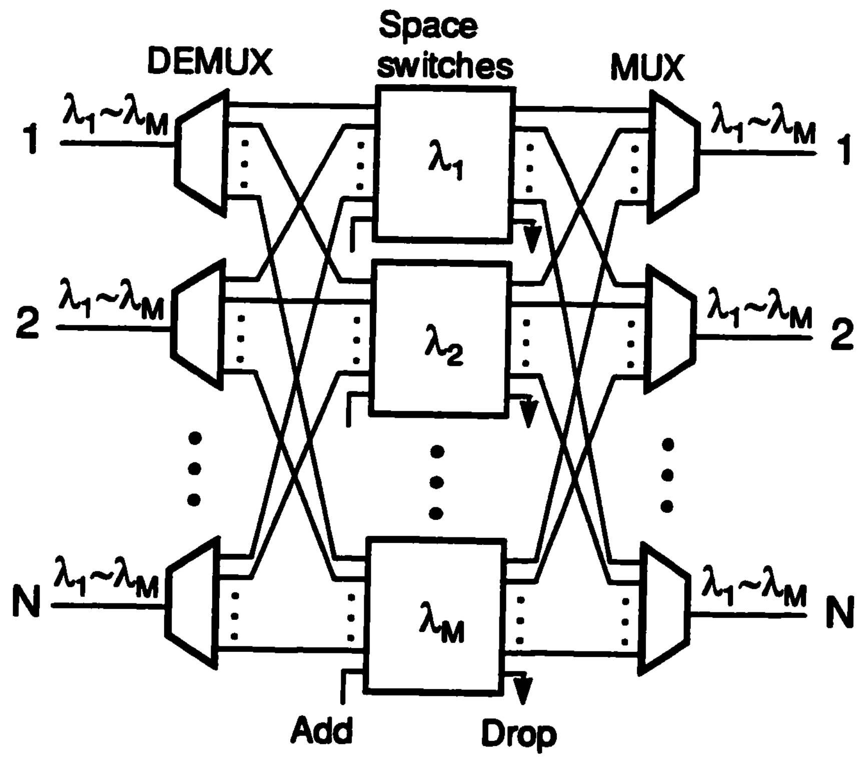

Figure 2.3: Architecture of a dynamic optical routing node using space switches.

These are crosstalk-signal beat interference and crosstalk-ASE (amplified spontaneous emission) beat noise to be discussed in Chapters 6 and 7.

Another approach to realize a dynamic routing node is using tunable acoustic-optic tunable filters (AOTF) to construct a cross-connect [27, 30]. The basic AOTF function is multi-wavelength exchange-bypass. The exchanged wavelengths are selected and controlled by *RF* drive signals injected into a surface acoustic transducer on the filter. With this basic wavelength exchange-bypass element, a large wavelength routing network can be constructed with a variety of space switch structures such as the Benes network [31]. The size of cross-connection networks will be mainly limited by the crosstalk of each AOTF device, to be discussed in Section 2.4.5.

Wavelength routing networks have a high scalability from local to global coverage, a good modularity, and a high survivability. With these features, they will become the base of future all-optical transport networks [9]. For realization, there are many technological constraints from related devices. For example, we need fast and wide tuning laser sources, fast tuning and high resolution wavelength-selective switches. High-performance wavelength converters are also necessary to make truly scaleable wavelength routing networks [32, 33]. The benefits of wavelength-routing networks are obtained at the cost of hardware and complexity of the network control.

In wavelength routing networks, wavelength assignments between access nodes have to be made globally so that there is no wavelength blocking in any links. The global wavelength assignment restricts efficient reuse of wavelengths among links and needs long and complex algorithms since the traffic pattern of the whole network must be dynamically monitored. Similar to the virtual path in ATM networks, an optical virtual wavelength path (VWP) concept is proposed [20]. In the VWP scheme, wavelengths are assigned on a link-by-link basis. In other words, the wavelength assigned to a path has only local significance. By using the VWP scheme, the number of wavelengths in a network can be further reduced, wavelength assignment can be simplified, and a large latency for reconfiguration can be avoided. However, the wavelength converters have to be used to transfer the optical signal at a wavelength to another wavelength in optical routing nodes. With the lack of effective wavelength converters, the optical transparency will be partially lost in VWP-based networks.

An alternative approach to avoid the problem of device tunability is using multihop packet-switched networks [34, 35]. This approach can be applied to centralized networks as well as distributed networks. In a multihop network, each station uses a small number of fixed-tuned optical transmitters and receivers but at unique wavelengths. A transmit packet can only be directly received by those nodes that have a receiver tuned to one of their transmit wavelengths. To reach other network nodes, the packets have to be routed through intermediate nodes, where the optical signal is received and its headers are decoded, and then it is re-transmitted on an appropriate wavelength to the destination. Over a physical topology of a multihop network, there is a logical topology which determines the actual connections between access nodes. A main research issue in multihop networks is how to minimize the average number of hops between a source node and a destination node since a significant portion of the network capacity is wasted at intermediate nodes [10]. Several routing algorithms have been studied for the uniform traffic distribution in regular logical topologies such as a shufflenet or a de Bruijn graph [35]. In contrast to single-hop wavelength routing networks, multihop networks may have large transit time latencies and the network throughput is reduced by a factor of at least the average number of hops. Another disadvantage is lack of optical transparency in the networks. The electronic processing of signals will invite the electronic bottlenecks due to retransmission of signals at intermediate nodes, which ultimately limit the network performance.

2.2.3 Photonic Switching

In a broad sense, photonic switching can be classified as photonic circuit switching and photonic packet switching as its electronic counterpart. With respect to switching techniques, photonic switching can also be categorized into space division switching, time division switching, wavelength division switching, and optical code division switching.

As for circuit switching, photonic switches primarily are dynamically reconfigurable optical cross-connects based on different path routing techniques. The reconfiguration time interval can be from microseconds to several hours in response to traffic changes. Depending on applications, the structures of photonic circuit switches can be very different. For example, small-size low-speed switches can be used for fault protection, while high-speed cross-connects should be fast and large enough to deal with fast traffic change. Even though, the techniques for optical cross-connections discussed in the following section can be applied to both. On the other hand, photonic packet switching fabrics could also be thought of as optical cross-connects with a fast reconfiguration speed enough to respond to each packet. For packet switching, buffering is necessary for temporary storage of packets as output contention happens, while buffering could be avoided in circuit switching.

Due to a lack of all-optical logical control, most of the proposed photonic switches use electronics for switching control. In these switches, optics and electronics are effectively combined to realize a broadband photonic switch [36, 37]. The switching speed of photonic switches is determined not only by the switching time, but also the processing time required to determine the appropriate state of the switch. Thus, a guard time is required for most of photonic switches. In photonic packet switching systems [5, 38, 39, 40], particularly photonic ATM switches, buffering takes place either at the input side or at the output side or at both sides. Unfortunately, there is no effective optical memory for packet storage as that in electronics. The only practical device available for optical buffering is the optical fiber delay line through which optical packets can be sequentially delayed or circulated [39]. Sequential fiber delay lines do not scale well for a large number of required delays. An optical fiber loop buffer is limited by accumulated ASE through the loop [41].

By using WDM, packet routing and buffering can be effectively combined, and the physical size of the buffers can be reduced. A good example is a photonic ATM switch architecture proposed by Gabriagues and Jacob [40, 42]. The routing fabric is a star coupler based wavelength routing structure. A set of sequential fiber delay lines are shared by ATM cells at different wavelengths. A space switch is employed to select different delay lines for buffering. A generic architecture using sequential fiber delay lines called "staggering switch" was proposed and discussed in [43].

In addition to SDM and WDM techniques, other techniques such as optical TDM and optical CDM have also been investigated for photonic switching [44, 45]. To realize TDM or CDM based photonic switching, we need some components which are not conveniently available. These include ultra-short pulse optical sources, nonlinear optics and optical logic, and time-division self-routing optical techniques. TDM may somehow be used in photonic switching systems when relevant technologies are available. CDM-based photonic switching is more complex to use in packet switches. However, these can be conveniently used as circuit switches in optical LANs. It appears that, only wavelength and space division switching makes use of the bandwidth in a way commensurable with the bandwidth of optical medium.

With presently available technologies, photonic switching can be applied to optical cross-connections without optical buffering [46, 47]. By using an ultra-high internal line rate, optical cross-connects can simplify the internal interconnect of large switching systems, such as SONET digital cross-connects and large ATM switches. An optical cross-connect architecture for large ATM switches was proposed by Munter [6], and since it has been prototyped. In this architecture, small satellite switches are cross-connected with a high-speed switching core at a line rate of 10 Gb/s. The optical splitting loss and electronic selectors will be problematic for a larger switch. To construct a large ATM switch using an optical switching core, we need to find a better optical cross-connect architecture and identify its strengths and limitations. In the following two sections, we briefly introduce different architectures of optical cross-connects and their enabling technologies.

2.3 Optical Cross-Connect Architectures

As discussed in the preceding section, optical cross-connects can play an important role in multi-wavelength transport networks and large switching systems. In this section, we discuss optical cross-connect architectures based on different division multiplexing techniques with respect to their potential and limitations. Multi-dimensional cross-connect architectures using hybrid division multiplexing techniques are considered for the improvement of single division multiplexing based cross-connects. Enabling technologies for constructing these optical cross-connects are briefly reviewed in order to understand the present state of related devices. An emphasis is placed on the devices for WDM and SDM.

Optical cross-connects, according to division multiplexing techniques they use, can be classified as: wavelength division cross-connects, space division cross-connects, time division cross-connects, and multi-dimensional cross-connects. Here, *multi-dimensional* means a combination of two or more division multiplexing techniques (orthogonal dimensions) . From the standpoint of their applications, optical cross-connects can be categorized into cross-connects for network routing and cross-connects for switching fabrics in switching systems. The first kind of cross-connect in the thesis is referred to as networking cross-connects such as the WDM cross-connects discussed in the preceding section. The second kind is referred to as switching cross-connects. For interconnections of network access nodes, it is preferred to avoid using E/O and O/E conversions in optical networking cross-connects so that the interconnections are transparent to data-formats. In

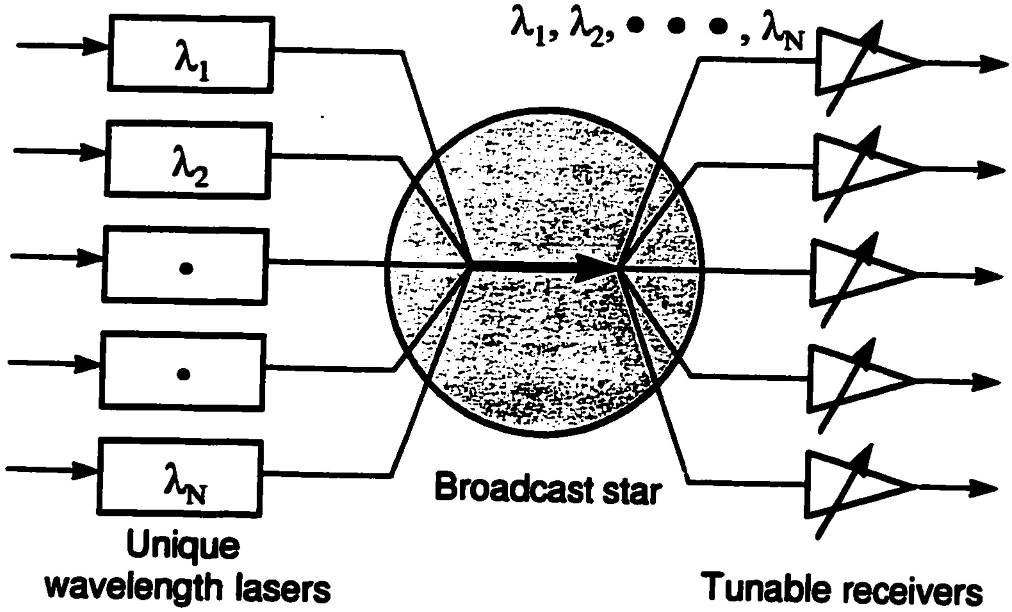

Figure 2.4: Broadcast-and-select structure.

switching cross-connects, E/O and O/E conversions are generally required at inputs and outputs.

There are various figures of merit for evaluation of optical cross-connects. Among them are: the number of components, complexity of control, limitation of switching speed, modularity, and scalability. Besides these, technological difficulties will determine whether a cross-connect can be implemented.

2.3.1 Wavelength Division Based Cross-Connects

WDM based cross-connects can be further categorized into two broad classes: a *broadcast-and-select* structure and a *wavelength routing* structure [27, 48].

In the broadcast-and-select structure, as shown in Figure 2.4, signals arriving at input ports are transmitted at fixed distinct wavelengths and broadcast to all output ports through a star coupler. At each output port, a tunable receiver selects a wavelength at which the signal intends to go to the output. As mentioned in the pervious section, due to using a single star coupler, for full cross-connections there are two limitations in this

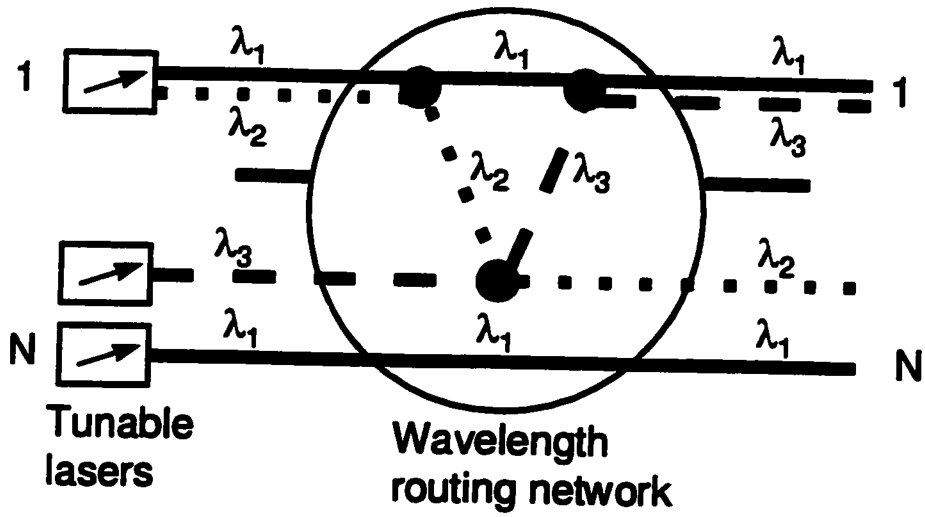

Figure 2.5: Wavelength routing structure.

structure: a lack of wavelength reuse and the inherent splitting losses. However, the simplicity of the structure makes is attractive.

Another structure of WDM based cross-connects is to use optical wavelengths as a routing tool as discussed in wavelength routing networks so that a signal traverses the cross-connect along a path determined by the signal wavelength. Figure 2.5 shows the wavelength routing structure. By selecting the wavelength of a tunable laser, the input is connected to an intended output. With just N wavelengths, every input can be connected to every output uniquely. The wavelength routing network is composed of passive wavelength-selective devices. One of specific routing networks is the WDM cross-connect [26] as shown in Fig. 2.2(a).

In an $N \times N$ broadcast-and-select network, the inherent splitting loss is $10\log(N)$ dB, and there has to be N wavelengths for the fully N to N cross-connections, so the maximum total capacity is $B \cdot N$, where B is the bit rate of each wavelength channel. One advantage of this network is its broadcast capability, realizable with fixed wavelength lasers and tunable filters. It is possible to partly reuse wavelengths in the broadcast-and-select network, but it is impossible to fully interconnect all the inputs to all the outputs. On the other hand, in the wavelength routing structure, there is no inherent loss with ideal wavelength routing devices and the wavelengths can be reused at distinct output ports so that the maximum cross-connection capacity can be $N^2 \cdot B$. The wavelength routing network has only one-to-one connections so it is difficult to have broadcast capability. Regarding cross-connection applications, the broadcast-and-select structure is attractive for a switching fabric [46, 47], while the wavelength routing structure is preferred for optical networking. The most important advantage of WDM-based cross-connects is the simple signal routing and the high transport capacity.

Based on two generic structures, many WDM cross-connects and switching networks have been proposed, and some of them have been demonstrated. Examples of such networks are: LAMBDANET, fast optical cross-connect, FOX, hybrid packet switching system, HYPASS, multi-stage λ-switch, and WDM cross-connect. Introductory discussion on these switching networks can be found in [27, 48].

The implementation of WDM cross-connects requires several essential components. Among them are: wavelength tunable sources and/or wavelength converters, star couplers, wavelength multiplexers/demultiplexers, tunable optical filters, and wavelength routers. Theses devices will be discussed in the next section.

To construct a large size WDM based cross-connect, we have to face some technological challenges. One is the tunability of WDM devices, including the tuning range and the tuning speed. Presently, the tuning range of tunable lasers is restricted within 20 nm with a high tuning speed in the order of nanoseconds [27]. Tunable filters can have a large tuning range of over 200 nm [30], but the tuning speed is only in micro-seconds. To overcome the problem of tunability, wavelength reuse can be introduced in cross-connection networks. Some approaches to realize wavelength reuse will be discussed in section 2.3.4.

2.3.2 Space Division Based Cross-Connects

Optical space division multiplexing has been extensively studied for optical cross-connection and photonic switching [37]. According to lightwave traveling modes, optical SDM based cross-connects (switching fabrics) can be classified as systems based on either guided-wave or free-space optics. A guided-wave structure is more attractive for high-speed communication systems because of the high compatibility of interconnection with

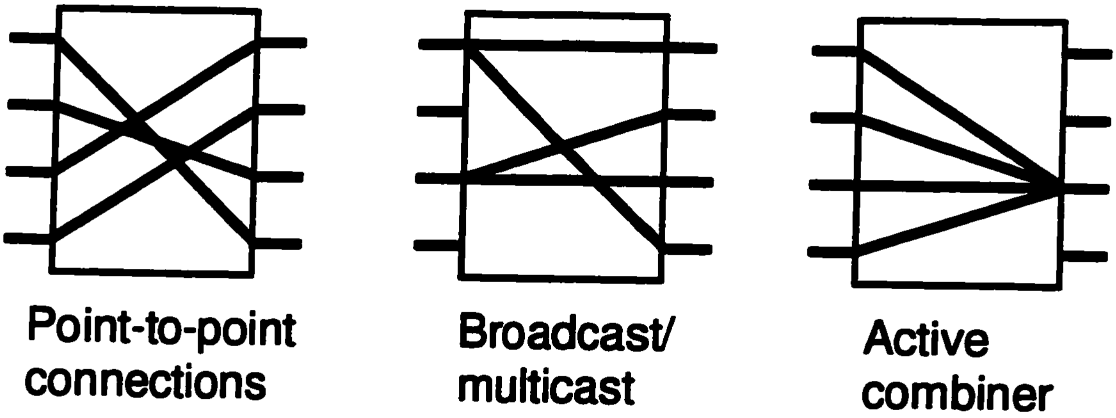

Figure 2.6: Functionality of space switches.

transmission components, robustness in different environments, and fast reconfiguration. Free-space optics is mainly used in optical interconnections with its high degree of connectivity [49, 50]. Performance of a specific optical space switching architecture is primarily characterized by the following parameters: the worst-case optical path loss, the worst-case crosstalk, a reconfiguration rate, and the number of switching elements necessary to implement the switch [37].

The functionality of space switches, as shown in Figure 2.6, depends on the requirements of their applications. The very basic function it has to perform is point-to-point connections. In some cases, multicast/broadcast function has to be achieved. Further, when WDM is used in combination with space switching, one may require connect several inputs at different wavelengths to a single output. For a given space switch, whether it has three functions or not is determined by its internal architecture.

According to their blocking characteristics, optical space switching fabrics can also be categorized into four types: strictly non-blocking, wide-sense non-blocking, and rearrangable non-blocking, and blocking [51]. For ultra-high-speed optical cross-connection and switching applications, it is desirable to use strictly or wide-sense non-blocking fabrics instead of rearrangable ones that may need to reconfigure some existing connections for setting a new connection. Bursts of high-speed data may be lost during rearrangement of the existing connections.

In guided-wave structures, the most widely investigated space-division switching device is a directional coupler [52, 53]. Such a coupler is a basic 2×2 non-blocking switching device in either the bar state or the cross state depending on the control signal. With directional couplers, we can build a larger space switching fabric using crossbar, Clos, Benes, banyan, or omega network topologies [37, 52].

The strength of directional couplers is their optical transparency which can support extremely high-bit-rate information. However, their use is restricted by several factors: the control electronics limits their maximum reconfiguration rate; the long length of each directional coupler prevents large-scale integration; and the losses and crosstalk associated with each device limit the maximum size of a possible network. Some approaches have been considered to solve these constraints. For example, semiconductor optical amplifiers have been used to compensate the loss in space switching system [54]. To reduce the crosstalk, dilated switching networks were proposed in [55]. In a dilated space switching fabric, there is one output in use at each 2×2 switching element while the other output is idle. The total number of switching elements in a dilated switching fabric is approximately doubled.

Another important space switching element is a semiconductor optical amplifier (SOA) switching gate. Its states (ON or OFF) are controlled by its injection current. With SOA gates and optical couplers, a basic 2×2 switch can be easily constructed, as shown in Figure 2.7. It should be noted that this 2×2 switch not only is strictly non-blocking, but also can perform all the three functions as illustrated in Figure 2.6, namely point-to-point connection, multicast and active combining. In section 2.3.4, it will be seen that this space switch is very important to the multi-dimensional cross-connects based on SDM and WDM. A 4×4 switch array using 24 SOAs has been monolithically integrated in a single chip and tested in an experimental network [56, 57].

A large size space switch based on SOAs can be constructed with the splitter-combiner structure and Benes structure [58, 59]. The size of switching fabrics is mainly limited by three factors: saturation power of SOAs, accumulation of amplified spontaneous emission (ASE) noise [59], and the multiple reflections due to residual facet

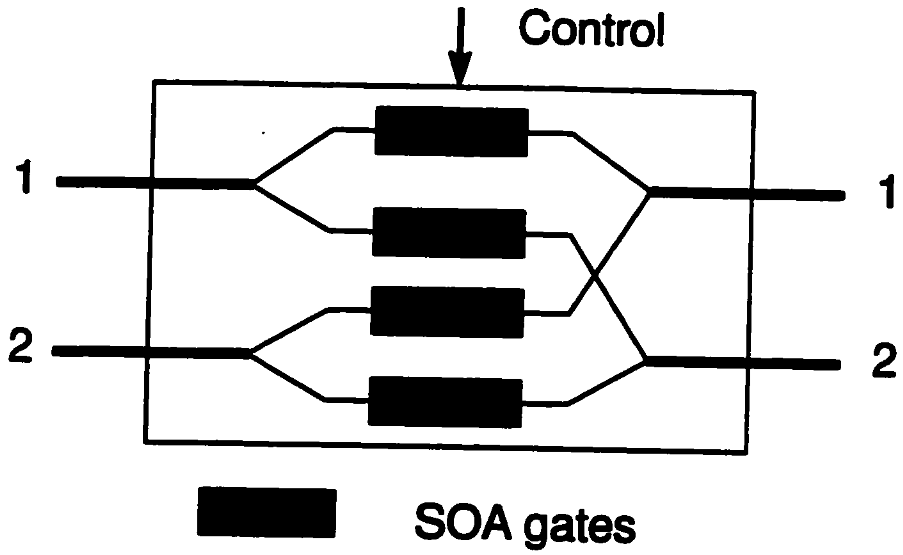

Figure 2.7: 2×2 space switch using SOAs.

reflections [58]. The splitter-combiner structure is inherently limited by the splitting losses. For an $N \times N$ switch, the power finally reaching an output is $1/N^2$ of the input power regardless of excess loss and amplifier gain. Fortunately, the gain of SOA gates can partially compensate for the splitting losses. In a large SOA-based switch, each input and output may use an SOA as an in-line amplifier in order to compensate for large splitting losses [60].

With free-space optics, there are a lot of proposed cross-connects and switching fabrics [37]. Two important ones are mentioned here. One is the symmetric self-electro-optic effect device (SEED) based extended generalized shuffle (EGS) networks, so far 128×128 switching fabrics have been demonstrated [50]. Another is cascaded-beam-shifter-type switches using liquid-crystal devices [61]. However, these switches either operate at a low-speed or with a long reconfiguration time.

2.3.3 Time Division Based Cross-Connects

There are two basic types of optical TDM, bit multiplexing and block-multiplexing, which can be applied in optical cross-connections. Bit multiplexing is preferred in transmission systems. However, for switching systems, block-multiplexing is attractive because it requires the switching fabric to reconfigure only at block boundaries. With a small amount of guard time between adjacent blocks (frames), the requirement on the reconfiguration time can be relaxed.

An example of time-division block-multiplexing based switching is a time-slot interchanger (TSI), through which the time slots of input frames are mapped into the desired output slots. The implementation of an optical TSI can be based on either a single-stage [62] or a multi-stage structure [63]. In all the proposed TSIs, optical fiber delay lines are used for time delay medium.

The size of block multiplexing switches is limited by the speed of electronic multiplexing. To cross-connect ultra-high-speed optical signals with TDM, we have to use bit-multiplexing with high-speed optical multiplexers and demultiplexers. Cross-connections are established by shifting the demultiplexing times. The size of this kind of cross-connect is limited by the highest possible optical bit-multiplexing. Synchronization is a formidable challenge for TDM based cross-connection systems [37]. More important is that in TDM based optical cross-connect there is no transparency for signal format and bit rate.

To realize a TDM cross-connect, we need several advanced optical components, namely ultra-short optical pulse sources, ultra-high speed optical multiplexers and demultiplexers, and high-speed optical bit synchronizers. These components have been demonstrated in some research laboratories [64, 65], but they are far from being practically used.

2.3.4 Multi-dimensional Optical Cross-Connects

With a single dimension (division-multiplexing), the size of optical cross-connects will be very limited due to the complexity of construction and control, and technological constraints such as wavelength tuning rang of tunable lasers, size limitation of space switches because of crosstalk and losses, and the highest TDM speed. To reduce the complexity and increase the connectivity, we can use two or more orthogonal dimensions to construct multi-dimensional cross-connects.

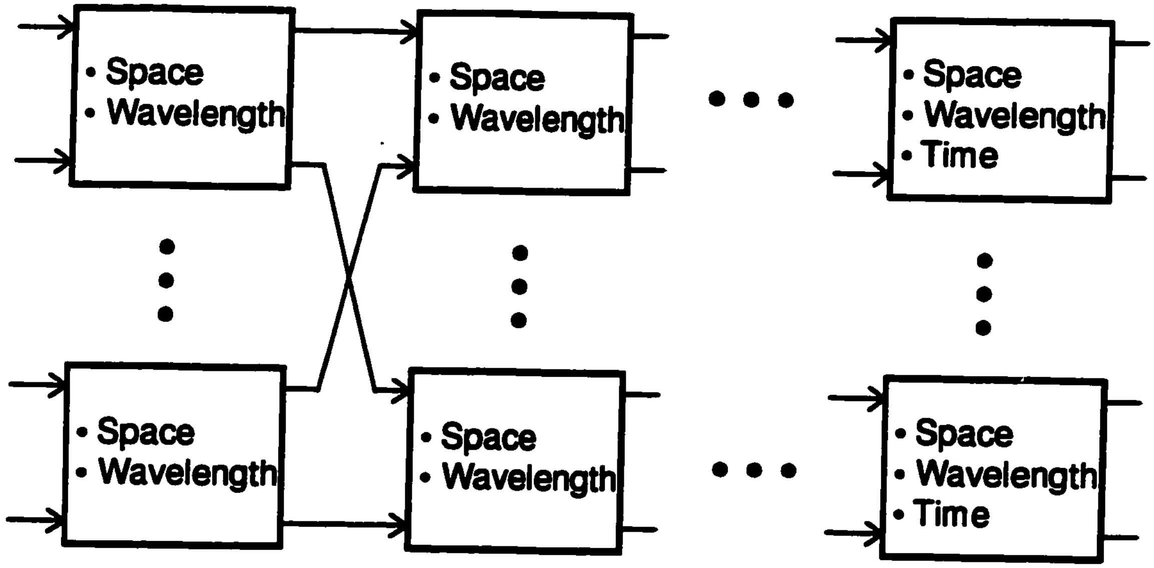

Figure 2.8: Multi-dimensional cross-connection and switching architecture.

Figure 2.8 shows a conceptual multi-dimensional cross-connect or switching architecture using the hybrid of three basic multiplexing techniques. Different techniques may be combined into one stage or used in different stages. For packet switching systems, a time-division stage is necessary to buffer packets for contention resolution, which may not be used in cross-connect systems. For optical cross-connection and switching, more practical hybrid architectures may be based on two multiplexing techniques, such as TDM and SDM, WDM and SDM, and WDM and TDM.

The combination of TDM and SDM has been widely used in modern telecommunications switching systems [51]. This kind of system is referred to as time-multiplexed space switches such as T-S-T and S-T-S switches. When similar architectures are used in optical cross-connects, challenges will come from TDM stages. For instance, for 5 Gb/s optical signals the switching time must be a few pico-seconds. It requires very fast optical AND gates which are still conceptually being investigated in research labs. Optical TSIs using space switches may be a possible application. Hunter *et al.* [63] proposed space switching architectures for cross-connecting optical TDM channels. For a large number of input channels, the complexity and crosstalk make them less practical [66].

TDM based switching and cross-connect systems can also be extended with WDM. Tsukada *et al.* [44] proposed an ultra-fast photonic ATM (ULPHA) switch based on TDM and WDM. In this switch, the input ATM cells are compressed and then broadcast through an optical star coupler. At the output side, cell selectors are used to switch and buffer the cells.

A more appropriate multi-dimensional solution is a combination of WDM and SDM. The hybrid of WDM and SDM can either increase the total capacity of a cross-connect system or reduce the size of space switches and the number of wavelengths. More importantly, they can provide transparent cross-connections for different signal formats and bit rates, a very important feature that optical cross-connects can provide.

There are several proposed multi-dimensional cross-connects for switching applications. In [67], Eng *et al.* proposed switching cross-connect based on WDM and SDM. There is some wavelength reuse. However, this switching fabric is not non-blocking. Obara *et al.* [68, 69] proposed two other cross-connect architectures using WDM and electrical SDM to ease the requirement on laser tunability. These architectures are only rearrangable non-blocking, also include electrical switches, which are very undesirable for transparent cross-connections. Also, complex routing algorithms make them harder to use in high-speed switching systems except for STM cross-connection applications. Another architecture called MONET (multi-dimensional optical network) cross-connect switch is proposed by Healey *et al.* [70]. This cross-connect is based on a bus structure. N input signals as a group are sent to a line of the bus with WDM. The wavelengths are reused at different input groups. At each output port, a space selector is used to select a line of the bus, and then select a wavelength channel. Use of the bus structure makes the power budget a very important concern in this switch.

For networking applications, we can also use multi-dimensional cross-connects. Figure 2.9 illustrates a 2×2 cross-connect composed of SDM and WDM for optical networking [4, 71]. WDM signals are first switched by a space-division switch. Then, corresponding

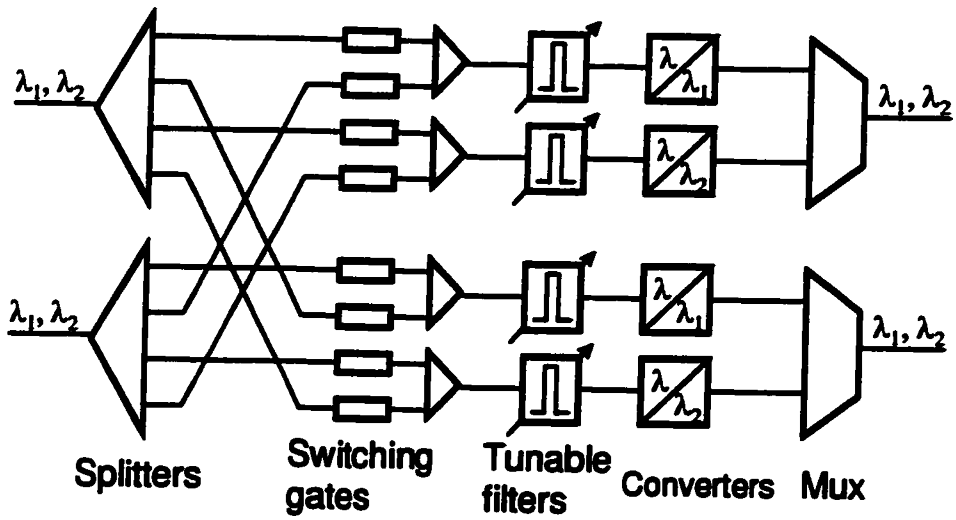

Figure 2.9: Networking cross-connect (routing node) based SDM and WDM.

wavelengths are selected and converted to their output wavelengths. In the space switch, SOAs are used as switching gates for two incoming wavelengths by taking advantage of SOAs' broad optical bandwidth. However, the interchannel crosstalk due to the gain saturation effect [97] will limit SOA application. Also, tunable optical filters used to select optical channels will restrict the reconfiguration speed of the cross-connections. Another optical cross-connect architecture applied in the multi-wavelength transport network (MWTN) [19] use a broadcast-and-select stage followed by space switches. There are no wavelength converters. Functionally, this is the same as the dynamic WDM cross-connect as shown in Figure 2.3. However, there is more loss at the inputs and the outputs.

Following the discussion, it can be concluded that multi-dimensional cross-connect architectures can potentially avoid the technological constraints of single dimensional cross-connect architectures so that we can construct large optical cross-connects for switching and networking applications.

2.4 Enabling Technologies

In this section, we discuss the present state of enabling device technologies for SDM and WDM. Research on new architectures in the absence of a sound knowledge of device capabilities and limitations may lead to unrealizable approaches.

2.4.1 Space Switching Waveguide Devices

By the materials for device fabrication, space switching devices can roughly be categorized into two classes: $LiNbO_3$ devices and semiconductor (mainly InP) devices. The most well-known space switching devices are titanium diffused $LiNbO_3$ directional couplers [53, 72]. Directional couplers are transparent to bit rates and information modulation formats. Their reconfiguration speed is generally limited by the electronic control. With basic 2×2 directional couplers, large size space switches can be built. However, the switching matrices in a single chip are limited by the long length of individual directional couplers and the large bending radii required in the integrated waveguide [52]. So far, the largest switching array implemented in a single chip is a 16×16, and this almost approaches the limits of the technology. For switching WDM signals, wavelength sensitivity of directional couplers is a constraining factor because of the wavelength dependence of switching characteristics. The optical bandwidth might be improved with an appropriate design of waveguide structures. Experimental study has shown that these can have an optical bandwidth of 10 nm with a crosstalk ratio of -30 dB [73]. Apart from the optical bandwidth limitation, large coupling losses at inputs and outputs are other limiting factors for wide applications [74].

Semiconductor space switching devices have attracted great attention recently [75]. These are suitable devices in the long run because of their low power consumption, compactness and integrability with other passive and active devices, and the possibility of having optical amplification. A further advantage of these devices is a large number of physical effects that allow one to modulate either the refractive index or the absorption. Among them are electro-optic modulation, carrier depletion modulation and carrier injection modulation. By using these modulation effects, we can construct various switching devices. Figure 2.10 illustrates four basic structures of InP-based optical switches. The first three are based on refractive index modulation and the last is based on intensity modulation.

Two devices are worth notice for their potential applications for switching WDM signals. One is the optical digital switch [76]. This kind of switch has two significant

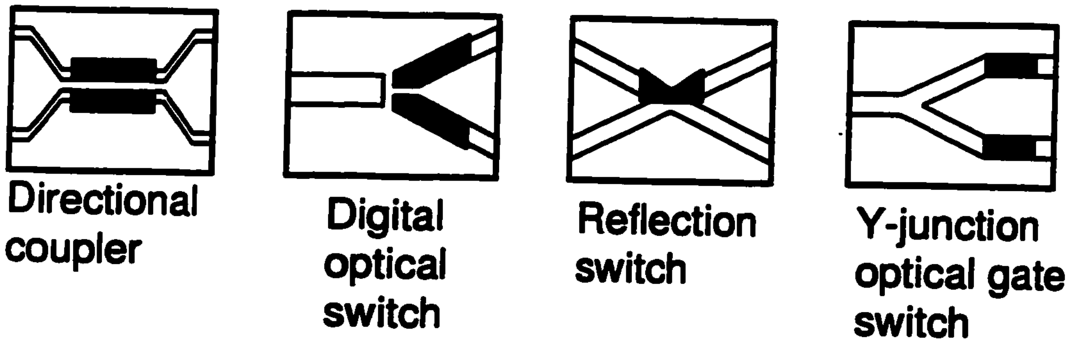

Figure 2.10: Semiconductor waveguide optical switches.

advantages: It can simultaneously switch an extremely broad optical bandwidth of over 100 nm. The second is that polarization independence can be achieved by simply increasing the voltage.

Another device is an SOA based space switch. SOAs as switching gates have several very attractive features [77, 78]. Among them are: possibility of a lossless switch because of the gain of SOAs, very low crosstalk of less than -40 dB because of a high contrast ratio of SOAs, and wavelength insensitivity owing to a large optical bandwidth, and a fast switching speed of about a nano-second. The cascadability of SOAs is limited by signal degradation due to amplified spontaneous emission, multiple reflections from facets and their saturation power [58, 59].

2.4.2 Wavelength Selective Sources

A wavelength selective source can be implemented with either a tunable laser or a laser array. In a WDM based system, wavelengths must be accurately specified and separated from their neighbors with precisely defined intervals. A wide tuning range and a fast tuning speed are preferable for most switching and networking applications.

There are various tunable lasers available for WDM applications. External tunable lasers can have a wide tuning range (50 ~ 200 nm) but a slow tuning speed, and are bulk and sensitive to environment [27]. Integrated tunable lasers are preferred for optical cross-connects. Two most common kinds of tunable lasers are multi-section distributed feedback Bragg (DFB) lasers and multi-section distributed Bragg reflector (DBR) lasers.

Wavelength tuning of a DFB laser is based on varying the refractive index of the active layer material with the carrier density which is controlled by the injection current into this layer. With this principle, the DFB laser gives a small but continuous tuning range of about 2 ~ 3 nm. Wavelength tuning of a DBR laser is based on variation of the current injected into the Bragg section and/or the phase section. The quasi-continuous tuning range of the DBR laser is from 8 nm to 10 nm [79]. A continuous tuning of the DBR laser is also possible, but the range is only 2 ~ 4 nm. An alternative to the DFB and DBR lasers is a tunable twin-guide (TTG) DFB laser [80], which has an extra passive waveguide transversely integrated on the top of another conventional DFB laser and biased separately from the active layer to change the Bragg wavelength through carrier-induced refractive index change. An important feature of TTG lasers is a large continuous tuning range of over 10 nm with a single tuning current.

For optical cross-connections, tunable lasers should have a wide tuning range. One approach proposed to extend the total tuning range is using three overlay DBR lasers working alternatively [81]. This can provide a total tuning range of 20 nm. Recently, several new types of widely tunable lasers (> 20 nm) have been introduced. Among them are: Y-lasers with a tuning range of 28 nm [82], vertical coupler filter (VCF) lasers with a tuning range of 57 nm [83], and super-structure grating (SSG) lasers with a tuning range of 105 nm [84]. For practical applications, these lasers need to be investigated further in terms of reliability and wavelength stability.

In addition to a wide tuning range, tunable lasers should have a fast tuning speed. The wavelength switching time of DFB lasers can be as short as a few hundred pico-seconds, which is determined by the effective carrier lifetime [85]. On the other hand, the switching time of DBR lasers can be from a few nano-seconds to several hundred nano-seconds, strongly dependent on the frequency space ΔF and allowable frequency deviation δf as follows: $T_{sw} = (\tau_s/2)\cdot\ln(\Delta F/\delta f)$ [86], where τ_s is the effective carrier life time. To reduce the wavelength switching time, Tada *et al.* [87] proposed a duplex transmitter using two DBR lasers and a high-speed space switching device such as a $LiNbO_3$ directional coupler. The wavelength switching speed totally depends on the device switching speed. An additional benefit is reducing the wavelength drift due to the thermal effect during wavelength tuning.

As an alternative to tunable lasers, laser arrays show promise as wavelength selective sources. Laser arrays allow a wider wavelength selective range and a more regular channel spacing than tunable lasers. Moreover, with proper configurations, multiple signals can be simultaneously transmitted so that we may have some multicast applications. A 16×1 DFB laser array with a star coupler and an optical amplifier has been monolithically integrated on a single chip [88].

2.4.3 Wavelength Converters

There are a variety of wavelength conversion configurations. The simplest way is to use a detected signal to modulate a laser running at the desired wavelength. However, we have to use O/E and E/O conversion, which is not transparent to date formats. To avoid this problem, all-optical wavelength converters are preferred. Presently, three kinds of all-optical wavelength converters are being vigorously investigated.

The first all-optical wavelength conversion approach uses non-degenerated four-wave mixing (FWM) in optical fibers [89] and in semiconductor optical amplifiers [90]. This approach has the potential for very fast operation and is modulation-format independent. The input and output wavelengths can be continuously tuned. The conversion range can be up to 20 nm. However, the conversion efficiency is relatively low, although the theoretical prediction shows a possible high efficiency [91].

Another approach to realize wavelength conversion is using the well-known cross-gain modulation of semiconductor optical amplifiers. Optical on-off keying (OOK) signals can be effectively converted to another wavelength. So far, a 10 Gb/s OOK signal has been successfully converted to another wavelength [92, 93]. Two-stage cascadability and signal multicasting have also been demonstrated at 2 Gb/s [94]. The speed limitation on the signal bit rate for this type of wavelength converter is determined by the gain recovery time of the SOA, which is strongly dependent on the input optical power. To increase the conversion speed, a higher input power will be required. The wavelength conversion range, determined by the amplified spectral width of SOAs, can be as wide as 40 nm. However, only conversion from a long wavelength to a short one can be efficient due to the gain profile shift to a long wavelength as the SOA saturates. The advantage of the wavelength conversion using SOAs is that it can be polarization insensitive and that variations in the signal input power and wavelength are less critical compared with other types.

A four-section DBR laser with a saturable absorber is another candidate as a wavelength converter [95]. The saturation absorber in the laser results in a bistability of the power via current (*L-I*) characteristic and allows the laser to be optically triggered. The lasing wavelength can be tuned electrically within several nano-meters. In contrast to SOA-based wavelength converters, the wavelength conversion is achieved by using a single component with low optical input power.

Wavelength converters will be the essential ingredients in constructing WDM cross-connection networks, but requirements of wavelength converters will depend on architectures and systems. For practical system applications, the main concerns are the cascadability, the range of input and output wavelengths, the sensitivity and required input signal power, and the frequency tolerance on input signals, which are still under investigation.

2.4.4 Optical Amplifiers

Optical amplifiers are key components in optical networks and cross-connect systems. They are required mainly to compensate for long-distant transmission loss and the losses at transport nodes. The most important is that optical amplifiers make an optical communication system modulation-format-transparent. There are two main kinds of optical amplifiers, semiconductor optical amplifiers (SOAs) and rare-earth doped fiber amplifiers (DFA).

The SOA type most widely used today is traveling-wave (TW) type. TW-SOAs have a large continuous optical bandwidth of over 40 nm with a gain of about 20 dB [96]. Although they have a large optical bandwidth, they have a relatively low output saturation power of less than 10 dBm. When they are used to amplify WDM signals, owing to their very short gain recovery time of hundreds of pico-seconds, there will be inter-channel crosstalk between WDM channels when SOAs work in their saturation region [97]. To avoid this interchannel crosstalk, one can use fixed amplitude modulation formats such as PSK and FSK for transmission. Another approach to increase the saturation power is using multi-quantum well (MQW) structure. A MQW semiconductor optical amplifier with a saturation power of 10 ~ 15 dBm has been reported [98]. Semiconductor optical amplifiers are attractive for their large optical bandwidth, compactness, and integratability with other optical and electrical devices. However, they have a relatively large input and output coupling loss, polarization dependence and inter-channel crosstalk for WDM signals. SOAs are mainly employed as functional devices for optical switching and networking instead of in-line amplifiers. More detailed introduction to SOAs will be given in Section 8.2.

As for rare-earth doped fiber amplifiers, the most important one is an erbium-doped fiber amplifier (EDFA) [99, 100]. EDFAs working at 1.5 μm have a high optical gain of 30 to 40 dB with a gain bandwidth of 35 nm and a high saturation power of over 15 dBm. They are inherently fiber compatible, insensitive to polarization, and immune to crosstalk among wavelength-multiplexed channels owing to their long carrier life time of about 10 ms. EDFAs are widely used in high-speed optical transmission systems as in-line and pre-amplifiers. In a cross-connect or switching system, they are primarily employed to compensate for the system losses such as splitting and coupling losses.

2.4.5 Wavelength Routing Devices

Wavelength routing devices are essential to WDM cross-connection networks. In a broad sense, they include optical filters, wavelength multiplexers/demultiplexers (MUX/DEMUX), and wavelength routers.

The most well-known kind of optical filter is Fabery-Perot (F-P) filters, which can have a very high finesse with a periodic response. By using optical fiber, very compact fiber F-P filters have been built with a finesse as high as 350 and a tuning range of 50 nm

[101]. However, the tuning speed is slow in the order of milliseconds. F-P filters are often used as fixed filters with a high finesse.

There are other two well-known tunable filters: electro-optic tunable filters and acousto-optic tunable filters (AOTF) [102]. They have a large tuning range and a relatively fast tuning speed. Electro-optic filters can be tuned within 16 nm at a speed of a few nano-seconds. AOTFs can be tuned over a range as large as 400 nm at a few micro-seconds. However, the resolution of AOTFs is relatively low, about 1 nm. From the discussion in Section 2.2.2, it is known that AOTFs as four-port components can be used as wavelength exchange-bypass components with which a large-size dynamic wavelength switch can be constructed. The construction of a large wavelength switch is limited by the crosstalk characteristics of AOTFs. There are three kinds of crosstalk in AOTFs [103, 104]: crosstalk due to the inband optical leakage and coherent optic ideal sinc-squared transmission function and coherent crosstalk due to the wavelength shift. An effective way to reduce the crosstalk is to use the dilated switching structure which will achieve the low crosstalk at a cost of an increase in the number of the components [104].

Wavelength demultiplexers/multiplexers are other kinds of essential components for WDM applications [105]. There are two main types of wavelength demultiplexers in terms of the mechanisms used to select wavelengths. These are: dispersion-based demultiplexers and interferometer-based demultiplexers. It is noted that, owing to the inherent reciprocity of lightwave, in all cases, the same device can be used as either a demultiplexer or a multiplexer.

In a dispersion-based demultiplexer, a diffraction grating as an angularly dispersive element disperses incident light spatially into various wavelength components. Most of recent implementations of this kind are realized with planar waveguides for integrating several optical components together [106, 107]. A typical interferometer-based demultiplexer is the cascaded Mach-Zehnder (M-Z) interferometer. A 128-channel demultiplexer has been fabricated by using seven serially connected M-Z interferometers [108].

Using optical filters or wavelength demultiplexers and multiplexers, one can construct the wavelength routing network shown in Figure 2.2. However, it is very desirable to have an integrated compact wavelength routing device. Drgone [108] proposed a very clever structure for realization of the integrated wavelength router. Two free-space couplers are connected by a waveguide phase array. With a proper design of the coupler and the array, different wavelengths from an input will be spatially separated on different outputs, and then they combine with different wavelengths from other inputs. Several successful fabrications have been reported with silica or InGaAsP material with wavelength channels up to 8 [109, 110]. Furthermore, a large size wavelength router can be constructed with small-size wavelength routers [111].

2.4.6 Optical Couplers

Optical couplers are passive components which realize optical power combination and/or power distribution independent of optical wavelengths. Optical couplers include optical splitter ($1 \times N$) and combiners ($N \times 1$), and optical star couplers ($N \times N$). In principle, any optical coupler with $N > 2$ can be constructed with 2×2 couplers [101]. However, the number of 2×2 couplers will be very high for a large N. An alternative is to use planar integrated waveguide optics [112]. Main advantages of the waveguide technology include the flexibility it offers since the coupler size is not restricted to 2×2 multiples and the possibility that it can be monolithically integrated with other optical components such as lasers and semiconductor optical amplifiers. An integrated 144×144 star coupler with an excess loss of about 5 dB has been reported [113]. Optical couplers are the most mature components for WDM applications.

2.5 Summary

In summary, we discussed architectures of optical cross-connect networks and enabling device technologies for implementing the cross-connects. It can be seen that multi-dimensional cross-connect networks using hybrid division multiplexing techniques show promise for practical large-size cross-connection applications with existing device technologies. Although some advanced devices are available, clever architectures are still required to relax the constraints on optical components. Cross-connect architectures should also be evaluated from the system point of view by considering the limitations of devices in order to know their feasibility for practical applications.

3. Optical Cross-Connect Based on Wavelength Division and Space Division Multiplexing Techniques

3.1 Introduction

In this chapter, we propose a novel optical cross-connect architecture by combining wavelength division and space division multiplexing techniques. The goal is to construct a large scale optical cross-connect with presently available technologies. WDM and SDM are selected mainly because they can provide optical signal transparency for optical cross-connection. It should be pointed out that this optical cross-connect is mainly proposed for a high-speed switching core within a switching system, not for multi-wavelength networking.

In the next section, we describe the principle behind this architecture. Section 3.3 presents some conceptual designs for its implementation. In Section 3.4 we further consider system loss for different design schemes.

3.2 Architecture

Figure 3.1 shows the architecture of the proposed optical cross-connect with N $(= L \cdot M)$ inputs and K $(= Q \cdot R)$ outputs. The optical cross-connect includes N wavelength tunable transmitters, L $M \times Q$ optical space switches, and Q $L \times R$ wavelength routing networks. M inputs, as a group, are connected to an $M \times Q$ space switch, then to Q wavelength routing networks. To set up a connection, the transmitter at an input is first tuned to a wavelength which can pass through the optical filter at the designated output; then the space switch, to which the input is connected, switches the input to an output connected to the wavelength routing network to which the designated output belongs. Finally, the wavelength, which the transmitter is tuned to, routes the optical signal to the output. To access R outputs of the wavelength routing network, the tunable transmitter at the input should be able to tune to R wavelengths. When the spatial

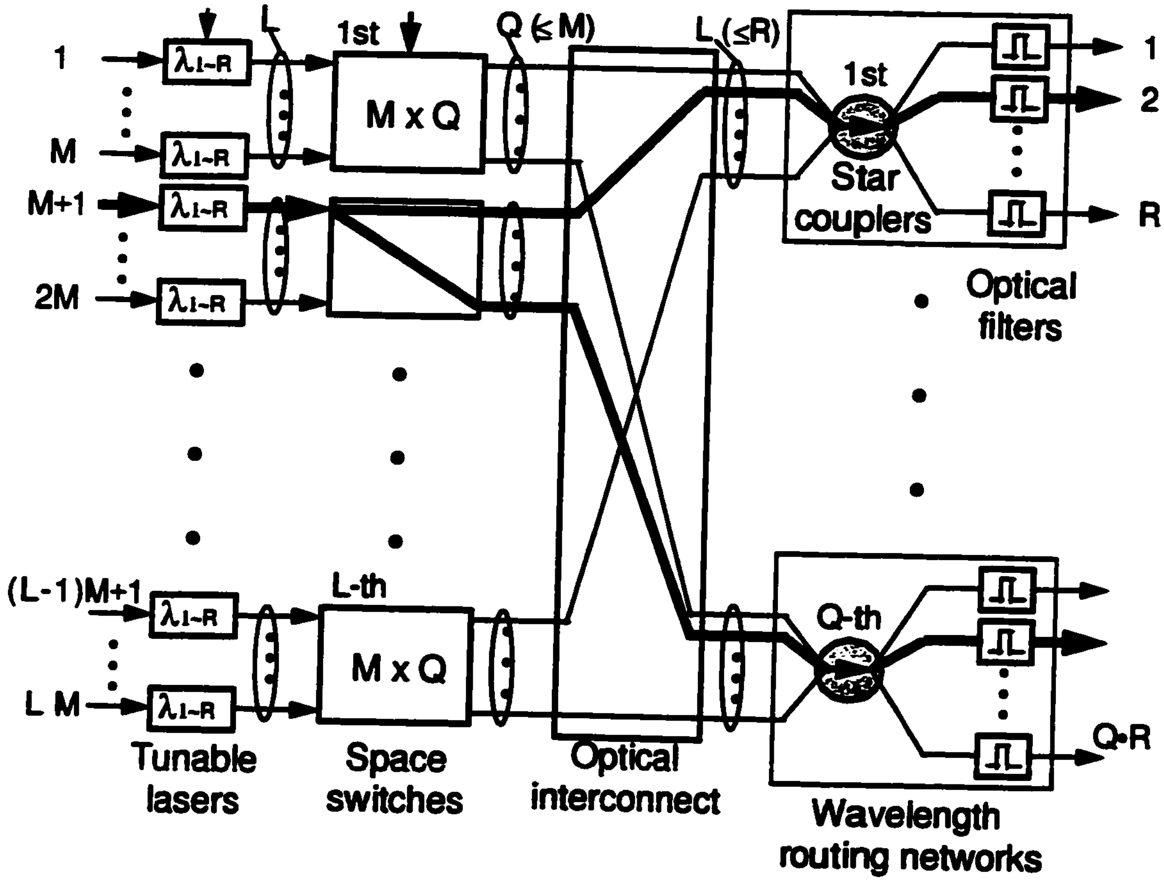

Figure 3.1: Architecture of the optical cross-connect based on WDM and SDM.

interconnects of all the space switches are set up, the optical cross-connect, in principle, becomes Q active routing WDM cross-connects as shown in Figure 2.5 [27]. With space switches, the active routing cross-connects are reconstructed dynamically, and all the wavelengths are reused at each sub-cross-connect.

To interconnect WDM sub-cross-connects and make the cross-connect strictly non-blocking, the space switches have to be strictly non-blocking and be able to combine inputs with different wavelengths for one output. The requirements can be well met by semiconductor optical amplifier based splitter-combiner space switches [56, 58], as shown in Figure 3.2. In this space switch, the number of outputs Q can be larger than the number of inputs M. Besides this kind of space switch, SOA-based space switches with other structures can also have this property, for instance, an SOA-based Clos switch [59]. However, the splitter-combiner space switch uses the least number of components.

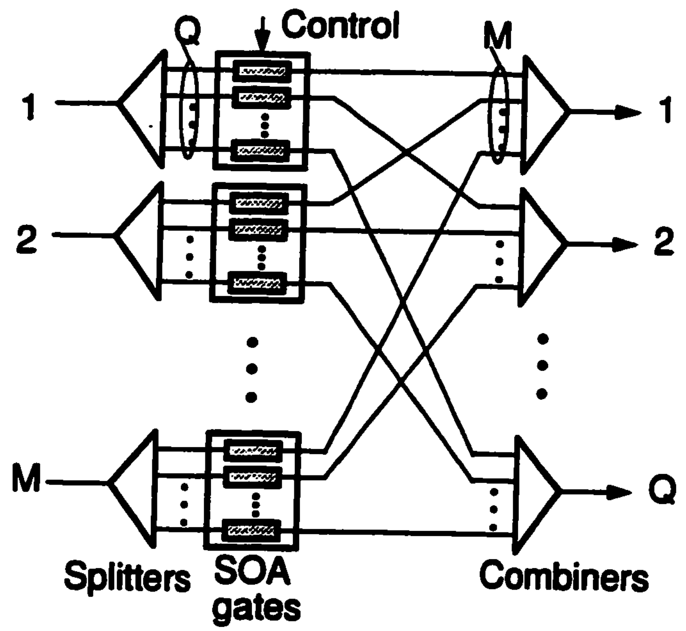

Figure 3.2: $M \times Q$ splitter-combiner space switch using SOAs.

The function of the wavelength routing networks is simply to rout optical signals at different wavelengths to their intended outputs. Figure 3.1 shows star-coupler based wavelength routing networks, which are made of star-couplers followed by sets of optical filters. In addition to this kind of wavelength routing network, we can also use wavelength routers as routing networks. This will be discussed in detail in Section 3.3.2.

Owing to the broadcast capability of the SOA-based splitter-combiner space switches, the cross-connect is able to multicast input signals under the appropriate control. The bold lines started from the (M+1)-th input in Figure 3.1 show the input being connected to two outputs. It should be noted that this multicasting is not arbitrary due to limited spatial interconnections of the space switches. That is, the (M+1)-th input tuned to λ_2 can only be connected to every 2nd output of each wavelength routing network. The multicast capability can be enhanced with tunable filters and a non-symmetrical architecture with K larger than N.

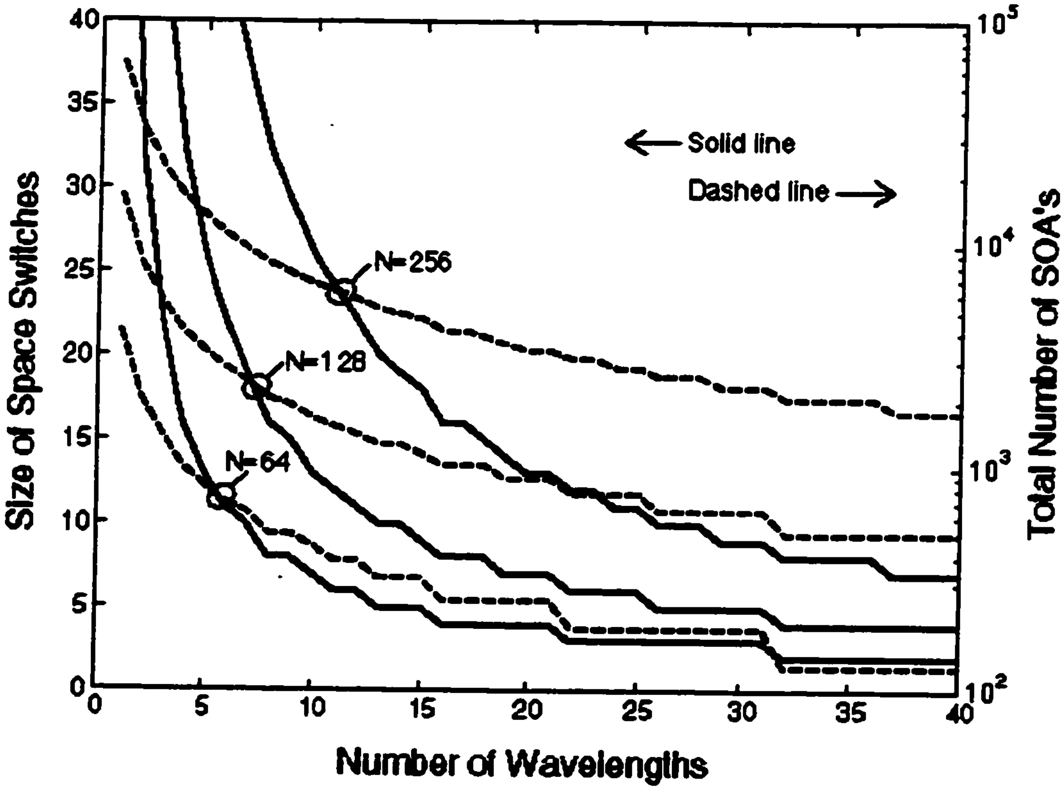

Figure 3.3: Size of the space switches and the total number of the SOAs of space switches versus the number of the wavelengths for 64×64, 128×128, and 256×256 optical cross-connects.

One of the main features of this architecture is wavelength reuse. This dramatically reduces the number of required wavelengths for a given-size optical cross-connect. From the space switch point of view, this optical cross-connect can be thought of as an expansion of space switches with WDM. In contrast to pure space switches, the proposed optical cross-connect needs much less components. The total number of SOAs used in splitter-combiner space switches for different combinations is plotted in Figure 3.3. For example, to construct a 64×64 cross-connect with four wavelengths, we need 16×16 space switches with 1024 SOAs in total instead of 4096 SOAs for a pure space-division cross-connect (with one wavelength).

The maximum size of the proposed optical cross-connect is determined by the number of the available wavelengths and the size of the space switches. For a symmetrical optical cross-connect, e.g., for M equal to Q and L equal to R, the number of the input/output ports of the cross-connect is given by

$$N = R \cdot M \tag{3-1}$$

Figure 3.3 shows different combinations of WDM and space switches for an $N \times N$ cross-connect with N = 64, 128, and 256. For a given-size cross-connect, the optimum combination will depend on many aspects, such as performance requirements, technological availability, reliability, and costs associated with each technologies, etc. In the next two sections we will discuss its implementation and related technologies, and consider the system loss for different combinations.

3.3 Design for Implementation

To see the feasibility of the proposed optical cross-connect, we describe some conceptual designs and the related technologies for implementing the cross-connect in this section. The detailed performance analysis based on the designs will be discussed in the next chapter..

As for the implementation, the system must be designed to be reliable, integral, and modular. Such a system would have three main parts: transmitter modules, receiver modules, and internal interconnect. To avoid crossovers on waveguides, we deliberately separate the optical splitters and combiners of the space switches on two separate modules the transmitter and the internal interconnect. For the sake of simplicity, we assume that four-wavelengths WDM is combined with 16×16 space switches to form a 64×64 optical cross-connect. Designs for other combinations such as eight-wavelength WDM with 8×8 space division switches can be simply obtained with some modifications.

3.3.1 Transmitter Modules

Transmitters are for wavelength tuning. Two designs are discussed here. The first, shown in Figure 3.4(a), uses a tunable laser as a wavelength tunable source. To avoid the problems induced by direct modulation of lasers, such as relaxation oscillation and large frequency chirp [24, 101], an external modulator is used to obtain an optical on-off keying (OOK) signal. The modulated signal is sent to a 1×16 ($1 \times M$) optical splitter which is followed by sixteen SOA switching gates controlled by their injection currents. It is noted that the optical splitter and SOA switching gates are a part of the space switch. With existing technologies, it is possible to monolithically integrate a tunable laser, an external modulator (electro-absorption type), a 1×16 optical splitter, and sixteen traveling wave SOA optical gates in a single chip. Similar integration fabrication has been demonstrated by Young *et al.* [88]. In case of difficulty in integrating all the components in a single chip, we can integrate a transmitter module on two chips, one for a tunable laser and an external modulator, the other for an optical splitter and SOA switching gates. The integration will make the system very compact and will reduce the coupling loss between different components.

An alternative to a tunable laser is a laser array, which consists of a group of lasers with fixed but unique wavelengths. Our second design of transmitter modules, shown in Figure 3.4(b), is based on the idea of using a laser array as a wavelength selective source. Following each laser in a laser array, an external modulator is used to select its wavelength and simultaneously modulate incident optical intensity in order to have an OOK signal, if the wavelength is selected. A problem when using laser arrays is that we have to adjust lasers to have the desired wavelengths and make sure that they are stable over a long time for proper system operation. Technically, we can use a wavelength stabilization system to control all the wavelengths, but this will be very costly for a switch system. To avoid this problem, we propose to use a set of central power lasers to supply optical power for all the transmitters, instead of using a laser array at each input port. The wavelengths of the central power lasers are stabilized. At each transmitter module we use a set of external modulators for wavelength selection and intensity modulation. In Chapter 4, it will be shown that with only a single intensity modulator with an ON/OFF ratio of about 20~25 dB, it is difficult to meet the system performance requirement for wavelength selection. Thus, two cascaded modulators may be needed to provide a high ON/OFF ratio for wavelength selection. If a wavelength is selected at a transmitter, one of the corresponding modulators modulates light intensity to have an OOK signal, the other one as a switch is set to the ON state. All other modulators in the transmitter are set to the OFF state in order to block optical power at other wavelengths.

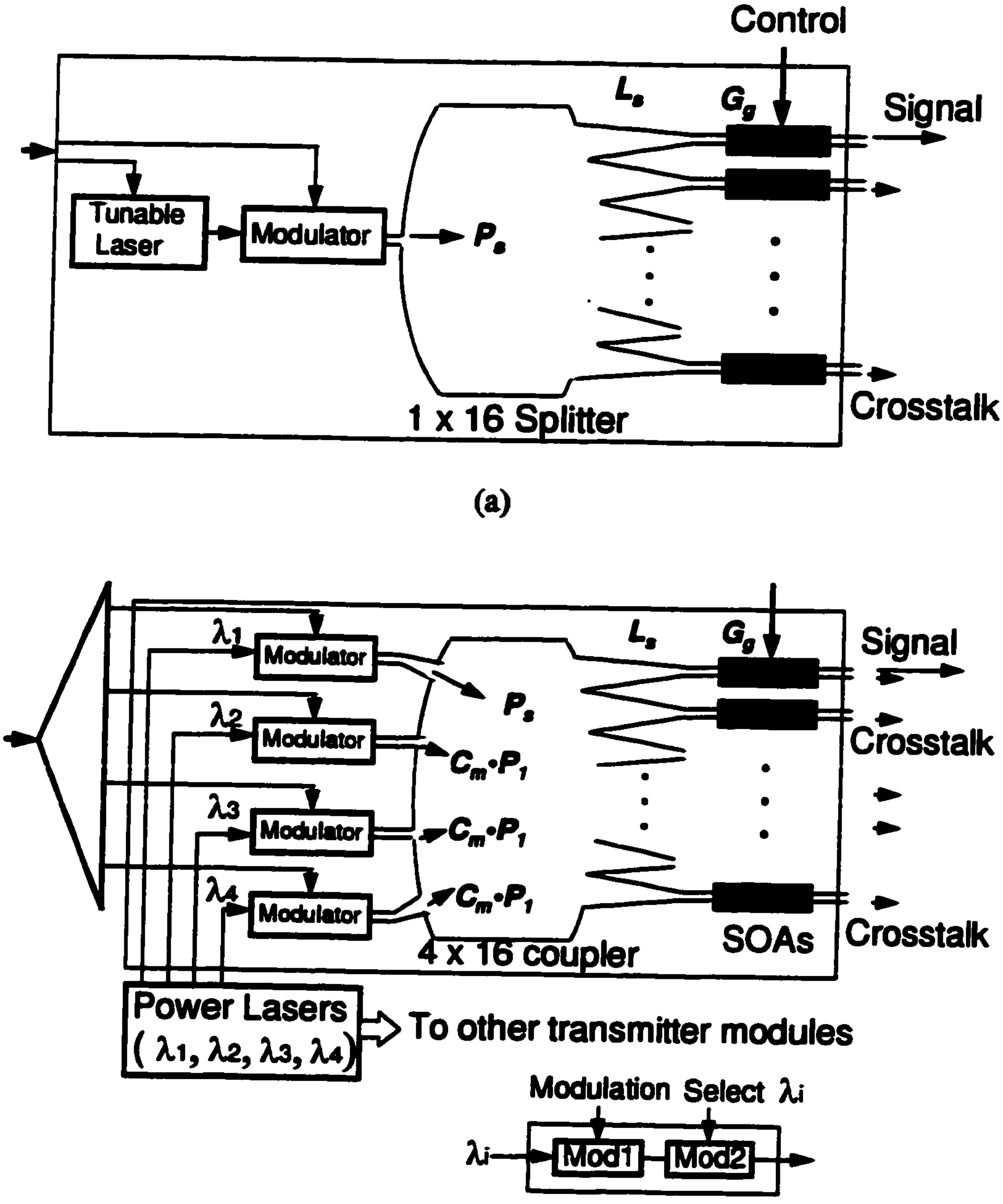

Figure 3.4: Schematics of transmitter modules. (a) Transmitter with a tunable laser. (b) Transmitter with a set of central high-power lasers and wavelength selectors.

In this transmitter, the wavelength selecting speed is merely determined by the modulators and can be hundreds of picoseconds. In place of a 1×16 splitter in the first transmitter module, a 4×16 ($R \times M$) star coupler is used as a shared optical power splitter for all four wavelengths. Use of central power lasers not only gets rid of wavelength difference among different transmitter modules, but also saves on the total number of lasers, thus, improves the system reliability. In contrast to the first transmitter module, in the second module, wavelengths for WDM with a large channel spacing (>1 nm) are easily obtained and stabilized for reliable system operation. The wavelength selecting speed is not only much faster but is also independent of the difference between the two switched wavelengths. Another feature of this design is that a transmitter may send more than one wavelength at a time, thus an input port can connect more output ports so as to enhance the multicast capability. Actually, each transmitter here can be thought of as a small broadcast-and-select WDM system. Limitation of this second design is power leakage from the blocked wavelength channels. The power leakage will introduce homo-wavelength crosstalk, which will be discussed in detail in the next chapter.

3.3.2 Receiver Modules

A receiver module is composed of a wavelength routing network and a photodiode array. The main concern is the wavelength routing network. In Figure 3.1, the wavelength routing networks are the star couplers followed by the optical filters. Optical signal power to a star coupler is distributed to each output and then the optical filters select the wavelengths. For one-to-one cross-connections, we can just use fixed optical filters following a star coupler. For a multicast/broadcast system, tunable filters may become necessary in accordance with the multicasting requirement.

One problem with the star coupler based wavelength routing networks is their inherent splitting loss due to the characteristic of power distribution of star couplers. To avoid this splitting loss, we can use wavelength routers based on a static WDM cross-connection network [114] as wavelength routing networks. Wavelength routers have no inherent splitting loss for ideal wavelength routing. This wavelength router has been discussed as a static optical router node in Section 2.2.2. In contrast to the application in optical networking as shown in Figure 2.2(a), in the optical cross-connect there is only one wavelength at each output port at a time instead of four wavelengths. When an input signal wavelength is changed, the signal will be routed to a different output in accordance with the wavelength matrix in Figure 2.2(b). To avoid contention, there must be only one

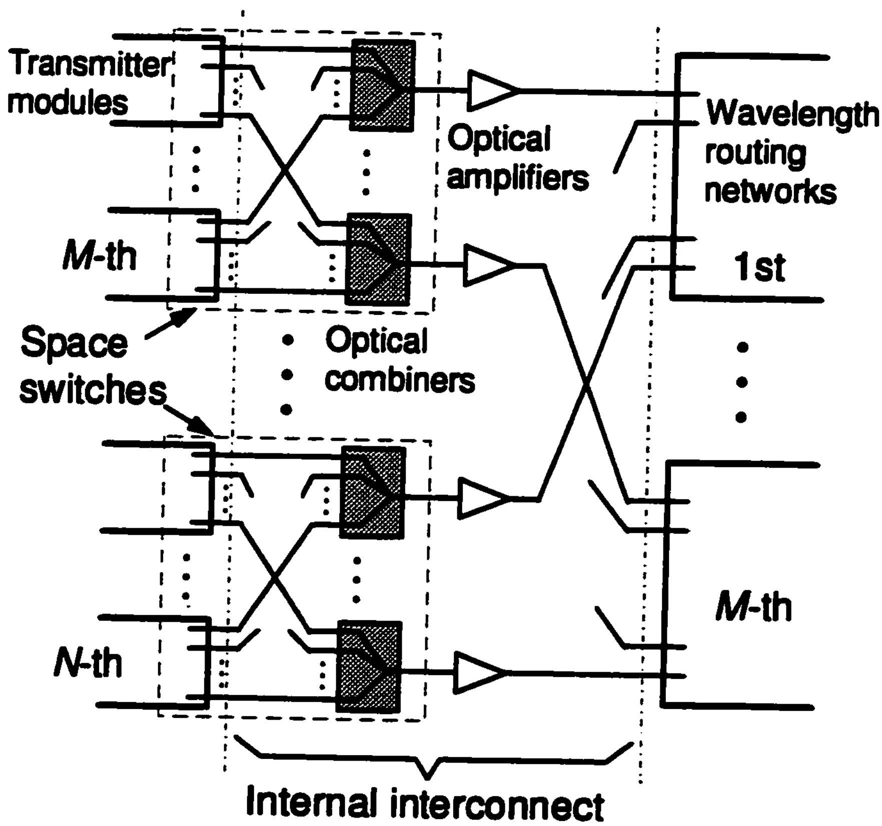

Figure 3.5: Schematic of internal interconnect of the optical cross-connect.

wavelength at each output port no matter how many wavelengths there are at each input port.

It should be noted that the wavelength control algorithm for tunable transmitters with the wavelength routers is different from that with the star coupler based wavelength routing networks. Due to fixed wavelength routing, the use of the wavelength routers limits the multicast capability of the optical cross-connect.

3.3.3 Internal Interconnect

The internal interconnect is for connecting the transmitter modules to the receiver modules. Figure 3.5 illustrates the schematic of this internal interconnect. Optical fibers connect the outputs of the transmitters to optical combiners, then to wavelength routing networks. Amplifiers are used following optical combiners to compensate for the splitting loss of the space switches. There are two ways to compensate for the system loss. One way is to use an optical amplifier as a power booster right after the external modulator. The alternative is using an EDFA to amplify multi-channel WDM signals after each optical combiner of the space switches. With a low input power, the EDFA can provide a higher optical gain. So, we choose the later scheme. To reduce the spontaneous emission noise, we may use an optical bandpass filter after each EDFA.

The internal interconnect uses $M^2 \cdot R$ optical fibers for space switch interconnections, $M \cdot R$ optical fibers for interconnections from space switches to the wavelength routing networks. The total number of optical fibers in the internal interconnect is $M^2 \cdot R + M \cdot R = N \cdot (M+1)$ which is almost proportional to the line number M of space switches. When $M = 1$, that is $N = R$, the two sets of interconnection fibers become one set with N the total number of optical fibers. The number of optical amplifiers compensating for the loss must be $M \cdot R = N$.

3.4 System Loss

In this section, we consider the system loss for different combinations of WDM and SDM. The system loss is an important parameter for selecting the number of WDM wavelengths and the size of space switches. In the optical cross-connect, it depends on the size of space switches and the structure of wavelength routing networks.

When we use tunable lasers in transmitters and wavelength routers, the total system loss L_{total} in decibels is given by

$$L_{total} = 10\log\left(M^2\right) - G_{net} + L_{ex} \qquad (3\text{-}2)$$

where G_{net} is the net gain of SOA switching gates, L_{ex} is the total excess loss including the insertion loss of an external modulator, the excess loss of an optical splitter and a combiner, and the insertion loss of a wavelength router. From equation (3-1), we have

$$L_{total} = 10\log\left[\left(\lceil N/R \rceil\right)^2\right] - G_{net} + L_{ex} \qquad (3\text{-}3)$$

where $\lceil N/R \rceil$ is the smallest rounded integer larger than or equal to N/R.

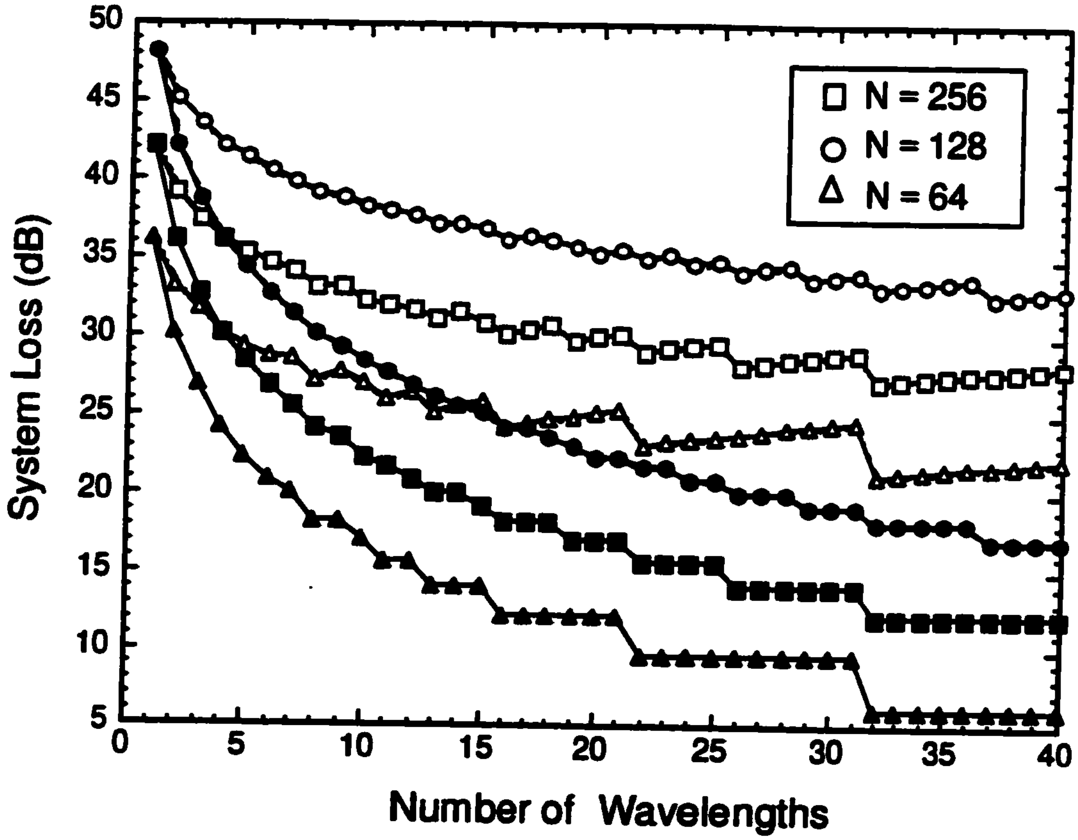

Figure 3.6: System loss of an $N \times N$ optical cross-connect. For each wavelength number, the lower curves show system loss when using wavelength routers while the upper curves show systems loss when using star-coupler-based routing networks.

With star-coupler based wavelength routing networks, the loss is increased to

$$L_{total} = 10\log\left[\left(\lceil N/R \rceil\right)^2 R\right] - G_{net} + L_{ex} \qquad (3\text{-}4)$$

This loss is the same as that when we use central power laser based transmitters and wavelength routers.

Figure 3.6 shows the system loss as a function of the number of wavelengths for WDM with the assumptions of $G_{net} = 15\,\text{dB}$ and $L_{net} = 15\,\text{dB}$. From Figure 3.3 and 3.6, it can be seen that using space switches to interconnect WDM sub-cross-connects reduces the number of wavelengths, but increases the system power budget comparing with the wavelength routing based optical cross-connects. It can be seen that the curves for using star-coupler-based routing networks will reach some asymptotes as the number of wavelengths increases. The asymptotes indicate the inherent losses of the star-couplers. To alleviate the splitting loss of space switches, we may use directional coupler based semiconductor active splitters instead of passive ones. To be successful, we have to reduce the crosstalk particularly within a wide optical bandwidth. Experimental studies [73] show that $LiNbO_3$ directional coupler can have a crosstalk ratio of -30 dB within 10 nm optical bandwidth with proper designs. Wavelength reuse may make it possible to use directional coupler based space switches to interconnect WDM sub-cross-connects because of a relative narrow optical bandwidth for WDM.

3.5 Conclusions

In this chapter, we have proposed an optical cross-connect architecture for a large size switching core. Space switches make full wavelength reuse in WDM sub-cross-connects so that the number of wavelengths is reduced. In turn, WDM makes it possible to expand the space switches to a large size one with significantly less components. With the conceptual designs for its implementation, we have shown that the system can be highly integrated and can be highly modular. As the size of the proposed optical cross-connect increases, the system loss may become a limiting factor, particularly when using star-coupler based wavelength routing networks.

4. Performance Analysis of the Proposed Optical Cross-Connect as a High-Speed Switching Core

4.1 Introduction

Following the design for the implementation in the last chapter, the system performance needs to be investigated and the degradation factors have to be identified before a possible practical system design. In this chapter, we consider the proposed optical cross-connect as a switching core used inside a switching system. For this application, optical to electrical (O/E) and electrical to optical (E/O) conversion interfaces may be used at the ends of the cross-connect system. The main factor degrading the system performance is homo-wavelength crosstalk due to using space switches for wavelength reuse. After investigating the crosstalk mechanisms, we will discuss a Gaussian approximation for calculating homo-wavelength crosstalk impact on the performance. Numerically, a 64×64 cross-connect is taken as an example for the performance evaluation. We believe this is a reasonably large size to be investigated with considerable engineering importance.

Some assumptions and simplifications are used in the following modeling and numerical calculations. First, the optical cross-connect is assumed to be fully loaded, that is, all the possible cross-connections are used all the time without output contention, which is resolved by the electronic control. The calculation is performed for connections in the steady state without any dynamic interruptions. Data signals are on-off keying (OOK) with the nonreturn-to-zero (NRZ) format, and received by direct detection with a *p-i-n* photodetector. Optical signals are represented by their optical power corresponding to data ONEs and ZEROs. Frequency chirp due to external intensity modulation and dispersion effects of all components are not taken into account since signals are transmitted only in short length fibers within the cross-connect. For simplicity of the analysis, all the light reflections in the system are ignored. All components are assumed to be polarization-insensitive.

The rest of the chapter is organized as follows. In Section 4.2, we describe the system models and then discuss the mechanisms of crosstalk degrading the system performance in Section 4.3. Section 4.4 describes the approach for our performance evaluation. Bit error rate performance and power penalty due to crosstalk are numerically evaluated and discussed in Section 4.5. Finally, in Section 4.6 we present our conclusions.

4.2 System Models

In this section, we describe system models for evaluating the system performance. The system models are based on the designs discussed in Section 3.3. Figure 4.1 shows the optical signal path through the cross-connect. In this figure, optical amplifiers are represented with their gains and other components are represented with their losses.

Optical amplifiers are key components in the optical cross-connect system. Two kinds of optical amplifiers, SOAs and EDFAs, are used. SOAs are considered to be in the steady state in our performance evaluation, although their dynamic characteristics are very important [77, 78]. Furthermore, SOAs will be treated as ideal traveling-wave optical amplifiers. As amplifiers, the gain of SOAs is wavelength-dependent even though the gain ripples have been ignored. For traveling-wave SOAs working at 1.5 μm at the unsaturated region, the -3 dB optical bandwidth is about 40 nm. In our present consideration, the utilized wavelength range is much smaller than SOAs' optical bandwidth. So, the gain of SOAs is assumed to be wavelength-independent. When more wavelengths are used for WDM, we have to consider the spectral dependence of the amplifier gain. In principle, we can provide a larger power margin to compensate for the gain drop for some signals.

The saturated gain of SOAs is calculated with [97]

$$P_{in} = \frac{P_{sat}}{G-1} \cdot \ln\frac{G_0}{G} \qquad (4\text{-}1)$$

where G is the amplifier saturated gain, G_0 is the gain with zero input power called the unsaturated gain, and P_{sat} is the optical saturation power.

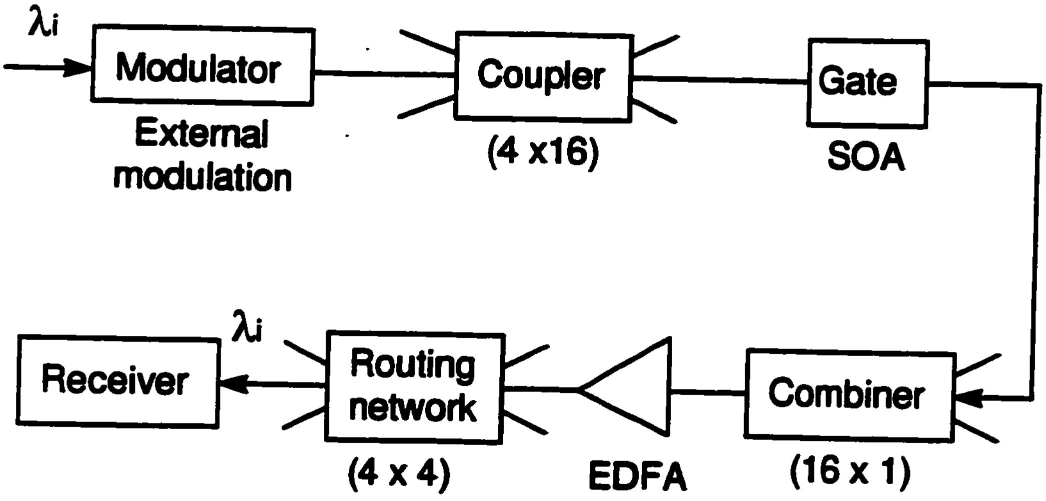

Figure 4.1: Model representation of an optical signal path of the optical cross-connect. Components are characterized with their losses or gains.

SOAs have a short gain recovery time of about several hundred picoseconds [115]. For a low-speed signal with a high input power, the gain will vary with signal data bits. For a high-speed optical signal at 10 Gb/s, the gain can be assumed to correspond to average optical power rather than power in each data bit, provided an appropriate line code is used to avoid long lines of data ZEROs or ONEs. This is the case we consider in this chapter. It is also well-known that the gain saturation of optical amplifiers, particularly SOAs, induces inter-channel crosstalk in WDM systems [97, 115]. Fortunately, in the proposed optical cross-connect system only one channel at a time is amplified by an SOA. So, the inter-channel crosstalk is avoided in this application.

EDFAs are also assumed to be gain-flat within the WDM wavelength range and their saturated gain is calculated with the average input power because of their long carrier lifetime of about 10 milliseconds [116]. Due to the same reason, inter-channel crosstalk resulting from gain saturation is negligible. Considering the input and output coupling losses, the optical output power is given by

$$P_{out} = L_{in} L_{out} G P_{in} \tag{4-2}$$

where L_{in} and L_{out} are the input and output coupling losses, respectively. Spontaneous emission noise power at the output from an amplifier is given by [97, 117]

$$P_{sp} = L_{out} p n_{sp} (G-1) h\nu B_o \quad (4\text{-}3)$$

where ν is the center frequency of the amplifier bandwidth, B_o is the effective optical bandwidth of optical filters, n_{sp} is the spontaneous emission factor, and p is a factor which ranges from 1 to 2 according to the polarization sensitivity of the amplifier. In the following evaluation, we assume that all the amplifiers are polarization insensitive, so p is taken to be 2 in our calculations.

In this optical cross-connect system, EDFAs are concatenated with SOAs, the signal output power and the total amplified spontaneous emission noise power can be calculated using the following iterative equations [118]

$$P_{out,i} = L_i G_i P_{out,i-1} \quad (4\text{-}4)$$

$$\begin{aligned} P_{ase,i} &= L_i G_i P_{ase,i-1} + P_{sp,i} \\ &= L_i G_i P_{ase,i-1} + L_{out,i} p n_{sp} (G_i - 1) h\nu B_o \end{aligned} \quad (4\text{-}5)$$

where $L_i = L_{in,i} L_{out,i}$ is the total coupling loss of the i-th optical amplifier, G_i is the internal gain of the i-th optical amplifier.

4.3 Mechanisms of Crosstalk

There are various crosstalk components degrading the system performance in the proposed optical cross-connect system. One is due to a finite ON/OFF ratio of SOA switching gates. Another component is induced by non-ideal response of wavelength routing networks which is a very common type of crosstalk in WDM systems. The third one results from the transmitter modules with central power lasers. The first and the third are unique in the cross-connect, so they will be emphasized in the following discussion. These three crosstalk components can be categorized into two types. One is referred to as hetero-wavelength crosstalk which can be taken into account by the power addition [119, 120, 121]. The second type is homo-wavelength crosstalk, as the crosstalk channels have the same nominal wavelength as the signal channel. When the signal-crosstalk beating falls

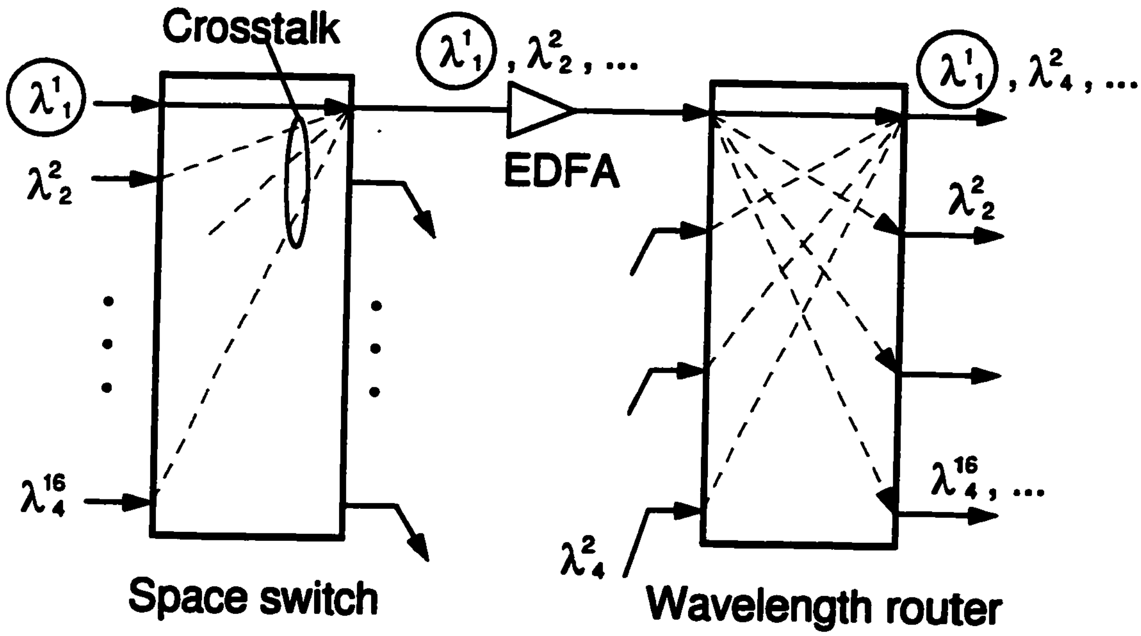

Figure 4.2: Crosstalk mechanism in space switches followed by wavelength routers. ___ represents a signal path; - - - represents a crosstalk path. Superscript and subscript of λ_j^i denote a signal from the *i*-th input port at the *j*-th wavelength. The circled wavelength is for the signal.

within the receiver electrical bandwidth, the homo-wavelength crosstalk is referred to as beat-noise crosstalk.

Let us first consider the cross-connect system with tunable laser transmitters and the wavelength routers. Each transmitter uses a separate tunable laser. Therefore, optical carrier phase of different signal channels are random and statistically independent.

As switching gates, SOAs work in the ON and OFF states controlled by their injection currents. An SOA in the OFF state (with a lower injection current) absorbs incident optical power and blocks the signal channel. However, some optical power can leak from the SOA. The power leakage becomes crosstalk to another signal channel when it gets combined with the signal at an output combiner of a space switch. Without loss of generality, we consider the first output port of a space switch in the cross-connect, as shown in Figure 4.2. With different wavelengths and space cross connections, there are the least and the worst case degradation due to crosstalk components.

The least degradation case corresponds to when the crosstalk channels in an input port group (which are connected to a single space switch) use different wavelengths compared to that of the signal channel. It can be seen that the crosstalk at the output of the combiner will be redistributed to different output ports of the wavelength routing network in accordance with their wavelengths. For instance, a crosstalk channel at λ_2 at the first input of the wavelength router becomes crosstalk at the second output port, as shown in Figure 4.2. In the same way, a crosstalk component at λ_4 at the fourth input of the router becomes crosstalk to the signal at the first output port. According to the wavelength routing relationship, one can note that all the crosstalk terms to a signal channel at an output of the wavelength router have different wavelengths compared to the signal channel. Thus, the crosstalk in this case is hetero-wavelength, so its power can directly add to the signal power with no beating falling within the receiver bandwidth. With the power addition, the crosstalk power in a signal channel at an output of a wavelength router is given by

$$P_{x,g}(t) = \sum_{\substack{k=1 \\ (k \neq i)}}^{M-1} C_g P_{out,k}(t) \tag{4-6}$$

where C_g is the reciprocal of the ON/OFF ratio of SOA gates, defined as $C_g = G_{off}/G_{on}$, and $P_{out,k}(t)$ is the output optical power of the k-th crosstalk channel at a wavelength different from λ_i, i.e., the signal wavelength, i denotes the signal channel. Equation (4-6) can be further simplified as

$$P_{x,g}(t) = C_g P_{out,1} \sum_{\substack{k=1 \\ (k \neq i)}}^{M-1} d_k(t) \tag{4-7}$$

where $P_{out,1}$ is the output optical power for data ONEs which is assumed the same for all the channels, $d_k(t)$ is a data indicator for the k-th crosstalk channel defined as $d_k(t) = 1$ for data ONEs and $d_k(t) = r$ for data ZEROs, where r is the reciprocal of a signal extinction ratio defined as $r = P_0/P_1$. Although there might be some beating among crosstalk terms when they have the same wavelength, it will be much smaller because of their small amplitudes. In the least case, we will have a lower bound on the performance degradation due to crosstalk from space switches.

In the cross-connect, there are interconnections for which all the channels in an input group use the same nominal wavelength, that is $\lambda^1_j = \lambda^2_j = ... = \lambda^{16}_j = \lambda_j$ in Figure 4.2. At the same wavelength, each input in an input group must be connected to a separate wavelength router after the space switch. Hence, at every output of the space switch, a signal is combined with all the leaked power from other M - 1 input channels. Since the crosstalk channels use the same wavelength as the signal, the crosstalk will be inseparable from the signal regardless of the type of the wavelength routing network. This kind of crosstalk was referred to as the homo-wavelength crosstalk [121]. If the polarization of the crosstalk channel is orthogonal to the polarization of the signal, there is no beating between the signal and the crosstalk and the power addition applies again.

When crosstalk channels have the same state of polarization as the signal channel or have a random polarization state, the crosstalk will beat with the signal. Considering the randomness of the optical carrier phase, the beating will convert the carrier phase noise to intensity noise, which is referred to as the signal-crosstalk beat noise in this thesis, and the signal-crosstalk beat noise will fall within the receiver electrical bandwidth. Here, we have assumed that the nominal central wavelengths of the transmitters are the same and the chirp of the external modulation is negligible. Small deviation among these central wavelengths will produce a low-frequency beating which is even worse than the normal signal-crosstalk beat noise since it may create long error bursts which are harder to correct. In our calculations, the low-frequency beating is included in the signal-crosstalk beat noise, provided the average time is sufficiently long. As the signal-crosstalk beat noise falls totally within the receiver bandwidth, the homo-wavelength crosstalk is referred to as beat-noise crosstalk, which is considered in the following for the safe system design. More detailed discussion about the homo-wavelength crosstalk will be presented in Chapter 7.

In addition to homo-wavelength crosstalk from space switches, when the central power lasers are used as optical sources at the transmitters, yet another form of homo-wavelength crosstalk due to optical power leakage of the wavelength selecting modulators can be introduced. Let C_m be the reciprocal of the ON/OFF ratio (which is the total ON/OFF ratio of the two cascaded modulators if they are used) of the modulators, defined as $C_m = P_{leak}/P_1$ where P_{leak} is the leaked optical power. When an optical wavelength, for instance λ_1, is selected, the corresponding modulator is set to the ON state and all others are set to the OFF state. Since the modulators in the OFF state can not completely block the input optical power, the power leakage $C_m P_1$ will be distributed to all the outputs through the star coupler. In Figure 3.4(b), the output from the first SOA gate includes signal power $L_s G_g P_s$ at a wavelength λ_1 and three crosstalk terms with constant optical power $C_m L_s G_g P_1$ but at different wavelengths λ_2, λ_3 and λ_4. The crosstalk with other signal channels is reduced to $(C_g C_m) L_s G_g P_1$ in which $C_g C_m <$ -50 dB is so small that makes the crosstalk negligible.

As for this crosstalk, the worst case is that R input channels in an input group are simultaneously cross-connected to R outputs of a wavelength router. Therefore, R input channels in the input group must be combined at an output port of the space switch. Figure 4.3 shows the wavelength distribution in this case before and after the combiner. Circled wavelengths are for the signals, the other ones in the same column at a circled wavelength are the homo-wavelength crosstalk terms at each output of the wavelength router.

If we assume that a signal channel and its crosstalk channels have the same polarization and their optical length is the same, that is, the signal carrier and the crosstalk carriers are totally in phase, the crosstalk will improve the signal extinction ratio. Unfortunately, this situation is very rare without a strict optical phase control.

With no control on the optical phase, the worst-case interference between the signal and the crosstalk may happen, that is, all the crosstalk carriers are in phase but out of phase with the signal and the polarization states of the signal and crosstalk channels are matched. The optical power of data ONEs may be significantly reduced by the interference. Considering the slow phase and polarization fluctuations in time, once this case happens, it would last for a long time (relative to the bit duration) during which the

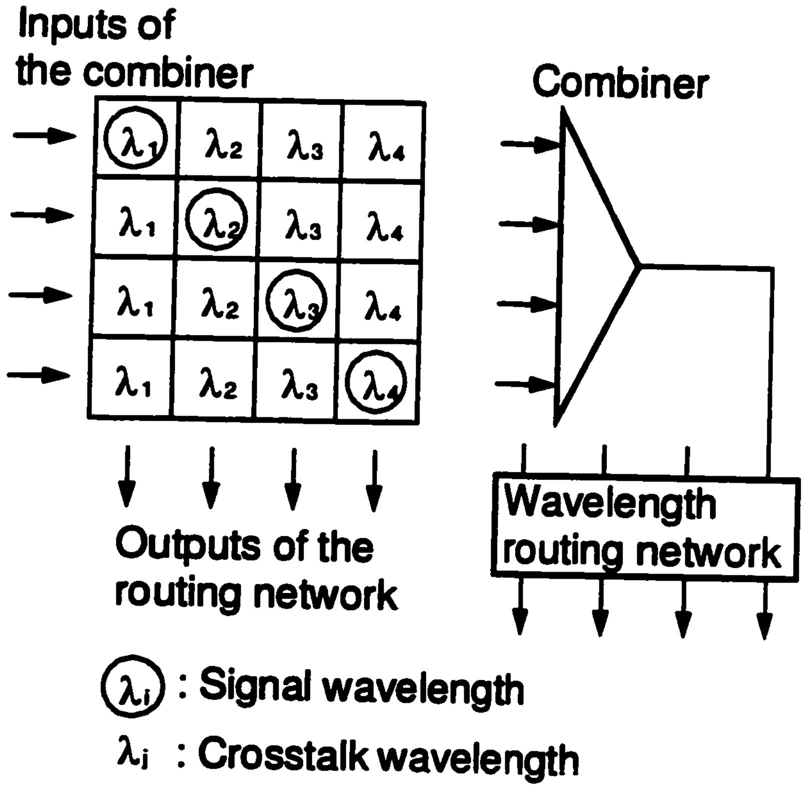

Figure 4.3: Wavelength distribution of homo-wavelength crosstalk when using central high-power lasers. Input wavelengths to the combiner are in rows, output wavelengths of the wavelength routing network are in columns.

system performance is seriously degraded. This is very undesirable because there is no way to recover a long length loss of data except by re-transmitting them and this is not possible in many communications situations.

To avoid the long-time out-of-phase worst case, we can randomize the phase of all the input wavelength channels through relative delays much longer than the laser coherent length. Therefore, the optical carrier phase values become uncorrelated and each can be assumed to have an independent phase uniformly distributed between $-\pi$ to π.

When we use the star coupler based wavelength routing networks, the worst-case crosstalk from the space switches and from the transmitters with central power lasers are the same as that with wavelength routers. In addition, the crosstalk always takes the worst case regardless of cross-connections since the inputs of a star coupler are always combined before they are distributed to the optical filters.

To evaluate the beat-noise crosstalk, we begin by considering the total received electrical field. It is assumed that there are K crosstalk channels with the same crosstalk ratio, C_x. On a photodetector, the optical field of the signal with the beat noise crosstalk is given by

$$E(t)=\sqrt{2P_s(t)}\bar{p}_s(t)\cos(\omega t+\phi_s(t))+\sum_{k=1}^{K}\sqrt{2C_xP_{x,k}(t)}\bar{p}_{x,k}(t)\cos(\omega t+\phi_{x,k}(t)) \quad (4\text{-}8)$$

where $P_s(t)$ is the optical signal power, $P_{x,k}(t)$ is the optical power of the crosstalk channel, $\bar{p}_s(t)$ and $\bar{p}_{x,k}(t)$ are unit vectors of the signal and the i-th crosstalk channel polarization, respectively, $\phi_s(t)$ and $\phi_{x,k}(t)$ are the optical phase of the signal carrier and the i-th crosstalk carrier, respectively. Considering the laser spectral linewidth of several tens of MHz being much smaller than the receiver bandwidth (≥ 1 GHz), we can assume the crosstalk carrier phase is constant at least within one bit duration. Thus, when a signal datum is ONE or ZERO, the detected optical power can be approximated by

$$\begin{aligned} P_d &= P_{out,1}d_s+2\sqrt{C_x}P_{out,1}\sum_{k=1}^{K}\sqrt{d_sd_{x,k}}\bar{p}_s\bar{p}_{x,k}\cos(\phi_s-\phi_{x,k}) \\ &+2C_xP_{out,1}\left[\sum_{k=1}^{K}\sqrt{d_{x,k}}\bar{p}_{x,k}\cos(\omega t+\phi_{x,k})\right]^2. \end{aligned} \quad (4\text{-}9)$$

The received optical power includes three terms. The first one represents the signal power, the second term is the beating between the signal and the crosstalk, and the third term is the power addition of crosstalk channels and the mutual beating. The second and the third terms contribute to the detected power fluctuation at the receiver with the second term being the dominant one.

Gimlett and Cheung [123] assumed the second beat term to be Gaussian and presented a power penalty relationship. The validation of this approximation is based on a large number of crosstalk channels, a low crosstalk ratio and a negligible optical power of the data ZEROs. To make the previously reported approach more accurate, we include the third term and data ZERO power effect on the signal-crosstalk beat noise, and then evaluate bit-error-rate performance and power penalty with the statistical methodology [120, 121].

With the assumption that crosstalk terms are small enough and their optical carrier phases are statistically independent, the total crosstalk in the electric field, $E_x(t)=\sqrt{C_x}\sum_{k=1}^{K}\sqrt{2P_{x,k}(t)}\bar{p}_{x,k}(t)\cos(\omega t+\phi_{x,k}(t))$, in accordance with the central limit theorem, can be approximated by a Gaussian random process $E_x(t)$. Through a square law detector, for a signal data ONE or ZERO, the received optical power has a non-central chi-squared distribution [124]. By using the probability distribution transformation, we have the variance of the non-central chi-squared distribution which can further be approximated by Gaussian statistics.

First, we assume that the polarization of each crosstalk channel matches the signal polarization, that is, $\bar{p}_s(t)=\bar{p}_{x,k}(t)$ for all k. For signal data ONE and ZERO, we assume there are K crosstalk channels with data ONEs. The average optical power and the optical power (fluctuations) variance due to the beat-noise crosstalk are

$$\overline{P}_{d,1/0}=P_1(d_{1/0}+KC_x) \tag{4-10}$$

$$\sigma^2_{x,1/0,K}=2P_1^2 d_{1/0}KC_x+K^2C_x^2P_1^2. \tag{4-11}$$

Here, we ignore the contribution from the crosstalk at data ZEROs. If the crosstalk channels are randomly polarized, the average optical power is kept the same but the power variances are reduced by a factor of 2,

$$\sigma^2_{x,1/0,K}=P_1^2 d_{1/0}KC_x+K^2C_x^2P_1^2/2. \tag{4-12}$$

From the above equations, it can be noted that the average optical power is the summation of the signal and crosstalk in power, and the power variance is strongly dependent on the power in the data ONEs and ZEROs. One term in the power variance is due to the beating among the crosstalk channels. With a low crosstalk ratio and a small number of crosstalk channels, this beating is usually negligible.

In addition to homo-wavelength crosstalk due to using space switches or wavelength selectors, there is another kind of crosstalk from wavelength routing networks due to their non-ideal spectral response. This kind of crosstalk is hetero-wavelength and can be easily taken into account with the power addition approach. For estimation, we only consider two adjacent crosstalk channels, so the crosstalk terms are independent of the number of the wavelength channels.

4.4 Bit-Error-Rate Evaluation

To evaluate the bit-error-rate performance of the optical cross-connect, we adopted a noise model of the signal current in the receiver from [97] with some modifications. Spontaneous emission noise of the amplifiers is assumed to be white within the signal optical bandwidth and to have Gaussian statistics. When the signal with spontaneous emission noise is detected by a photodetector, an electric current includes the signal current corresponding to the input optical power and noise components corresponding to thermal noise, shot noise, signal-spontaneous beat noise, and spontaneous-spontaneous beat noise contributions. The thermal noise, independent of the received optical power, is an equivalent noise including all the noise terms from the photodetector and the subsequent electrical pre-amplifier.

The thermal noise, shot noise, signal-spontaneous beat noise, and spontaneous-spontaneous beat noise electrical power with a loading resistance of one ohm are given by

$$N_{th} = I_{th}^2 B_e \qquad (4\text{-}13)$$

$$N_{shot,1/0} = 2\frac{\eta e^2}{h\nu}\left(P_{out,1/0} + N_{eff}B_o\right)B_e \qquad (4\text{-}14)$$

$$N_{s-sp,1/0} = 4\left(\frac{\eta e}{h\nu}\right)^2\left(P_{out,1/0}N_{eff}/p\right)B_e \qquad (4\text{-}15)$$

$$N_{sp-sp} = \left(\frac{\eta e}{h\nu}\right)^2 N_{eff}^2/p\left(2B_oB_e - B_e^2\right) \qquad (4\text{-}16)$$

where N_{eff} is the effective power spectral density of the amplified spontaneous emission noise from all optical amplifiers, $P_{out,1/0}$ is the output power of the optical signal corresponding to data ONEs and ZEROs. All the noise components are assumed to be Gaussian. Therefore, the total noise power can be expressed as

$$N_{1/0} = N_{th} + N_{shot,1/0} + N_{s-sp,1/0} + N_{sp-sp}. \tag{4-17}$$

Now we consider a signal in crosstalk. With wavelength routers, the crosstalk not only increases the shot noise but also contributes to crosstalk-spontaneous beat noise since spontaneous emission noise along with the crosstalk is simultaneously routed to the same output port with the information. Figure 4.4 shows a spectral distribution at an output of a wavelength router. Spontaneous emission noise and crosstalk from other three inputs are routed to the signal output port.

With the power addition assumption of hetero-wavelength crosstalk, the crosstalk power will be added to $P_{out,1/0}$ in equations (4-14) and (4-15). The spontaneous-spontaneous beat noise is increased by R times as a single channel does. With these arguments in mind, equations (4-14) to (4-16) become

$$N_{shot,1/0} = 2\frac{\eta e^2}{h\nu}\left[P_{out,1/0} + P_x + N_{eff}(RB_o)\right]B_e \tag{4-18}$$

$$N_{s-sp,1/0} = 4\left(\frac{\eta e}{h\nu}\right)^2\left[\left(P_{out,1/0} + P_x\right)N_{eff}/p\right]B_e \tag{4-19}$$

$$N_{sp-sp,1/0} = 2\left(\frac{\eta e}{h\nu}\right)^2 N_{eff}^2/p\left(2B_oB_e - B_e^2\right)R. \tag{4-20}$$

As for the beat-noise crosstalk, since it has been considered as the beat noise to the signal using the Gaussian approximation, the average optical power $\overline{P}_{d,1/0}$ is used as in equations (4-18) and (4-19) to calculate the shot noise and signal-spontaneous beat noise.

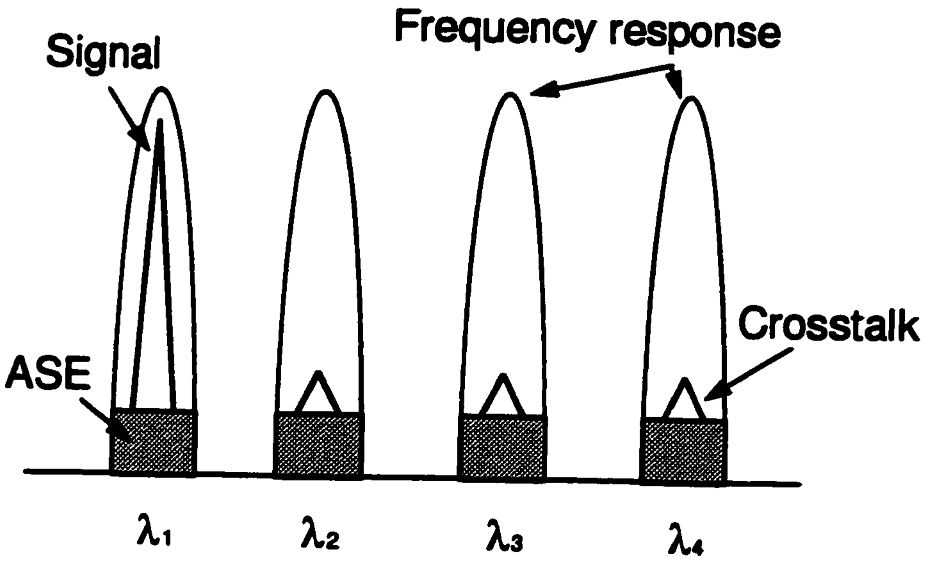

Figure 4.4: Spectral distribution of an optical signal and its crosstalk at an output of a wavelength router.

If it is assumed that the OOK signals have equal probability ($1/2$) in data ONEs and ZEROs and are statistically independent, with the power addition assumption and disregarding non-ideal signal waveform distortion, the total crosstalk power at the sampling point for threshold detection will be binomially distributed. This is due to the fact that the total power is the summation of many (say M-1 from a space switch) two-level power crosstalk channels. This may overestimate the crosstalk impact on the performance when the signal with asynchronous crosstalk channels is received by a receiver with a finite electrical bandwidth. For the hetero-wavelength crosstalk from the space switches, the total crosstalk power takes on M possible power levels with the probability given by

$$\begin{aligned} P_b(j) &= P_b\left[P_{x,j} = jC_g P_{out,1} + (M-1-j)C_g P_{out,0}\right] \\ &= \frac{(M-1)!}{j!(M-1-j)!}\cdot\frac{1}{2^{M-1}}, \qquad j = 0,\ 1,\ \dots\dots,\ M-1. \end{aligned} \tag{4-21}$$

The average BER may be evaluated for each possible crosstalk level at the receiver. Thus,

$$P_e = \sum_{j=0}^{M-1} \frac{1}{2\sqrt{2\pi}} \left\{ \int_{Q_{0,j}}^{\infty} \exp(-t^2/2)dt + \int_{Q_{1,j}}^{\infty} \exp(-t^2/2)dt \right\} P_b(j) \tag{4-22}$$

where

$$Q_{0,j} = \frac{T_{opt} - \left(S_{out,0,j} + S_{x,j}\right)}{\sqrt{N_{0,j}}}, \quad Q_{1,j} = \frac{\left(S_{out,1,j} + S_{x,j}\right) - T_{opt}}{\sqrt{N_{1,j}}}. \tag{4-23}$$

Also, $S_{out,1/0,j} = \frac{\eta e}{h\nu} P_{out,1/0,j}$ and $S_{x,j} = \frac{\eta e}{h\nu} P_{x,j}$, $N_{0,j}$ and $N_{1,j}$ are the total noise power for data ONEs and ZEROs, respectively, as the crosstalk power is $P_{x,j} = jC_g P_{out,1} + (M-1-j)C_g P_{out,0}$. T_{opt} is the optimal decision threshold which results in the minimum average BER. Unfortunately, the optimal threshold level is analytically intractable. Numerical calculations must be used to obtain accurate results.

In addition to using the statistical averaging, we can use the worst case analysis to evaluate the performance degradation. It should be noted that this worst case is for hetero-wavelength crosstalk components under the power addition assumption. With the worst case analysis, all the crosstalk channels are assumed to always have data complementary to that of the signal channel. Therefore, the bit error rate is calculated by

$$P_e = \frac{1}{2\sqrt{2\pi}} \left\{ \int_{Q_{0,min}}^{\infty} \exp\left(-t^2/2\right) dt + \int_{Q_{1,min}}^{\infty} \exp\left(-t^2/2\right) dt \right\} \tag{4-24}$$

$$Q_{0,min} = \frac{T_{opt} - \left(S_{out,0} + (M-1)C_g S_{out,1}\right)}{\sqrt{N_0}}, \quad Q_{1,min} = \frac{\left(S_{out,1} + (M-1)C_g S_{out,0}\right) - T_{opt}}{\sqrt{N_1}}. \tag{4-25}$$

In the following numerical calculations, the crosstalk due to non-ideal filter response of wavelength routing networks is considered under this worst-case analysis.

For the beat-noise crosstalk from space switches, the variance of the optical power taking on a certain level is also a binomial distribution as given in equation (4-21). The bit error rate could be evaluated for each possible power variance level due to the beat noise crosstalk at the receiver. Thus, we can calculate the bit error rate using equation (4-22) with

$$Q_{0,j} = \frac{T_{opt} - \left(S_{out,0,j} + \overline{S}_{x,j}\right)}{\sqrt{N_{0,j}}}, \quad Q_{1,j} = \frac{\left(S_{out,1,j} + \overline{S}_{x,j}\right) - T_{opt}}{\sqrt{N_{1,j}}} \tag{4-26}$$

where $\overline{S}_{x,j} = \frac{\eta e}{h\nu}\left[jC_g P_{out,1} + (M-1-j)C_g P_{out,0}\right]$, $N_{1/0,j} = N_{1/0} + N_{g,1/0,j}$ is the total noise power of the signal with a signal-crosstalk beat-noise power $N_{g,1/0,j} = \left(\frac{\eta e}{h\nu}\right)^2 \sigma^2_{g,1/0,j}$. It should be stressed that the performance degradation obtained using the beat-noise analysis of homo-wavelength crosstalk is an upper bound. The beat interference between the signal and the crosstalk can be reduced by some factors such as crosstalk central wavelength shift from the signal wavelength larger than the receiver electrical bandwidth and the large frequency chirp due to the modulation.

For the beat-noise crosstalk due to using central power lasers, since crosstalk channels have a constant power level, we can simply calculate the power variance for signal data ONEs and ZEROs, and add them to the total noise power. One can note that the worst case crosstalk may also include the beat-noise crosstalk from space switches since there are R input ports from an input group at most to connect to a wavelength routing network, and there can be $M-R$ beat-noise crosstalk channels from the same space switch. To emphasize the crosstalk due to using the central power lasers, we assume the ON/OFF ratio of the SOA switching gates is large enough so that the crosstalk terms can be dealt with, separately.

4.5 Numerical Results and Discussions

For the following numerical calculation, the default values of the system parameters are listed in Table 4.1 at the end of the chapter. We first consider using tunable lasers at the transmitters and wavelength routers as the wavelength routing networks, thus there are only the homo-wavelength beat-noise crosstalk from space switches in the worst case. The crosstalk of the wavelength routing networks is taken into account with two adjacent crosstalk channels. The worst case analysis is applied as discussed in equations (4-24) and (4-25).

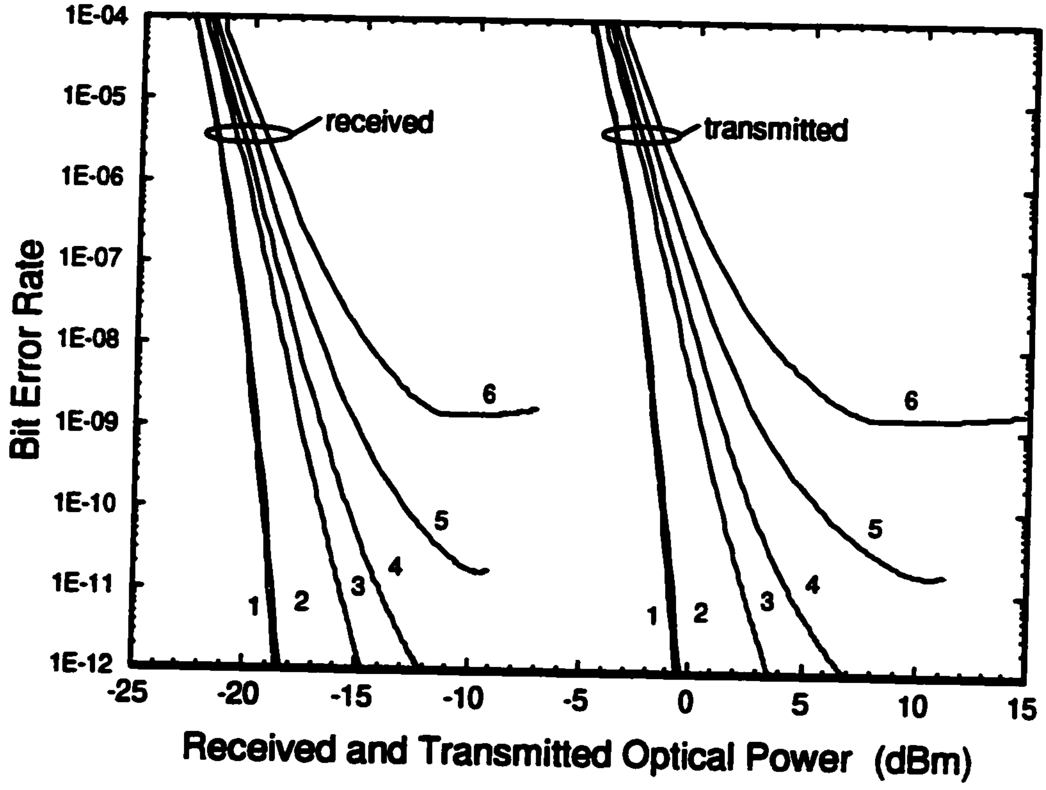

Figure 4.5: Bit error rate versus received and transmitted average optical power with different crosstalk ratios of SOA switching gates. Crosstalk channels are assumed to be randomly polarized. The signal extinction ratio is 20 dB. Crosstalk ratios corresponding to curve 1, 2, 3, 4, 5, and 6 are -∞, -40, -30, -29, -28, and -27 dB.

With the beat noise analysis, Figure 4.5 shows the bit error rate performance of the 64×64 optical cross-connect with the four-wavelength WDM and the 16×16 space switches. In the worst case, there are 15 (that is, $M-1$) beat noise crosstalk channels. To be realistic, we assume that the crosstalk channels have random states of polarization. The extinction ratio for all these channels is 20 dB. Without the crosstalk, the bit error rate performance is limited by the signal-spontaneous beat noise due to the use of optical amplifiers. The receiver sensitivity for a signal at 10 Gb/s is about -18.5 dBm with a BER of 10^{-12}. With a crosstalk ratio of -40 dB which is a reasonable value for the SOA gates [78] (or see Figure 8.6), there is almost no degradation. As the crosstalk ratio increases and approaches -28 dB, the BER performance will reach a floor of 10^{-12}. With a crosstalk

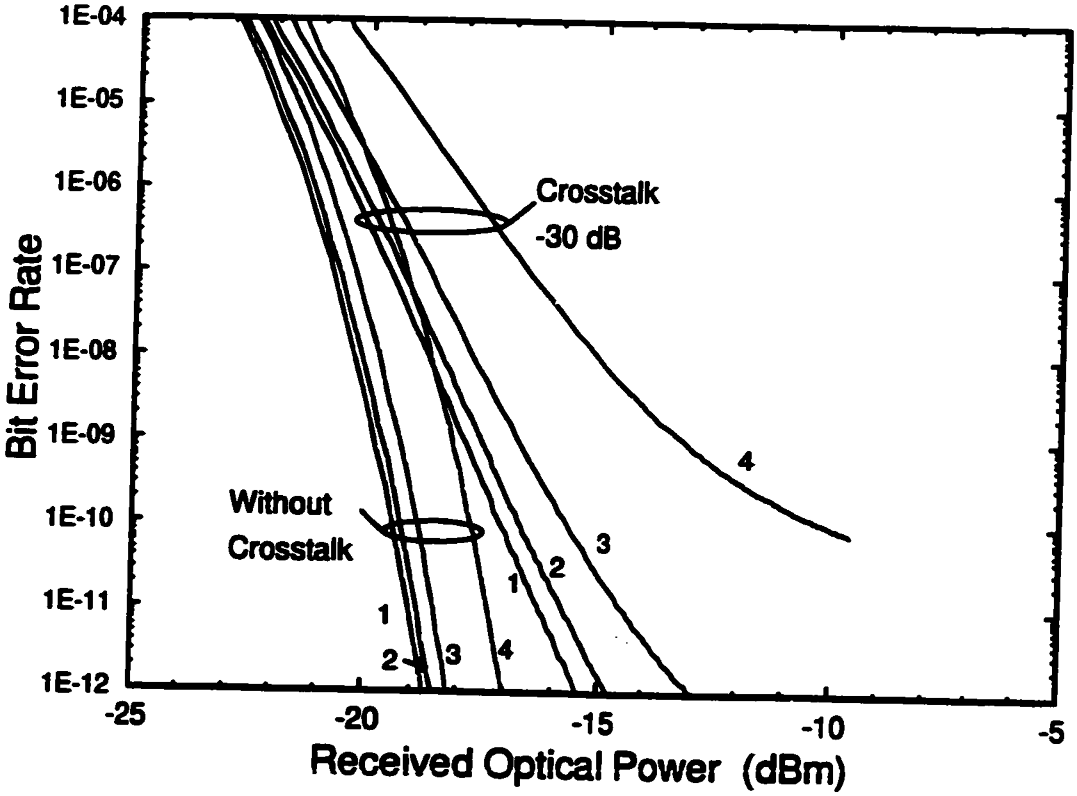

Figure 4.6: Bit error rate versus received average optical power for the signals with different signal extinction ratios. Curve 1, 2, 3, and 4 correspond to $r = -\infty$, -20, -15, and -10 dB.

ratio of -27 dB, we have a BER floor at 10^{-9}. From Figure 4.5, one can see another important point that the power penalty due to the beat-noise crosstalk is strongly BER dependent, that is, for a certain crosstalk ratio we have a larger power penalty for a lower BER. This strong dependence is due to the noise-like characteristic of signal-crosstalk beat interference and its field addition treatment instead of power addition treatment.

BER values as a function of the transmitted optical power is also shown in Figure 4.5. To have the required BER, we have to increase the input power to compensate for the crosstalk. However, the gain of SOA switching gates will be saturated by high input optical power. Thus, the transmitted power will be increased to a level higher than what we expected from the output power penalty. For example, to compensate 6.5 dB power penalty for the crosstalk ratio of -29 dB, the transmitted power need to be increased by over 7.5 dB.

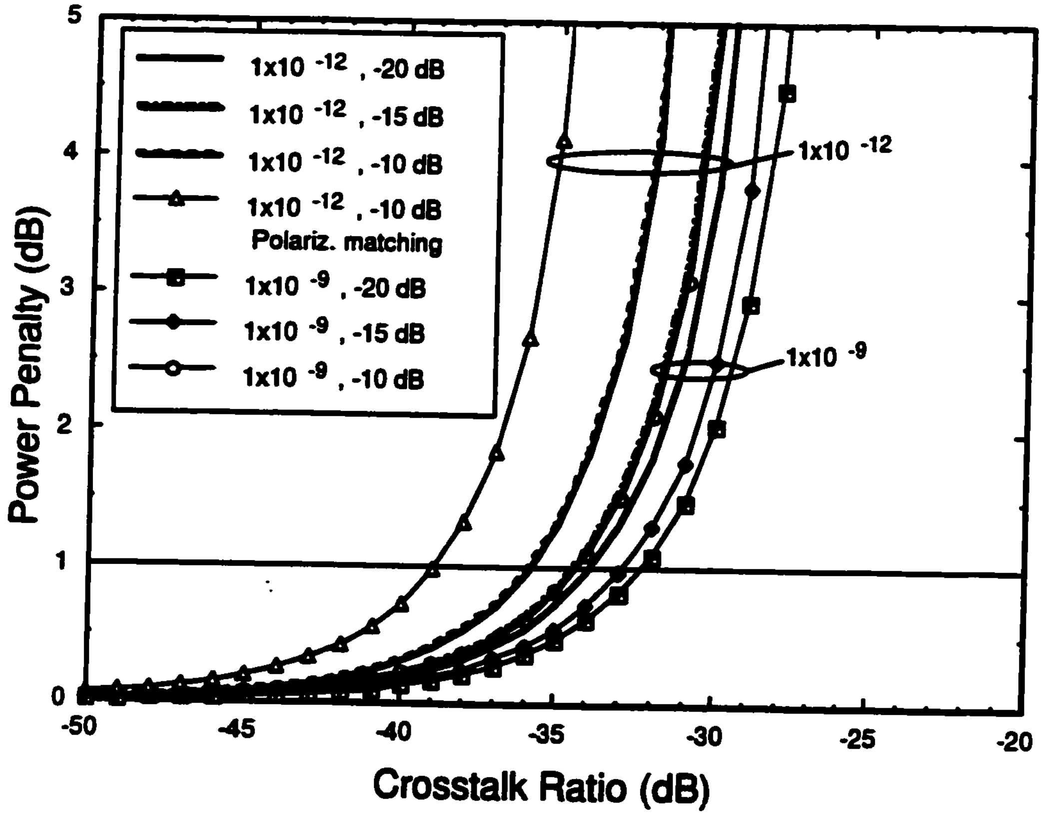

Figure 4.7: Power penalty versus crosstalk ratio of space switches with different signal extinction ratios. The optical cross-connect utilizes 16×16 space switches and the four-wavelength WDM. Crosstalk channels are randomly polarized except the case shown by the curve with triangles.

With the same system parameters as those in Figure 4.5, Figure 4.6 shows the BER performance for signals with different signal extinction ratios. Without the beat-noise crosstalk, the power penalty due to finite signal extinction ratios is independent of bit error rates, as shown by the four parallel solid lines in Figure 4.6 where curve 1 (solid line) is for the signal with the ideal extinction ratio ($r=-\infty$) and no crosstalk. With a beat-noise crosstalk ratio of -30 dB, the power penalties for these four signals with $r=-\infty,\ -20,\ -15,\ -10$ dB are strongly dependent on the bit error rates. It is important to see that with the same crosstalk ratio, the receiver sensitivity for the signal with an extinction ratio of 20 dB is about -15 dBm at a BER of 10^{-12} while the signal with an extinction ratio of 10 dB reaches the BER floor. This is because signals with lower extinction ratios have a relatively larger ZERO power with which the signal-crosstalk beat

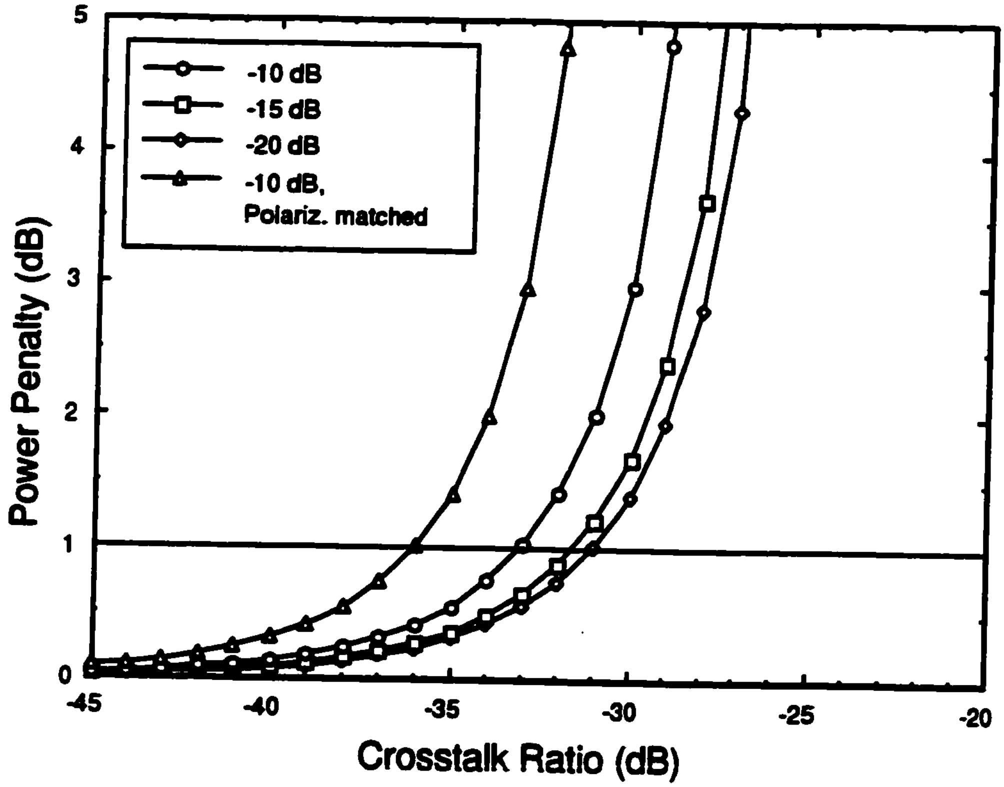

Figure 4.8: Power penalty versus crosstalk ratios of space switches when the cross-connect uses 8×8 space switches and eight-wavelength WDM. Crosstalk channels are randomly polarized except the case shown by the curve identified with triangles. BER is set to 10^{-12}.

noise can be significant. This effect was neglected in the previous power penalty evaluations [123]. To alleviate the performance degradation due to the beat-noise crosstalk, we should make the signal extinction ratio so high that the beating between the signal data ZEROs and the crosstalk be negligible. A signal extinction ratio of 20 dB will be appropriate with a power penalty of less than 0.5 dB.

Figure 4.7 shows the receiver power penalty as a function of the crosstalk ratio of SOA switching gates. The calculations are based on the same system parameters as those used for the BER performance evaluation in Figure 4.5. The dependence of power penalty on the signal extinction ratios is clearly shown in the figure. When the signal extinction ratio increases from 10 dB to 20 dB, the crosstalk ratio can be relaxed by about 2.2 dB as the BER approaches the floor. Figure 4.7 also shows the power penalty difference for two

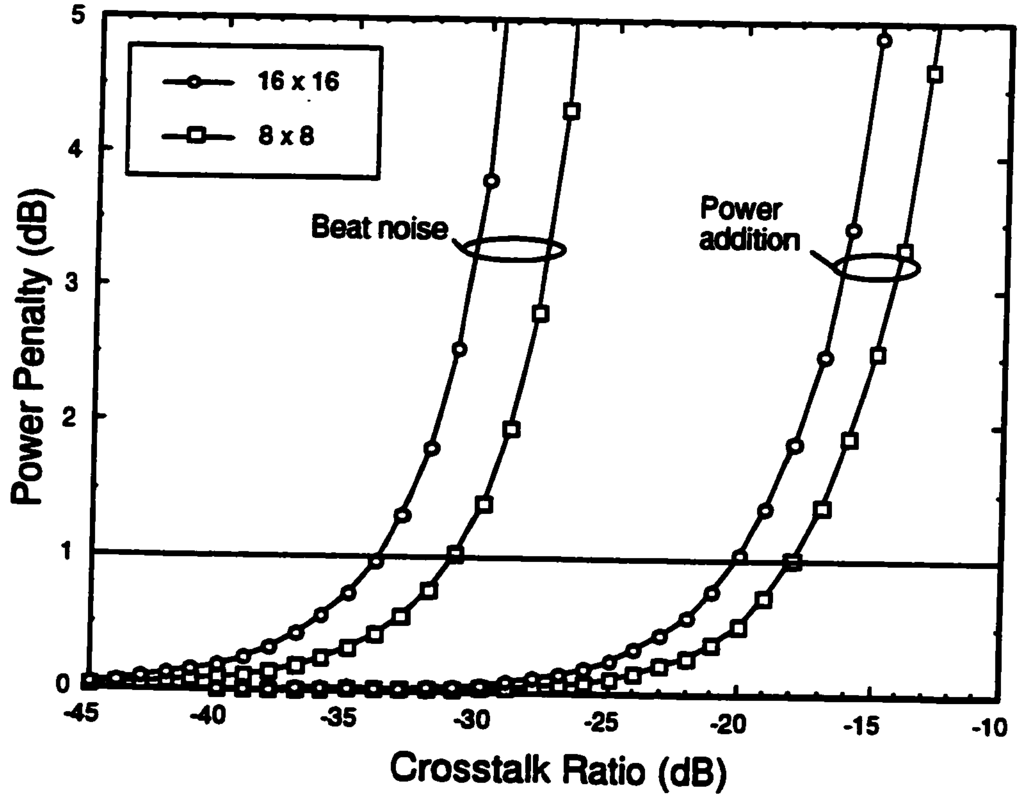

Figure 4.9: Upper and lower bounds of power penalty from space switches for the 64×64 optical cross-connect with 8×8 and 16×16 space switches. Signal extinction ratio is 20 dB. BER is set to 10^{-12}.

BER requirements of 10^{-12} and 10^{-9}. The requirement on the crosstalk ratio for a BER of 10^{-12} is less by about 1.5 dB than that for a BER of 10^{-9}. In all the above evaluations we have assumed the crosstalk channels have been randomly polarized. This is a reasonable assumption in practical systems. However, if the polarization of the crosstalk channels all match that of the signal channel, we will have more power penalty. From Figure 4.7, it is seen that the requirement for a crosstalk ratio is by 3 dB lower than that for the crosstalk channels with random polarization.

To ensure the power penalty stay within 1 dB, we must make the crosstalk ratio less than -35 dB for the signal with an extinction ratio of 15 dB at a BER of 10^{-12}. In general, crosstalk ratio of -35 dB is easily obtained with SOA switching gates. So, for 16×16 space switches, homo-wavelength beat-noise crosstalk will not be a serious problem. It is

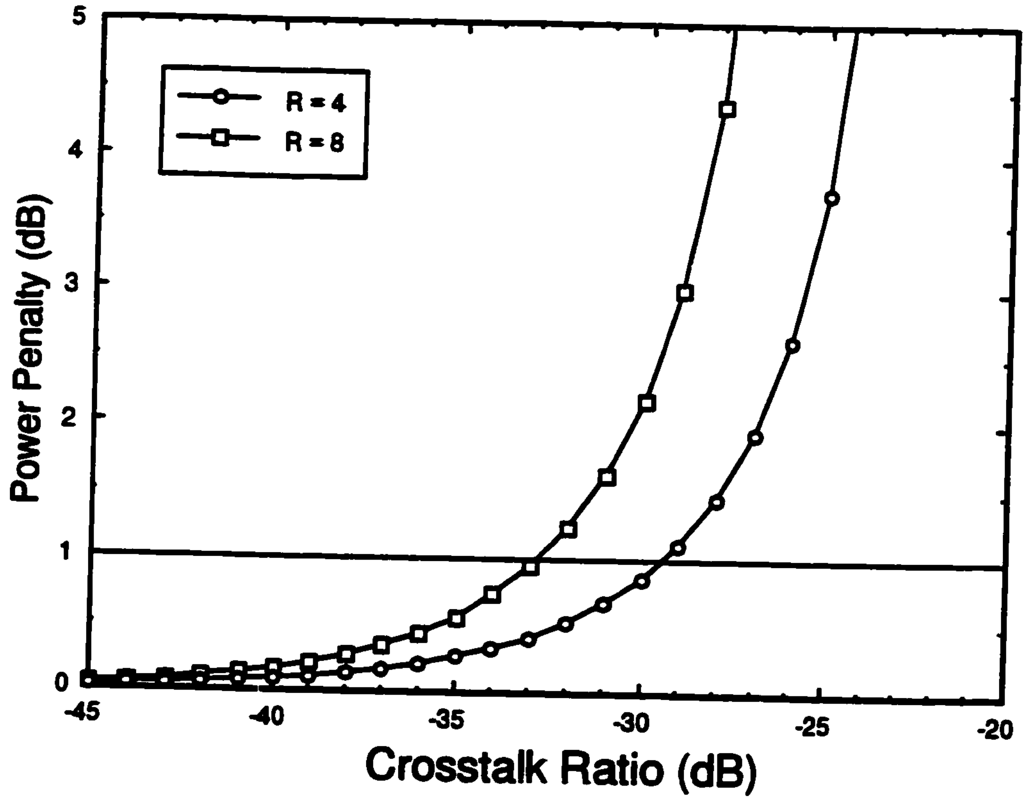

Figure 4.10: Power penalty due to using central high-power lasers for the four-wavelength WDM and the eight-wavelength WDM. Crosstalk channels are randomly polarized. Signal extinction ratio is 20 dB. BER is set to 10^{-12}.

worth seeing that the power penalty is independent of the number of wavelengths for WDM, that is, with more wavelengths we will not get more performance degradation from the space switches.

From equations (4-10)-(4-12), we see that the crosstalk beat-noise power depends on the size of the space switches. To reduce the power penalty of space switches, we can use more wavelengths for WDM and smaller size space switches. For a 64×64 optical cross-connect we consider the combination of eight-wavelength WDM with 8×8 space switches. It can be expected that the system loss will be reduced by 6 dB from equation (3-3). Figure 4.8 shows the power penalty due to the crosstalk level of the 8×8 space switches. When the crosstalk polarization matches the signal polarization, the required crosstalk ratio is 3 dB lower than that when the crosstalk channels have a random polarization. To keep the power penalty to within 1 dB, we must make the crosstalk ratio be less than -31 dB.

As we mentioned in the last section, the beat-noise analysis of homo-wavelength crosstalk gives an upper bound on the crosstalk power penalty. Considering the homo-wavelength crosstalk under the power addition assumption, we can have a lower bound on the power penalty. In Figure 4.9, we show the two bounds for the two combinations with the four-wavelength WDM and the eight-wavelength WDM. It is seen that for a power penalty of 1 dB, the difference between the required crosstalk ratios is about 13 dB. Considering this large difference, we may introduce some ways to reduce the beat noise effect of homo-wavelength crosstalk in order to relax the crosstalk requirements.

When central power lasers are used at the transmitters, there is another homo-wavelength crosstalk. Figure 4.10 shows the power penalty of these crosstalk terms under the beat-noise analysis. The signal extinction ratio is 20 dB. We assume that the phase of all the crosstalk channels have been randomized, and each crosstalk channel has an independent random polarization. The difference in the crosstalk ratio requirement for the four-wavelength WDM and the eight-wavelength WDM is 3.5 dB. To make the power penalty be within 1 dB, the crosstalk ratios must be less than -29.5 dB and -33 dB for the four wavelength WDM and the eight-wavelength WDM. With a single optical modulator, this requirement on the crosstalk ratio is hard to meet. With two cascade modulators with a total ON/OFF ratio of about 40 dB, there will be no problem to realize this transmitter scheme.

4.6 Conclusions

To assess the feasibility of the proposed optical cross-connect system, we have discussed and analyzed the system performance. With wavelength reuse, it is identified that homo-wavelength crosstalk is introduced in space switches. When using central power lasers for the transmitters, we have also similar homo-wavelength crosstalk due to finite ON/OFF ratio of the wavelength selectors. An upper bound on the performance degradation due to the homo-wavelength crosstalk has been evaluated using the beat-noise analysis.

A 64×64 optical cross-connect at an internal line rate of 10 Gb/s has been numerically evaluated. With a four-wavelength WDM and 16×16 space switches, the results show that we can have a power penalty of as low as 0.2 dB at a BER as low as 10^{-12} with a crosstalk ratio of -40 dB in the space switches. The crosstalk from the space switches will not be a concern in this system even with consideration of its beat noise effect. To reduce the beat-noise effect of homo-wavelength crosstalk, we should use a high extinction ratio for the signal and take proper measures to reduce the beating, in order to approach the lower bound on the power penalty as presented in this work. To use the central power lasers configuration, we have to have the wavelength selector with an ON/OFF ratio higher than 30 dB for a less than 1 dB power penalty. The cascade of the two modulators for wavelength selection at the transmitters will meet the requirement. From the system performance point of view, the discussion and analysis show that implementation of a 64×64 optical cross-connect is possible, at the present state-of-the-art.

Table 4.1: Default values used in the numerical calculations

Parameter	Symbol	Default Value
Bit rate	R_b	10 Gb/s
Bit error rate	BER	10^{-9} or 10^{-12}
Receiver electrical bandwidth	B_e	7 GHz
Central optical wavelength	λ_s	1550 nm
Size of optical cross-connect	N	64
Number of wavelengths	R	4 or 8
Size of space switches	M	16 or 8
Excess loss of optical splitters	L_s	3 dB
Excess loss of optical combiners	L_c	3 dB
Loss of external modulators	L_m	5 dB
Effective optical bandwidth	B_o	50 GHz
Channel crosstalk of wavelength routers	C_d	-15 dB
Thermal noise current	I_{th}	10 pA/√(Hz)
Optical gain of SOA with zero input	$G_{o,g}$	15 dB
Saturation power of SOAs	$P_{sat,g}$	3 dBm
Spontaneous emission factor	$n_{sp,g}$	3.5
Input coupling loss of SOAs	$L_{in,g}$	3 dB
Output coupling loss of SOAs	$L_{out,g}$	5 dB
Optical gain of EDFAs with zero input	$G_{o,a}$	20 dB
Saturation power of EDFAs	$P_{sat,a}$	13 dBm
Spontaneous emission factor of EDFAs	$n_{sp,a}$	1.5
Input coupling loss of EDFAs	$L_{in,a}$	2 dB
Output coupling loss of EDFAs	$L_{out,a}$	3 dB

5. Experimental Demonstration of a 4 × 4 Optical Cross-Connect

5.1 Introduction

In the previous two chapters, we presented the proposed optical cross-connect using WDM and SDM and the analysis of system performance for a 64 × 64 cross-connect as a switching core. To further prove the concept of the proposed optical cross-connect, in this chapter we present an experimental demonstration of a 4 × 4 optical cross-connect. The demonstration shows that it is promising to construct a practical system based on the proposed architecture. This experimental system can be further developed as a 4 × 4 optical cross-connect prototype.

5.2 Experimental Setup

The schematic of a 4 × 4 optical cross-connect is shown in Figure 5.1. This is a small version of Figure 3.1. In this system we use two optical wavelengths for WDM and two 2 × 2 SOA-based space switches for interconnections. A wavelength selective transmitter is made of two DFB lasers, two wavelength selectors, and a 3-dB coupler since we do not have wavelength tunable lasers. Due to lack of components, we only construct a part of this system to demonstrate the switching functions. Neglected parts have no effects on the operation of the working part.

Semiconductor optical amplifiers used in the following experiments are MQW semiconductor optical amplifiers operating at the wavelength window of 1300 nm which are specially designed for their polarization independence. The fiber-to-fiber gain is about 10 ~ 12 dB at an injection current of 100 mA. Polarization dependence of the gain is less than 0.5 dB. More detailed characteristics of these components will be discussed in Chapter 8.

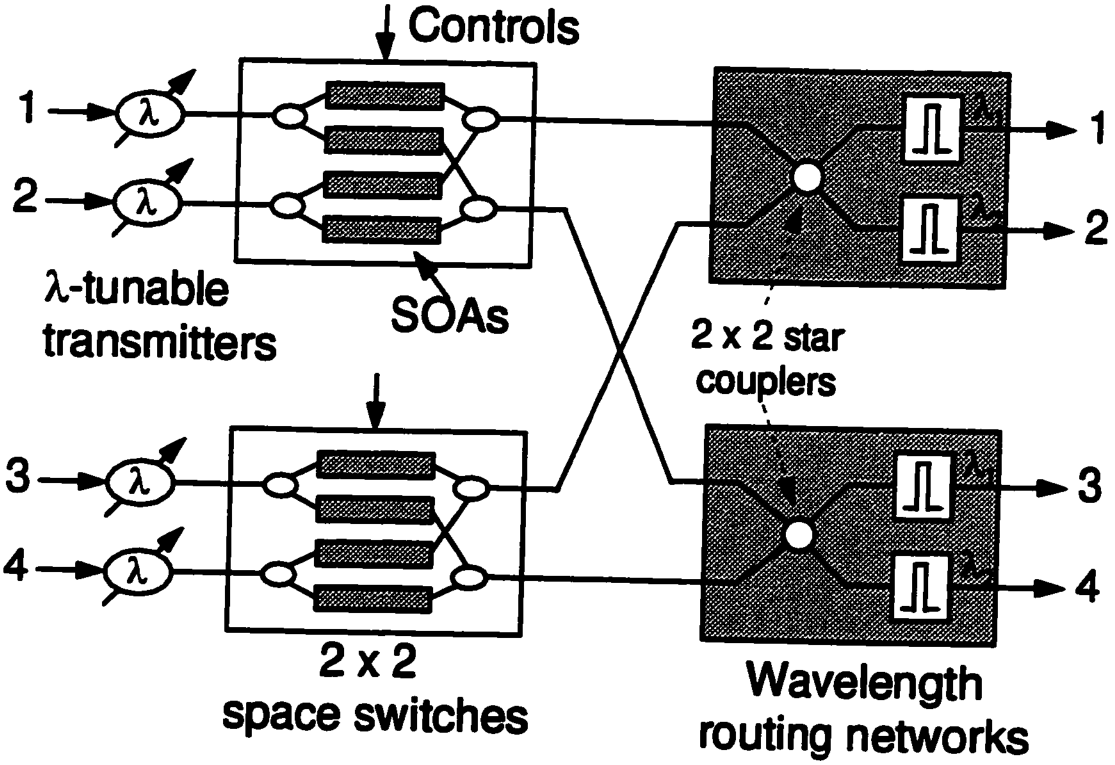

Figure 5.1: Schematic of a 4 × 4 optical cross-connect using WDM and SDM.

Two experimental setups are used to demonstrate different switching operations. First of all, we investigate a 2×2 SOA-based optical switch, which is a basic part of the 4×4 optical cross-connect. Figure 5.2 illustrates the setup for the 2×2 switch. A DFB laser operating at 1302.7 nm is directly modulated with a PRBS with a word length of 2^7-1 at a bit rate of 1 Gb/s. A semiconductor laser pumped Nd:YAG laser operating at 1318.6 nm with an external modulator is used to generate an optical sine-wave signal at 1 GHz. Optical isolators are used before and after SOAs in order to avoid optical reflections. Two optical receivers are a *p-i-n* receiver (PD1) with a frequency response up to 2 GHz and a high-sensitivity Ge-APD receiver (PD2) with a response up to 1.2 GHz. Control signals are from a pulse generator with a rise time of 1 ns. They are amplified with pulse RF amplifiers before being injected into the SOAs. A digital oscilloscope is employed to display switched signals.

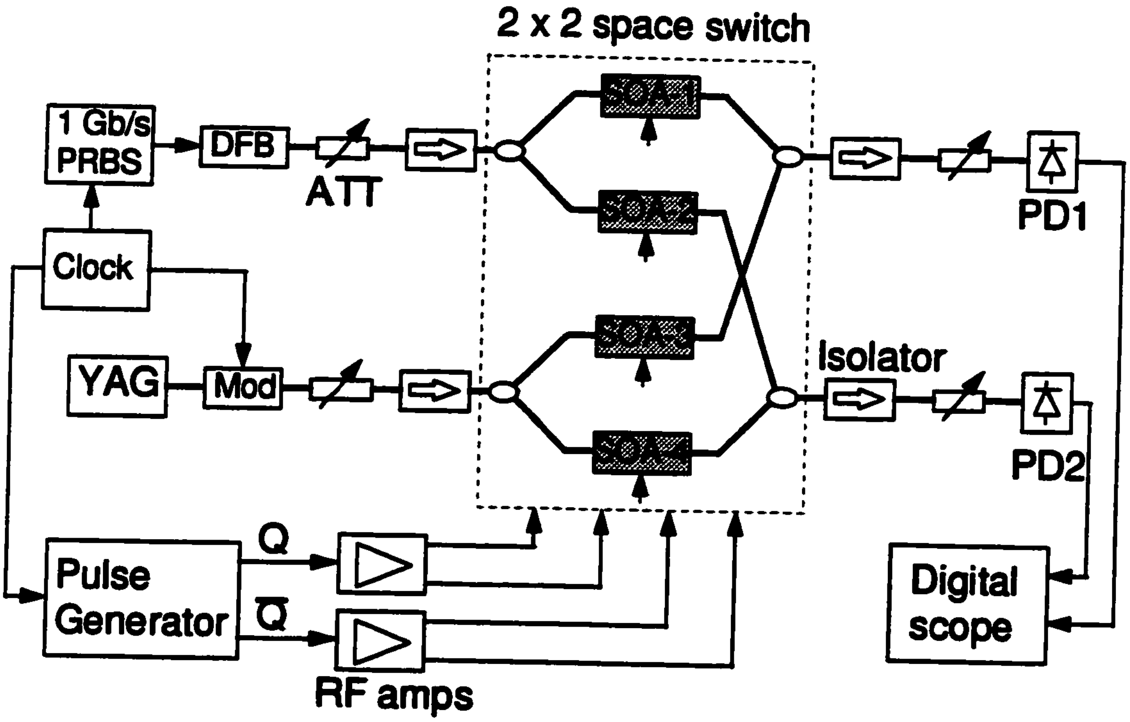

Figure 5.2: Experimental setup for an SOA-based 2×2 space switch.

The second experimental setup is for a 4×4 optical cross-connect. In this setup, there are one wavelength tunable transmitter, two SOAs for an optical space switch, and a 2×2 coupler and two optical filters for a wavelength routing network. The tunable transmitter is made of two DFB lasers operating at 1302.7 nm and 1307.5 nm, which are directly modulated with the same signal current, and two SOA gates followed by a 2×1 coupler for wavelength selection. Although we use much less components in the setup than a real 4×4 cross-connect system, we can demonstrate all the switching functions of the 4×4 cross-connect. As to the SOA-4 in the setup, there are two different connections, one for cross-connection denoted by (a), and the other for simulating a homo-wavelength crosstalk channel denoted by (b).

5.3 Switching Demonstration and Experimental Results

First, we use the setup in Figure 5.2 to demonstrate a 1×2 space switch, where the Nd:YAG laser is turned off. The switched output signals are shown in Figure 5.4. In Figure 5.4(a) the input PRBS signal is switched to the first output of the 2×2 space switch. When

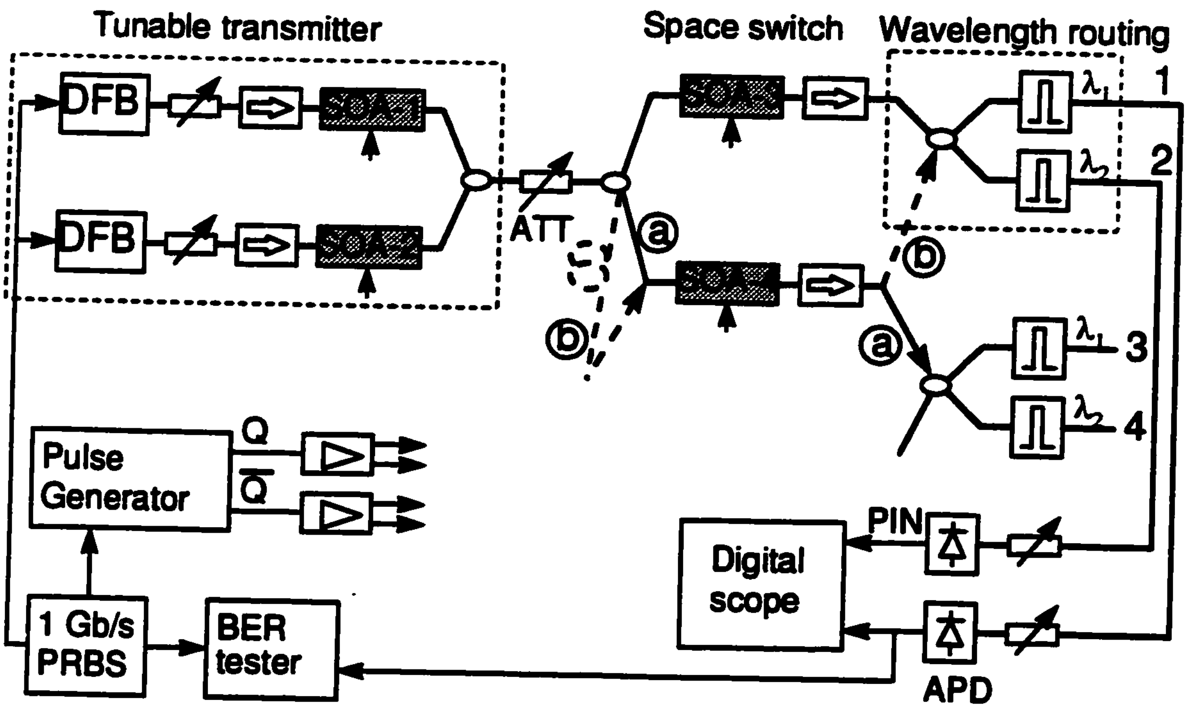

Figure 5.3: Experimental setup for a 4×4 optical cross-connect using SDM and WDM.

two complementary control signals are applied to the first and second SOAs simultaneously, we have two output signals shown in Figure 5.4(b). Traces 3 and 4 in Figure 5.4(b) clearly show no bit loss of the switched signal during the switching transient. One-bit guard time should be sufficient for switching transient in this SOA-based switch. For a 2×2 switch, we turn on the second transmitter. Figure 5.5 shows the two input signals and the switched signal from the first output. The switching transient shows the fast switching speed of the SOAs.

Combining space division switching with wavelength division multiplexing, we can expand 2×2 space switches to a 4×4 switch using the proposed architecture. With the second experimental setup shown in Figure 5.3 , we directly modulate the two DFB lasers with the same PRBS signal, then switch the first and second SOAs in a complementary fashion to select a required wavelength. The optical signal from the transmitter is then splitted into two switching paths where the third and fourth SOAs control connections to the wavelength routing stage. Finally, the signal is routed to its intended output by a wavelength routing network.

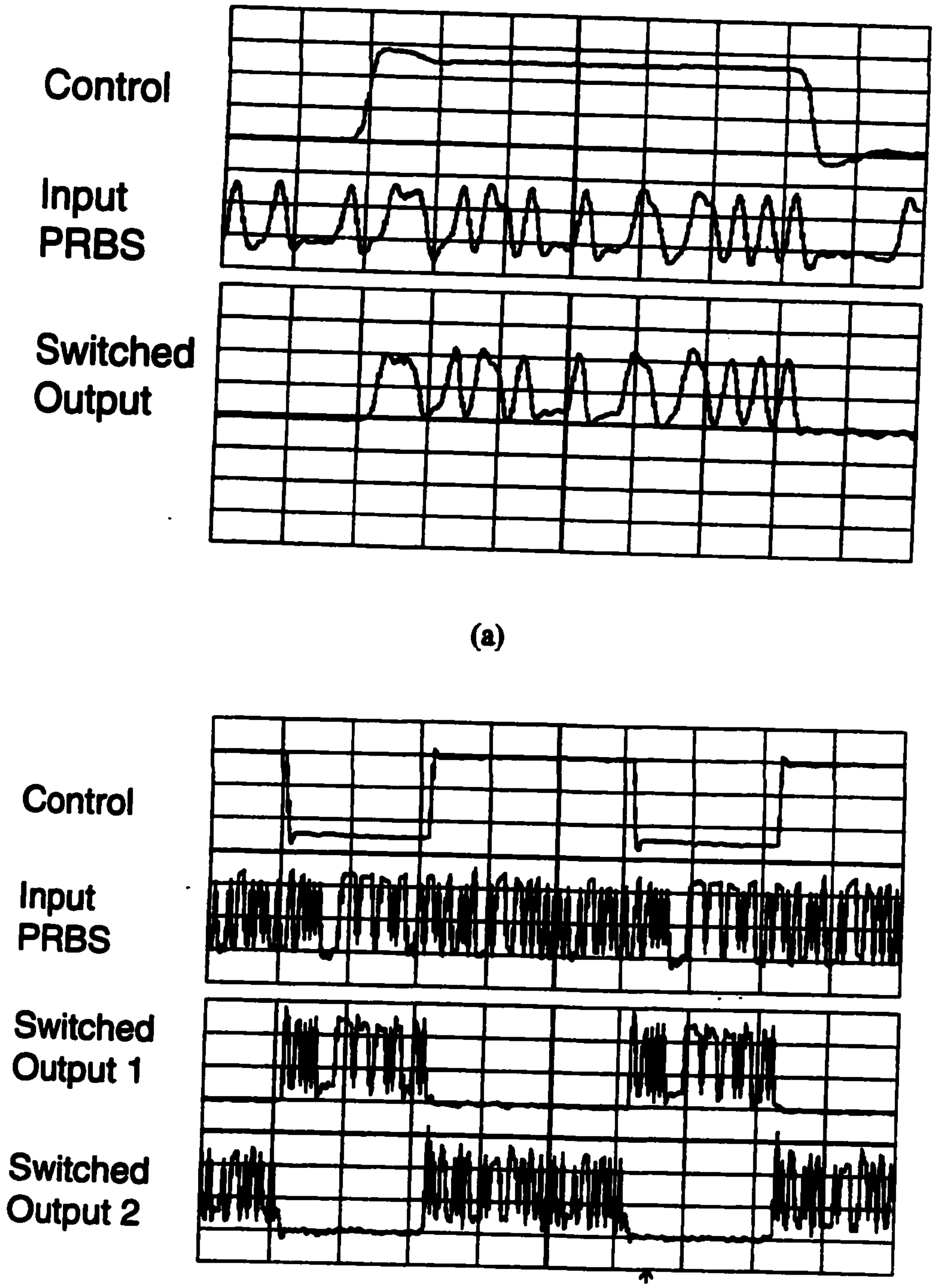

(a)

(b)

Figure 5.4: Demonstration of a 1×2 space switch. (a) Input and output of an SOA switching gate (SOA-1 in Figure 5.2). (b) Two outputs of the 1×2 switch with a PRBS input.

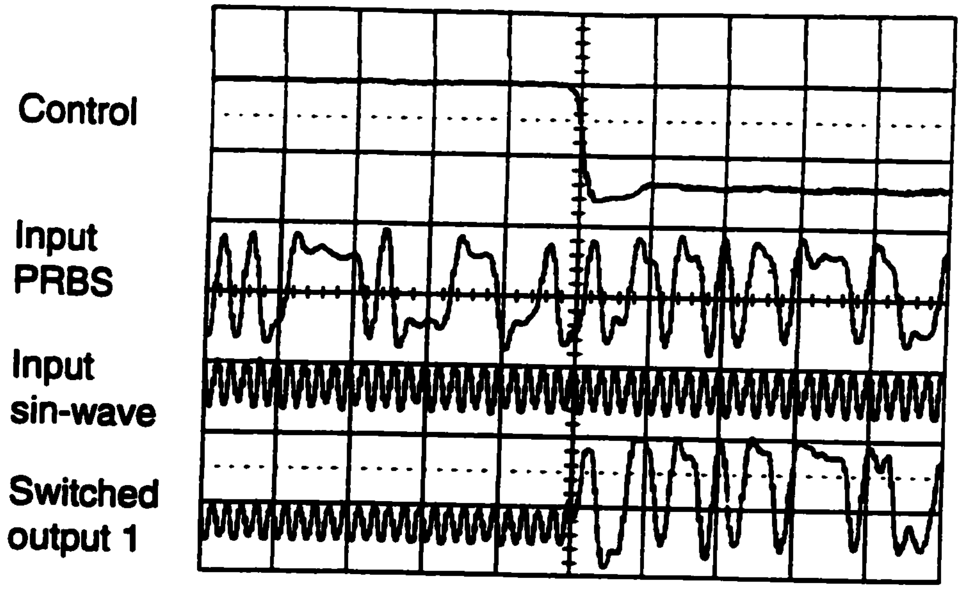

Figure 5.5: Demonstration of a 2×2 space switch. Two inputs are a PRBS and sine-wave signals.

Figure 5.6 illustrates the scope traces for switching functions of the 4×4 cross-connect. Two sets of control signals are used. One is for wavelength switching, another is for space switching. In Figure 5.6, trace 1 shows an input signal at λ_1 from the transmitter, trace 3 denotes an input signal at λ_2. The two signals are alternatively sent to the two SOA switching gates. The control signals for space switching are deliberately delayed from the wavelength control signals as shown at the top of Figure 5.6. Trace 2 is the output signal at λ_1 from the first output after wavelength and space switching, the signal at λ_2 from the second output is illustrated by trace 4.

With connection (a) for the fourth SOA, Figure 5.7 shows the signals at λ_1 coming out from the first and third outputs. These two output signals are switched by the space switch. Similar trace display is observed from the second and fourth outputs of the cross-connect.

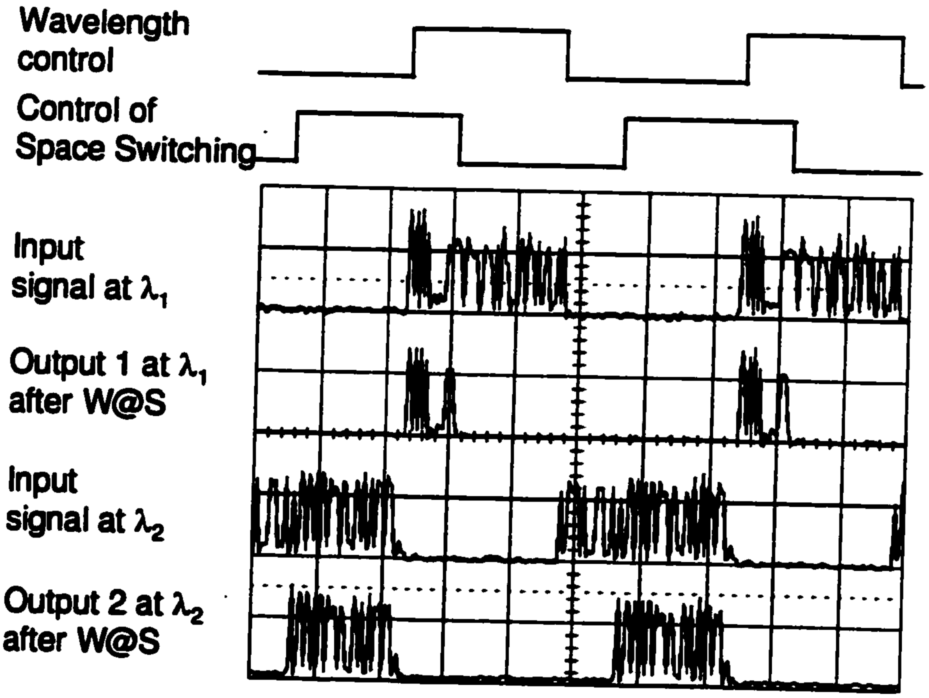

Figure 5.6: Demonstration of wavelength tuning and space switching of a 4×4 optical cross-connect. W@S denotes wavelength tuning and space switching.

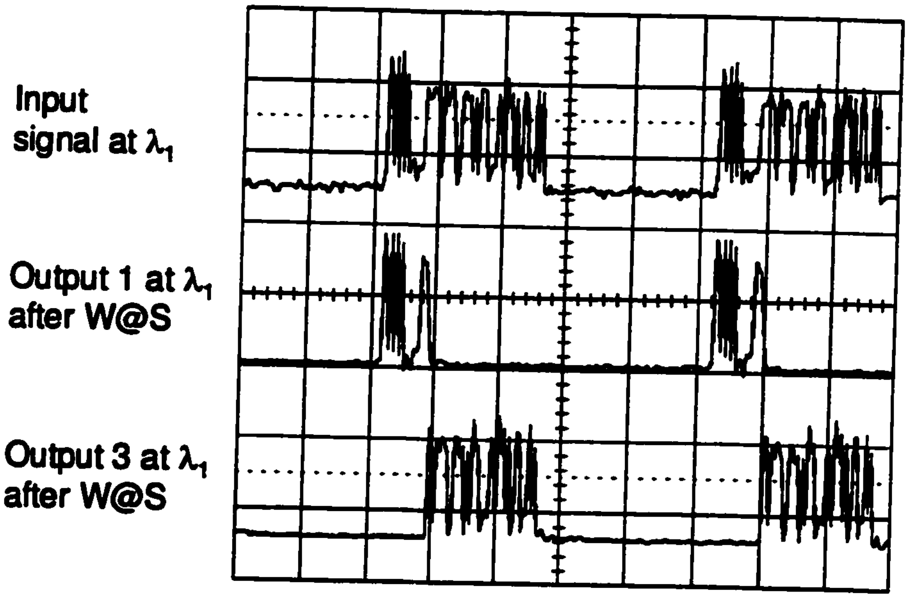

Figure 5.7: Outputs from two wavelength routing networks. The input signal at λ_1 is switched to two outputs, alternatively.

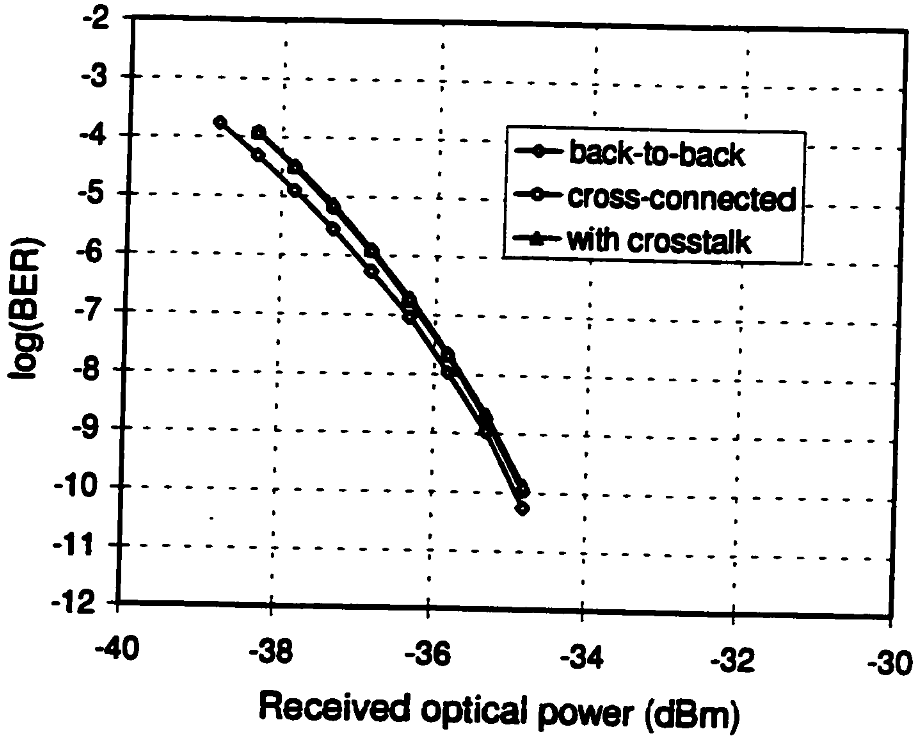

Figure 5.8: BER versus received optical power for a static cross-connection of the 4×4 optical cross-connect.

After successfully demonstrating the switching functions of the proposed optical cross-connect, we further measure system performance in terms of bit error rate for a static cross-connection. We mainly investigate the impact of the homo-wavelength crosstalk from the space switches in this small 4×4 optical cross-connect. First, we set injection currents to four SOAs as follows:

$I_1 = I_3 =$ 85 mA for the ON state,

$I_2 = I_4 =$ 15 mA for the OFF state.

The ON/OFF ratio of the SOAs is about 30 dB. In this experiment, the fourth SOA is assumed to be connected to the second transmitter which is turned to the same wavelength as the first transmitter. When setting connection (b) for the fourth SOA, we use 1.2 km fiber before the SOA to de-correlate the optical phase for two signal paths. The output of the fourth SOA is connected to another input of the first 2×2 coupler. Thus, we have two virtual paths in a 2×2 space switch. Since the fourth SOA is set in the OFF state, the signal leakage from this path becomes homo-wavelength crosstalk to the signal from the third SOA.

The measured BER as a function of received optical power is shown in Figure 5.8. The back-to-back receiver sensitivity is about -35.3 dBm with no space switches. For the cross-connection without crosstalk (the second path is disconnected), the power penalty is 0.12 dB at a bit error rate of 10^{-9}. This penalty is primarily due to ASE noise of SOAs. With the homo-wavelength crosstalk from the second path, there is almost no more power penalty compared with the cross-connection without crosstalk. Homo-wavelength crosstalk impact on system performance will be further investigated experimentally in Chapter 7.

5.4 Conclusions

In this chapter, we experimentally demonstrate a 4×4 optical cross-connect based on the proposed architecture. The wavelength and space switching functions have been proved. The experiment shows that 1-ns guard time (corresponding to 1 bit of a 1-Gb/s signal) is enough for protecting signals at switching transient. The successful demonstration of the proposed optical cross-connect shows the promise of constructing an 8×8 or 16×16 prototype.

6. Performance Degradation due to Crosstalk in Multi-wavelength Optical Networks Using Dynamic Routing

6.1 Introduction

Multi-wavelength optical networks using wavelength routing have been recognized to be very attractive over other optical networks by virtue of their information transparency, wavelength reuse and a good degree of scalability [9, 10]. For non-uniform traffic, dynamic reconfiguration of the wavelength routing interconnections is required in response to changing traffic patterns [10]. Dynamic wavelength routing can be realized by introducing optical space switches at the wavelength routing nodes, as discussed in section 2.2.2.

For the evaluation of end-to-end transmission performance, two crosstalk mechanisms have been identified in the dynamic wavelength routing nodes [28]. One is due to the non-ideal response of the optical multiplexers and demultiplexers, the other is due to the non-ideal signal switching of the space switches. Thus, we have two kinds of crosstalk, homo-wavelength and hetero-wavelength crosstalk as discussed in Chapter 4. The homo-wavelength crosstalk is accumulated as the signal is transmitted through the routing nodes. When optical amplifiers such as EDFAs are used in the network, the accumulated ASE noise will intensify the impact of the crosstalk on the performance. Also, the homo-wavelength crosstalk may introduce signal-crosstalk beat-noise, so the system performance may be severely degraded.

In [28] only a simplified network without EDFAs was considered under the power addition assumption. From the discussion in Chapter 4, it can be known that the homo-wavelength impact on the system performance is far underestimated in [28]. In this chapter, we use the approach employed in Chapter 4 to analyze an end-to-end transmission performance in a multi-wavelength optical network using dynamic wavelength routing with EDFAs for loss compensation. A lower bound and an upper bound on the performance degradation due to the homo-wavelength crosstalk will be evaluated. In the next section, we describe the system model for performance evaluation. Then, we present a numerical example for a network with moderate-size dynamic routing nodes.

6.2 System Model

The structure of the dynamic wavelength routing node is shown in Figure 2.3. The routing node consists of N wavelength demultiplexers at the input side and N multiplexers at the output side, and M $(N+1)\times(N+1)$ optical space switches. M incoming signals in an optical fiber are first demultiplexed and then sent to M space switches through which they are connected to different multiplexers where the signals at different wavelengths are multiplexed and coupled into a single output fiber. Each space switch only switches incoming signals at the same optical wavelength. Here, the space switches are considered as general optical switches instead of very specific ones. Except for introducing losses and crosstalk, the switches contribute no noise to the system.

An optical path with a fiber link (one transmission stage) through two routing nodes is shown in Figure 6.1. An optical signal is added through the i-th space switch, then multiplexed with other signals at different wavelengths. The signals go through an EDFA, then a fiber link and another EDFA just before a wavelength demultiplexer in the $(i+1)$-th node. The signal added at the i-th node can be switched to drop to the $(i+1)$-th node. In the following we assume that the signal goes through K transmission stages with $(K+1)$ space switches. For the end-to-end performance evaluation, the optical components, except for the amplifiers, are represented by their losses. The EDFAs amplify the signals and at the same time contribute ASE noise. The same lumped amplifier model for calculating the EDFA gain and accumulated ASE and the current noise model at the receivers discussed in Section 4.2 are employed.

As for the crosstalk at the routing nodes, first we consider there is no signal-crosstalk beat noise falling within the receiver electrical bandwidth. Therefore, the crosstalk power can simply be added to the signal power. We assume the multiplexers and the

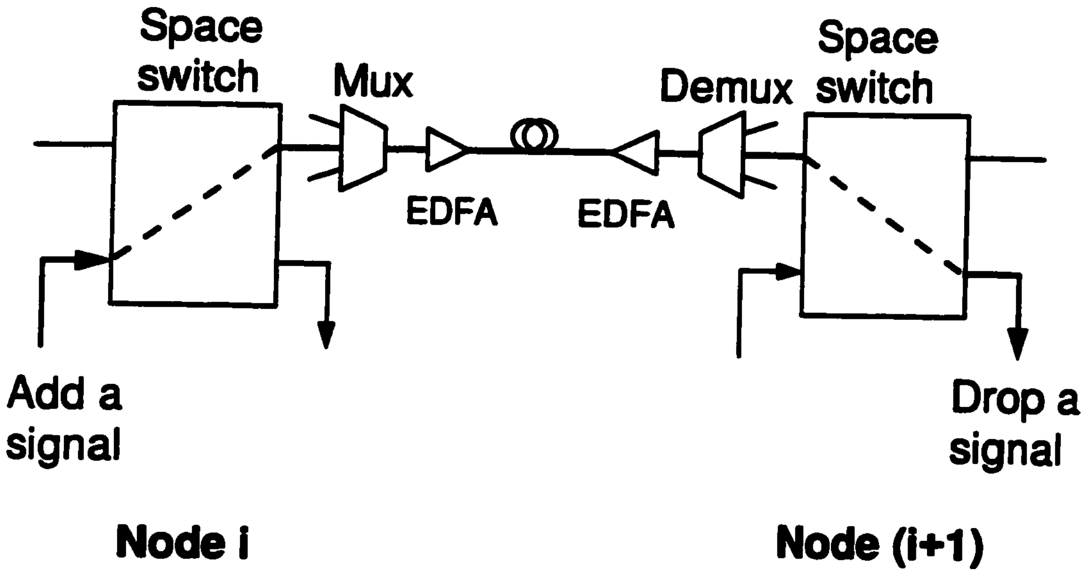

Figure 6.1: Schematic of an optical path of one transmission stage from node i to node i+1.

demultiplexers have identical characteristics with each channel causing the same amount of crosstalk into other channels. Also, each output of a space switch includes the same amount of crosstalk from every other output. For a signal datum, the total homo-wavelength crosstalk power is given by

$$P_x = \sum_{l=1}^{K}\sum_{i=1}^{M-1} C_{mux}^2 d_{il} P_1 + \sum_{l=1}^{K+1}\sum_{j=1}^{N} C_{space} d_{jl} P_1 \qquad (6\text{-}1)$$

where K is the number of the signal transmission stages, C_{mux} and C_{space} are the crosstalk ratios of the multiplexers/demultiplexers and the space switches, respectively, P_1 is the optical power of the signal data ONEs, d is a signal data indicator defined as $d = \{^{1,\text{ for data ONEs}}_{r,\text{ for data ZEROs}}$, where r is the reciprocal of the signal extinction ratio. Here, we have neglected the higher order terms of the crosstalk [28]. In the worst case, the total homo-wavelength crosstalk power is

$$P_x = K(M-1)C_{mux}^2 P_1 + (K+1)NC_{space} P_1. \qquad (6\text{-}2)$$

If it is assumed that the OOK signals have equal probability in data ONEs and ZEROs and are statistically independent, the total crosstalk power is a binomial variable. It takes on, for example, the crosstalk from a space switch, $[(K+1)N+1]$ possible power levels with a probability given by

$$P_b\left(P_{x,i}=C_{space}\left\{iP_1+[(K+1)N-i]rP_1\right\}\right)=\frac{[(K+1)N]!}{i!\,[(K+1)N-i]!}\cdot\frac{1}{2^{(K+1)N}}$$

$$\text{for } i=0,\,1,\,\ldots,\,(K+1)N. \tag{6-3}$$

The bit error rate can be evaluated for each possible crosstalk power level, defined as $P_{x,i}=C_{space}\left\{iP_1+[(K+1)N-i]rP_1\right\}$, at the receiver. Thus, the average bit error rate can be obtained from

$$P_e=\sum_{i=0}^{(K+1)N}\frac{1}{2\sqrt{2\pi}}\left\{\int_{Q_{0,i}}^{\infty}\exp\left(-t^2/2\right)dt+\int_{Q_{1,i}}^{\infty}\exp\left(-t^2/2\right)dt\right\}P_b(i) \tag{6-4}$$

$$Q_{0,i}=\frac{T_{opt}-\left(S_0+S_{x,i}\right)}{\sqrt{N_{0,i}}},\quad Q_{1,i}=\frac{\left(S_1+S_{x,i}\right)-T_{opt}}{\sqrt{N_{1,i}}} \tag{6-5}$$

where $S_{1/0}=\frac{\eta e}{h\nu}P_1d_{1/0}$ and $S_{x,i}=\frac{\eta e}{h\nu}P_{x,i}$ are the electrical currents corresponding to the signal and the crosstalk at the receiver, respectively, T_{opt} is the optimum decision threshold which is chosen to minimize the average bit error rate, and $N_{1/0,i}$ is the current noise power corresponding to data ONEs and ZEROs with the crosstalk power . The total noise power is given by

$$\begin{aligned}N_{1/0,i}&=N_{thermal}+N_{spont-spont}\\&+N_{shot,\,signal,\,1/0}+N_{signal-spont,\,1/0}\\&+N_{shot,\,crosstalk,\,i}+N_{crosstalk-spont,\,i}\,.\end{aligned} \tag{6-6}$$

The six noise terms are given as follows:

$$N_{thermal}=I_{th}^2B_e \tag{6-7}$$

$$N_{spont-spont}=\left(\frac{\eta e}{h\nu}\right)^2N_{ase}^2/p\left(2B_oB_e-B_e^2\right) \tag{6-8}$$

$$N_{shot,1/0} = 2\frac{\eta e^2}{h\nu} P_{1/0} B_e \tag{6-9}$$

$$N_{signal-spont,1/0} = 2\left(\frac{\eta e}{h\nu}\right)^2 \left(2P_{1/0} N_{ase} B_e / p\right) \tag{6-10}$$

$$N_{shot,crosstalk,i} = 2\frac{\eta e^2}{h\nu} P_{x,i} B_e \tag{6-11}$$

$$N_{crosstalk-spont,i} = 2\left(\frac{\eta e}{h\nu}\right)^2 \left(2P_{x,i} N_{ase} B_e / p\right) \tag{6-12}$$

where η is the quantum efficiency, e is the electron charge, h is Planck's constant, ν is the signal optical frequency, B_o is the bandwidth of the optical filter, B_e is the electrical bandwidth of the receiver, and N_{ase} is the optical power of the ASE noise.

The crosstalk-spontaneous beat noise, the last noise term in equation (6-6) may become comparable to the other noise terms at the receivers where the signal (and crosstalk)-spontaneous beat noise dominates. Thus, the crosstalk impact on the performance is intensified by the ASE noise.

The degradation evaluated by using the above model is a lower bound, when the signal-crosstalk beat noise falls within the receiver bandwidth. To obtain an upper bound, we consider the extreme case in which the crosstalk and the signal have exactly the same wavelength and a negligible frequency chirp due to modulation. We consider the crosstalk from the space switches and assume all the crosstalk channels are randomly polarized. When i crosstalk channels have data ONEs, with Gaussian approximation introduced in Section 4.3, we have the average crosstalk power and the signal power variance given by

$$\overline{P}_{x,i} = C_{space}\left\{iP_1 + \left[(K+1)N - i\right]rP_1\right\} \tag{6-13}$$

$$\sigma^2_{x,1/0,i} = iC_{space} d_{1/0} + i^2 C^2_{space} P_1^2 / 2 \tag{6-14}$$

They have the same probability distribution as given by equation (6-3). Again, we use equation (6-4) to evaluate the average bit error rate, provided the noise term of the power fluctuation due to signal-crosstalk beating is included in equation (6-6).

Table 6.1: Values of the parameters used in the numerical calculations

Bit rate		2.5 Gb/s
Wavelength	λ_s	1550 nm
Receiver electrical bandwidth	B_e	1.75 GHz (0.7 bit rate)
Equivalent thermal noise	I_{th}	5 pA/√(Hz)
Bandwidth of optical channels	B_o	0.2 nm
Channel spacing		1.2 nm
Loss of a fiber link	L_{link}	25 dB
Loss of space switch	L_{space}	10 dB
Crosstalk ratio of mux/demux	C_{mux}	-20 dB
Loss of mux/demux	L_{mux}	2.5 dB
Unsaturated gain of EDFAs	G_0	25 dB
Saturation power of EDFAs	P_{sat}	13 dBm
Spontaneous emission factor	n_{sp}	1.5
Input coupling loss of EDFAs	L_{in}	2 dB
Output coupling loss of EDFAs	L_{out}	3 dB

6.3 Numerical Results

The values of the parameters used in the following calculations are listed in Table 6.1. We mainly consider the degradation due to crosstalk from the space switches. Other crosstalk components are taken into account in the worst case. In this numerical example, a general power penalty is defined as the ratio of the receiver sensitivity of an end-to-end transmission to the receiver sensitivity of a single-stage transmission with no crosstalk from the space switches. A relative power penalty is defined as the degradation of the receiver sensitivity compared to the receiver sensitivity with no crosstalk from the space switches. The average bit error rate is set to 10^{-9} for the power penalty evaluation.

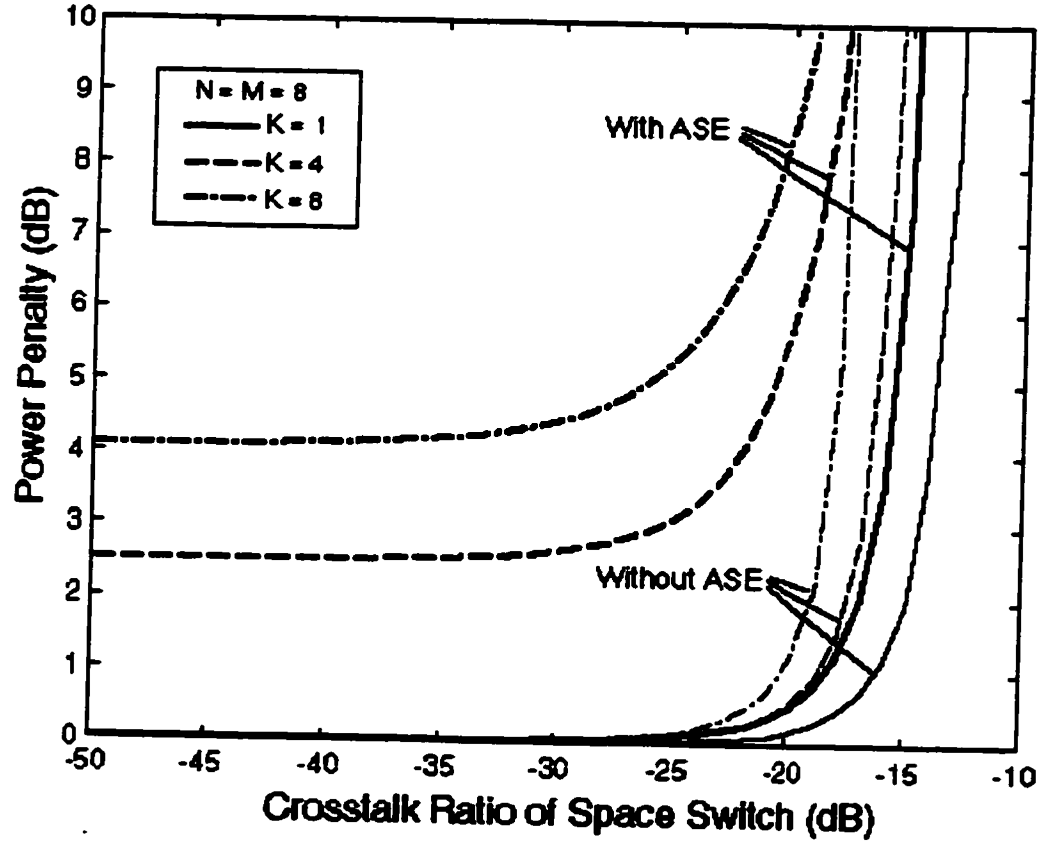

Figure 6.2: Power penalty as a function of crosstalk ratio of the switches for various transmission stages with and without the ASE noise.

We consider moderate size network nodes with $N = M = 8$. Figure 6.2 shows the general power penalty as a function of the crosstalk ratio of the space switches under the power addition assumption. Without considering the accumulated ASE noise, for a 1 dB power penalty, the crosstalk ratio is -16.2 dB for $K = 1$ (one transmission stage), and -20.5 dB for $K = 8$. Considering the accumulated ASE noise, for a 1 dB relative power penalty due to crosstalk from the space switches, the crosstalk ratio is -18.5 dB for $K = 1$, and -25.8 dB for $K = 8$. The vertical shift of the curves with the ASE noise shows the degradation resulting from accumulated ASE noise. One part is contributed by spontaneous-spontaneous beat-noise. The other is due to the accumulated homo-wavelength crosstalk from the optical multiplexers and demultiplexers, which beats with the ASE noise. Compared with the results without the ASE, the crosstalk ratio is 5 dB lower for a 1 dB power penalty with eight transmission stages. One can expect there is a

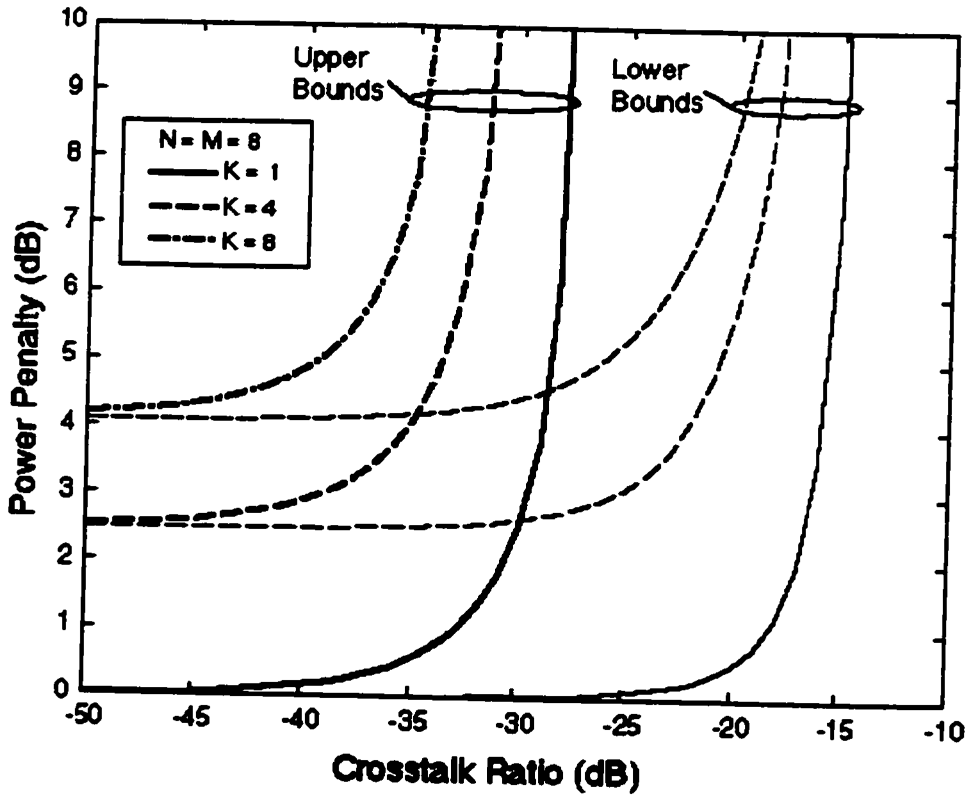

Figure 6.3: Lower and upper bounds on the power penalty for three different numbers of transmission stages.

larger difference for more transmission stages. The reason for this is that the ASE noise intensifies the effect of homo-wavelength crosstalk.

The power penalties evaluated above with consideration of the ASE noise can be thought of as a lower bound on the performance degradation. An upper bound on the degradation considering the signal-crosstalk beat noise is shown in Figure 6.3. As shown in the figure, the lower bound and the upper bound of the penalty approach the same values as the crosstalk becomes very small. For a 1 dB power penalty due to crosstalk from space switches, the crosstalk ratio is -32.8 dB for $K = 1$, and -38.5 dB for $K = 8$. This requirement is hard to meet with general space switches, such as $LiNbO_3$ based waveguide switching arrays. For a 1 dB penalty, the difference between the acceptable crosstalk ratios calculated from the upper bound and the lower bound is about 13 to 14 dB. To meet this requirement, an SOA-based optical space switch may be used.

6.4 Conclusions

We analyzed the end-to-end transmission performance of multi-wavelength optical networks incorporating optical amplifiers and using wavelength dynamic routing. It has been shown that the degradation due to homo-wavelength crosstalk is intensified by the accumulated ASE in this kind of network. More stringent requirement on the components of optical space switches is needed in order to obtain an acceptable end-to-end performance. The upper bound on the degradation evaluated by considering the signal-crosstalk beat noise gives an estimate for the worst-case situation which should be considered in designing the multi-wavelength routing networks.

7. Implications of Homo-Wavelength Crosstalk on System Performance

7.1 Introduction

Optical crosstalk in optical networking and switching is one of the most important factors degrading the system performance. As discussed in Chapters 4 and 6, optical crosstalk can come from a number of different sources and behave quite differently in terms of degradation effects and accumulation fashions. In this chapter, we will extend our discussions on optical crosstalk in Chapters 4 and 6 and consider optical crosstalk for more general situations including optical networking, switching, and transmission. Some parts of the contents may be repeated to emphasize a few points.

In Chapter 4, we have considered homo-wavelength crosstalk for the performance evaluation and used a simple Gaussian approximation to incorporate the crosstalk impact. Also, in Chapter 6, we further investigate the end-to-end transmission performance in a multi-wavelength optical network using a dynamic wavelength routing scheme. We show that the performance degradation due to homo-wavelength crosstalk can be intensified by ASE noise from optical amplifiers. In those two chapters, only a Gaussian approximation is used for an upper bound estimation of power penalty. This may be enough for engineering design and analysis. Further detailed theoretical and experimental studies are required to fully understand this kind of optical crosstalk from its origin to its impact on systems.

Most considerations on optical crosstalk is based on power addition assumption [28, 29, 120]. However, several recent experimental studies [122, 125] show that homo-wavelength crosstalk has more serious impact on the performance as the signal-crosstalk beating falls within the receiver bandwidth. Glodstein [125, 126, 127] carried out a series of experiments on performance implications of homo-wavelength crosstalk in multi-wavelength optical networks. In time-division switches, homo-wavelength crosstalk has also been reported in [122]. There are several papers which present the theoretical analysis for performance degradation due to homo-wavelength crosstalk [78, 123, 128, 129, 130]. Most of these are based on Gaussian approximation for the signal-crosstalk beat noise.

In this chapter, we investigate homo-wavelength crosstalk and its impact on the system performance both theoretically and experimentally. First, we survey several mechanisms of homo-wavelength crosstalk. To evaluate its impact on system performance, we use moment generating functions (MGF) to derive an accurate statistical description of the signal-crosstalk beat noise. Then, a saddlepoint approximation is employed to evaluate the performance degradation due to crosstalk. Further experiments are carried out to verify the theoretical analysis.

7.2 Theoretical Analysis

7.2.1 Mechanisms of Homo-Wavelength Crosstalk

Optical crosstalk considered here is optical power sneaking from non-signal channels into a signal channel. Optical crosstalk due to inter-modulation or cross-coupling such as gain saturation is excluded in the following analysis since this kind of crosstalk has to be evaluated with different approaches. According to the wavelength, optical crosstalk can be categorized into two main groups: hetero-wavelength and homo-wavelength.

Hetero-wavelength crosstalk has a different optical wavelength compared to the signal, which falls outside of the bandwidth of optical filters in a system or before a receiver. This kind of crosstalk can be easily reduced by sharpening the response of the optical filters and its impact on the performance can be evaluated with a power addition approach [28, 120]. Hetero-wavelength crosstalk is not-accumulative, but often it can become homo-wavelength crosstalk to another signal as it transverses along more optical components. At an optical detector, hetero-wavelength crosstalk is like a power fluctuation reducing the signal extinction ratio. No beating would be expected for this kind crosstalk. Crosstalk polarization has no effects on the performance degradation. Randomness of the crosstalk data bits can be evaluated with either a worst case approach or a statistical method by taking into account different combinations of crosstalk patterns, as discussed in Chapters 4 and 6.

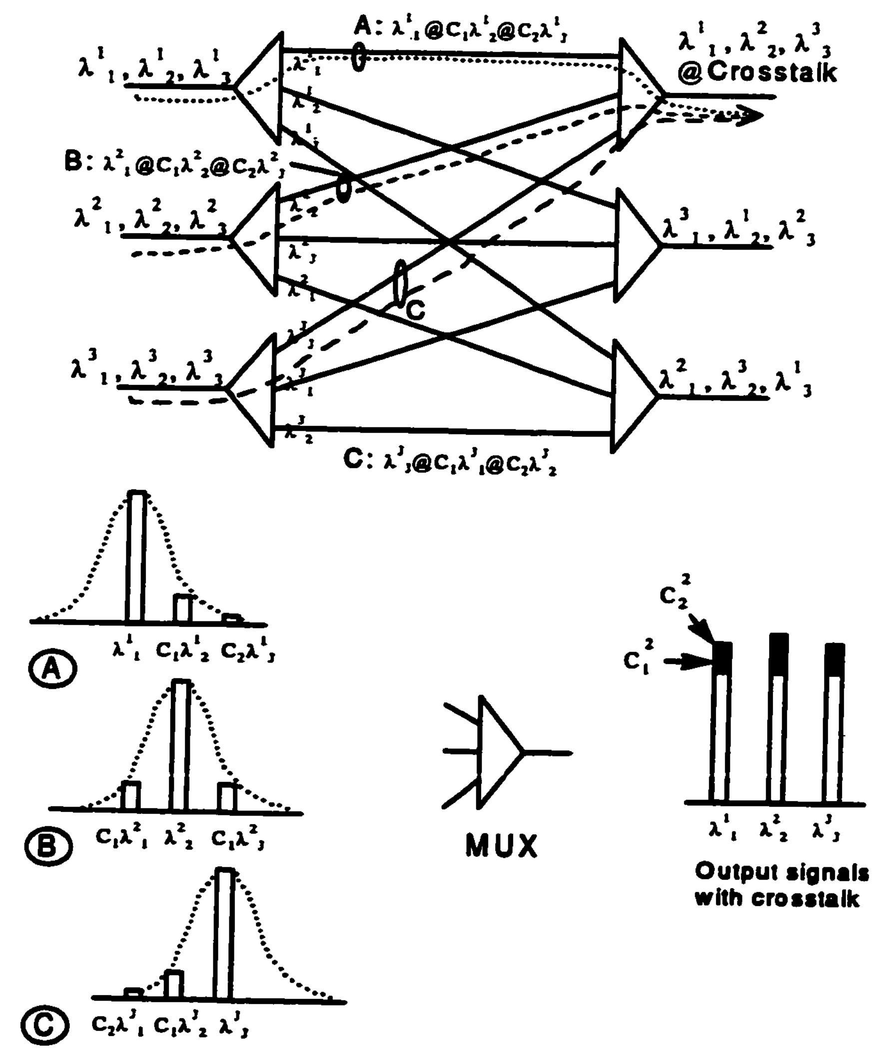

Figure 7.1: Schematic of a static wavelength routing node and its various crosstalk components. Superscripts denote inputs and subscripts denote wavelengths. C_1 and C_2 are the crosstalk ratios of mux and demux.

Homo-wavelength crosstalk has the same nominal wavelength as the signal. It passes through any optical filter with the same attenuation as the signal. After the homo-wavelength crosstalk is combined with the signal, there is no optical way to separate or reduce it. In contrast to hetero-wavelength crosstalk, homo-wavelength crosstalk is more detrimental to the system performance since beating between the signal and crosstalk during detection would fall within the receiver bandwidth in high-speed systems using narrow linewidth transmitter sources such as DFB lasers. The beating not only could

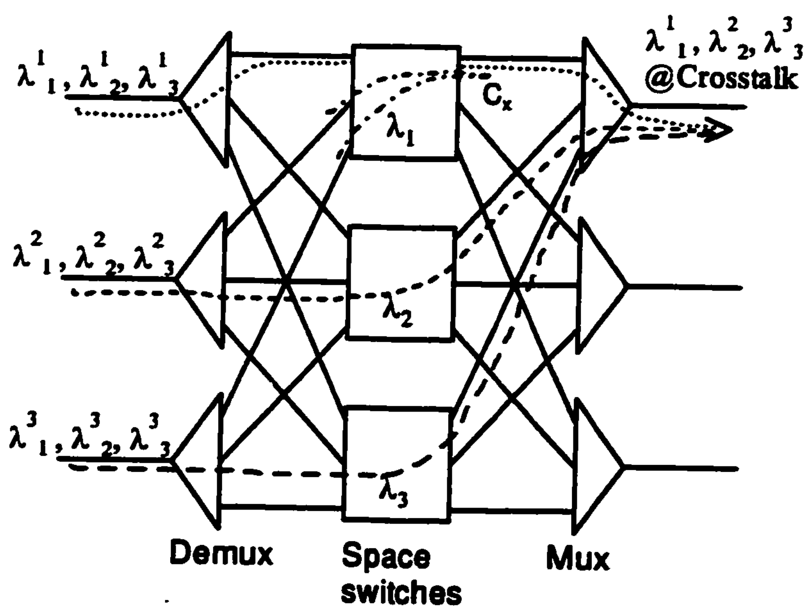

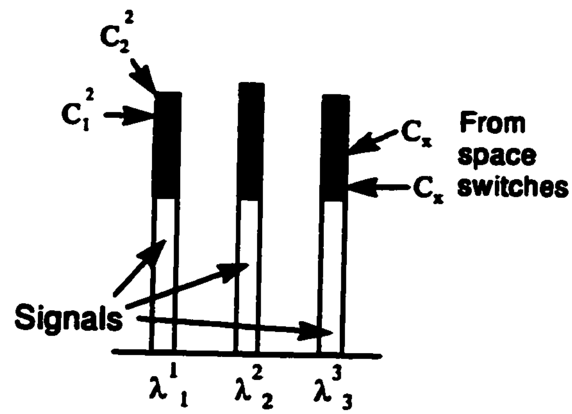

Figure 7.2: Schematic of a dynamic wavelength routing node and its crosstalk components within an output signal. C_x is the crosstalk ratio of space switches.

introduce a periodic fluctuation of the received signal, but also converts the phase noise of the optical sources to intensity noise. In the following, we concentrate our discussion only on the homo-wavelength crosstalk.

There are various well-known mechanisms introducing optical homo-wavelength crosstalk. Among them are optical wavelength reuse [28, 29, 125, 129, 130], four-wave mixing of WDM channels [128, 131], optical multiple reflections [123, 132], and acousto-optic interaction in acousto-optical tunable filters [103, 104]. Improper switching

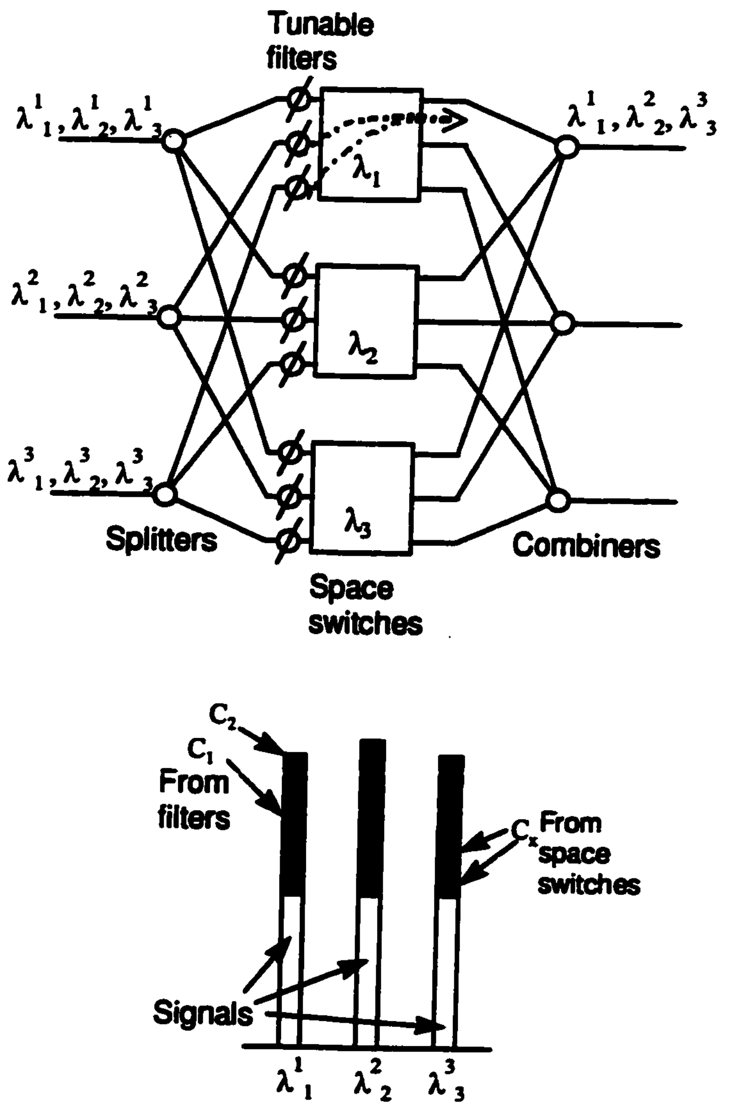

Figure 7.3: Schematic of a reconfigurable wavelength routing node and various crosstalk components with an output signal.

architecture designs may also introduce homo-wavelength crosstalk [66]. Our discussions will focused on optical wavelength reuse in optical networking and switching.

Spatial wavelength reuse is a very primary reason for introducing homo-wavelength crosstalk. As we pointed out in Chapter 2, optical wavelengths similar to radio spectrum are very limited resources over the useable transmission band of the optical fiber, particularly when they are used for signal path routing. It is inevitable to reuse available wavelengths spatially or in the time domain in order to meet the requirements for networking. Homo-wavelength crosstalk is introduced at optical routing nodes and/or add/drop multiplexers as the wavelengths are reused.

Three widely-discussed wavelength routing schemes are shown in Figures 7.1, 7.2 and 7.3. The first node structure has been discussed in Chapter 2 as a static wavelength routing node. The second is the dynamic wavelength routing node discussed in Chapter 2 and 6. The last one is employed by the RACE project [19, 29] as a reconfigurable multi-wavelength routing node. Two most important kinds of wavelength routing components used in these routing nodes are optical filters and wavelength multiplexers/demultiplexers. Optical space switches are utilized for dynamic wavelength configuration. The non-ideal response of these components will introduce hetero- and homo-wavelength crosstalk at wavelength routing nodes.

First of all, let's see the crosstalk in a static wavelength routing node. Coming signals over a fiber are first separated by optical demultiplexers, as shown in Figure 7.1. Due to the non-ideal filtering response of the demultiplexers, there are residual (crosstalk) channels along with each signal channel. Let's take a signal at λ_1 in the first input as an example. After the first demultiplexer, $C_1 \cdot \lambda_2 @ C_2 \cdot \lambda_3$ on the path A becomes crosstalk to the signal at λ_1, where C_1 and C_2 are the crosstalk ratios for the adjacent and next adjacent channels in demultiplexers. Following certain internal connections, the separated signals on the path A, B and C are multiplexed together into a single output fiber. The multiplexing is just a reverse process of demultiplexing, and the same crosstalk ratios can be assumed. The two crosstalk terms along with the signal at λ_1 are reduced to $C_1^2 \cdot \lambda_2$ and $C_2^2 \cdot \lambda_3$ and become homo-wavelength to other two signals at λ_2 and λ_3, respectively. Accordingly, the signal at λ_1 also has two homo-wavelength crosstalk components from the path B and C, as shown in Figure 7.1. The homo-wavelength crosstalk will go with the signals to the next routing node. At the following nodes, more homo-wavelength crosstalk will be added to the signals, and hetero-wavelength crosstalk will be further reduced by demultiplexers to be negligible.

The second and third cross-connects are all designed for dynamic wavelength routing. In addition to the crosstalk components discussed just before, there is new homo-

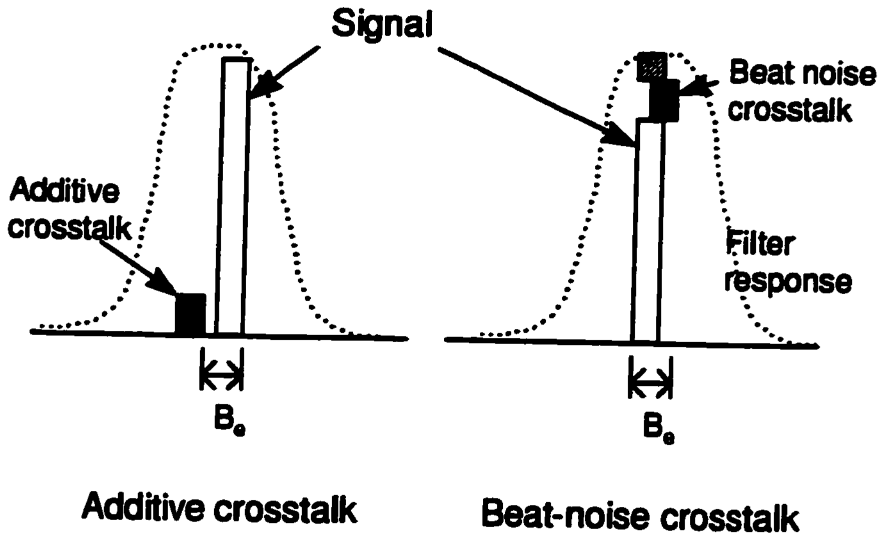

Figure 7.4: Classification of homo-wavelength crosstalk.

wavelength crosstalk resulting from the non-ideal switching of the space switches. Traditionally, optical crosstalk in space switches is considered with the power addition assumption with no beating term [37]. However, with a narrow-linewidth optical source such as a DFB laser, as signal wavelengths are precisely aligned, beating between a signal and its crosstalk components will severely affect the system performance. The performance degradation resulting from homo-wavelength crosstalk of the space switches has been evaluated in Chapter 6 by using a Gaussian approximation.

The third routing node utilizes an optical splitter followed by optical filters as a demultiplexer. There are two sources for homo-wavelength crosstalk. One is due to the non-ideal response of optical filters. As shown in Figure 7.3, at the output side of the node an optical combiner combines the signals with hetero- and homo-wavelength crosstalk from different space switches. After this combination, two hetero-wavelength crosstalk components to a signal become homo-wavelength crosstalk to the other two signal channels. This is similar to the situation illustrated in Figure 4.3. It is important to note the difference between the second and the third routing nodes in terms of their homo-wavelength crosstalk ratios.

Homo-wavelength crosstalk can be further classified into *additive* crosstalk and *beat-noise* crosstalk according to whether the signal-crosstalk beating could fall within the receiver electrical bandwidth. Although the additive crosstalk has the same nominal wavelength as the signal, there is no signal-crosstalk beating because its beating with the signal lies outside the receiver electrical bandwidth. The power addition approach can be used to evaluate this kind of crosstalk. However, the additive crosstalk differs from hetero-wavelength crosstalk in that it can be accumulated along routing nodes. Beat-noise crosstalk is assumed to have the same central wavelength as the signal but statistically independent optical phases. The signal-crosstalk beating converts the phase noise of the optical sources to intensity noise which is called signal-crosstalk beat noise. In the following subsection, we will present a detailed analysis of the beat noise crosstalk.

7.2.2 Theoretical Formulation

There are three main approaches for evaluating the system performance by incorporating beat-noise crosstalk. These are Gaussian approximation [123, 130], calculation with an actual probability density function of the signal-crosstalk beat noise [104, 123], and numerical simulation [133, 134]. Complexity of the last two approaches limits them to be useful only for a small number of crosstalk components. A widely cited Gaussian approximation was given by Gimlett and Cheung in [123] in which multiple signal reflections from optical slices are investigated. With assumptions of low reflections and negligible logic ZEROs' power, a Gaussian approximation is applied to arrive at that power penalty due to crosstalk given by

$$Penalty = -5\log\left[1 - 4Q^2 N \cdot 10^{C_x/10}\right] \qquad (7\text{-}1)$$

where N is the number of crosstalk channels, C_x is the crosstalk ratio in dB and $Q = 5.9$ for a BER of 10^{-9}.

In this subsection we introduce the moment generating function (MGF) of the signal-crosstalk beat noise in order to derive a more accurate statistical expression. On-off keying (OOK) with a nonreturn-to-zero (NRZ) signal format is assumed for the signal and crosstalk channels. For the sake of simplicity, we only consider crosstalk components just before the optical receiver regardless of their generating mechanisms. The optical power for data ONEs and ZEROs at the detector are P_{on} and P_{off}, respectively, which are related to the average received signal power P_{ave} as

$$P_{on} = \frac{2}{1+r} P_{ave} \tag{7-2}$$

$$P_{off} = \frac{2r}{1+r} P_{ave} \tag{7-3}$$

where r is the reciprocal of the signal extinction ratio.

The electrical field of the received signal with the crosstalk can be expressed as

$$E(t) = \sqrt{2P_{on} d_s(t)}\bar{p}_s(t)\cos(\omega_s t + \phi_s(t)) + \sum_{i=1}^{N} \sqrt{2C_i P_{on} d_i(t)}\bar{p}_i(t)\cos(\omega_i t + \phi_i(t)) \tag{7-4}$$

where N is the number of crosstalk channels, C_i is the crosstalk ratio of the i-th crosstalk component, ϕ_s and ϕ_i are the phases of the signal carrier and crosstalk carriers, respectively, $\bar{p}_s(t)$ and $\bar{p}_i(t)$ are the unit vectors indicating the polarization states of the signal and crosstalk channels, respectively. $d_s(t)$ and $d_i(t)$ are the data indicators for the signal and crosstalk channels, defined by

$$d_{s/i}(t) = \begin{cases} 1, & \text{for ONEs} \\ r, & \text{for ZEROs} \end{cases} \tag{7-5}$$

Here, we assume that all crosstalk channels have the same extinction ratio as the signal.

The total detectable optical power at the receiver is computed by

$$\begin{aligned} P_{det}(t) &= Lp\left[\left(E_s(t) + \sum_{i=1}^{N} E_i(t)\right)^2\right] \\ &= P_{on} d_s(t) + \sum_{i=1}^{N} C_i P_{on} d_i(t) \\ &\quad + 2\sum_{i=1}^{N} P_{on}\sqrt{C_i d_s(t) d_i(t)}\bar{p}_s(t)\bar{p}_i(t)\cos(\Delta\omega_{s,i} t + \Delta\phi_{s,i}(t)) \\ &\quad + 2\sum_{i=1}^{N}\sum_{j=i+1}^{N} P_{on}\sqrt{C_i C_j d_i(t) d_j(t)}\bar{p}_i(t)\bar{p}_j(t)\cos(\Delta\omega_{i,j} t + \Delta\phi_{i,j}(t)) \end{aligned} \tag{7-6}$$

where $Lp[\cdot]$ denotes the low-pass response of the photodetector, and $\Delta\omega_{s,i} = \omega_s - \omega_i$, $\Delta\phi_{s,i} = \phi_s - \phi_i$, $\Delta\omega_{i,j} = \omega_i - \omega_j$, $\Delta\phi_{i,j} = \phi_i - \phi_j$. The received signal current is given by

$$i(t) = \frac{\eta e}{h\nu} P_{det}(t) = RP_{det}(t) \tag{7-7}$$

where η is the photodetector quantum efficiency, e is the elementary charge, ν is the optical carrier frequency in Hz, h is Planck's constant, and R is the receiver responsivity.

The first, second, third and fourth terms on the right side of equation (7-6) represent the signal power, the *dc*-component of the crosstalk, and the signal-crosstalk beating, and crosstalk-crosstalk beating, respectively. Using one ohm load resistance for current to voltage conversion, we have the output voltage after the low-pass filter of the receiver as

$$v(t) = \int_{-\infty}^{\infty} i(\tau)h(t-\tau)d\tau \tag{7-8}$$

where h(t) is the impulse response of the low-pass filter.

From equation (7-6) it can be seen that several factors have strong effects on the received signal. The first factor is the difference between the signal and crosstalk carrier frequencies. If the frequency difference is larger than the receiver bandwidth determined by h(t), the third term will be filtered out. Thus, only the *dc*-crosstalk term needs to be considered in the calculation if the crosstalk-crosstalk beating is negligible. From the performance evaluation point of view, the homo-wavelength crosstalk can be treated as hetero-wavelength crosstalk in this case. However, the worst case can happen if the crosstalk channels have the same central frequency (wavelength) as the signal. The two beat noise terms could be maximized. Even all the crosstalk channels are aligned with the signal in their frequency, the beat noise also depends on their polarization states. If $\bar{p}_i(t)$ for all i are orthogonal to $\bar{p}_s(t)$, the signal-crosstalk beating will disappear.

In addition to the central frequencies and the polarization states, the linewidth of the optical sources also influence the beat noise. For a high-speed optical transmission system (a bit rate > 500 Mb/s), DFB lasers with a linewidth of a few tens of MHz are used. Hence, the linewidth of the optical sources is negligible in general compared with the receiver electrical bandwidth. Additionally, transient effects and chirp of the signal and crosstalk channels, and asynchronization can reduce the beating effect.

Analysis of the homo-wavelength crosstalk including all related factors would be too involved to be tractable. In the following, we only consider the worst-case, that is,

$$\Delta\omega_{s,i} = \Delta\omega_{i,j} = 0, \quad \text{for all } i$$
$$\bar{p}_s(t)\bar{p}_i(t) = \bar{p}_i(t)\bar{p}_j(t) = 1, \quad \text{for all } i \text{ and } j \tag{7-9}$$

We further assume that crosstalk ratios for all crosstalk components are the same, $C_i = C_x$ for all i, and $\Delta\phi_{s,i}$ and $\Delta\phi_{i,j}$ for all i and j are statistically independent variables with a probability distribution given by

$$P(\Delta\phi) = \frac{1}{2\pi}, \qquad \Delta\phi \in [-\pi, \pi] \tag{7-10}$$

To make the analysis tractable, we consider the beat noises for signal logic ONEs and ZEROs separately, on the condition that K of N crosstalk channels have logical ONEs during the detection. The probability is given by

$$P_b(K) = \frac{N!}{K!(N-K)!} \cdot \frac{1}{2^N}. \tag{7-11}$$

The bit error rate can be calculated by averaging BERs for signal ONEs and ZEROs over different pattern combinations of the crosstalk components with the probability given by equation (7-11).

First, we consider signal ONEs on the condition that K of N crosstalk channels have logical ONEs. For the simplicity of derivation, we use the following notations

$$x_{1,1,i} = 2RP_{on}\sqrt{C_x}\cos(\Delta\phi_{s,i}) = A_{1,1}\cos(\varphi_{s,i}) \tag{7-12}$$

$$x_{1,0,i} = 2RP_{on}r\sqrt{C_x}\cos(\Delta\phi_{s,i}) = A_{1,0}\cos(\varphi_{s,i}). \tag{7-13}$$

We take the predominant beat noise term to illustrate the analysis as follows. The probability density function (PDF) of random variable $x_{1,1,\ell}$ is given by [135]

$$P(x_{1,1,\ell}) = \frac{1}{A_{1,1}\pi\sqrt{1-(x_{1,1,\ell}/A_{1,1})^2}}, \qquad |x_{1,1,\ell}| < A_{1,1} \tag{7-14}$$

Its moment generating function (MGF) can be found as

$$MGF_{1,1,\ell}(s) = I_0(A_{1,1}s) \tag{7-15}$$

where $I_0(\cdot)$ is the modified Bessel function of order zero. Following the same way, we can have the MGF of $x_{1,0,\ell}$ as

$$MGF_{1,0,\ell}(s) = I_0(A_{1,0}s) \tag{7-16}$$

Since the terms in the summation of the signal-crosstalk beat noise are statistically independent, the MGF of the signal-crosstalk beat noise is given as

$$MGF_{1,K}(s) = [MGF_{1,1}(s)]^K \cdot [MGF_{1,0}(s)]^{N-K} = [I_0(A_{1,1}s)]^K [I_0(A_{1,0}s)]^{N-K}. \tag{7-17}$$

To calculate the BER for signal ONEs, we have to consider other two noise terms: thermal noise and shot noise. These two kinds of noises can be assumed to have a Gaussian distribution. Hence, the total noise power, its PDF and MGF are expressed as follows;

$$\sigma^2_{g,1,K} = \sigma^2_{th} + \sigma^2_{shot,1,K} \tag{7-18}$$

$$P(x_{g,1,K}) = \frac{1}{\sqrt{2\pi}\sigma_{g,1,K}} \exp\left[-\frac{(x_{g,1,K} - \langle i_{1,K}\rangle)^2}{2\sigma^2_{g,1,K}}\right] \tag{7-19}$$

$$MGF_{g,1,K}(s) = \exp\left(\langle i_{1,K}\rangle s + \frac{s^2\sigma^2_{g,1,K}}{2}\right) \tag{7-20}$$

where $\sigma^2_{g,1,K}$ is the total Gaussian noise power for a signal ONE. $\langle i_{1,K}\rangle$ is the average current including the *dc*-crosstalk term.

The MGF of the received signal current for data ONE is obtained by multiplexing (7-17) and (7-20). Thus,

$$MGF_{1,K}(s)=\exp\left(\langle i_{1,K}\rangle s+\frac{s^2\sigma^2_{g,1,K}}{2}\right)\left[I_0\left(A_{1,1}s\right)\right]^K\left[I_0\left(A_{1,0}s\right)\right]^{N-K} \tag{7-21}$$

where

$$\langle i_{1,K}\rangle = R\cdot\left[P_{on}+(K+(N-K)r)C_xP_{on}\right]$$

$$\sigma^2_{1,K}=\sigma^2_{th}+\sigma^2_{shot,1,K}=I^2_{th}B_e+2e\langle i_{1,K}\rangle B_e$$

$$A_{1,1}=2RP_{on}\sqrt{C_x}$$

$$A_{1,0}=2RP_{on}r\sqrt{C_x}.$$

Following the same way for deriving the MGF of the received signal ONEs, we can have the MGF of received signal ZEROs, expressed as

$$MGF_{0,K}(s)=\exp\left(\langle i_{0,K}\rangle s+\frac{s^2\sigma^2_{g,0,K}}{2}\right)\left[I_0\left(A_{0,1}s\right)\right]^K\left[I_0\left(A_{0,0}s\right)\right]^{N-K} \tag{7-22}$$

where

$$\langle i_{0,K}\rangle = R\cdot\left[rP_{on}+(K+(N-K)r)C_xP_{on}\right]$$

$$\sigma^2_{0,K}=\sigma^2_{th}+\sigma^2_{shot,0,K}=I^2_{th}B_e+2e\langle i_{0,K}\rangle B_e$$

$$A_{0,1}=2RP_{on}r\sqrt{C_x}$$

$$A_{0,0}=2RP_{on}r^2\sqrt{C_x}.$$

It is noted that if any optical amplifiers are involved in the system, the signal-spontaneous beat noise and spontaneous-spontaneous beat noise can be either included in the total Gaussian noise or taken into account by multiplexing their MGFs to the right side of equations (7-21) and (7-22).

In the following, a saddlepoint approximation method [136, 137] is adopted to evaluate the average bit error rate using the MGFs given in equations (7-21) and (7-22). Compared to other numerical methods [138], the saddlepoint approximation is simple and accurate. A brief introduction to the principle of the saddlepoint approximation is given in Appendix 7.1 at the end of this chapter.

With the saddlepoint approximation, the BER on the condition that K of N crosstalk channels have logical ONEs can be expressed as

$$P_e(K) = \frac{1}{2}\left[q_{+,K}(\alpha) + q_{-,K}(\alpha)\right] \tag{7-23}$$

where $q_{+,K}(\alpha)$ and $q_{-,K}(\alpha)$ are the upper and lower tails, respectively, which are approximated by

$$q_{+,K}(t) \approx \left[2\pi\psi''_{0,K}\left(s_{0,K}\right)\right]^{-\frac{1}{2}} \exp\left[\psi_{0,K}\left(s_{0,K}\right)\right], \qquad s_0 > 0 \tag{7-24}$$

$$q_{-,K}(t) \approx \left[2\pi\psi''_{1,K}\left(s_{1,K}\right)\right]^{-\frac{1}{2}} \exp\left[\psi_{1,K}\left(s_{1,K}\right)\right], \qquad s_1 > 0 \tag{7-25}$$

$$\psi_{0,K}(s) = \log\left[MGF_{0,K}(s)\right] - s\alpha - \log(s) \tag{7-26}$$

$$\psi_{1,K}(s) = \log\left[MGF_{1,K}(s)\right] - s\alpha - \log(s) \tag{7-27}$$

$s_{0,K}$ and $s_{1,K}$ is the positive and negative roots of $\psi'_{0,K}(s) = 0$ and $\psi'_{1,K}(s) = 0$, respectively.

By taking account of all possible data pattern combinations of the crosstalk channels, the average bit error rate can be calculated as

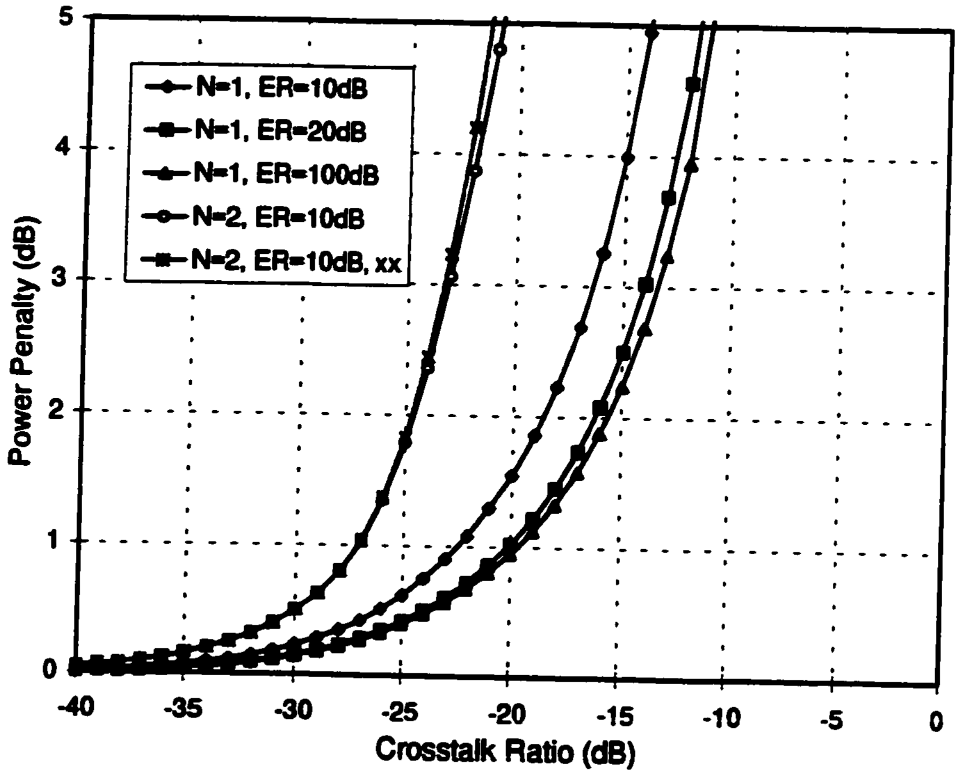

Figure 7.5: Power penalty versus crosstalk ratio for three different signal extinction ratios with one crosstalk channel (N=1). For N=2, the effect of crosstalk-crosstalk beat noise is compared. 'xx' indicates the curve with consideration of crosstalk-crosstalk beat noise.

$$P_e = \sum_{K=0}^{N} \frac{1}{2}\left[q_{+,K}(\alpha_{opt}) + q_{-,K}(\alpha_{opt})\right] P_b[\text{Number of ONEs} = K] \tag{7-28}$$

where α_{opt} is the optimum threshold so that the average BER is minimized. To evaluate the value of equation (7-28), $s_{0,K}$, $s_{1,K}$ and α_{opt} have to be solved, numerically.

In the above analysis, we have deliberately ignored the crosstalk-crosstalk beat noise. To take into account this beat noise term, we assume all crosstalk-crosstalk beat noise terms in the summation are statistically independent in order to simplify the analysis. Thus, the MGF of the crosstalk-crosstalk beat noise can be found as

$$MGF_{xx,K}(s) = \left[I_0(2RC_x P_{on} s)\right]^{K(K-1)/2} \tag{7-29}$$

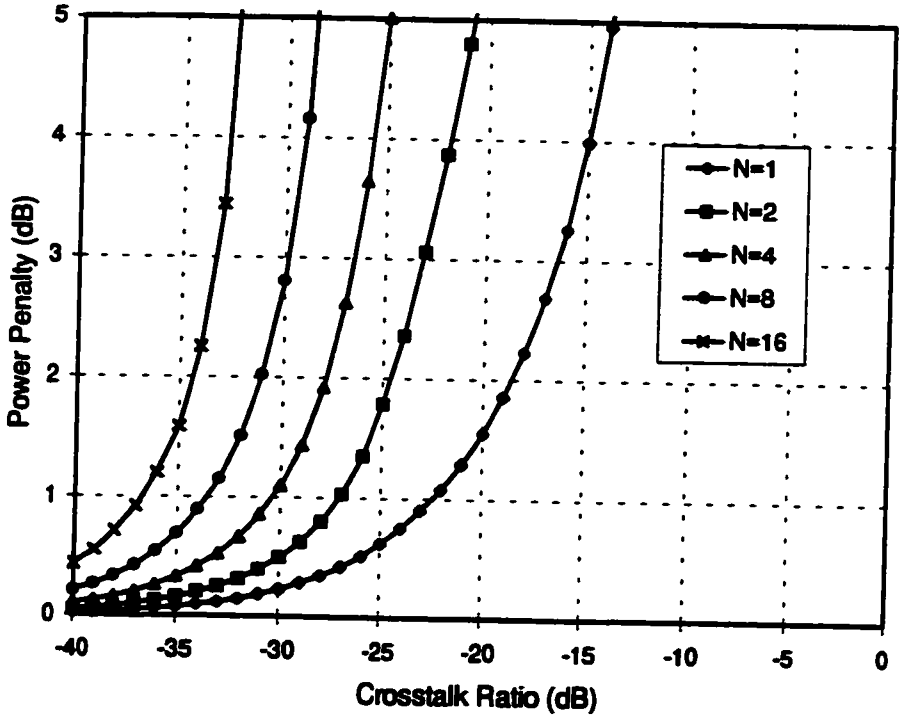

Figure 7.6: Power penalty versus crosstalk ratio for different numbers of crosstalk channels calculated by using the saddlepoint approximation method with optimum threshold setting.

Here, the higher order crosstalk-crosstalk beat noise due to logic ZEROs of the crosstalk channels has been excluded. It will be shown that the crosstalk-crosstalk beat noise is negligible in practical systems. To include the crosstalk-crosstalk beat noise in the evaluation, the right side of equation (7-29) can be directly multiplexed to the right sides of equations (7-21) and (7-22).

7.2.3 Numerical Examples

In this section we present several numerical examples using the saddlepoint approximation to evaluate a BER with the MGFs of signal-crosstalk and crosstalk-crosstalk beat noises. The Gaussian approximation used in Chapter 4 and 6 are compared with the MGF-saddlepoint approximation numerically. The worst case is always assumed here, that is, the crosstalk channels are aligned with the signal in polarization and central frequency.

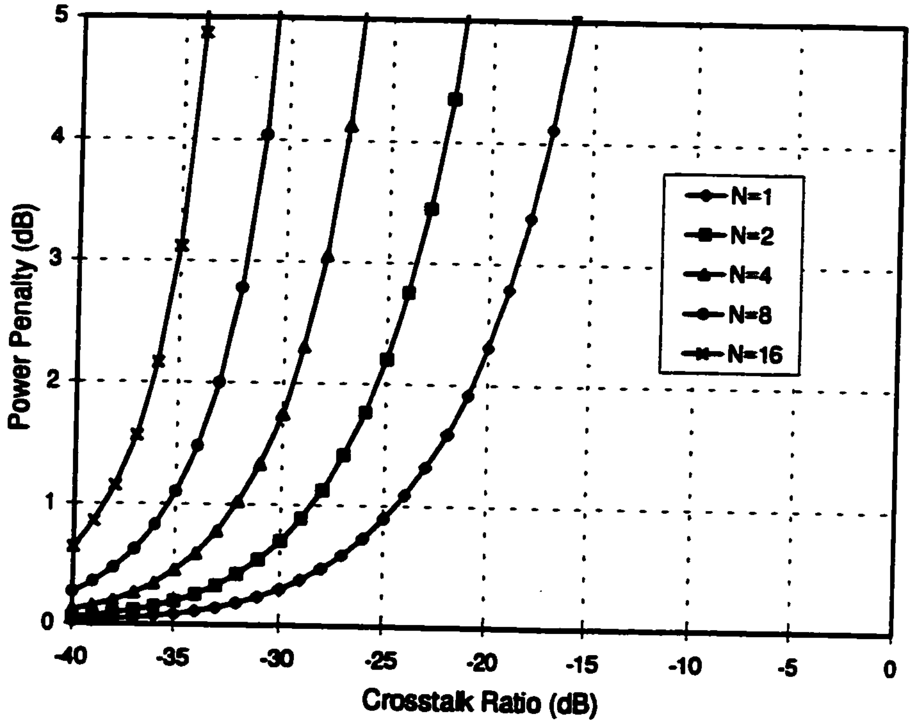

Figure 7.7: Power penalty versus crosstalk ratio for different numbers of crosstalk channels, calculated by using the saddlepoint approximation method with a fixed threshold setting.

To compare with experimental results in the next section, we assume an APD receiver for the following calculations. The symbols and values of used parameters are listed in Table 7.1. Shot noise introduced by the APD photodiode is assumed a white Gaussian noise calculated by

$$\sigma^2_{shot,0/1} = 2e\langle M\rangle^2 F(M)\left(R\overline{P}_{0/1} + I_{dark}\right)B_e \tag{7-30}$$

Figure 7.5 shows the receiver power penalty as a function of the crosstalk ratio with $N=1$ and $N=2$. For $N=1$, there are three curves plotted for three different signal extinction ratios. As the signal extinction ratio decreases, the crosstalk introduces more degradation since the ZEROs from the crosstalk channels contributing more to the degradation and the ZEROs of the signal also get stronger beating with crosstalk ONEs. With an extinction ratio of 10 dB, the crosstalk ratio at a 1-dB penalty is about 2.5 dB lower than that with an extinction ratio of 20 dB. Further increasing the signal extinction

Table 7.1: Symbols and values of the parameters used in numerical calculations

Symbols	Parameters	Default values
B_r	Bit rate	1 Gb/s
λ_s	Wavelength	1300 nm
B_e	Receiver bandwidth	$0.75B_r$
I_{th}	Thermal noise	8.5 pA/√Hz
η	Quantum efficiency	0.85
$\langle M \rangle$	Avalanche gain	10
$F(M)$	Excess noise factor	9
I_{dark}	Multiplied dark current	20 pA

ratio to 100 dB, we only relax 0.2 dB of the crosstalk ratio at a 1-dB penalty. An extinction ratio of 20 dB would be enough in terms of degradation due to beat-noise crosstalk. For the rest of the simulations, an extinction ratio of 10 dB is used so that simulation results can be compared with experimental ones.

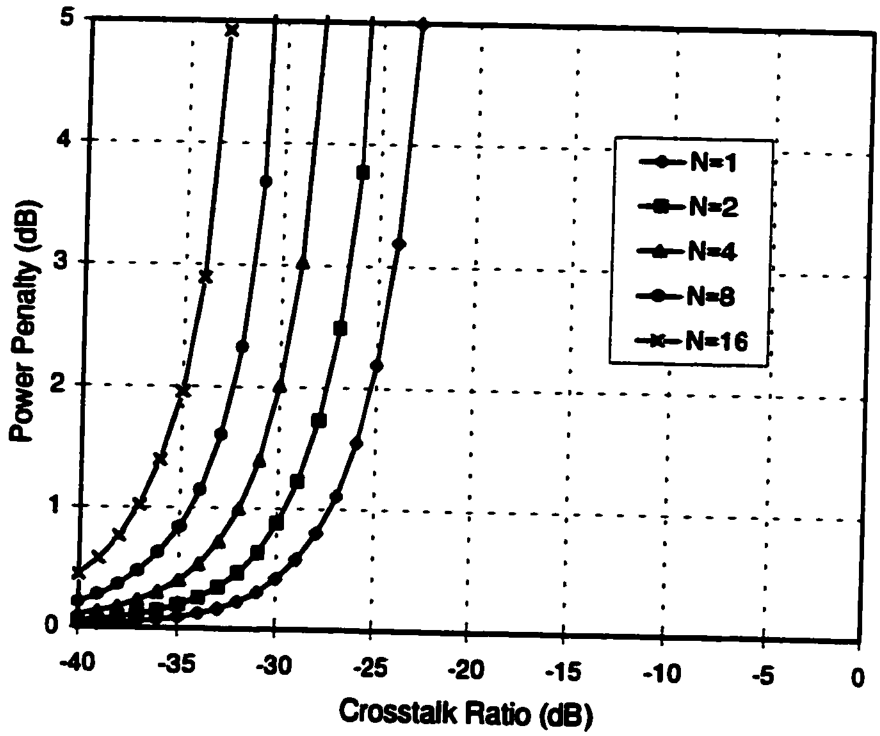

Figure 7.8: Power penalty versus crosstalk ratio for different numbers of crosstalk channels, calculated by using the Gaussian approximation method with optimum threshold setting.

Other two curves for $N = 2$ in Figure 7.5 illustrate the effect of crosstalk-crosstalk beat noise. 'xx' in the legend indicates the curve with crosstalk-crosstalk beat noise terms. At a 1-dB power penalty, there is almost no difference in crosstalk ratio. In the following calculations of power penalty, the crosstalk-crosstalk beat noise is excluded in order to speedup calculations.

For different numbers of crosstalk channels, their power penalties versus crosstalk ratios are plotted in three figures, Figures 7.6, 7.7 and 7.8, by using three different approximations. With the saddlepoint approximation method, the curves in Figure 7.6 are calculated by setting optimum threshold levels, while the curves in Figure 7.7 are obtained by using a fixed threshold level which is optimized to the signal without crosstalk. It can be seen that setting a fixed threshold level enhances the power penalty, thus makes the requirements stronger for the crosstalk ratio. The reason is that the optimum threshold

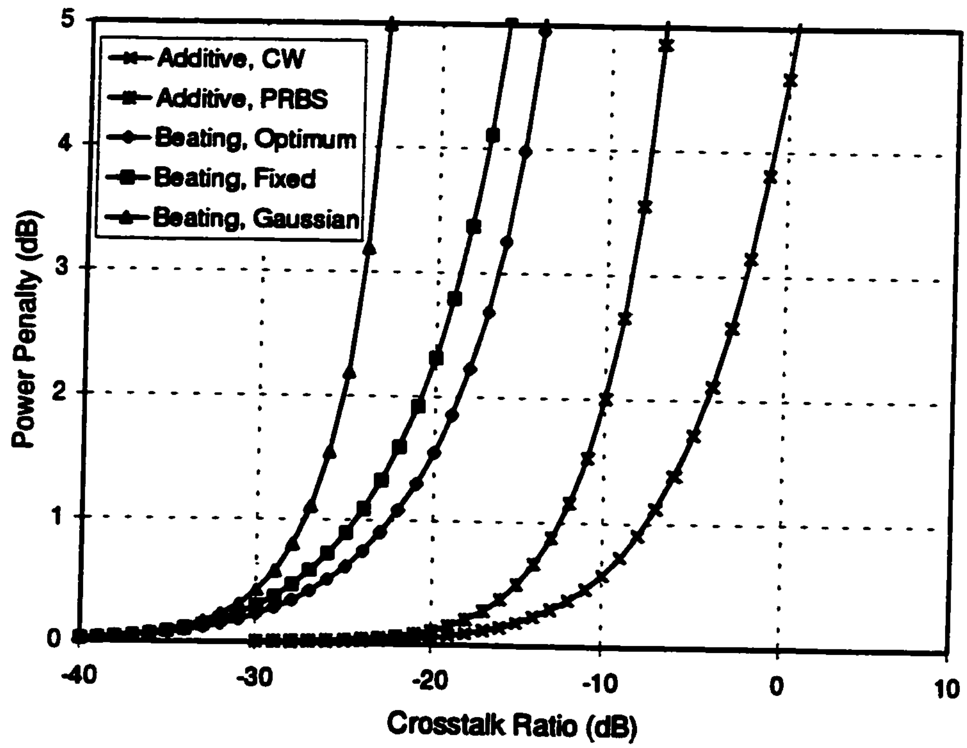

Figure 7.9: For N =1, power penalty versus crosstalk ratio for two kinds of homo-wavelength crosstalk. Three different approximations are used to calculate power penalty for the beat-noise crosstalk.

level goes lower as the beat-noise crosstalk is introduced because signal ONEs have more beat noise than signal ZEROs have. In general, any shift of the threshold level from its optimum will introduce more error bits, thus a higher bit error rate. Hence, a dynamic optimum threshold setting is required to achieve the best system performance when there is beat-noise crosstalk.

In Figure 7.8, the power penalties are calculated with the Gaussian approximation by setting an optimum threshold level, as used in Chapters 4 and 6. Compared with Figure 7.6, it is apparent that the Gaussian approximation overestimates the power penalties. This is simply because a bounded PDF of the signal-crosstalk beat noise is replaced by a Gaussian PDF.

To clearly compare the results evaluated with three approximations, three curves for $N = 1$ from Figure 7.6, 7.7 and 7.8 are plotted in Figure 7.9 with two extra curves for

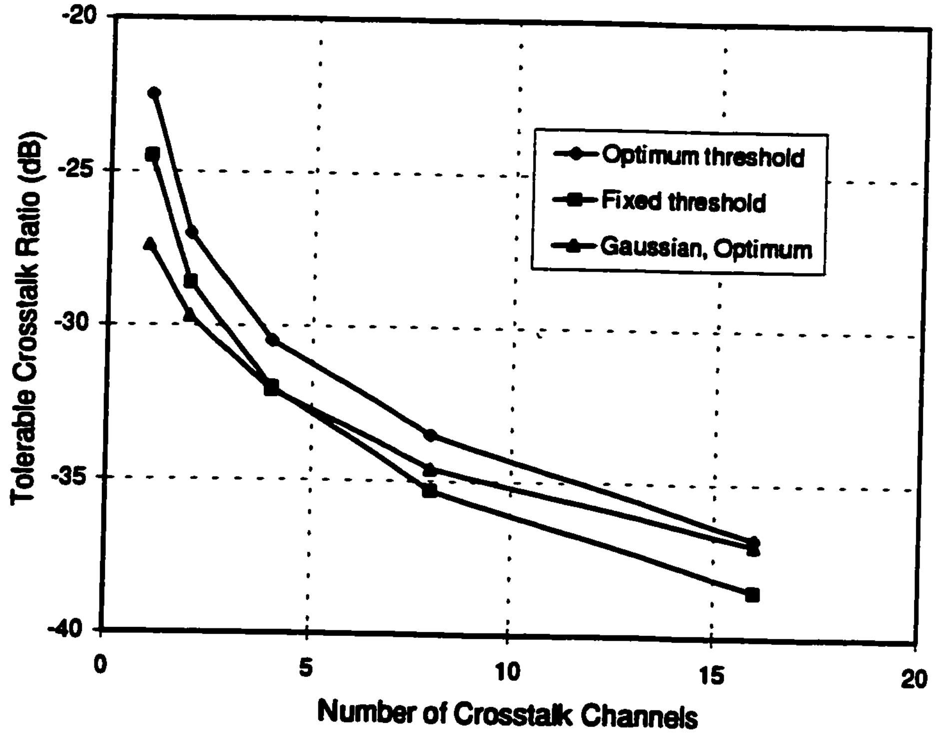

Figure 7.10: Tolerable crosstalk ratio with less than 1-dB power penalty versus the number of beat-noise crosstalk channels. The curves with diamonds and squares are calculated by using the saddlepoint approximation method.

additive crosstalk. For $N > 1$, the comparison among other curves follow the same trend as shown in Figure 7.9. Compared with beat-noise crosstalk, additive crosstalk deduces much less degradation. At a 1-dB penalty, the crosstalk ratio to the additive crosstalk can be 10 dB higher than that to the beat-noise crosstalk.

Figure 7.10 shows the crosstalk ratio at a 1-dB penalty as a function of the number of beat-noise crosstalk channels. With a fixed threshold level setting, the crosstalk requirements are always more stringent than that with an optimum threshold level setting. Another important point is that as the number of the crosstalk channels increases, the curve calculated by using the Gaussian approximation approaches that calculated by using the saddlepoint approximation with an optimum threshold level setting. That means the Gaussian approximation can give a good estimation to the required crosstalk ratio for a large number ($N > 4$) of crosstalk channels. For $N = 4$, the Gaussian approximation estimates only about 2 dB higher on the required crosstalk ratio than that calculated with the accurate saddlepoint approximation. This conclusion justifies our analysis approach based on the Gaussian approximation used in Chapter 4 and Chapter 6.

7.3 Experimental Study

7.3.1 Experimental Setup

To study crosstalk effects on the system performance, three experimental setups are used here. We start from a setup for studying hetero-wavelength crosstalk, shown in Figure 7.11(a). Two DFB lasers operating at two different wavelengths of 1302.7 nm and 1307.5 nm are used as optical sources for a signal and a crosstalk channel. The signal is generated by directly modulating the first DFB laser at 1 Gb/s with a PRBS word length of 2^7-1. The signal extinction ratio is about 10 dB. The crosstalk channel from the second DFB laser can have three crosstalk formats, namely, a CW light, a signal modulated directly by the same PRBS driving signal to the first DFB laser, and a signal modulated directly by a data sequence 1010 at 250 Mb/s from a pulse generator. The reason for using the third crosstalk format is to de-correlate the signal and crosstalk channels. The signal and crosstalk from the two DFB lasers are properly attenuated, then combined at a 3-dB coupler. No polarization controllers are required for this experiment because of only an additive effect of the crosstalk on the signal. Several optical isolators are inserted after the DFB lasers and before the detector to avoid possible disturbance due to optical reflections. The optical receiver is the BCP-51R high-sensitivity Ge-APD, which is followed by a BCP-210 BER tester.

The second experiment is designed to verify the theoretical analysis discussed in the preceding section. Figure 7.11(b) shows the experimental setup. To avoid any chirp resulting from direct modulation of a DFB laser, an external modulator is employed here to generate a chirp free signal. A semiconductor laser-pumped Nd:YAG laser operating at 1318 nm provides CW light to the external modulator. The same PRBS generator and BER tester as in the first setup are used for testing a BER and a power penalty. The signal from the external modulator is splitted by a 1×2 coupler into two data paths. The upper one is referred to as a signal path, the lower one as a crosstalk path. On the crosstalk path,

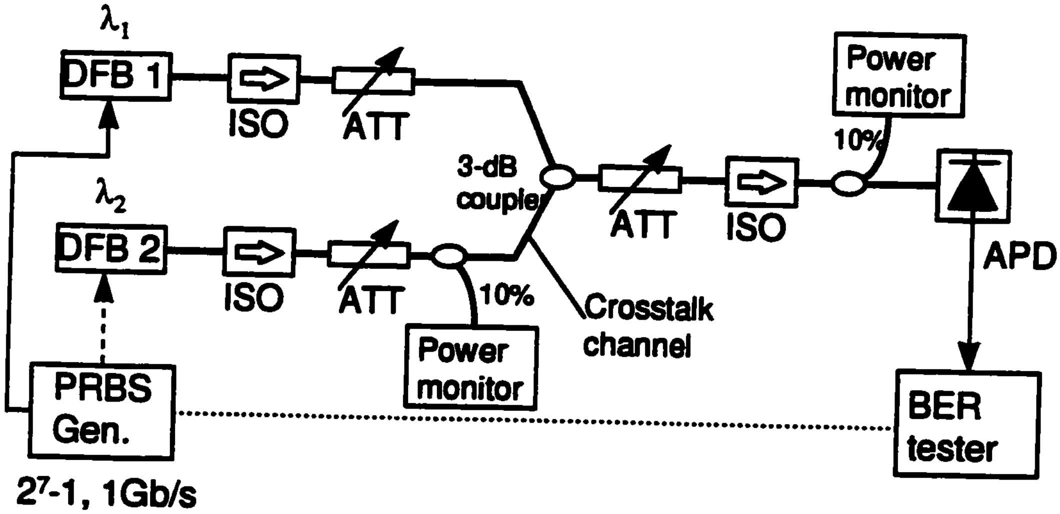

(a)

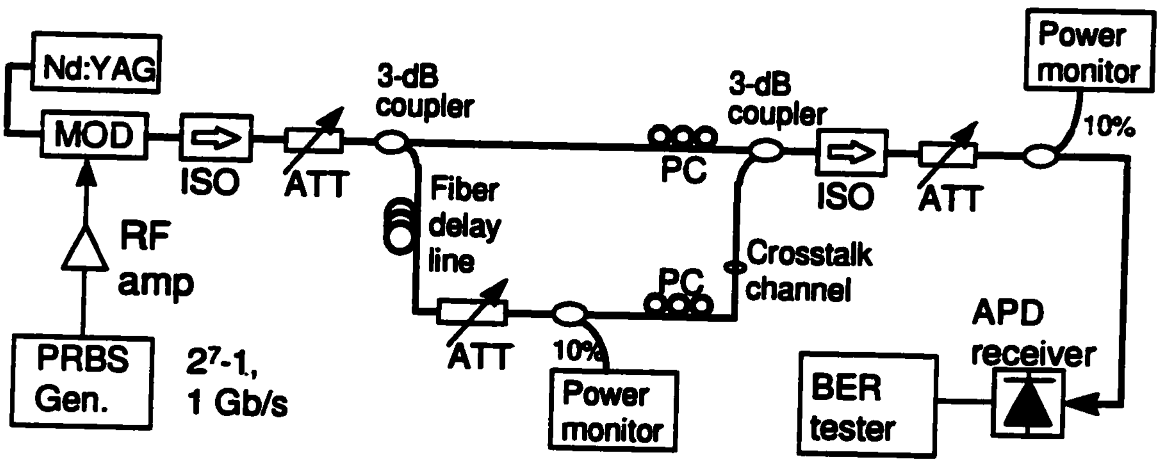

(b)

Figure 7.11: Experimental setups for power penalty measurement. (a) Hetero-wavelength crosstalk experiment. (b) Beat-noise crosstalk experiment using an external modulator.

about 1.2-km fiber delay line is inserted to de-correlate the carrier phases between the signal and crosstalk channels. Before the two paths are combined, polarization controllers are utilized to align their polarization states so that worst-case effect of the crosstalk could be measured.

The third experimental setup as shown in Figure 7.12 is designed to investigate the difference between the power penalty measurement using a single laser source and two

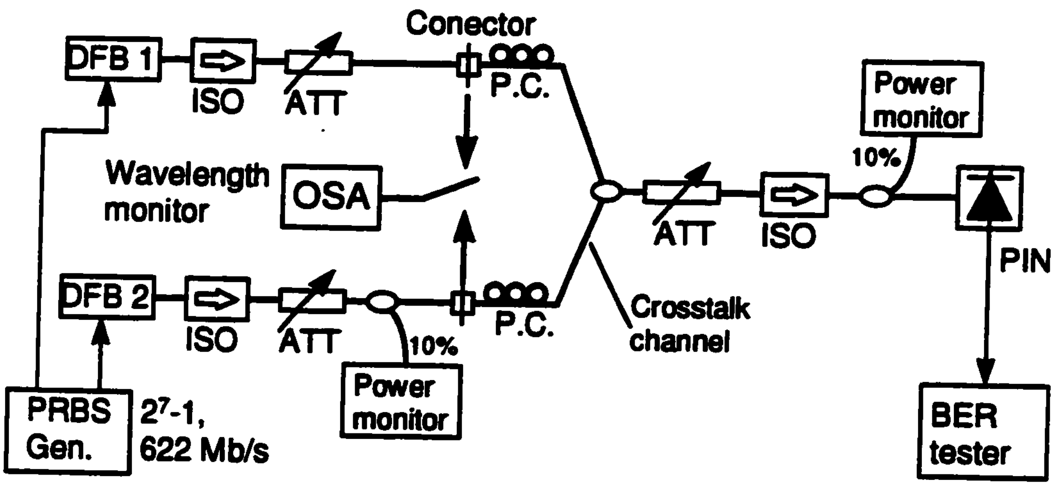

Figure 7.12: Experimental setup for measuring power penalty using two separate DFB lasers.

separate laser sources, and also how the wavelength difference between the signal and crosstalk channels could affect the power penalty. In this setup, two DFB lasers operating around 1553 nm are used to generate a signal and a crosstalk channel. Their wavelengths are tuned by controlling their temperature with thermal-electric coolers, and monitored by using an optical spectrum analyzer (OSA). The wavelength difference is measured in terms of their peak wavelengths displayed on the OSA. Due to the change of operating wavelength window, a PIN optical receiver (BCP-50R) is used to detect the optical signal. The signal bit rate is set to 622 Mb/s. At this bit rate, the back-to-back receiver sensitivity is -25 dBm at a BER of 10^{-9}. All other parts of the setup are similar to those of the second experimental setup.

7.3.2 Results and Discussions

First, we measure the power penalty due to the hetero-wavelength crosstalk as a function of the crosstalk ratio. Figure 7.13 shows the measured and calculated results. Among three kinds of crosstalk forms, the CW crosstalk has the minimum impact on the performance since it only degrades the signal extinction ratio. The crosstalk ratio at a 1-dB power penalty is about -8 dB and there is no BER floor with a crosstalk ratio up to 5 dB. As for two other kinds of hetero-wavelength crosstalk, the PRBS crosstalk has a little stronger effect on the performance than that due to the 1010 sequence crosstalk. One

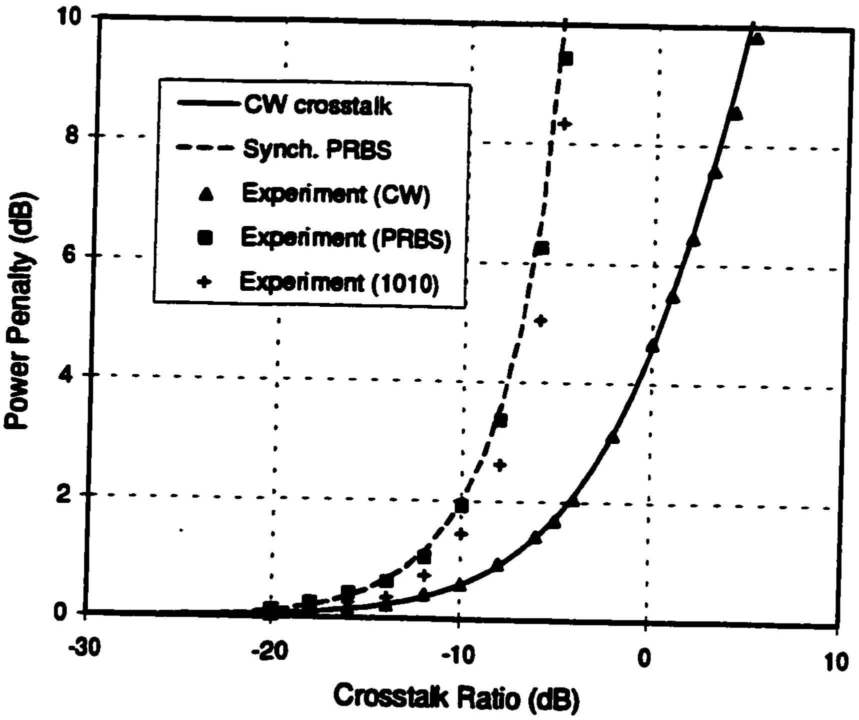

Figure 7.13: Measured power penalty versus crosstalk ratio for hetero-wavelength crosstalk with three formats. The solid and dashed curves show calculation results.

possible reason for this is the correlation between the signal and crosstalk channels. The crosstalk ratio of the PRBS crosstalk at a 1-dB penalty is -12.5 dB. The theoretical results for the PRBS crosstalk is calculated by using the statistical approach discussed in Chapter 4. A very good agreement is shown in Figure 7.13.

Figure 7.14 shows the power penalty versus the crosstalk ratio of beat-noise crosstalk. The results are measured by using the second experimental setup illustrated in Figure 7.11(b). For the externally modulated signal and crosstalk, the experimental results agree well with the calculated ones by assuming a signal extinction ratio of 10 dB. When the laser is directly modulated, a crosstalk ratio at a 1-dB penalty is about 3 dB less than that with the external modulation. This we believe results from the chirp of direct modulation which extends the bandwidth of the signal-crosstalk beat noise so that a part of the beat noise falls outside the receiver bandwidth.

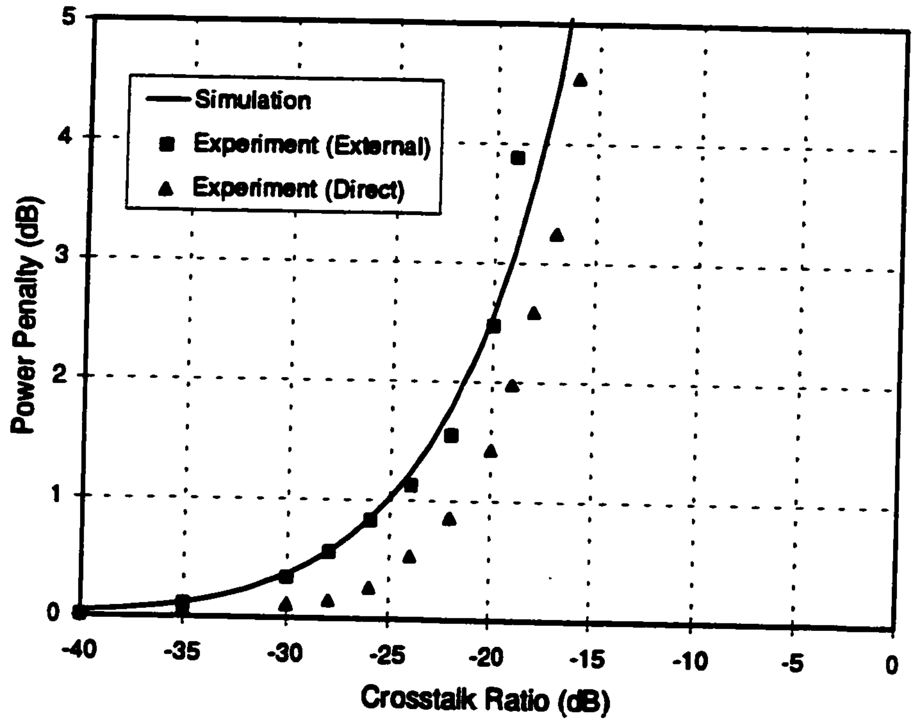

Figure 7.14: Measured power penalty versus crosstalk ratio for beat-noise crosstalk. The solid curve is the results calculated by using the saddlepoint approximation with fixed threshold setting.

Most of the reported experiments on homo-wavelength crosstalk were done by using a single laser for the signal and crosstalk channels. Here, we use two separate lasers to measure the power penalties due to homo-wavelength crosstalk. Two DFB lasers are aligned in their peak wavelengths by adjusting their temperature. Figure 7.15 shows the experimental results and comparison of the results measured by using a single laser. It can be seen that a single laser has accurately simulated two separate lasers with a sufficient long delay between the signal and crosstalk channels. CW homo-wavelength crosstalk imposes a lower degradation than the PRBS crosstalk does.

Using two separate lasers, we further study the influence of the wavelength difference between the signal and the crosstalk on degradation. The power penalty as a function of the peak wavelength difference between the signal and the homo-wavelength crosstalk is shown in Figure 7.16. The results are measured by using the third experimental setup as

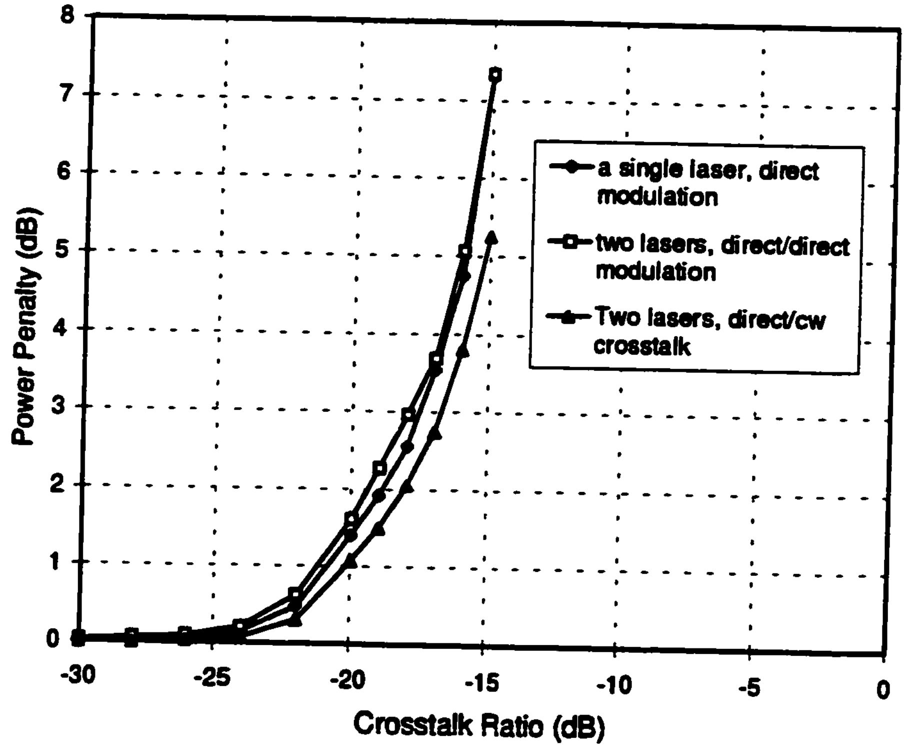

Figure 7.15: Comparison of measured power penalties by using a single laser and two separate lasers for beat-noise crosstalk.

illustrated in Figure 7.12 with a crosstalk ratio of -18 dB. The signal peak wavelength is fixed at 1553.2 nm while the crosstalk peak wavelength is tuned by changing the temperature of the second DFB laser. It can be seen from Figure 7.16 that the beat-noise effect of the homo-wavelength crosstalk decreases as the peak wavelength of the crosstalk is shifted away from the peak wavelength of the signal. As for the PRBS crosstalk, the wavelength range for generating signal-crosstalk beat noise is larger than that for the CW crosstalk because of a wider linewidth due to chirp of direct modulation. When the peak wavelength of the crosstalk channel is far from the signal peak wavelength (> 0.04 nm), we only have the penalty due to additive crosstalk (about 0.2 dB penalty).

As for the signal and crosstalk generated by directly modulating the lasers, we find the second peak of power penalty. It is somewhat a strange phenomenon. Further study on the optical spectrum of the crosstalk channel shows that the second peak of power penalty is due to asymmetrical spectral broadening resulting from chirp [139], which is shown in

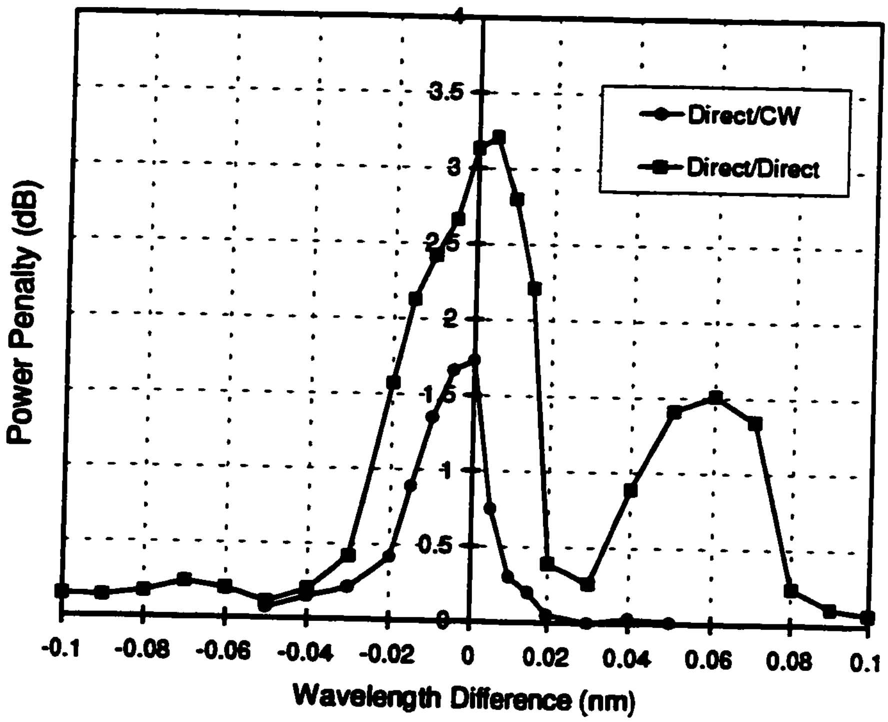

Figure 7.16: Measured power penalty versus peak wavelength difference between the signal and the crosstalk channel. There are two formats of crosstalk, CW light and direct modulated data.

Figure 7.17. This phenomenon becomes very important when the minimum wavelength shift is considered to avoid the beat-noise effect of homo-wavelength crosstalk. The wavelength range for generating beat-noise is 0.03 nm and 0.05 nm for CW and directly modulated crosstalk without considering the second penalty peak, respectively, which corresponds to 3.75 GHz and 6.3 GHz. As the bit rate increases, a wider wavelength range would be expected.

7.4 Conclusions

Homo-wavelength crosstalk is a primary kind of optical crosstalk, particularly as optical wavelengths are reused for wavelength routing. Three basic kinds of optical wavelength routing nodes have been discussed in terms of the mechanisms of homo-

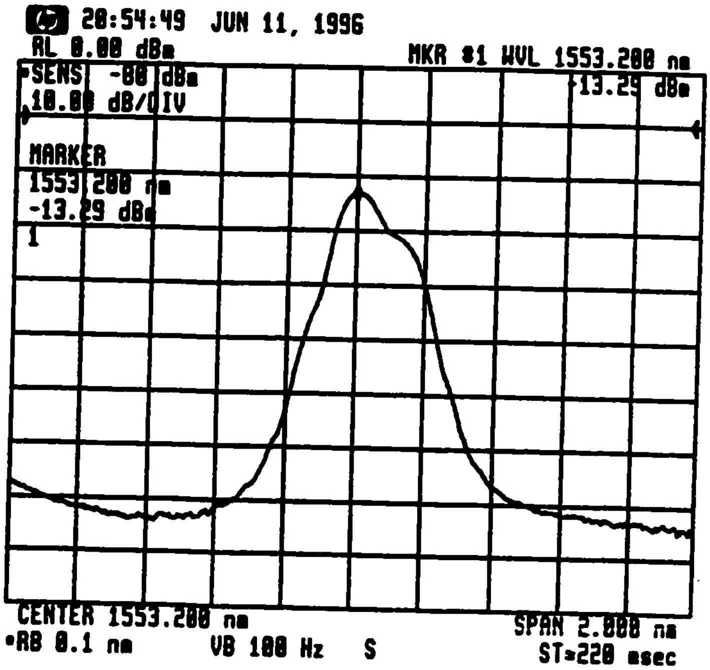

Figure 7.17: Optical spectrum of a directly modulated DFB laser at 622 Mb/s.

wavelength crosstalk. According to its impact on system performance, homo-wavelength is categorized into additive and beat-noise crosstalk.

As for beat-noise crosstalk, the signal-crosstalk beat noise is studied with its moment generating function. Further, a simple and accurate numerical method, the saddlepoint approximation, was employed to evaluate the system performance. With the numerical examples, we find the Gaussian approximation used in Chapter 4 and 6 can give good estimates for the required crosstalk ratio at a 1-dB power penalty.

The experimental study on the homo-wavelength crosstalk has verified the MGF-saddlepoint approach for performance evaluation by comparing the experimental results with the calculated ones for a single crosstalk channel. With two separate lasers, the effect of wavelength shift between the signal and the crosstalk has been investigated. It was found that there can be another power penalty peak in addition to one at the peak wavelength for directly modulated signals. The study in this chapter provides an insightful understanding of homo-wavelength crosstalk for optical networking and switching.

Appendix 7.1 Saddlepoint Approximation

Following [136, 137] the saddlepoint approximation is derived as follows.

Let $q_+(\alpha)$ and $q_-(\alpha)$ denote the upper and lower tails of a continuous variable with the probability density function (PDF) $P(x)$

$$q_+(\alpha) = \int_{\alpha}^{\infty} P(x)dx \tag{A7-1}$$

$$q_-(\alpha) = \int_{-\infty}^{\alpha} P(x)dx. \tag{A7-2}$$

The moment generating function (MGF) of $P(x)$ can be found by taking bilateral Laplace transform, as

$$MGF(-s) = \int_{-\infty}^{\infty} P(x)e^{-sx}dx \tag{A7-3}$$

The PDF $P(x)$ is equal to inverse integral

$$P(x) = \frac{1}{2\pi j}\int_{c-j\infty}^{c+j\infty} MGF(-s)e^{sx}ds \tag{A7-4}$$

where C is the convergence region of the transform.

Replace $P(x)$ in equation (A7-1) by (A7-4) and choose the integration contour such that $C > 0$ to guarantee convergence of the integral. Thus,

$$q_+(\alpha) = \frac{1}{2\pi j}\int_{c-j\infty}^{c+j\infty} MGF(-s)\frac{e^{-s\alpha}}{s}ds, \qquad C > 0 \tag{A7-5}$$

Then, the parameter C is chosen to be the value of s for which the integrand is minimal. It turns out that this point $s = s_0$ corresponds to a saddlepoint in the complex plane.

We express the integrand in terms of its phase function defined by

$$\exp[\psi(s)] = |s|^{-1} \exp(-s\alpha) MGF(s) \tag{A7-6}$$

Further, $\psi(s)$ can be expanded in a Taylor series around the point $s = s_0$

$$\psi(s) = \psi(s_0) + \frac{1}{2}\psi''(s_0)(s - s_0)^2 + \ldots \tag{A7-7}$$

where the first derivative disappears since $s = s_0$ is an extremum of $\psi(s)$.

Substitute (A7-7) into (A7-5) and neglect higher order terms, we have the zero-order saddlepoint approximation

$$\begin{aligned} q_+(\alpha) &\approx \frac{1}{2\pi} \exp[\psi(s_0)] \int_{-\infty}^{\infty} \exp\left[-\frac{1}{2}\psi''(s_0) y^2\right] dy \\ &= [2\pi\psi''(s_0)]^{-\frac{1}{2}} \exp[\psi(s_0)] \end{aligned} \tag{A7-8}$$

The parameter s_0 is the value of s for which $\psi(s)$ has a minimum, equal to the positive root of the equation

$$\psi'(s) = 0. \tag{A7-9}$$

For the lower tail, analogously to (A7-8), we have

$$q_-(\alpha) \approx [2\pi\psi''(s_1)]^{-\frac{1}{2}} \exp[\psi(s_1)] \tag{A7-10}$$

with s_1 equal to the negative root of equation (A7-9).

The approximation can be improved by including higher-order terms as shown by Helstrom [137].

8. Fundamentals and Characterization of Semiconductor Optical Amplifiers

8.1 Introduction

Semiconductor optical amplifiers (SOAs) are one of the two most widely used optical amplifiers. In contrast to erbium doped fiber amplifiers (EDFAs), small-size and electrical pumping properties of SOAs make them attractive for many applications such as photonic switching, optical interconnection, and photonic integration for optical transmitters and receivers. Recently, several major breakthrough have been made in multiple quantum well (MQW)-SOAs [98]. SOAs with a high-gain, low gain ripples, low noise, low polarization sensitivity, and high saturation power have been reported [142].

In this thesis, SOAs as optical switching gates are one of basic components in the proposed optical cross-connect. Starting from this chapter, the following three chapters concentrate on SOA applications in photonic switching. In this chapter, we first present the principles of SOAs, with emphasize on their gain and noise characteristics. After the introduction of the principles, available SOAs are tested and characterized for switching applications.

8.2 Principles of Semiconductor Optical Amplifiers

8.2.1 Gain Characteristics

Figure 8.1 shows a schematic diagram of an SOA with active region width w, thickness d, and length L. Optical amplification in the SOA takes place in its active region. For a traveling-wave SOA, the input and output facets are anti-reflection coated with reflectivity $R_1 = R_2 < 10^{-4}$.

The material gain coefficient per unit length, g_m, can generally be expressed as [143, 144]

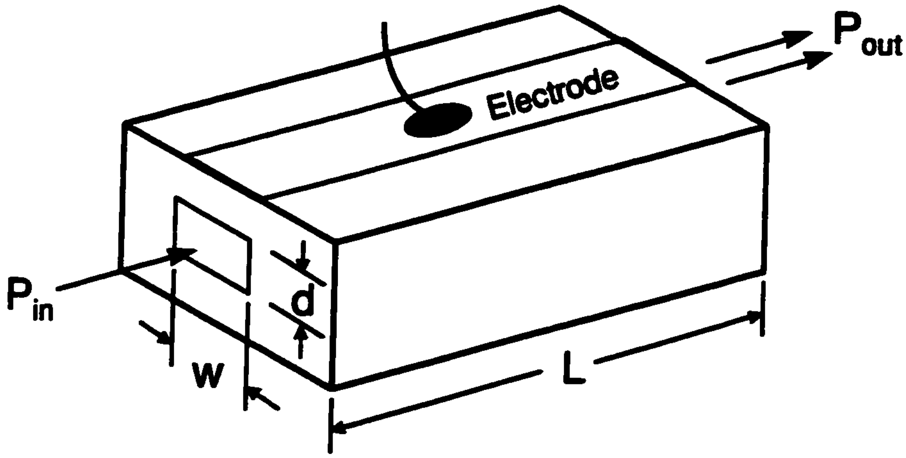

Figure 8.1: Schematic diagram of a semiconductor optical amplifier.

$$g_m = a_1(N - N_0) - a_2(\lambda - \lambda_p)^2 \tag{8-1}$$

where a_1 and a_2 are the gain constants, N is the carrier density, N_0 is the transparency carrier density, and λ_p is the peak gain wavelength which can be related to the carrier density by

$$\lambda_p = \lambda_0 - a_3(N - N_0) \tag{8-2}$$

with a constant a_3 and the peak gain wavelength λ_0 at the transparent state. The net gain per unit length can be calculated by considering the power distribution of the guided modes and the loss of the cavity, as

$$g = \Gamma g_m - \alpha \tag{8-3}$$

where Γ is the optical confinement factor, α is the effective loss coefficient. Thus, the total gain of the SOA will be

$$G = P_{out}/P_{in} = \exp[(\Gamma g_m - \alpha)\cdot L] \tag{8-4}$$

where P_{in} and P_{out} are the input and output power of the signal being amplified.

From equations (8-1) to (8-4), it can be noted that the optical gain of the SOA is wavelength dependent. As the carrier density increases, the wavelength at the gain peak shifts to a lower one. The 3-dB optical bandwidth for the unsaturated SOA can be estimated as [144]

$$2\Delta\lambda = 2\sqrt{\frac{\ln 2}{a_2 \Gamma L}} \tag{8-5}$$

The carrier density in the SOA can be obtained by solving the well-known rate equation [139]

$$\frac{dN}{dt} = \frac{I}{eV} - R(N) - S_{signal} - S_{spont} \tag{8-6}$$

where $V = wdL$ is the active volume, $R(N)$ is the spontaneous recombination rate, I is the injection current, e is the elementary charge, S_{signal} is the recombination rate due to the stimulated emission caused by the input optical signal, and S_{spont} is the recombination rate due to amplified spontaneous emission (ASE).

The spontaneous recombination rate $R(N)$ can be modeled by [139]

$$R(N) = AN + BN^2 + CN^3 \tag{8-7}$$

where A, B, and C are the coefficients corresponding to non-radiative recombination, radiative recombination, and Auger recombination, respectively. A simple recombination rate is often assumed to estimate the gain saturation effect,

$$R(N) = \frac{N}{\tau_c} \tag{8-8}$$

where τ_c is the equivalent carrier life time.

The recombination rate due to the stimulated emission caused by the input signal is calculated by [145]

$$S_{signal} = \frac{P_{in}}{h\nu} \cdot \frac{\Gamma g_m}{gL \cdot wd}\left(e^{gL} - 1\right) \tag{8-9}$$

where P_{in} is the optical input power, h is Planck's constant, and v is the optical frequency of the signal. The recombination rate due to ASE is given by [145]

$$S_{spont} = \sum \frac{\Gamma g_m}{g} 2R_{sp}\beta\left[\frac{e^{gL}-1}{gL}-1\right] \tag{8-10}$$

where R_{sp} is the spontaneous emission rate, and β is the fraction of the spontaneous emission coupled into the guided modes. In general, the term S_{spont} is negligible as it only incurred a small correction [146].

By setting $dN/dt = 0$ in the rate equation and using equation (8-8), we can have [144, 147]

$$g_m = \frac{g_0}{1 + P/P_{sat}} \tag{8-11}$$

where g_0 is the unsaturated material gain coefficient, P_{sat} is the internal saturation power, which can be approximated as follows by setting the loss coefficient α to zero.

$$P_{sat} = \frac{hv(wd)}{\Gamma a_1 \tau_c}. \tag{8-12}$$

A lumped SOA model for the gain saturation has been widely used for estimation of the system performance [97, 147]. The saturated gain can be simply calculated by

$$P_{out} = \frac{P_{sat}G}{G-1}\ln\left(\frac{G_0}{G}\right) \tag{8-13}$$

where G_0 is the unsaturated gain. A quantity of practical interest is the output saturation power P_{out}^s defined as the output power for the amplifier gain G reduced by 3 dB from its unsaturated value G_0. From equation (8-13), P_{out}^s can be expressed as

$$P_{out}^s = \frac{G_0 \ln 2}{G_0 - 2} P_{sat} \tag{8-14}$$

For a large unsaturated gain, $G_0 >> 2$, $P_{out}^s \approx 0.69 P_{sat}$.

In practice, even AR-coated facets will exhibit some residual reflectivity. Thus, small gain ripples can be observed from the gain profile of SOAs. To take optical reflections of the facets into account, we can calculate the optical gain at a frequency ν using the following equation [145, 148]

$$G(\nu)=\frac{(1-R_1)(1-R_2)G_s}{\left(1+\sqrt{R_1R_2}G_s\right)^2+4\sqrt{R_1R_2}G_s\sin^2\left[\pi(\nu-\nu_0)/\Delta\nu\right]} \tag{8-15}$$

where G_s is the single pass gain, R_1 and R_2 are the input and output residual facet reflectivities, respectively, ν_0 is one of the F-P resonant frequencies, and $\Delta\nu$ is the free-spectral range of the SOA. A well-designed SOA can have gain ripples less than 0.5 dB.

In addition to the gain dependence on the signal wavelength, the SOA gain is also dependent on the polarization of the input signal. Due to different optical confinement factors for TE and TM polarizations, i.e., $\Gamma_{TE} \neq \Gamma_{TM}$, the G_{TE} and G_{TM} can differ as much as 5~8 dB [147]. The gain dependence on polarization is undesirable for most of lightwave and optical switching systems. Several schemes have been devised to reduce this gain dependence, such as using two SOAs or two passes through the same SOA [147, 149]. The most recent approach for reducing the polarization sensitivity is using multiple quantum wells (MQWs) with alternating tensile and compressed strains in the active region of an SOA [98, 150]. With this scheme, the gain difference caused by different confinement factors is compensated by different material gains. The polarization sensitivity can be less than 0.5 dB as shown in the next section.

8.2.2 Noise Characteristics

Optical output from any optical amplifier is composed of an amplified optical signal and amplified spontaneous emission (ASE) of a broad spectral width. The ASE is generated randomly in the amplified medium, creating interference both between the ASE and the signal, and between ASE components. According to the photo-statistic master equation [151, 152], the average photon number at the output end of the optical amplifier $\langle n_{out}\rangle$ and the variance σ^2_{out} are

$$\langle n_{out}\rangle = G\langle n_{in}\rangle + (G-1)n_{sp}p\Delta\nu \tag{8-16}$$

$$\sigma_{out}^2 = G\langle n_{in}\rangle + (G-1)n_{sp}p\Delta\nu + 2G(G-1)n_{sp}\chi\langle n_{in}\rangle + (G-1)^2 n_{sp}^2 p\Delta\nu + G^2\left(\langle n_{in}^2\rangle - \langle n_{in}\rangle^2 - \langle n_{in}\rangle\right) \tag{8-17}$$

where n_{sp} is the population inversion factor or called the spontaneous emission factor, $\Delta\nu$ is the equivalent noise bandwidth and p is the effective mode number for transverse modes from 1 to 2, χ is the excess noise coefficient for signal spontaneous beat noise, which is determined by the gain and reflections. For TW-SOAs, $\chi = 1$. The terms on the right side of equation (8-17) represent the amplified signal shot noise, ASE shot noise, signal-ASE beat noise, spontaneous-spontaneous beat noise, and signal excess noise. The signal excess noise disappears when the input signal is completely coherent [148], that is $\langle n_{in}^2\rangle - \langle n_{in}\rangle^2 = \langle n_{in}\rangle$. The two beat noises dominate the total noise since the beat noise levels are G times larger than the shot noise levels, as shown in equation (8-17).

Generally, the second term in equation (8-16) is referred to as amplified spontaneous emission noise. Its power can be expressed as

$$P_{ase} = (G-1)n_{sp}ph\nu\Delta\nu \tag{8-18}$$

where the spontaneous emission factor is given by [148]

$$n_{sp} = \frac{N}{N-N_0}\cdot\frac{\Gamma g}{\Gamma g - \alpha} \tag{8-19}$$

which is ranged from 1.4 to 5 for SOAs.

Another parameter characterizing the noise property of an SOA is its noise figure which is defined by the degradation in the signal-to-noise ratio (SNR) values before and after amplification. As the signal-spontaneous beat noise dominates over the spontaneous-spontaneous beat noise, the noise figure F_n can be reduced to the simple expression

$$F_n = 2n_{sp}. \tag{8-20}$$

For ideal optical amplification with $n_{sp} = 1$, the noise figure will be 2 or 3 dB, which is the minimum noise figure limited by the quantum characteristics of photons.

The derivation of equation (8-17) does not require the photon detection process. That means, the photon number fluctuation is an intrinsic process during the optical amplification. However, it is interesting and useful that almost the same results can be obtained by considering the square-law detection of an amplified signal with ASE noise. The total noise power of the received signal is given by [97, 116, 117]

$$\begin{aligned}\sigma_d^2 &= N_{thermal} + N_{shot} + N_{s-ase} + N_{ase-ase} \\ &= I_{th}^2 B_e + 2e\eta B_e\left(GP_{sig} + P_{ase}\right) + 2\eta^2 GP_{sig} P_{ase} \frac{B_e}{B_o} + \eta^2 P_{ase}^2 \frac{2B_e}{B_o^2}\left(B_o - B_2/2\right)\end{aligned} \quad (8\text{-}21)$$

where η is the quantum efficiency of the photodetector, B_e is the effective electrical bandwidth, and B_o is the optical bandwidth of the filter before the detector. The last two terms represent signal-spontaneous beat noise and spontaneous-spontaneous beat noise.

In practical amplified fiber transmission systems, the input and output coupling losses have to be taken into account when calculating the beat noises. By doing so, the first three noise terms in equation (8-21) become

$$N_{shot} = 2e\eta B_e L_{out}\left(GL_{in} P_{sig} + P_{ase}\right) \quad (8\text{-}22)$$

$$N_{s-ase} = 4GP_{sig} L_{in} L_{out}^2 P_{ase} B_e / B_0 \quad (8\text{-}23)$$

$$N_{ase-ase} = \eta^2 P_{ase} L_{out}^2 \frac{2B_e}{B_o^2}\left(B_o - B_e/2\right). \quad (8\text{-}24)$$

where L_{in} and L_{out} are the input and output coupling losses of the SOA, respectively. All the noise terms can be assumed to be Gaussian noise processes with reasonable accuracy for performance evaluation. Equations (8-21) to (8-24) have been used in the analysis in Chapter 4 and Chapter 6.

8.2.3 System Applications

In optical fiber transmission systems, SOAs can be employed as power boosters, in-line amplifiers, pre-amplifiers of optical receivers, and switching gates. Two main issues are involved in the performance of SOA-based systems. One is the ASE noise as discussed in the last section, the other is the gain saturation due to high input optical power. In general, for one input signal channel, the lowest input power level is limited by the ASE noise, while the highest one is often restricted by the gain saturation.

In contrast to EDFAs, SOAs have a much faster gain recovery time of less than 1 ns due to their short carrier life time. At a low bit rate (< 1 Gb/s), the gain saturation simply degrades the signal extinction ratio as data ONEs and ZEROs have different gains. At a much higher bit rate (> 10 Gb/s), the average saturated gain for data ONEs and ZEROs can be assumed, although the data pattern effect due to waveform distortion may be seen in the amplified signal. As the bit rate falls within 1 to 10 Gb/s, the signal will be degraded by both the reduction of the extinction ratio and waveform distortion as the SOAs are saturated.

Furthermore, if WDM signals are simultaneously amplified by an SOA, the gain to each WDM signal will be modulated by other signals when the SOA is saturated. This is because as the gain is modulated by one of the WDM signals, the remaining signals are subjected to the same modulation due to homogeneous gain saturation. This phenomena is well known as the cross-gain modulation [97]. It should be noted that for equal-power input WDM channels, the saturation power for each channel becomes $1/N$. In addition to the cross-gain modulation, WDM signals with an equal frequency spacing also suffer from another kind of inter-modulation crosstalk induced by a non-linear effect known as four-wave mixing as their frequency spacing is narrowed to a few GHz [96, 115].

SOAs can be applied to a variety of optical functional devices [78, 93]. One of the most important applications is to switch optical signals. As switching gates, three main issues are closely related to the system performance. First, the contrast ratio of SOAs has to be sufficiently high in order to achieve the required system performance. The contrast ratio can be improved by lowering the injection current for the OFF state. The second issue is the input dynamic range of SOAs. This is more important in a switching system than in a point-to-point transmission system. As mentioned before, the dynamic range of an SOA is determined by its noise characteristic and saturation power. The last one is the switching speed of SOAs. The speed is primarily determined by SOAs' carrier lifetime [77, 78]. Since the carrier life time is dependent on input signal power, the speed can be improved by increasing the input optical power. Among three issues the contrast ratio and switching speed will be measured and estimated in the next section, the input dynamic range will be studied in detail in Chapter 9.

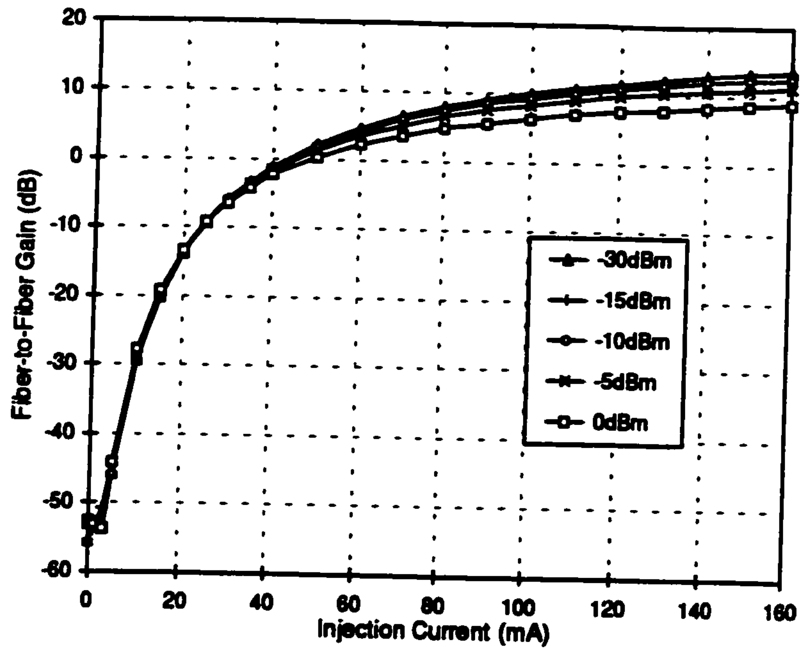

(a)

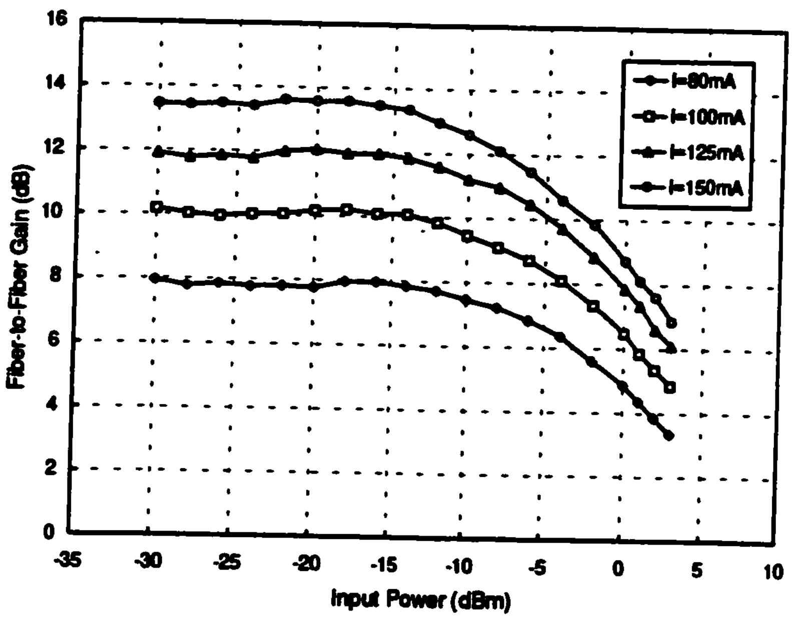

(b)

Figure 8.2: (a) Fiber-to-fiber gain versus injection current for five different input power levels. (b) Fiber-to-fiber gain versus optical input power at different injection currents.

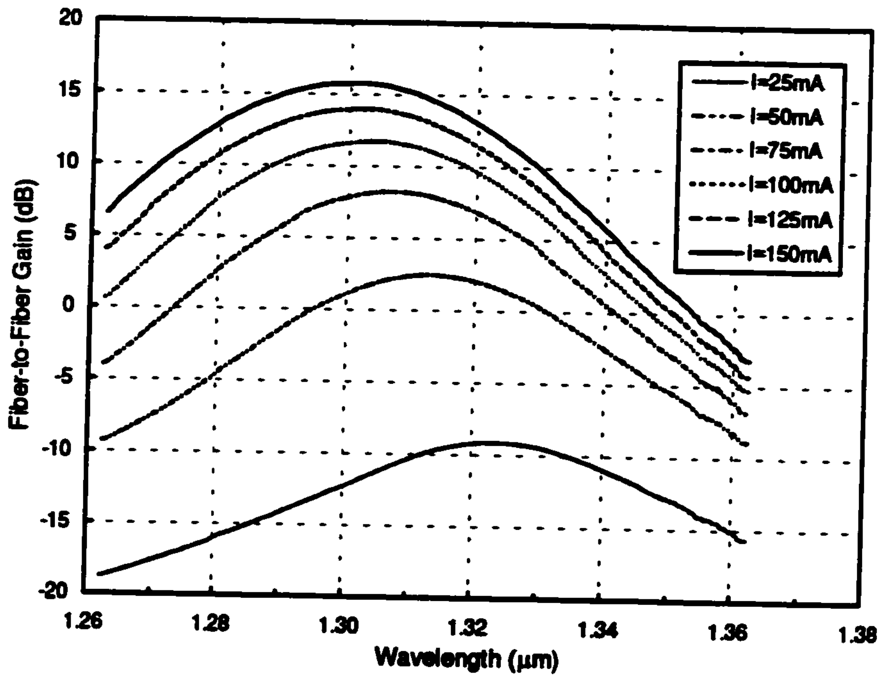

Figure 8.3: Gain profile of the SOA at different injection currents.

8.3 Characterization of Semiconductor Optical Amplifier

The SOAs used in the experiment in Chapter 4 and the next chapter are specially designed for their low polarization sensitivity with a ridge waveguide structure. A combination of 3 tensile strained QWs and 4 compressively strained QWs (3T/4C) is used to compensate for the gain difference for TE and TM modes. To reduce the facet reflections, the chips contain a 10-degree angled strip and AR coatings. All optical gains are tested at a wavelength of 1318.6 nm. The results are for a typical packaged SOA and tested at a temperature of 25 °C unless stated otherwise.

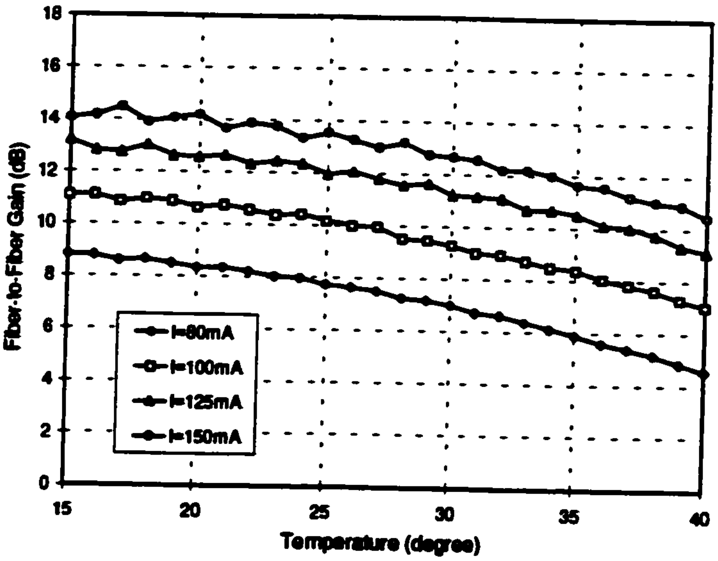

(a)

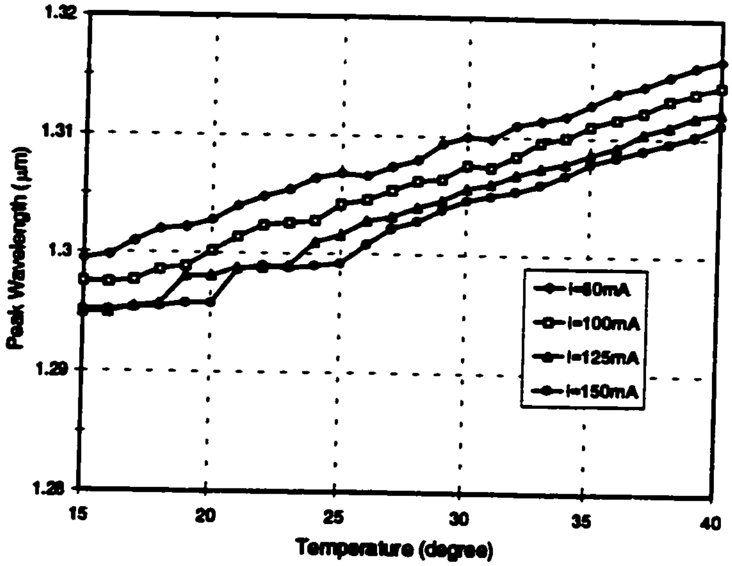

(b)

Figure 8.4: (a) Fiber-to-fiber gain versus temperature of the SOA at different injection currents. (b) Peak wavelength of the gain profile versus temperature of the SOA.

8.3.1 Gain

Figure 8.2(a) shows the fiber-to-fiber gain as a function of the injection current for different input optical power levels. At a low input power level the gain can be up to 10

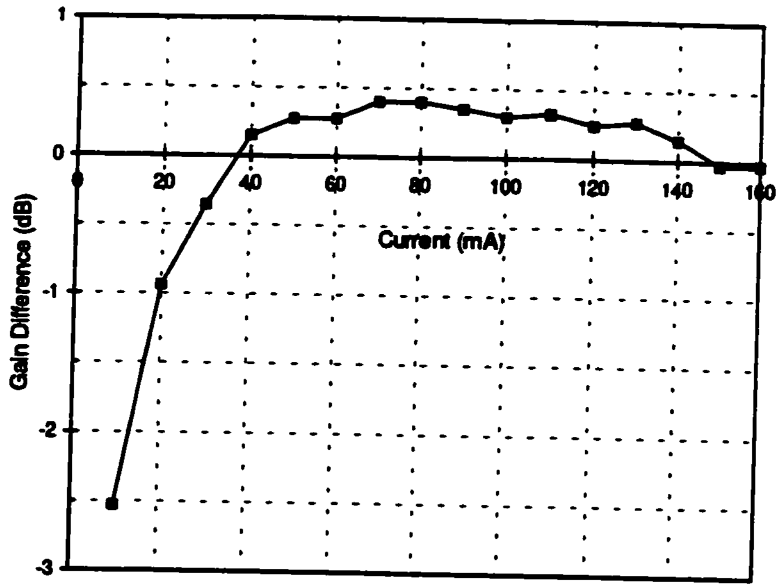

Figure 8.5: Difference of the maximum and minimum gains versus injection current.

dB at an injection current of 100 mA. Gain saturation characteristic is shown in Figure 8.2(b) for different injection currents. The output saturation power up to 7 dBm can be calculated from the figure.

The gain spectra versus wavelengths at different injection currents are shown in Figure 8.3. These gain profiles are derived from the spontaneous emission spectra by calibrating the gain at a wavelength of 1318.6 nm. It can be seen that the gain peak is shifted to a shorter wavelength as the injection current increases. The 3-dB optical bandwidth is about 40 nm.

Temperature sensitivity of the optical gain and gain profiles are also tested. Figure 8.4(a) illustrates the change of the fiber-to-fiber gain with SOA's temperature. A gain change of up to 4 dB is observed for the temperature change from 0 to 40 °C. The change of the peak wavelength of the gain profile is about 15 nm for the same temperature range, as shown in Figure 8.4(b). From Figures 8.3 and 8.4, it can be concluded that the gain change at a wavelength shorter than the peak wavelength would be larger than 4 dB

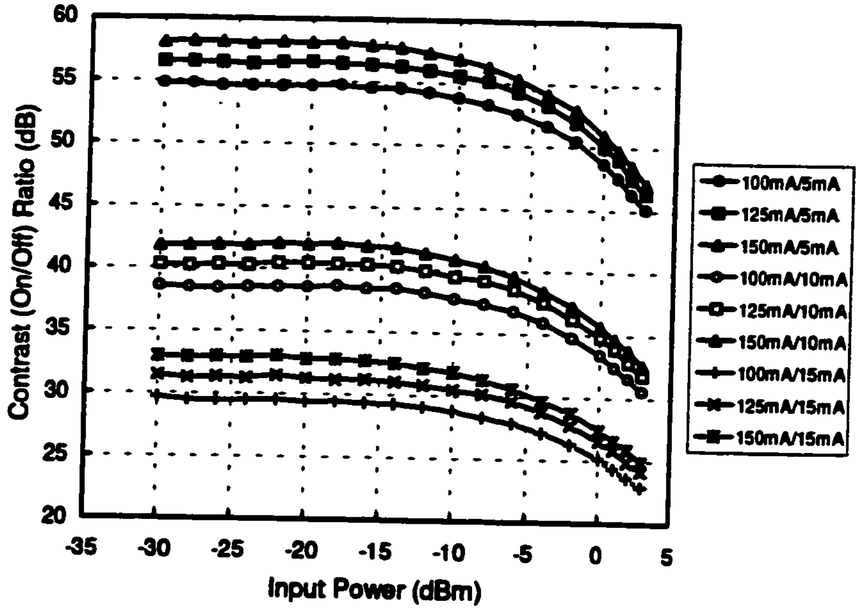

Figure 8.6: Contrast ratio versus optical input power for different combinations of injection currents for the ON and OFF states.

since the gain spectral profile shifts to a longer wavelength with the increase of temperature.

The SOA that we tested performs very well in terms of polarization sensitivity. The maximum and minimum gains have been measured by adjusting the polarization state of the input signal and are shown in Figure 8.5. It can be seen that the polarization sensitivity is less than 0.5 dB at the injection current from 40 mA to 160 mA.

8.3.2 Contrast Ratio

Figure 8.6 shows three sets of contrast ratios with different combinations of injection currents for the ON and OFF states. A high contrast ratio over 55 dB can be achieved with this SOA. Due to the gain saturation in the ON state and the saturated absorption in the OFF state, the contrast ratios deteriorate as the input optical power increases over -10 dBm. It can be seen that the contrast ratio of an SOA strongly depends on its gain in the OFF state since increasing the injection current for the ON state does not change the gain very much. Although a low injection current for the OFF state is preferred for a high

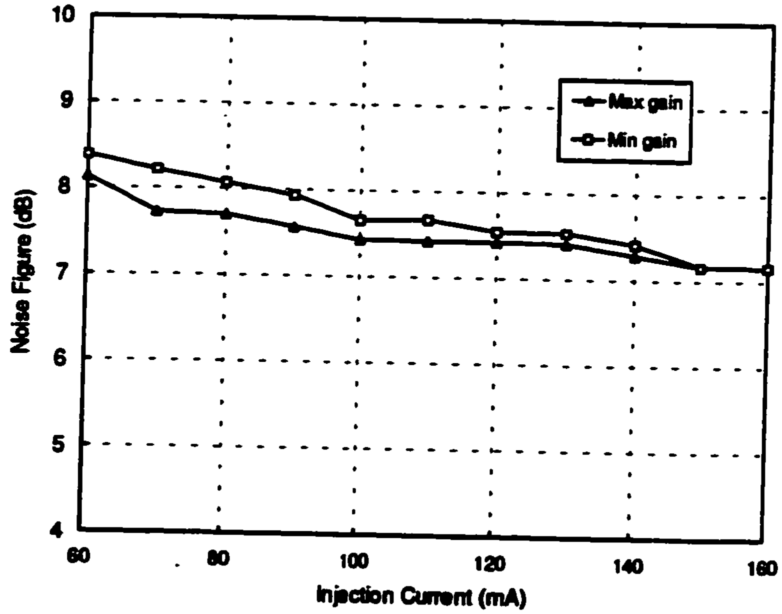

Figure 8.7: Fiber-to-fiber noise figure versus injection current of the SOA.

contrast ratio, but it will increase the switching rise time [77, 78] and may also make it difficult to protect the SOA.

8.3.3 Noise Figure

Figure 8.7 shows the measured fiber-to-fiber noise figure versus the injection current of the SOA. The maximum and minimum noise figure curves correspond to the minimum and maximum gains measured by adjusting the polarization state of the input signal. The input optical power is set to -20 dBm. For an injection current of over 100 mA, the minimum noise figure is less than 7.5 dB.

8.3.4 Switching Speed

Due to a lack of a high-speed pulse generator, the speed of switching has not been fully characterized. Only the electrical modulation response was measured as illustrated in Figure 8.8. The 3-dB bandwidth is about 600 MHz at an optical input power of 3 dBm. Thus, its rise time can be estimated to be about 580 ps. Reducing input optical power to -10 dBm, the rise time increases up to 850 ps. The measured rise times are longer than the reported results [153]. This could be improved by optimizing the packaging design.

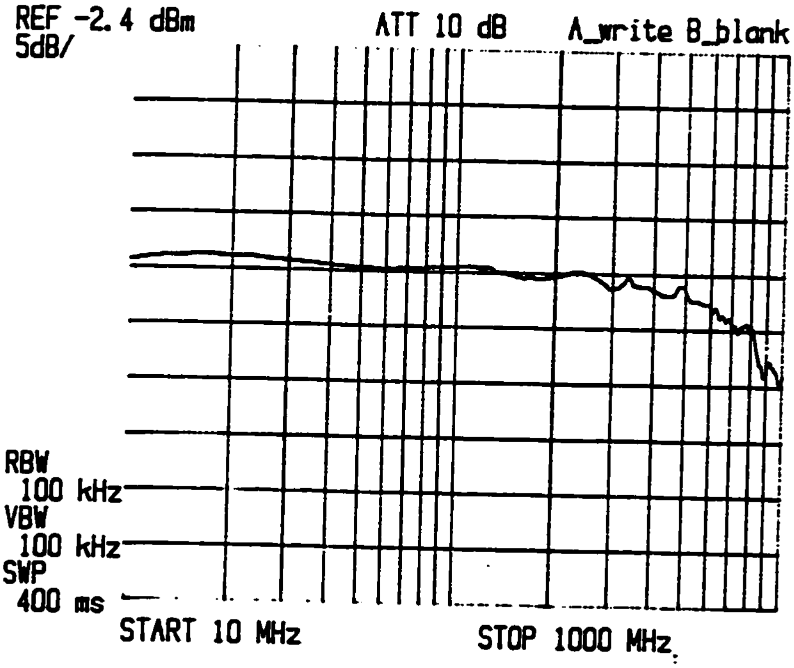

Figure 8.8: Frequency response of the SOA modulated by an injection current. The RF input power is 22 dBm and the optical input power of the SOA is 3 dBm.

In addition, other four SOAs of the same kind have also been tested. Figure 8.9 shows the fiber-to-fiber gains and noise figures as functions of the injection currents. Two of them have no temperature controllers as indicated by 'nc' in the legends. These four SOAs show similar optical gains and noise figures as one that we tested before.

8.4 Conclusions

In this chapter, the fundamentals of semiconductor optical amplifiers were briefly introduced. The gain and noise characteristics were discussed in detail. Also, the several important system issues were addressed. Further, we presented the tested results of a typical SOA used in our system demonstration and experiments. The SOA performs very well in terms of polarization sensitivity, contrast ratio, and noise figure. The same type of SOA will be further investigated from a system point of view in the next chapter.

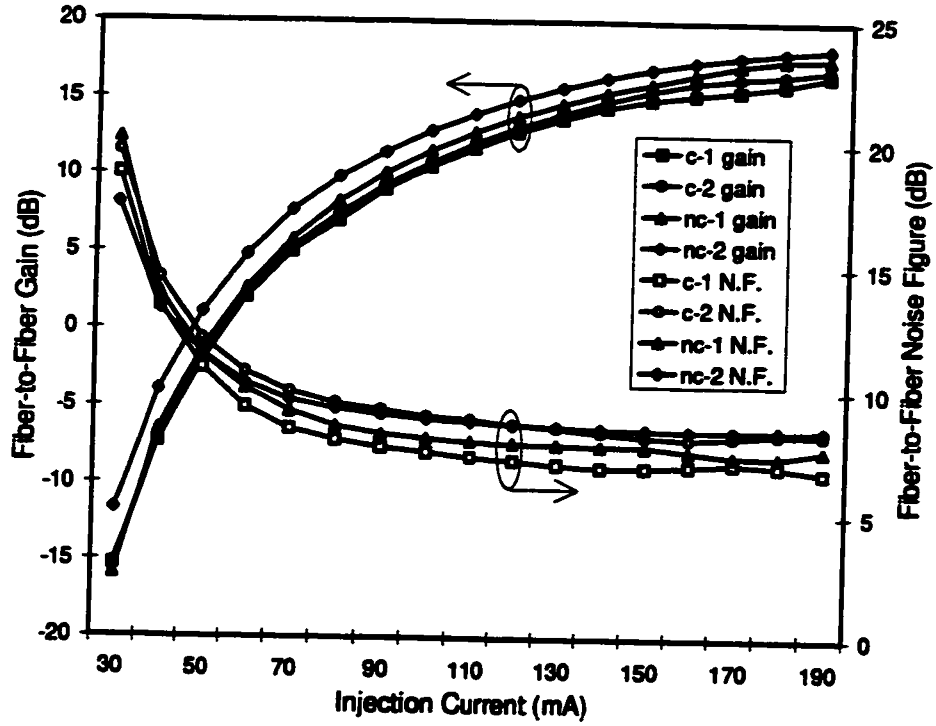

Figure 8.9: Fiber-to-fiber gain and noise figure versus injection current for other four SOAs.

9. System Applications of Semiconductor Optical Amplifiers

9.1 Introduction

In Chapter 8, we characterized available SOAs, but only on a component level basis. From a system point of view, other issues in SOA-based optical switching systems have to be considered [154, 155, 156, 157]. One of these is an input dynamic range. Optical switching systems should be designed to have a large input dynamic range to accept different input signal power levels. Several papers [146, 156, 157, 158] investigated an input dynamic range of SOAs by using numerical simulation but only very few experimental studies were done [57, 155]. Most of simulation studies were based on lumped SOA models [146, 157] with no direct comparison with experimental studies. In this chapter, we concentrate on the transmission performance of SOA-based switching systems, particularly the input dynamic range. First, experiments are carried out to measure the input dynamic ranges of an single-stage SOA system and a three-stage SOA system. Then, numerical simulations are used to compare with the experiments and to further predict the performance at higher bit rates.

9.2 Transmission Experiments

9.2.1 Experimental Setup

The experimental setup for an SOA-based system is shown in Figure 9.1. Figure 9.1(a) is for a single-stage SOA system. The transmitter is a directly modulated DBF laser operating at 1302.7 nm. The signal is a PRBS of a length 2^7-1 at a bit rate of 1 Gb/s. At the receiver end, an optical filter with a bandwidth of 1.6 nm is inserted before the receiver to reduce the ASE noise. The signal is detected by a high-sensitivity Ge-APD receiver and then fed to a BER tester. Optical isolators are utilized before and after the SOA in order to avoid reflections.

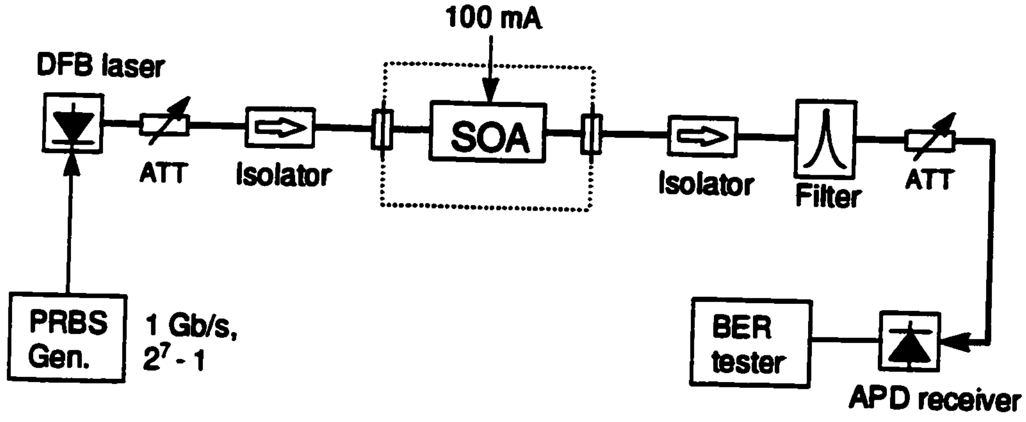

(a)

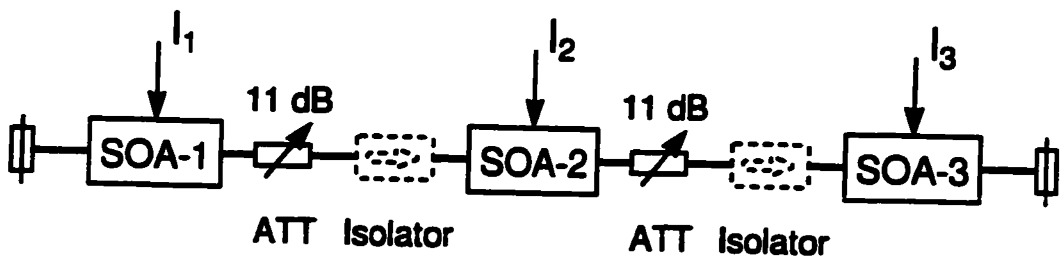

(b)

Figure 9.1: (a) Experimental setup for a single-stage SOA system. (b) Setup for a three-stage SOA system.

To compensate for splitting losses in a large switching system, we may use an SOA at each input and output as an in-line amplifier. This is referred to as a three-stage SOA system. For a three-stage SOA system, the setup in Figure 9.1(b) replaces the single SOA in Figure 9.1(a). The losses of 11 dB between the SOAs are set to simulate the splitting loss and typical insertion loss in an 8×8 SOA-based switch.

9.2.2 Results and Discussions

In the following, the power penalty is defined as the increase in the receiver sensitivity at a BER of 10^{-9} for a certain input power level compared to the back-to-back sensitivity, and an input dynamic range is defined as the optical input power range within which a system introduces a power penalty of less than 1 dB.

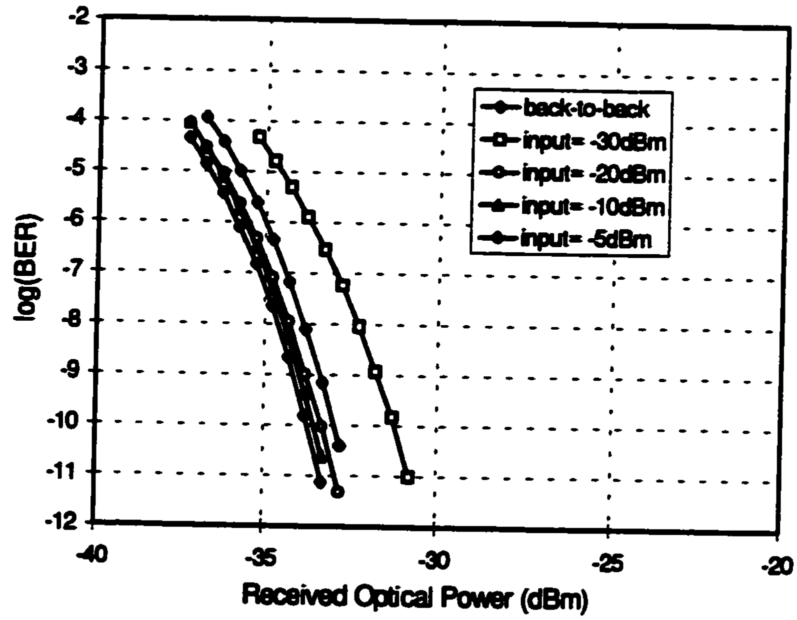

Figure 9.2: Bit error rate versus received optical power for the single-stage SOA system.

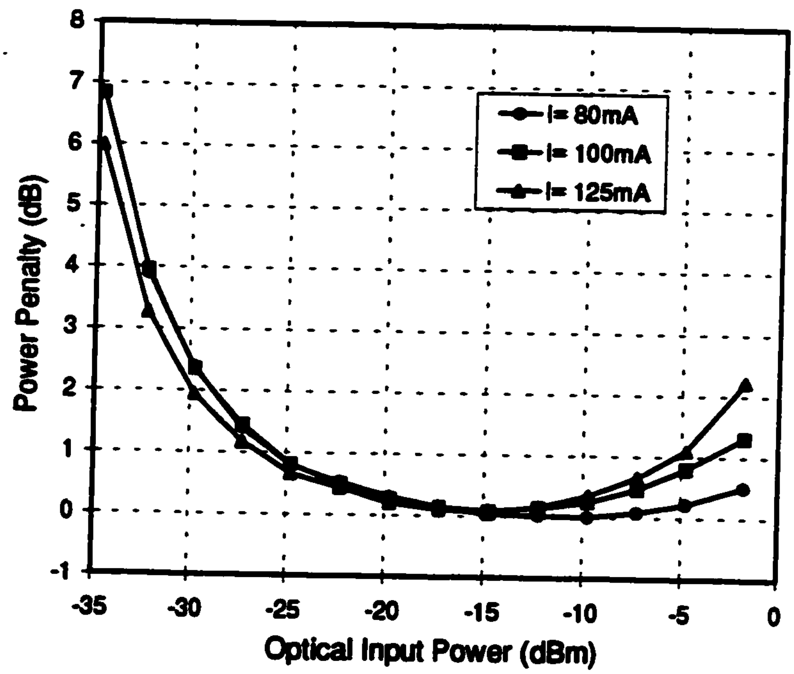

Figure 9.3: Power penalty versus optical input power for three different injection currents of the SOA in the single SOA system.

Figure 9.2 shows the BER as a function of the received optical power for a single-stage SOA system with an injection current of 100 mA. At a very low input power level such as -30 dBm, there is a relatively large power penalty of about 2.5 dB. As the input power increases, the power penalty goes down, and then goes up again. To illustrate this penalty trend clearly, we measured the power penalty against the input optical power. Figure 9.3 shows the penalty curves for three different injection currents of the SOA. At a low input optical power, the power penalty mainly results from SOA's ASE noise since there is too much ASE noise compared with the signal [57, 155]. As the input power increases, it can be expected that the penalty due to ASE noise decreases. However, further increasing the input optical power will saturate the gain of the SOA and introduce new degradation, which results from the gain reduction and waveform distortion [57, 158]. Thus, there is the optimum optical input power level at which the total effect of ASE and gain saturation is minimized. The optimum input power for the tested SOA is about -15 dBm at injection currents 100 mA and 125 mA, and -10 dBm at an injection current of 80 mA.

By comparing the power penalties for three different injection currents of the SOA, it is noted that at the low input power side, a higher injection current makes a higher gain thus a lower penalty, while at the high input power side, the same higher injection current renders a lower input saturation power as shown in Figure 8.3(b) thus a higher penalty. For the injection currents of 125 mA, 100 mA, and 80 mA, the input dynamic ranges are 21 dB , 22 dB, and over 25 dB, respectively. An SOA with a lower injection current tends to have a wider input dynamic range.

It should be pointed out that the power penalty for high optical input power in Figure 9.3 might be under-measured because of a non-ideal electrical driving signal to the DFB laser. The reason for this is that the gain saturation could 'correct' a non-ideal optical signal by mitigating the distortion in the optical signal [159]. When we use long PRBS word lengths of 2^{15}-1 and 2^{23}-1, we observed some negative penalty, that is, an improved receiver sensitivity compared to the back-to-back one. To reduce this effect on measurement, the shortest word length of 2^{7}-1 is used for all measurements.

Table 9.1: Three current combinations for a three-stage SOA system

Injection currents ↘	SOA 1	SOA 1	SOA 1
Combination 1	100 mA	100 mA	100 mA
Combination 2	70 mA	100 mA	150 mA
Combination 3	150 mA	100 mA	70 mA

For the three-stage SOA system, we use three combinations of injection currents as listed in Table 9.1 in order to study the influence of the SOA gains on the power penalty and input dynamic range. The total unsaturated gains for all three combinations are approximately the same.

Figure 9.4 shows the measured BER as a function of the received optical power for the first combination of injection currents. Input optical power of the first SOA is set at -20 dBm. For this combination, optical isolators improve the receiver sensitivity by 0.15 dB.

For the second and third combinations of injection currents, the power penalty is measured against the optical input power, as shown in Figure 9.5. At a low optical input power level, the third combination performs better than the second combination as the system performance is limited by the ASE noise, whereas at a high optical input power level, the second combination performs better than the third combination as the system performance is limited by the gain saturation. Although a high injection current of the first SOA (high gain and low noise figure) can extend the input power level to the lower end, the high gain makes the SOA easily saturated so that the highest optical input power is lower. The systems with the second and third combinations of injection currents have approximately the same input dynamic range, about 11 dB. From Figure 9.5, it can also be seen that optical isolators do improve the system performance at the low optical input power end, while at the high input power end the curves show better performance with no isolators. A possible reason is that as the SOA is saturated, the backward ASE noise with a complementary form of the input signal could compensate for the degradation due to the gain saturation of the first and/or second SOAs.

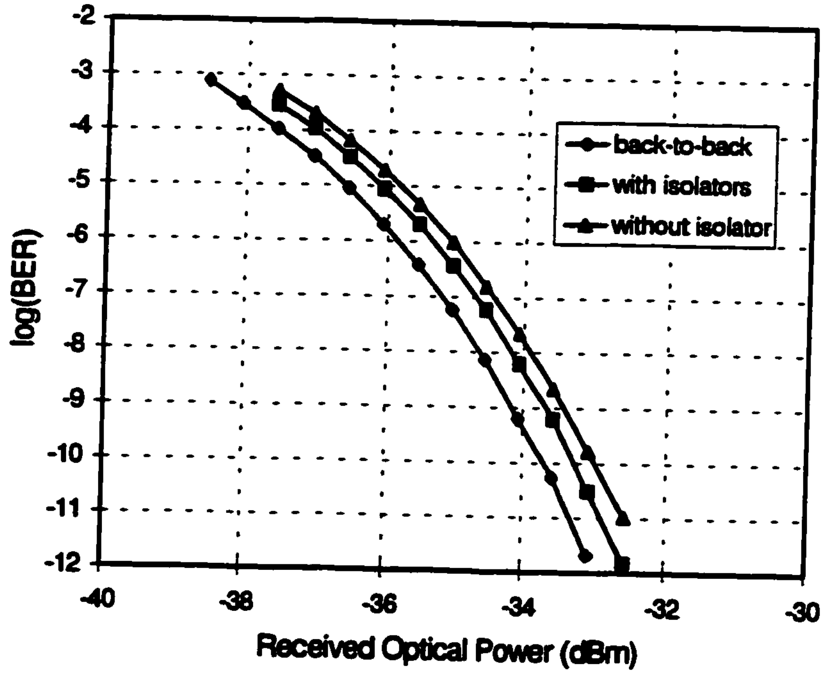

Figure 9.4: Bit error rate versus received optical power for the three-stage SOA system with the first combination of the currents.

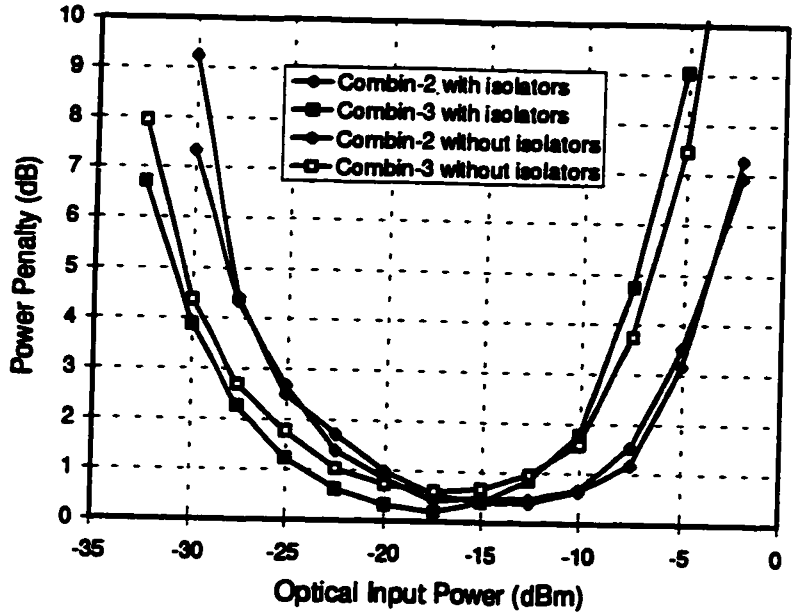

Figure 9.5: Power penalty versus optical input power for the three-stage SOA system.

9.3 System Simulation

Figure 9.6 shows the schematic diagram of the simulated SOA system, which is similar to the experimental setup in Figure 9.1(a). A time-domain model is used to simulate this system. For the sake of simplicity, several assumptions are made hereafter. First, we neglect all effects of fiber except for its attenuation. Second, we assume that the an ideal electrical signal from a PRBS generator directly modulates a DFB laser with an ideal response. Third, optical isolators are used between SOAs so that any reflections and backward ASE noise are ignored. Also, ideal clock recovery (timing) is assumed for the threshold detection.

9.3.1 System Model

First of all, we describe the model of SOAs used in the simulation. To effectively incorporate the gain saturation effect, we use a distributed numerical model of the SOAs [78, 160] instead of a lumped model. As shown in Figure 9.7, an SOA is divided into M sections ($M = 20$), each of which is assumed to have a constant carrier density $N(z_m, t_k)$. At each time step t_k, the carrier density at the m-th section is obtained by solving the following difference rate equation

$$\frac{N(z_m, t_k) - N(z_m, t_{k-1})}{\Delta t} = \frac{I}{eV} - R(N(z_m, t_k)) - S_{signal}(z_m, t_k) \tag{9-1}$$

where m is the section index, k is the time index, I is the injection current, V is the cavity volume, e is the elementary charge, $R(N(z_m, t_k))$ is the spontaneous recombination rate given by equation (8-7), and $S_{signal}(z_m, t_k)$ is the recombination rate due to the stimulated emission caused by the signal. Here, the internal ASE is neglected in equation (9-1) because of its minor effect [57].

The term $S_{signal}(z_m, t_k)$ is given as

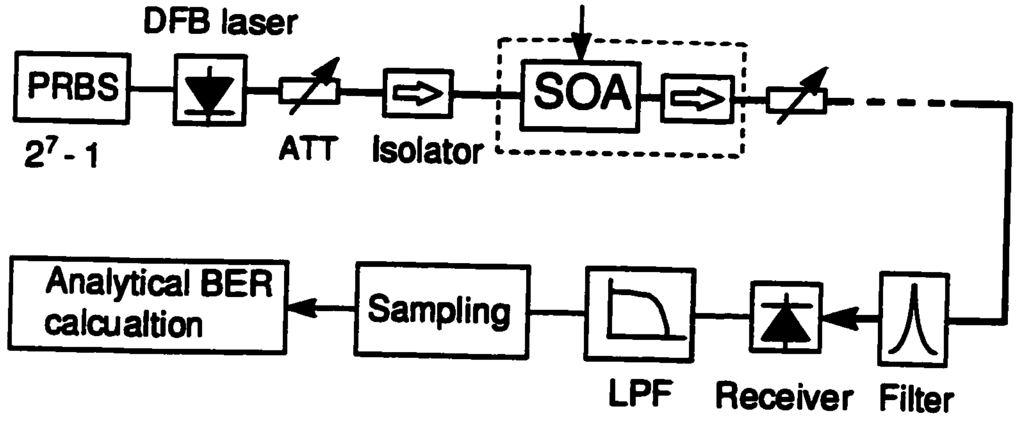

Figure 9.6: Schematic of an SOA-based simulation system.

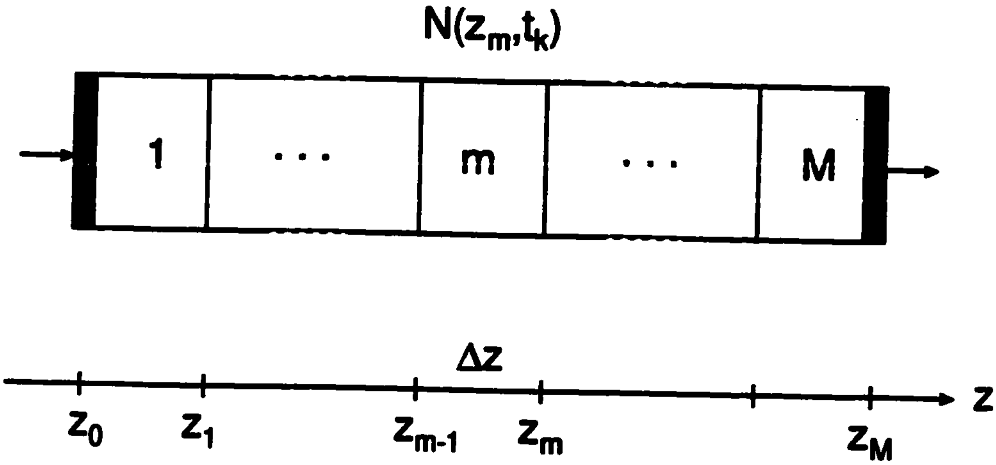

Figure 9.7: Distributed SOA model.

$$S_{signal}(z_m,t_k)=\frac{P_{sig}(z_{m-1},t_k)}{hv}\cdot\frac{\Gamma g_m(z_m,t_k)}{g(z_m,t_k)\Delta z\cdot wd}\cdot\left[\exp\left(g_m(z_m,t_k)\Delta z\right)-1\right] \qquad (9\text{-}2)$$

where h is Planck's constant, v is the optical frequency of the signal, Γ is the optical confinement factor, Δz is the length of a section, w and d are the width and thickness of the cavity, respectively. $g_m(z_m,t_k)$ and $g(z_m,t_k)$ are the material gain coefficient and net gain per unit length which are calculated with equations (8-1) and (8-3), respectively.

$P_{sig}(z_{m-1}, t_k)$ is the optical input power of the m-th section, which can be iteratively calculated as

$$P_{sig}(z_{m-1}, t_k) = P_{sig}(z_{m-2}, t_k)\exp\left[g(z_{m-1}, t_k)\Delta z\right] \tag{9-3}$$

with the optical input power of the SOA as $P_{sig}(z_0, t_k)$. Here, the signal delay due to the SOA cavity length has been neglected since the signal bit duration is much longer than the SOA delay.

After solving the rate equation at each section, the gain of the SOA can be calculated by

$$G(t_k) = \exp\left[\sum_{m=1}^{M}\left(\Gamma g_m(z_m, t) - \alpha\right)\Delta z\right] \tag{9-4}$$

and the ASE noise spectral density from the SOA is calculated by

$$R_{ase}(t_k) = \left(G(t_k) - 1\right)h\nu p n_{sp} \tag{9-5}$$

with an estimated spontaneous emission factor n_{sp} obtained from the measured noise figures in Figure 8.9, and the effective number of modes $p = 2$.

An optical input signal to the system is a PRBS with a word length of 2^7-1 in the non-return-to-zero (NRZ) format. The time step is set at 1/64 bit duration. At the receiver side, an optical filter is employed to filter out ASE noise. After detected by a photo-detector, the signal passes through an electrical low-pass filter. The filter here is a fourth-order Bessel filter with a cutting frequency of 0.75 times bit rate, which is standardized for SONET transmission systems [161, 162]. The filter for simulation is generated with the Matlab signal processing toolbox [163]. The filtering is performed by a direct convolution between the signal input and the impulse response of the filter. After the filter, the sampling instant for the threshold detection is chosen as the one with the largest eye opening over the bit duration.

As for the electrical noise, as discussed in the previous chapter, there are five noise terms, namely, receiver noise (thermal noise), signal shot noise, ASE shot noise, signal-ASE beat noise, and ASE-ASE beat noise. All the noise terms except for the receiver noise are time-dependent due to the gain variation during SOA amplification. Thus, these noise processes are not ergodic and the noise terms can not be simply calculated with the effective bandwidth of the low-pass filter. A reported method [57] for bypassing this difficulty is to assume that the optically induced noises have a δ-function relative to the modulation time constant and that the impulse response of the low-pass filter is rectangular, so that the signal and ASE noise can pass through the filter separately and then calculate the beat noise terms with the filtered signal and ASE noise. This approach can not be justified when there is a large signal waveform distortion due to the gain saturation.

We have noted that a Bessel filter has a very important property that within the pass band, it has a linear phase change with the frequency so that the signal and noises at different frequencies within the pass band will have the same time delay. Thus, the sampling instant for the threshold detection can be traced back to the corresponding point before the filter, at which the noise terms are calculated by using the equivalent electrical bandwidth of the low-pass filter.

With the filtered signal and the noise terms, the average BER can be calculated by

$$P_e = \min_T \left(\frac{1}{N_b \sqrt{2\pi}} \sum_{i=1}^{N_b} \int_{Q_i}^{\infty} \exp\left(-t^2/2\right) dt \right) \tag{9-6}$$

$$Q_i = \begin{cases} \dfrac{S_{1,i} - T}{\sqrt{N_{1,i}}}, & \text{for ONEs} \\[2ex] \dfrac{T - S_{0,i}}{\sqrt{N_{0,i}}}, & \text{for ZEROs} \end{cases} \tag{9-7}$$

where $N_b = 127$ (the number of PRBS bits), $S_{1,i}$ and $S_{0,i}$ are the sampled values of the electrical signal for data ONEs and ZEROs, $N_{1,i}$ and $N_{0,i}$ are the total noise power per

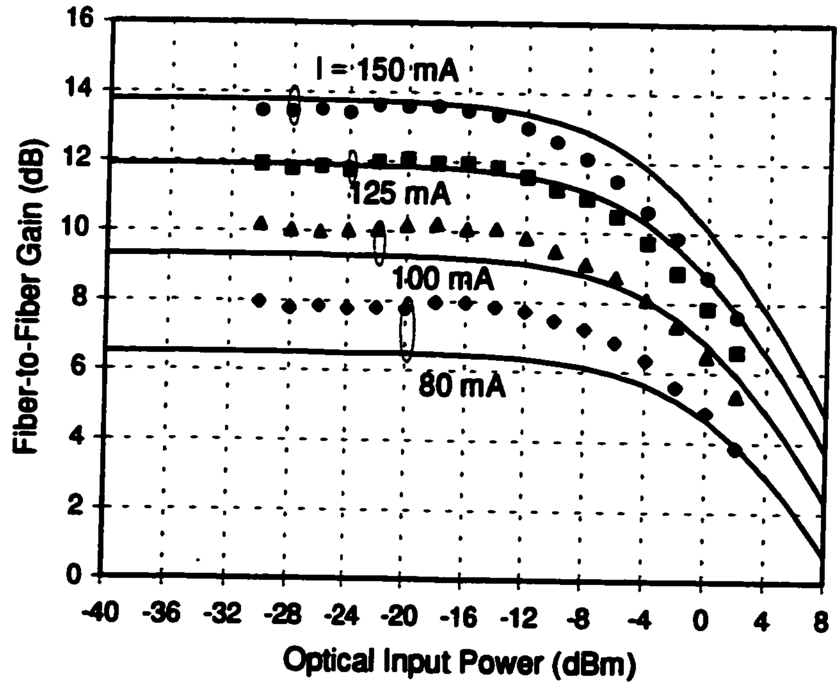

Figure 9.8: Fiber-to-fiber gain versus optical input power for the simulated SOA with four different injection currents. Solid lines denote the simulation results and symbols denote the tested results.

unit load resistance which are calculated by using equation (8-21). The optimum threshold is set to minimize the average BER. The values of all the parameters for the simulation are listed in Table 9.2 at the end of the chapter.

9.3.2 Numerical Results and Discussions

Figure 9.8 shows the gain versus the optical input power of the simulated SOA for four different injection currents. The 3-dB input and output coupling losses are included here. Compared with the tested results, the simulation results show a little bit higher saturation power.

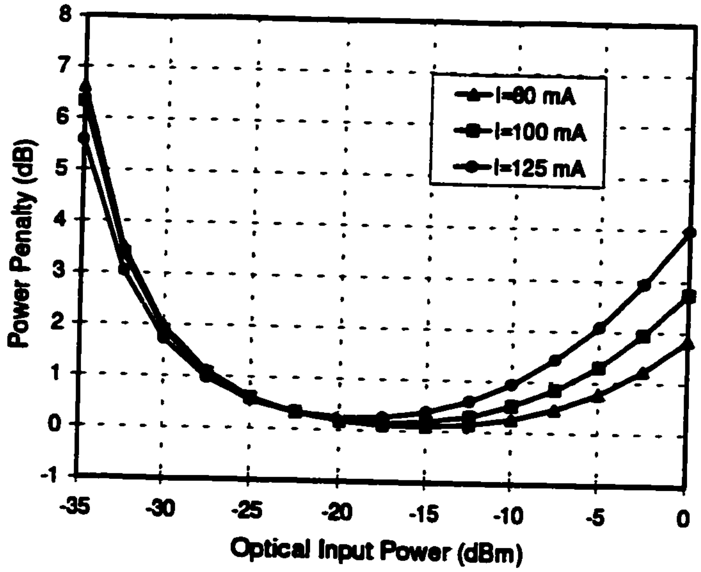

Figure 9.9: Power penalty versus optical input power for a single-stage SOA system, evaluated using simulation.

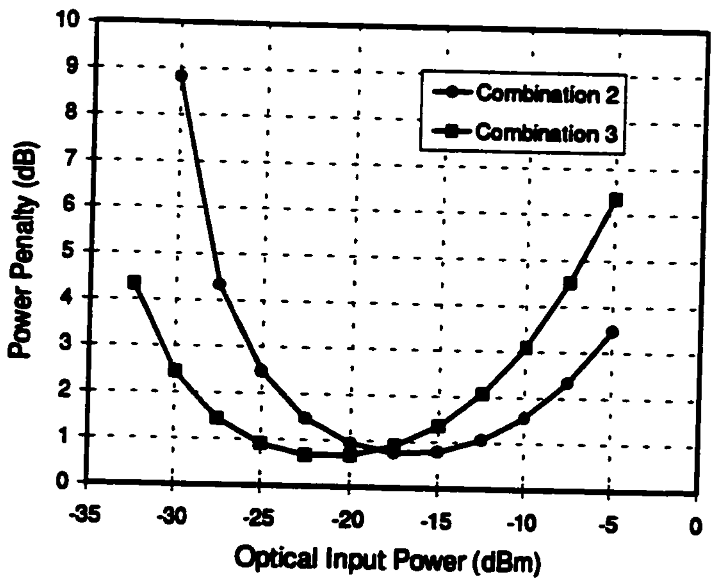

Figure 9.10: Power penalty versus optical input power for a three stage SOA system with the second and third combination of the currents, evaluated using simulation.

To compare to the experimental results, the dynamic ranges for three different injection currents for a single-stage SOA system at a bit rate of 1 Gb/s are evaluated using simulation. The simulation was done with an APD receiver and no low-pass filter. The electrical bandwidth is obtained from the frequency response of the receiver. The parameters of the receiver are listed in Table 7.1. Figure 9.10 shows the simulation results. They have a good agreement with the experimental results for low input power. For high optical input power, the simulation shows a larger power penalty than the experiment. This could be due to the mitigation of the distortion of the input signal by the gain saturation as mentioned in the last section.

We use the same system parameters as those for Figure 9.9 to simulate a three-stage SOA system for the second and third combinations of injection currents listed in Table 9.1. The simulation results in Figure 9.10 show a reasonable agreement with the experimental results. The third combination performs better for low input powers, while the second combination does better for high input powers. The input dynamic ranges for these two combinations are very close although the optimum input power levels are different.

In addition to the comparison with the experiments, we further investigate the system performance with simulation at higher bit rates at which we lack facilities to test the system. In the following simulations, we use a *p-i-n* photodetector and a standard SONET low-pass filter. The quantum efficiency of the *p-i-n* is 0.85, and the thermal noise power density of the receiver is 8.5 pA/√Hz that is assumed to be the same at all bit rates.

For a single-stage SOA system, Figure 9.11 shows the power penalty as a function of optical input power at six different signal bit rates. The injection current of the SOA is set at 100 mA. As the bit rate increases, the power penalty increases at the low input power end because the signal-spontaneous and spontaneous-spontaneous beat noises are enhanced with enlargement of the receiver electrical bandwidth. At the high input power end, the power penalty is primarily determined by the gain saturation. At a very low bit rate (< 0.5 Gb/s), the signal mainly suffers from signal extinction ratio reduction although there is some distortion at the leading edge of the data ONEs, with little effect on the sampling instant for the threshold detection. In this case, the gains for data ONEs and ZEROs can be evaluated separately. As the bit rate increases, the leading edge distortion of data ONEs starts to have an effect on the threshold detection whereas the signal extinction ratio is not improved high enough to compensate for the distortion, thus the degradation due to the gain saturation rises. From Figure 9.11, it can be noted that at a bit rate of around 2.5 Gb/s the total degradation resulting from the waveform distortion and signal extinction ratio reduction reaches its maximum. Then, the degradation decreases as the bit rate increases. The input dynamic range at different bit rates is plotted in Figure 9.13, ranging from 22 to 26 dB.

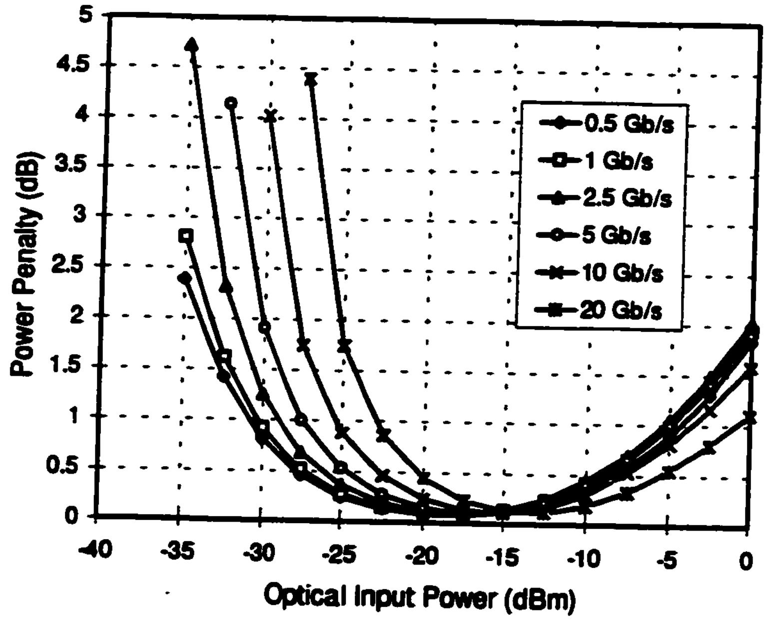

Figure 9.11: Power penalty versus optical input power for a single-stage SOA system at six different bit rates, evaluated using simulation.

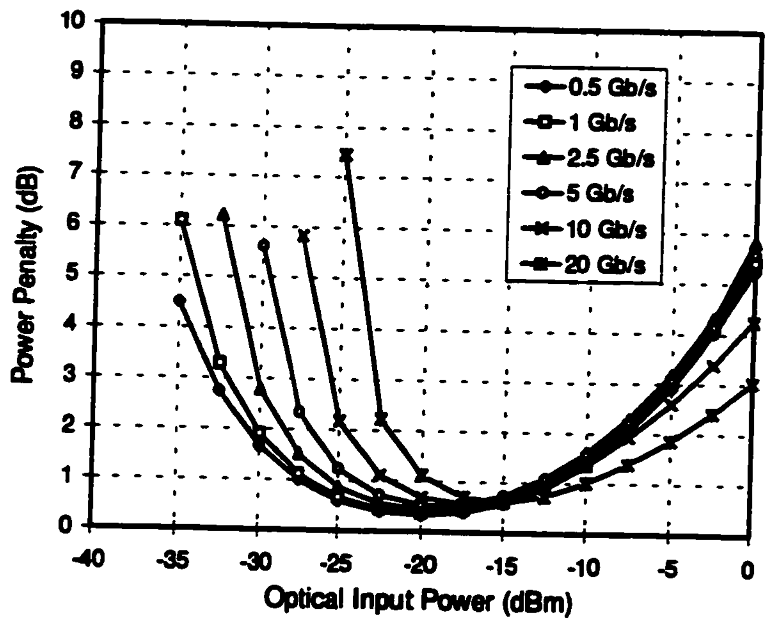

Figure 9.12: Power penalty versus optical input power for a three-stage SOA system at six different bit rates, evaluated using simulation.

For a three-stage SOA system, we only simulate the first combination of injection currents, that is, injection currents of the three SOAs are each 100 mA. The simulation

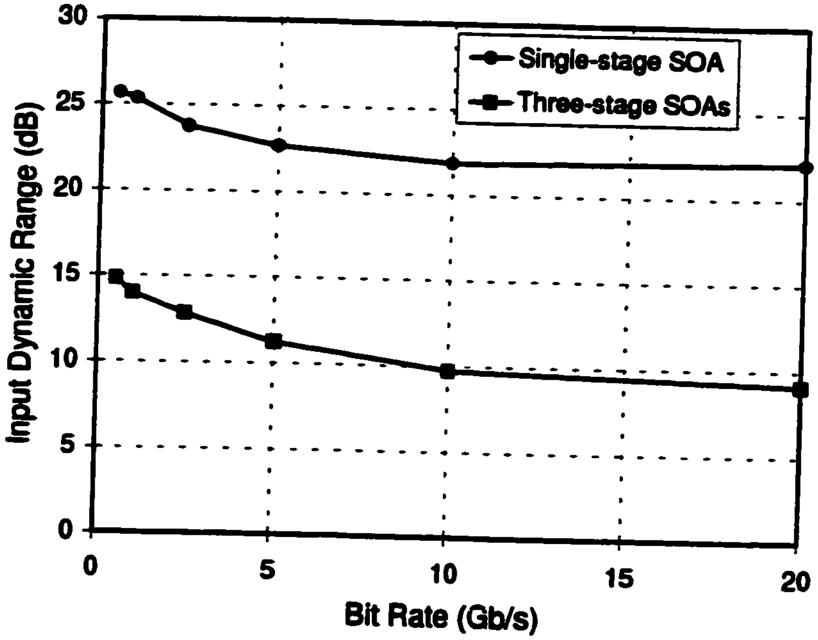

Figure 9.13: Input dynamic range versus signal bit rate for single-stage and three-stage SOA systems, evaluated with simulation.

results are plotted in Figure 9.12. The same penalty trend is obtained as that in Figure 9.12 except a smaller input dynamic range as shown in Figure 9.13.

9.4 Conclusions

In this chapter, the input dynamic range of SOA-based systems has been investigated experimentally and further studied with numerical simulation. It is found that for a single-stage SOA system, a lower injection current can have a larger input dynamic range because of a higher input saturation power. For a three-stage SOA system, the different current combinations show the similar input dynamic range although the absolute input power ranges are different. Optical isolators between the SOAs only improve the performance marginally. Further simulations at higher bit rates show that SOA-based systems can have large input dynamic ranges. It can be over 20 dB for a single-stage SOA system and about 10 dB for a three-stage SOA system at a bit rate of 20 Gb/s. Thus, SOA-based switching systems can operate at up to 20 Gb/s with a reasonably large input dynamic range.

Table 9.2: Symbols and default values of simulation parameters.

Parameters	Symbols	Values
SOA Parameters		
Cavity length	L	750×10^{-6} m
Cavity width	w	2.0×10^{-6} m
Cavity thickness	d	0.15×10^{-6} m
Optical confinement factor	Γ	0.05
Transparent carrier density	N_0	1.2×10^{24} m^{-3}
Gain constant	a_1	8.9×10^{-20} m^{-2}
Gain constant	a_2	1.8×10^{19} m^{-3}
Peak wavelength at transparent state	λ_0	1.306×10^{-6} m
Wavelength shift constant	a_3	1.35×10^{-32} m^4
Loss coefficient	α	2.0×10^3 m^{-1}
Non-radiate recombination coeff.	A	2.0×10^8 s^{-1}
Radiative recombination coefficient	B	8.5×10^{-17} m^3/s
Auger recombination coefficient	C	4.7×10^{-41} m^6/s
Number of sections	M	20
Input and output coupling loss	L_{in}/L_{out}	3 dB
Equivalent ASE noise bandwidth	$\Delta\lambda$	35×10^{-6} m
System Parameters		
Signal bit rate	B_r	1.0 Gb/s
Signal wavelength	λ	1.3×10^{-6} m
Electrical bandwidth	B_e	1.2 GHz for APD, $0.75 \cdot B_r$ for *p-i-n*
Input signal extinction ratio	$1/r$	10 dB
Bandwidth of optical filter	B_o	1.6×10^{-9} m

10. Bi-directional Optical Cross-Connect Using Semiconductor Optical Amplifiers

10.1 Introduction

Recently, bi-directional transmission has become an attractive option for upgrading existing fiber transmission systems [164, 165, 166, 167]. There are two wavelength schemes for bi-directional transmission. One is using the same optical wavelength for the two signal channels. Another scheme is using two different wavelengths for the forward and backward channels. Although the single wavelength scheme is easy and simple to be implemented, the reflections and back-scattering can severely degrade the system performance [168, 169]. In contrast, bi-directional systems using two wavelengths can have much better transmission performance by eliminating reflections and back-scattering with optical filters. Nevertheless, optical subsystems such as optical switches or cross-connects have to be redesigned to support two-wavelengths bi-directional operation.

In this chapter, we propose an SOA-based bi-directional optical cross-connect for bi-directional transmission systems using two wavelengths. A main feature of the SOA-based bi-directional cross-connect is a wide optical bandwidth for easy channel separation. In the rest of the chapter, we will investigate the feasibility of the SOA-based bi-directional optical cross-connects, experimentally.

10.2 Experimental Setup

The bi-directional optical cross-connect is an SOA-based splitter-combiner space switch. Figure 10.1(a) shows a 2×2 cross-connect where there is only a single-stage SOA in each cross-connection path. For a large cross-connect, we may use an SOA at each input and output port in order to compensate for the losses from optical splitters and combiners. To investigate both situations, we use two cross-connect arrangements in our experiment, as shown in Figure 10.1(b), referred to as a single-stage-SOA and three-

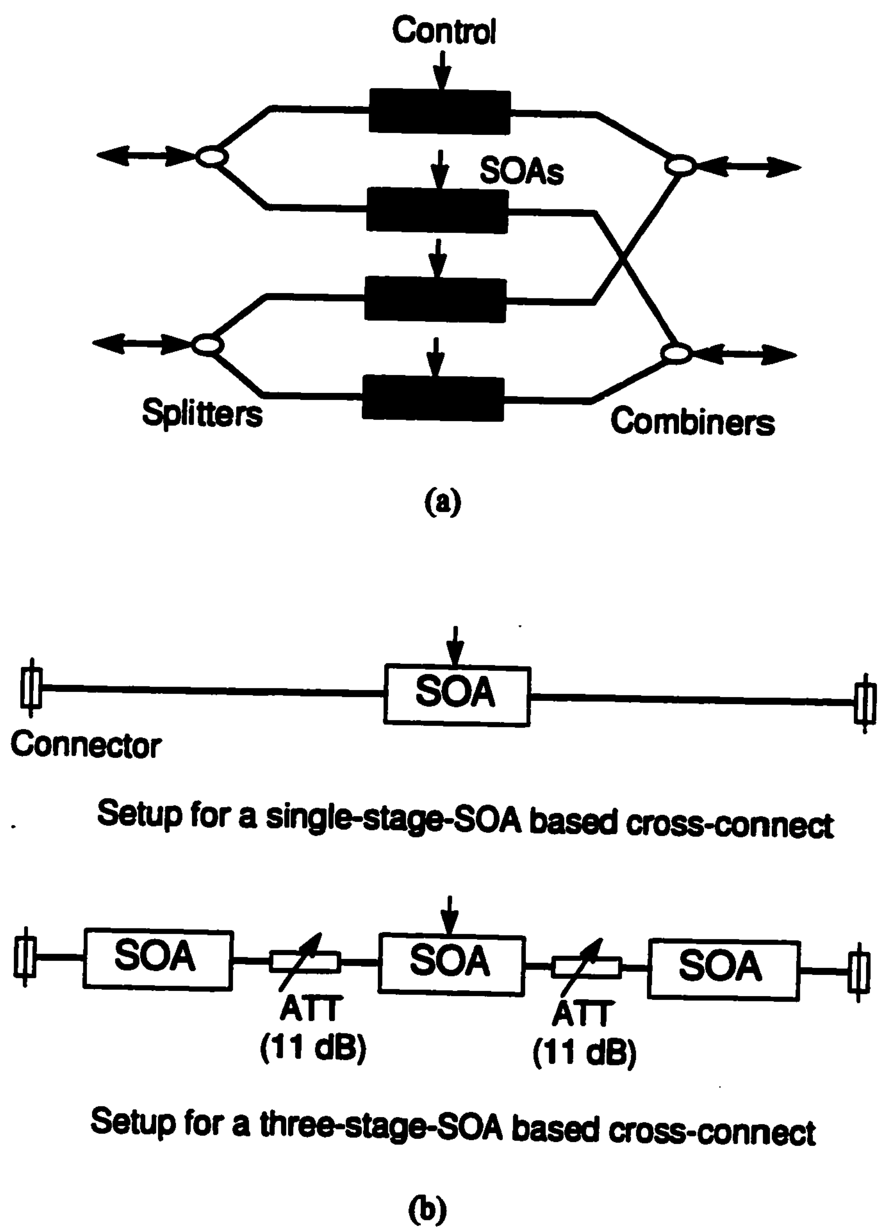

Figure 10.1: (a) Schematic of a 2 × 2 SOA-based optical cross-connect. (b) Experimental arrangements for single-stage-SOA and three-stage-SOA cross-connects.

stage-SOA cross-connects hereafter, respectively. It is noted that only one bi-directional cross-connection path is tested in the experiment, and splitting losses at the input and output sides are excluded here.

Semiconductor optical amplifiers used in the experiment are those tested in Chapter 8. For the single-stage-SOA cross-connect, we set the SOA fiber-to-fiber gain to 11 dB with

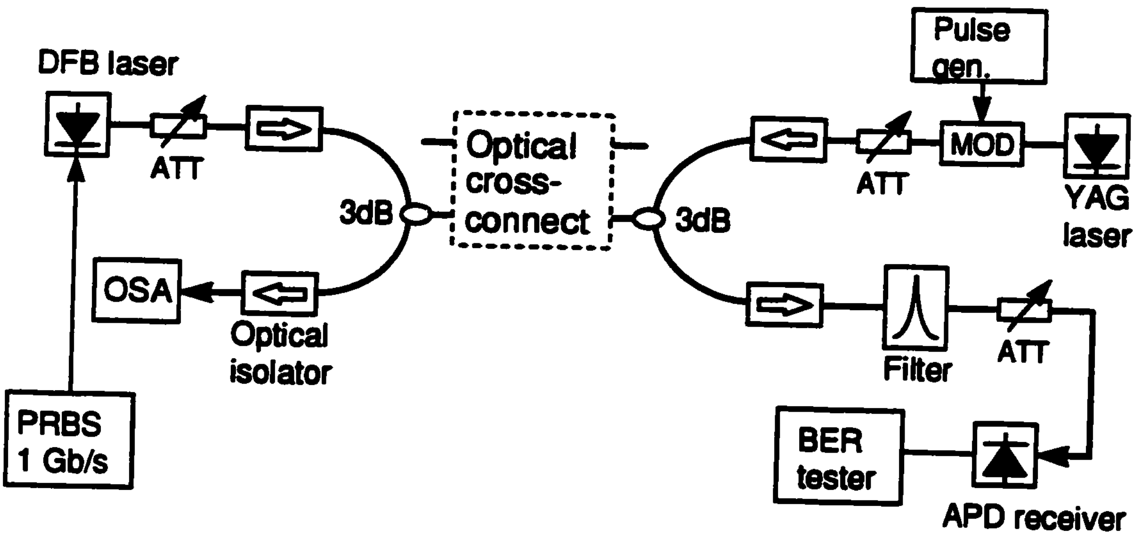

Figure 10.2: Experimental setup for bi-directional optical cross-connection.

an injection current of 100 mA. As for a three-stage-SOA arrangement, the loss between SOAs is set to 11 dB, which is equal to the unsaturated gain of the SOAs. So, the input optical power to each SOA is approximately the same with no gain saturation. For bi-directional cross-connection, no optical isolators are used between three cascaded SOAs.

The experimental setup for the bi-directional cross-connections is shown in Figure 10.2. There are two transmission channels at different wavelengths, forward and backward ones. As for the forward channel, a DFB laser at 1302.7 nm is directly modulated at 1 Gb/s with a PRBS length of 2^7-1. A variable optical attenuator is used to adjust the optical input power of the cross-connect. The backward channel is an externally modulated 1010 sequence at 250 Mb/s. The optical source is a semiconductor laser-pumped Nd:YAG laser at 1318.6 nm. The extinction ratios of the forward and backward channels are about 10 dB and 15 dB, respectively. Two 3-dB couplers are employed at the two sides of the cross-connect in order to separate the forward and backward channels. Back reflection of the couplers is approximately -50 dB. They may be replaced with optical circulators or WDM couplers with no intrinsic loss. For the forward channel, a manually tunable optical filter with a bandwidth of 1.6 nm is used before the receiver in order to select the forward channel. A high-sensitivity Ge-APD receiver is employed for bit error rate testing. Four

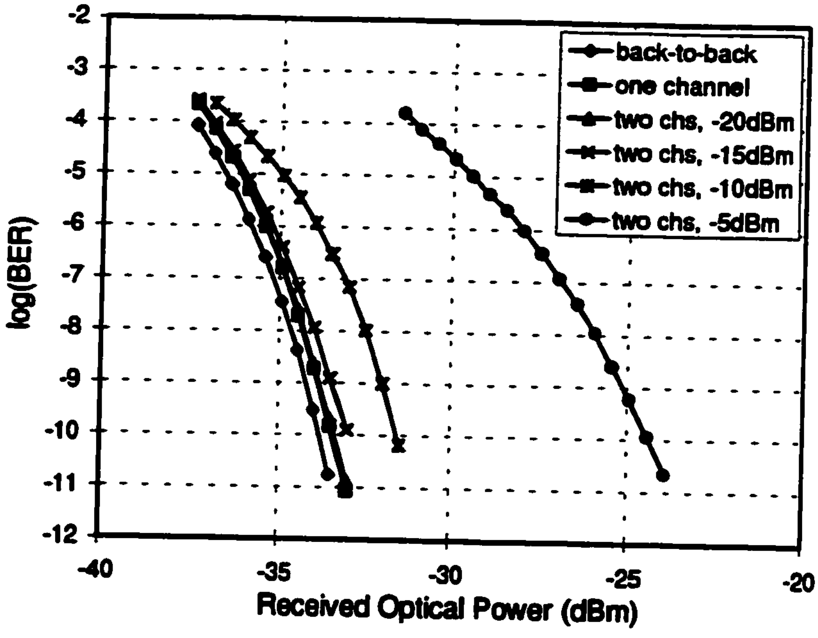

Figure 10.3: Bit error rate versus received optical power at different input power levels of the backward channel. The input power of the forward channel is -20 dBm.

optical isolators are inserted as shown in Figure 10.2 in order to block reversed channels and reflections to optical sources.

10.3 Results and Discussions

10.3.1 Single-stage-SOA cross-connect

Figure 10.3 shows the measured BER for the forward channel with different input power levels of the backward channel for the single-stage-SOA cross-connect. The average input power from the forward channel is kept to -20 dBm. Comparing the BERs of the back-to-back and only one forward channel, we see a power penalty of about 0.4 dB at a BER of 10^{-9}. This is mainly due to amplified spontaneous emission (ASE) noise from the SOA. With the increase of the backward input, the power penalty to the forward channel increases. This results from the cross-gain modulation among the WDM channels as SOAs saturate [97, 170]. With the backward input power up to -5 dBm, a power penalty is about 9 dB. However, there is no BER floor.

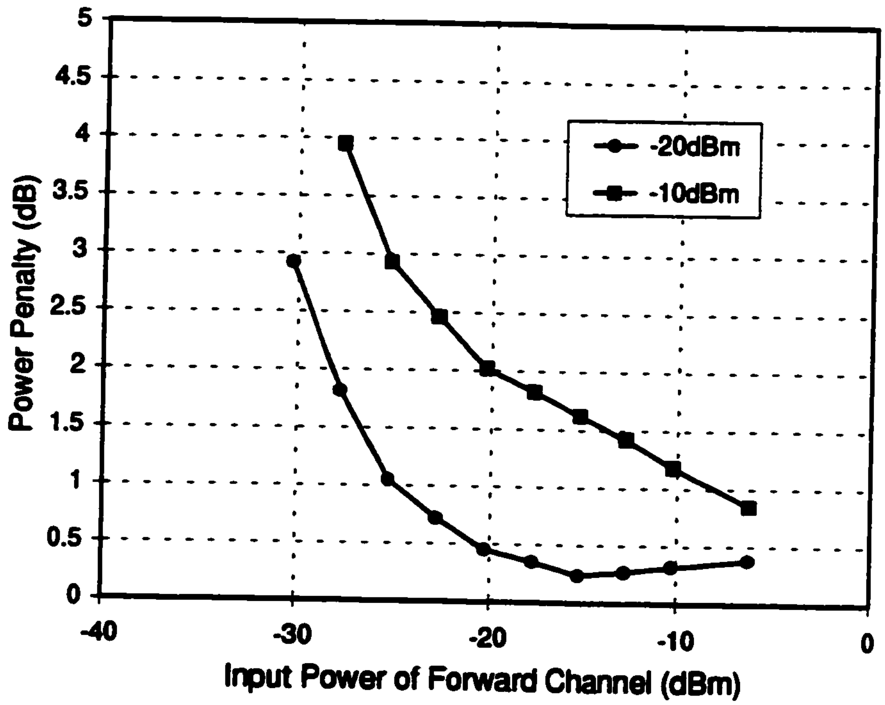

Figure 10.4: Power penalty versus input power of the forward channel at two different input power levels of the backward channel in the single-stage-SOA based cross-connect.

Figure 10.4 shows the power penalty versus the input power of the forward channel at two input power levels of the backward channel. At a low backward input power of -20 dBm, the lower curve shows that the input power can be as low as -25 dBm with a 1-dB penalty. The highest input power can not be measured because of low input power from the DFB laser, but it is expected to be over 0 dBm. The resulting dynamic range is about 25 dB. At a higher backward input power of -10 dBm, the dynamic range of the forward channel within a 1-dB penalty is very limited. If the margin for power penalty is relaxed to 2 dB, the input power can be as low as -20 dBm.

At three forward input power levels, the power penalty of the forward channel is measured against the backward input power, as shown in Figure 10.5. Each curve is plotted compared to its corresponding receiver sensitivity with zero backward input power level. The power penalty increases with the increase of the backward input power. With a higher forward input power level, the penalty is lower than that with a lower forward input

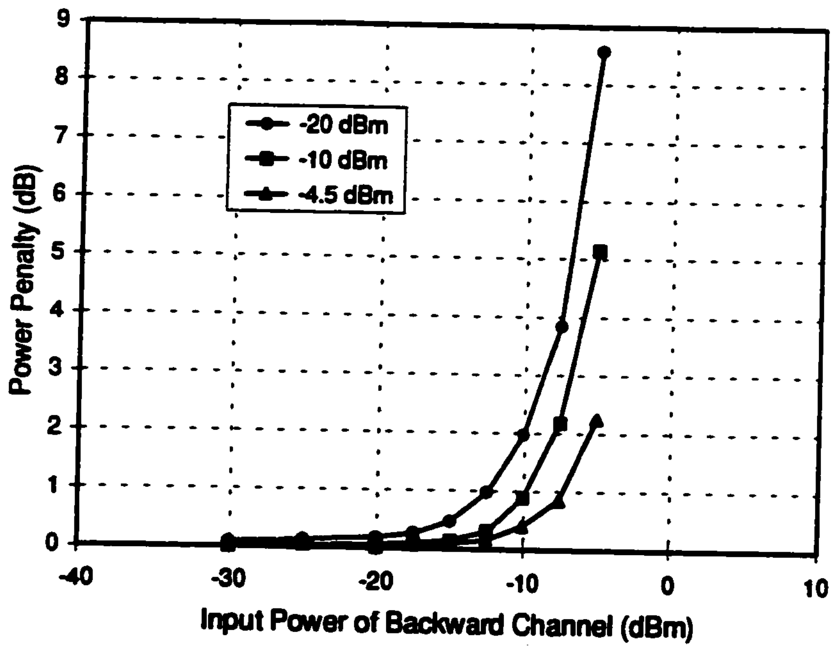

Figure 10.5: Power penalty versus input power of the backward channel at three different input power levels of the forward channel in the single-stage-SOA based cross-connect.

power level. The reason is that the forward channel with a higher input power level is less cross-modulated by the backward channel, since the gain is mainly saturated by the forward channel. When the two channels have the same input power less than -10 dBm, the relative power penalty for the two channels can be less than 1 dB. With the input power levels over -10 dBm, the power penalty may not be limited to 1 dB.

10.3.2 Three-stage-SOA cross-connect

Figure 10.6 shows the power penalty versus the forward input optical power at three different backward input power levels for the three-stage-SOA optical cross-connect. As we increase the backward input power, the input dynamic range of the forward channel decreases rapidly. The margin for power penalty has to be relaxed in order to have reasonable input dynamic range. The input dynamic range is about 7.5 dB with a 2-dB power penalty at a backward input power level of less than -15 dBm. It is also noted that the optimum input power level of the forward channel corresponding to the minimum power penalty becomes higher as the backward channel power increases. From channel inter-modulation point of view, the more stages of SOAs are in cascade, the stronger

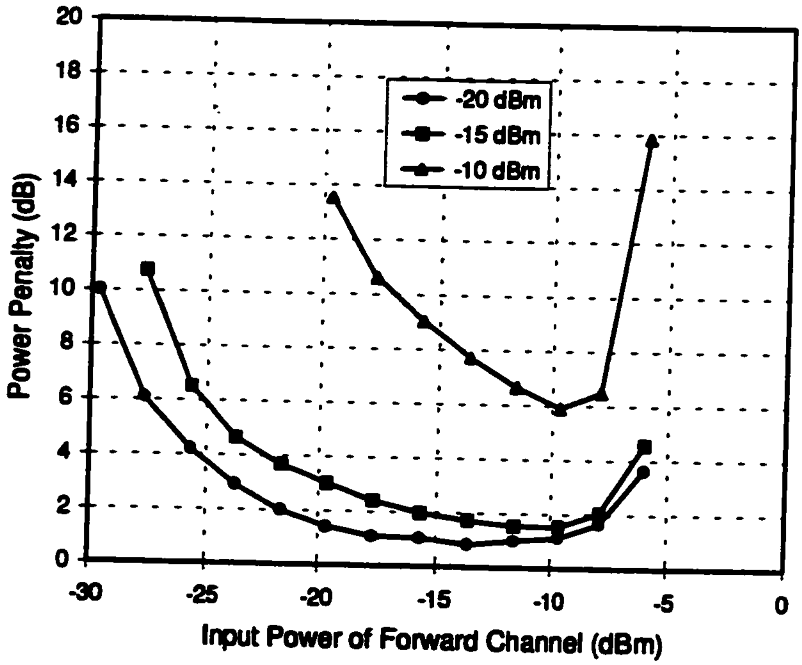

Figure 10.6: Power penalty versus input power of the forward channel at three different input power levels of backward channel in the three-stage-SOA based cross-connect.

cross-gain modulation is. The conclusion drawn from Figure 10.6 may also apply to three cascaded single-stage-SOA based cross-connects.

10.4 Conclusions

In this chapter, we presented a bi-directional cross-connection experiment using semiconductor optical amplifiers. The experiment shows the feasibility of constructing SOA-based optical cross-connects. For single-stage-SOA based cross-connects, the input dynamic range is 15 dB starting from -25 dBm extending to -10 dBm at a bit rate of 1 Gb/s with a power penalty of less than 1 dB. For three-stage-SOA based cross-connects, a dynamic range of 7.5 dB is obtained with a 2-dB power penalty.

11. Summary and Suggestions for Future Work

11.1 Summary

In this thesis, we investigated the architecture and system perspective of optical cross-connects using semiconductor optical amplifiers. The studies on the optical cross-connects include theoretical analysis, simulations and experiments. The thesis can be summarized in three main parts.

From Chapters 3 to 5, the study is concentrated on the proposed optical cross-connect. First, the proposed optical cross-connect was presented in Chapter 3. In the proposed cross-connect, WDM and SDM techniques are effectively combined to reuse optical wavelengths and reduce the size of space switches. The system performance of the proposed optical cross-connect as a high-speed switching core is further investigated in Chapter 4. Due to wavelength reuse, homo-wavelength crosstalk was identified as a very important degradation factor in the cross-connect. When the shared central power lasers are used for all transmitters, another homo-wavelength component will be introduced by wavelength selectors at the transmitters. The analysis shows that the size of the high-speed switching core at a line rate of 10 Gb/s can be up to 64×64 with four or eight optical wavelengths. The cross-connect can be constructed with presently available technologies. In Chapter 5, a small version (4×4) of the proposed optical cross-connect has been experimentally demonstrated. The successful demonstration shows the promise to construct an 8×8 or 16×16 prototype.

As a primary performance degradation factor in optical cross-connects and multi-wavelength networks, homo-wavelength crosstalk has been investigated in Chapters 6 and 7 in detail. Chapter 6 presented the performance degradation due to homo-wavelength crosstalk in multi-wavelength optical networks using dynamic wavelength routing. It was identified that the degradation due to homo-wavelength crosstalk can be enhanced by ASE noise of the optical amplifiers. In Chapter 7, several mechanisms of homo-wavelength crosstalk were reviewed. According to its impact on the performance, homo-wavelength crosstalk is classified as additive and beat-noise crosstalk. Beat-noise crosstalk was investigated by using the moment generating function (MGF) of the signal-crosstalk beating. Saddlepoint approximation was applied to evaluate the system performance with the MGF of the total noise in the signal. Calculated results for one cosstalk channel have a very good agreement with the experimental results. Also, numerical calculations verify the performance estimations obtained with Gaussian approximation in Chapters 4 and 6. The effect of wavelength shift between the signal and crosstalk channels has also been studied, experimentally.

As basic optical switching gates, semiconductor optical amplifiers were studied in Chapters 8 to 10. A brief introduction to the principles of SOAs was given in Chapter 8. This chapter also presented the tested results of available SOAs. The components show good performance as switching gates, particularly their low polarization sensitivity and high contrast ratio. Chapter 9 addressed the input dynamic range of SOA-based systems. For a single-stage SOA system, an experiment at a bit rate of 1 Gb/s shows a wide input dynamic range up to 25 dB. For a three-stage-SOA system, experimental results indicate that different current combinations have quite similar input dynamic range except for the shift of their absolute input power ranges. Optical isolators between the SOAs only improve the system performance marginally. Further simulations show that SOA-based systems can have a reasonably large input dynamic range at a very high bit rate. Finally, Chapter 10 described an experimental work on bi-directional cross-connects using SOAs. The experiment shows the feasibility of SOA-based bi-directional cross-connects.

11.2 Suggestions for Future Work

As for the future work on optical cross-connect systems, two research topics are suggested. One is research on the control protocol for the proposed optical cross-connect. The best protocol would maximize the system switching capability with a minimum blocking probability. The work in this direction will be very important when the whole system is designed to meet the required network or switch performance.

Another direction is further experimental study on the proposed cross-connect and semiconductor optical amplifiers. Several experiments at a high bit rate (~ 10 Gb/s) are required to validate the analysis and simulations presented in the thesis, and to understand unforeseen problems in SOA-based switching systems. Other experiments on system control and synchronization may also be suggested.

In conclusion, a large size optical cross-connects can be constructed with state-of- the-art technologies by using the proposed cross-connect architecture. We hope the work presented in the thesis provide a helpful understanding for the future system design and implementation of optical cross-connect systems.

References

1. S. Minger, "Broadband ISDN and asynchronous transfer mode (ATM)," *IEEE Commun. Mag.*, Vol. 27, No. 9, pp. 17-24, Sept. 1989.
2. M. De Prycher, *Asynchronous Transfer Mode: Solution For Broadband ISDN*, 3rd Ed. London: Prentice Hall, 1995.
3. R. Ballart and Y. C. Ching, "SONET: now it's the standard optical network," *IEEE Commun. Mag.*, Vol. 29, No. 3, pp. 8-15, March 1989.
4. C. Baack and G. Walf, "Photonics in future telecommunications," *Proc. IEEE*, Vol. 81, No. 11, pp. 1624-1631, Nov. 1993.
5. T. Egawa, K. Yukimatsu, and K. Yamasaki, "Recent research trends and issues in photonic ATM switching technologies," *NTT Rev.*, Vol. 5, No. 1, pp. 30-37, 1993.
6. E. Munter, J. Parker, and P. Kirkby, "A high-capacity ATM switch based on advanced electronic and optical technologies," *IEEE Commun. Mag.*, Vol. 33, No. 11, pp. 64-71, November 1995.
7. M. Buhrgard, "Photonic switching of optical interconnects in large telecom nodes," *OSA Topical Meeting on Photonic Switching'95*, PThC2-1, 1995.
8. L. Thylen, G. Karlsson, and O. Nilsson, "Switching technologies for future guidedwave optical networks: potentials and limitations of photonics and electronics," *IEEE Commun. Mag.*, Vol. 34, No. 2, pp. 106-113, February 1996.
9. Special issues on All-Optical Networks, *J. Lightwave Technol.*, Vol. 11, No. 5/6, May/June, 1993.
10. R. Ramaswami, "Multiwavelength light networks for computer communication," *IEEE Commun. Mag.*, Vol. 31, No. 2, pp. 78-88, Feb. 1993.
11. Y. D. Jin and M. Kavehrad, "Optical cross-connect based on WDM and space division multiplxing," *IEEE Photon. Technol. Lett.*, Vol. 7, No. 11, pp. 1300-1302, Nov. 1995.

12. Y. D. Jin and M. Kavehrad, "Optical cross-connect architecture based on WDM and space division multiplexing," *Tech. Digest of LEOS Summer Topical Meeting on Global Information Infrastructure*, Keyston, CO, Aug. 1995.

13. Y. D. Jin and M. Kavehrad, "Optical cross-connect based on WDM and space division multiplexing and its performance as a high-speed switching core," *J. Lightwave Technol.*, Vol. 14, No. 6, pp. 1183-1197, June 1996.

14. Y. D. Jin and M. Kavehrad, "Performance analysis of an optical cross-connect as high-speed switching core," *Technical Digest of ICAPT'96*, Montreal, July 1996.

15. Y. D. Jin, Q. Jiang, and M. Kavehrad, "Performance degradation due to homo-wavelength crosstalk in all-optical networks using dynamic wavelength routing," *IEEE Photon. Technol. Lett.*, Vol. 7, No. 10, pp. 1210-1212, Oct. 1995.

16. Y. D. Jin, P. Myslinski, J. Chrostowski, and M. Kavehrad, "Wavelength-division bidirectional optical cross-connection experiment using semiconductor optical amplifiers," *Technical Digest of LEOS'96*, Boston, November 1996.

17. A. S. Acampora, *An Introduction to Broadband Networks*, New York: Plenum Press, 1994.

18. T. Miki, "Optical transport networks," *Proc. IEEE*, Vol. 81, No. 11, pp. 1594-1609, Nov. 1993.

19. G. R. Hill *et al.*, "A transport network layer based on optical network elements," *J. Lightwave Technol.*, Vol. 11, No. 5/6, pp. 667-676, May/June 1993.

20. K. Sato, S. Okamoto, and H. Hadama, "Network performance and integrity enhancement with optical path layer technologies," *IEEE J. Select. Areas. Commun.*, Vol. 12, No. 1, pp. 159-170, Jan. 1994.

21. *Report on all-optical network workshop*, Washington, D. C., Jan. 1993.

22. Special Issue on Optical Networks, *IEEE J. Select. Areas Commun.*, Vol. 14, No. 6, June 1996.

23. Special Issue on Multi-wavelength Networking Technologies, *J. Lightwave Technol.*, Vol. 14, No. 6, June 1996.

24. D.J.G. Mestdagh, *Fundamentals of Multiaccess Optical Fiber Networks*, Boston: Artech House, 1995.

25. R. A. Barry and P. A. Humblet, "Bounds on the number of wavelengths used in WDM networks," *Tech. Digest of LEOS'92 Summer Topical Meeting*,1992, pp. 21-22.

26. H. Kobrinski, "Crossconnection of WDM high-speed channels," *Electron. Lett.*, Vol. 23, No. 18, pp. 974-976, Aug. 1987.

27. C. A. Bracket, "Multiwavelength Switching and interconnection networks," in *Photonics in Switching*, Vol. II, Systems, Ed. by J. E. Midwinter, Boston: Academic Press, Inc., 1993.

28. C-S. Li and F. Tong, "Crosstalk penalty in an all-optical network using dynamic wavelength routers," *OFC'94 Technical Digest*, Paper WN4, Feb. 1994.

29. J. Zhou, M. J. O'Mahony, and S. D. Walker, "Analysis of optical crosstalk effects in multipath switched networks," *IEEE Photon. Technol. Lett.*, Vol. 6, No. 2, pp. 302-305, Feb. 1994.

30. K.-W. Cheung, "Acousto-optic tunable filters in narrowband WDM networks: system issues and network applications," *IEEE J. Select. Areas Commun.*, Vol. 8, No. 6, pp. 1015-1025, Aug. 1990.

31. V. E. Benes, "On rearrangeable three-stage connecting networks," *Bell Syst. Tech. J.*, Vol. 41, pp. 148-1492, 1962.

32. C. A. Bracket, "The principles of scalability and modularity in multiwavelength optical networks," *OFC'93 Technical Digest*, paper TuJ2, Feb. 1992.

33. C. A. Bracket *et al.*, "A scaleable multi-wavelength multihop optical network: a proposal for research on all-optical networks," *J. Lightwave Technol.*, Vol. 11, No. 5/6, pp. 736-753, May/June, 1993.

34. A. S. Acampora, "A multi-channel multihop local lightwave network," *Proc. GLOBECOM'87*, 1987, pp. 37.5.1-9.

35. B. Mukherjee, "WDM-based local lightwave networks, part II: multihop systems," *IEEE Network*, Vol. 6, No. 4, pp. 20-32, July 1992.

36. H. S. Hinton, "Photonics in switching," *IEEE LTS*, Vol. 6, No. 4, pp. 26-35, Aug. 1992.

37. H. S. Hinton, *An Introduction to Photonic Switching Fabrics*, New York: Plenum Press, 1993

38. A. Jajszczyk and H. T. Mouftah, "Photonic fast packet switching," *IEEE Commun. Mag.*, Vol. 31, No. 2, pp. 58-65, Feb. 1993.

39. D. J. Blumenthal, P. R. Prucnal, and J. R. Sauer, "Photonic packet switches: architectures and experimental implementations," *Proc. IEEE*, Vol. 82, No. 11, pp. 1650-1667, Nov. 1994.

40. J. M. Gabriagues, J. B. Jacob, "Photonic ATM switching matrix based on wavelength routing," *Proc. SPIE*, Vol. 1807, Minsk, July 1992, pp. 355-359.

41. W. Pieper *et al.*, "Crosstalk in a fiber-loop optical buffer," *OFC'94 Tech. Digest*, paper ThD1, San Jose, Feb. 1994

42. J. M. Cabriagues *et al.*, "Design, modeling and implementation of ATMOS project fiber delay line photonic switch matrix," *Opt. and Quantum Electron.*, Vol. 26, pp. 497-516, 1994.

43. Z. Hass, "The 'staggering switch': an electronically controlled optical packet switch," *J. Lightwave Technol.*, Vol. 11, No. 5/6, pp. 925-936, May/June 1993.

44. M. Tsukata and Y. Shimazu, "Ultrafast photonic ATM switches based on time-division broadcast-and-select network," *Proc. GLOBECOM'91*, 1991, pp. 1230-1234.

45. A. M. Weiner and J. A. Salehi, "Optical code-division multiple-access," *Photonics in Switching*, Vol. II, Systems, Ed. J. Midwinter, Boston: Academic Press, Inc., 1993.

46. K. Y. Eng, M. A. Santoro, T. K. Koch, J. Stone, and W. W. Snell, "Star-coupler-based optical cross-connect switch experiments with tunable receivers," *IEEE J. Select. Areas Commun.*, Vol. 8, No. 6, pp. 1026-1031, Aug. 1990.

47. Y. Tada, N. Shibata, O. Ishida, K. Nosu, and H. Ishii, "Optical cross-connect configuration based on FDM technologies," *Proc. ICC'92*, Chicago, June 1992, pp. 1588-1592.

48. C. A. Brackett, "Dense wavelength division multiplexing networks: principles and applications," *IEEE J. Select. Areas Commun.*, Vol. 8, No. 6, pp. 948-964, Aug. 1990.

49. F. B. McConnick, "Free-space interconnection techniques," *Photonics in Switching*, Vol. II, System, Chapter 4. Ed. J. Midwinter, Boston: Academic Press, Inc., 1993.

50. H. S. Hinton *et al.*, "Free-space digital optical systems," *Proc. IEEE*, Vol. 82, No. 11, pp. 1632-1649, Nov. 1994.

51. J. C. McDonald, *Fundamentals of Digital Switching*, 2nd Edition, New York: Plenum Press, 1990.

52. H. S. Hinton, "Photonic switching using directional couplers," *IEEE Commun. Mag.*, Vol. 25, No. 5, pp. 16-25, May 1987.

53. R. C. Alferness, "Waveguide electrooptic switch arrays," *IEEE J. Select. Areas Commun.*, Vol. 6, No. 7, pp. 1117-1130, Aug. 1988.

54. M. Fujiwara, H. Nishimoto, T. Kajitani, M. Itoh, and S. Suzuki, "Studies on semiconductor optical amplifier for line capacity expansion in photonic space-division-switching system," *J. Lightwave Technol.*, Vol. 9, No. 2, pp. 155-159, Feb. 1991.

55. K. Padmanabhan and A. N. Netravali, "Dilated networks for photonic switching," *IEEE Trans. on Commun.*, Vol. 35, No. 12, pp. 1357-1365, Dec. 1987.

56. M. Gustavsson *et al.*, "Monolithically integrated 4 × 4 InGaAsP/InP laser amplifier gate switch arrays," *Electron. Lett.*, Vol. 28, No. 24, Nov. 1992.

57. E. Almstrom *et al.*, "Experimental and analytical evaluation of packaged 4 × 4 InGaAsP/InP semiconductor optical amplifier gate switch matrices for optical networks," *J. Lightwave Technol.*, Vol. 14, No. 6, pp. 996-1004, June 1996.

58. R. F. Kalman, L. G. Kazovsky, and J. W. Goodman, "Space division switches based on semiconductor optical amplifiers," *IEEE Photon. Technol. Lett.*, Vol. 4, No. 9, pp. 1048-1051, Sept. 1992.

59. J. D. Evankow and R. A. Thompson, "Photonic switching modules designed with laser diode amplifiers," *IEEE J. Select. Areas Commun.*, Vol. 6, No. 7, pp. 1087-1094, 1988.

60. G. Jeong and J.W. Goodman, "Gain optimization in switches based on semiconductor optical amplifiers," *J. Lightwave Technol.*, Vol. 13, No. 4, pp. 598-605, April 1996.

61. M. Yamaguchi, H. Yamazaki, and S. Shirai, "Free-space photonic switches," *NTT Rev.*, Vol. 5, No. 1, pp. 62-69, Jan. 1993.

62. R. A. Thompson and P. R. Giordana, "An experimental photonic time-slot interchanger using optical fibers as reentrant delay-line memories, " *J. Lightwave Technol.*, Vol. 5, No. 1, pp. 154-162, Jan. 1987.

63. D. K. Hunter, P. E. Barnsley, I. Andonovic, and B. Culshaw, "Architectures for optical TDM switching," *Proc. SPIE*, Vol. 1787, pp. 204-214, Sept. 1992.

64. S. Shimada, K. Nakagama, M. Saruwatari, and T. Matsumoto, "Very-high-speed optical signal processing," *Proc. IEEE*, Vol. 81, No. 11, pp. 1633-1646, Nov. 1993.

65. D. M. Spirit, A. D. Ellis, and P. E. Barnsly, "Optical time division multiplexing: systems and networks," *IEEE Commun. Mag.*, Vol. 32, No. 12, pp. 56-62, Dec. 1994.

66. P. J. Legg, D. K. Hunter, I. Andonovic, and P. E. Barnsley, "Inter-channel crosstalk phenomena in optical time division multiplexed switching networks," *IEEE Photon. Technol. Lett.*, Vol. 6, No. 5, pp. 661-663, May 1994.

67. K. Y. Eng, M. J. Karol, and I. Chih-lin, "A Modular broadband (ATM) switch architecture with optimum performance," *Proc. 13th ISS*, Vol. IV, Stockholm, 1990, pp. 1-6.

68. H. Obara and Y. Hamazumi, "Star coupler based WDM switch employing tunable devices with reduced tunability range," *Electron. Lett.*, Vol. 28, No. 13, pp. 1268-1270, June 1992.

69. H. Obara and Y. Hamazumi, and M. Teshima, "Multiwavelength routing using tunable laser and arrayed-waveguide grating multiplexer for wavelength-division and space-division multiplexed cross-connects," *Electron. Lett.*, Vol. 28, No. 23, pp. 2172-2173, Nov. 1992.

70. P. Healey, D. W. Smith, and S. A. Cassidy, "Photonic switching and interconnect for future network nodes," *BT Technol. J.*, Vol. 9, No. 4, pp. 19-28, Oct. 1991.

71. R. P. Braun *et al.*, "Transport switching node for optical frequency division multiplexed signals," *Electron. Lett.*, Vol. 29, No. 10, pp. 912-913, May 1993.

72. H. S. Hinton, "A non-blocking optical interconnection network using directional couplers," *Proc. GLOBALCOM'84*, Atlanta, Nov. 1984, pp. 885-889.

73. I. Januar, R. J. Feuerstein, A. R. Michelson, and J. R. Sauer, "Wavelength sensitivity in directional couplers," *J. Lightwave Technol.*, Vol. 10, No. 9, pp. 1202-1209, Sept. 1992.

74. R. A. Spanke, "Architectures for large non-blocking optical space switches," *IEEE J. Quantum Electron.*, Vol. 22, pp. 964-986, June 1986.

75. E. Marko, "InP optoelectronic devices and photonic integrated circuits for high speed packet switching," *Proc. SPIE*, Vol. 1807, Minsk, 1992, pp. 295-306.

76. J. F. Vinchant *et al.*, "InP digital optical switch: key element for guided-wave photonic switching," *IEE Proc.*, Vol. 140, pt. J No. 5, pp. 301-307, Oct. 1993.

77. M. Ikeda, "Switching characteristic of laser diode switch," *IEEE J. Quantum Electron.*, Vol. 19, No. 2, pp. 157-164, Feb. 1983.

78. A. Ehrhardt *et al.*, "Semiconductor laser amplifier as optical switching gates," *J. Lightwave Technol.*, Vol. 11, No. 8, pp. 1287-1295, Aug. 1993.

79. C. E. Zah and T. P. Lee, "Wavelength-tunable semiconductor lasers for optical fiber communications," *Proc. ICC'90*,1990, pp. 1286-1290.

80. T. Wolf, S. Illek, J. Rieger, B. Borchert, and M. C. Amann, "Tunable twin-guide (TTG) distributed feedback (DFB) laser with over 10 nm continuous tuning rage," *Electron. Lett.*, Vol. 29, No. 24, pp. 2124-2125, Nov. 1993.

81. U. Koren *et al.*, "An integrated tunable light source with extended tunability range," *Proc. IOOC'89*, paper 19A2-3, Kobe 1989.

82. M. Schilling *et al.*, "Multifunctional photonic switching operation of 1500 nm Y-coupled cavity laser with 28 nm tuning capacity," *IEEE Photon. Technol. Lett.*, Vol. 3, pp. 1054-1057, 1991.

83. R. C. Alferness *et al*, "Broadly tunable InGaAs/InP laser based on a vertical coupler filter with 57 nm tuning rage," *Appl. Phys. Lett.*, Vol. 60, pp. 3209-3211, 1992

84. H. Ishii, Y. Tohmori, Y. Yoshikuni, T. Tamamura, and Y. Kondo, "Multiple-phase-shift super structure grating DBR laser for broad wavelength tuning," *IEEE Photon. Technol. Lett.*, Vol. 5, No. 6, pp. 613-615, June 1993.

85. S Kuwano, Y. Tada, and N. Shibata, "100 ps frequency switching without bit loss for a 10 Gb/s ASK modulated signal," *IEEE Photon. Technol. Lett.*, Vol. 5, No. 3, Mar. 1993.

86. Y. Tada, O. Ishida, N. Shibata, and K. Nosu, "Design consideration a DBR-lasers transmitter for fast frequency switching in an optical FDM cross-connect system," *J. Lightwave Technol.*, Vol. 11, No. 5/6, pp. 813-818, May/June 1993.

87. Y. Tada, N. Shibata, O. Ishida, K. Nosu, and H. Ishii, "Duplex transmitter configuration for bit-error-free operation in an optical FDM cross-connect system," *IEEE Photon. Technol. Lett.*, Vol. 4, pp. 1051-1053, 1992.

88. M. G. Young *et al.*, "A 16 × 1 wavelength division multiplexer with integrated distributed Bragg reflector lasers and electroabsorption modulators," *IEEE Photon. Technol. Lett.*, Vol. 5, No. 8, pp. 908-910, Aug. 1993.

89. K. Inoue and H. Toba, "Wavelength conversion experiment using fiber four-wave mixing," *IEEE Photon. Technol. Lett.*, Vol. 4, pp. 69-72, 1992.

90. M. C. Tatham, G. Sherlock, and L. D. Westbrook, "20-nm optical wavelength conversion using nondegenerate four-wave mixing," *IEEE Photon. Technol. Lett.*, Vol. 5, No. 11, pp. 1303-1306, Nov. 1993.

91. J. Zhou *et al.*, "Efficiency of broadband four-wave mixing conversion using semiconductor traveling-wave amplifiers," *IEEE Photon. Technol. Lett.*, Vol. 6, No. 1, pp. 50-52, Jan. 1994.

92. J. M. Wiesenfeld, B. Glance, J. S. Perino, and A. H. Gnauck, "Wavelength conversion at 10 Gb/s using a semiconductor optical amplifier," *IEEE Photon. Technol. Lett.*, Vol. 5, 11, pp. 1300-1306, Nov. 1993.

93. C. Joergensen *et al.*, "Efficient wavelength conversion at 10 Gbit/s in a polarization-insensitive simple configuration," *OFC'94 Technical Digest*, paper ThQ2, San Jose, Feb. 1994.

94. B. S. Glance, J. M. Wiesenfeld, U. Koren, and R. W. Wilson, "New advances on optical components needed for FDM optical networks," *J. Lightwave Technol.*, Vol. 11, No. 5/6, pp. 882-889, May/June 1993.

95. S. Yamakoshi, "Gigabit operation of a wavelength conversion laser," *OFC'88 Technical Digest*, Postdeadline paper, PD10, 1988.

96. T. Saitoh and T. Mukai, "Traveling-wave semiconductor laser amplifiers," *Coherence, Amplifications and Quantum Effects in Semiconductor Lasers*, Ed. Y. Yamamoto, Chapter 7, New York: John Wiley & Sons, Inc., 1990, pp. 257-322.

97. R. Ramaswami and P. A. Humblet, "Amplifier induced crosstalk in multichannel optical networks," *J. Lightwave Technol.*, Vol. 8, No. 12, pp. 1882-1896, Dec. 1990.

98. P. J. A. Thijs, F. Tiemeijer, J. J. M. Binsma, and T. Dongen, "Progress in long-wavelength strained-layer InGaAs(P) quantum-well semiconductor lasers and amplifiers," *IEEE J. Quantum Electron.*, Vol. 30, No. 2, pp. 477-499, Feb. 1994.

99. J. L. Zyskind, C. R. Giles, J. R. Simpson, and D. J. DiGiovanni, "Erbium-doped fiber amplifiers and the next generation of lightwave systems," *AT&T Bell Tech. J.*, Jan./Feb. 1992, pp. 53-62.

100. E. Desurvire, *Erbium-Doped Fiber Amplifiers: Principles and Applications*, New York: John Wiley & Sons, Inc., 1994

101. P. E. Green, Jr., *Fiber Optic Networks*, Englewood Cliffs: Prentice Hall, 1993.

102. H. Kobrinski and K-W. Cheung, "Wavelength tunable optical filters: applications and technologies," *IEEE Commun. Mag.*, Oct. 1989, pp. 53-63.

103. A. d'Alessandro, D. A. Smith, and J. E. Baran, "Devices for wavelength switching in optical networks," *Proc. SPIE*, Vol. 2144, 1994, pp. 20-30.

104. M. Fukutoku, K. Oda, and H. Toba, "Optical beat-induced crosstalk of an acousto-optic tunable filter for WDM network application," *J. Lightwave Technol.*, Vol. 13, No. 11, pp. 2224-2235, Nov. 1995.

105. J. M. Senior and S. D. Cusworth, "Devices for wavelength multiplexed and demultiplexing," *IEE Proc.*, Vol. 136, Pt. J, No. 3, pp. 183-202, June 1989.

106. K. Liu and F. K. Tong, "Planar grating waveguide wavelength demultiplexer," *Proc. SPIE*, Vol. 2024, pp. 278-283, July 1993.

107. F. Tong, Y. H. Kwark, and A. E. Stevens, "A four-channel monolithic optical/electronic selector for fast packet-switched WDMA networks," *IEEE Photon. Technol. Lett.*, Vol. 6, No. 1, pp. 68-70, Jan. 1994.

108. H. Toba *et al.*, "100-channel optical FDM transmission/distribution at 622 Mb/s over 50 km," *OFC'90*, Postdeadline paper PD1, San Francisco, 1990.

109. C. Dragone. C. A. Edwards, and R. C. Kistler, "Integrated optics $N \times N$ multiplexer on silicon," *IEEE Photon. Technol. Lett.*, Vol. 3, No. 10, pp. 896-899, Oct. 1991.

110. B. H. Verbeek *et al.*, "Polarization-insensitive 8 × 8 arrayed waveguide grating multiplexer," *OFC'94*, Postdeadline paper, PD13-2, San Jose, Feb. 1994.

111. T. Ozeki, "Ultra optoelectronic devices for photonic ATM switching systems with tera-bits/sec throughput," *IEICE Trans. Commun.*, Vol. E77-B, No. 2, pp. 100-108, Feb. 1994.

112. C. Dragone, "Efficient $N \times N$ star coupler using Fourier optics," *J. Lightwave Technol.*, Vol. 7, No. 3, pp. 479-489, Mar. 1989.

113. K. Kato, K. Okamoto, H. Okazaki, Y. Ohmori, and I. Nishi, "Packaging large-scale integrated-optic $N \times N$ star-couplers," *IEEE Photon. Technol. Lett.*, Vol. 4, No. 3, pp. 348-351, Mar. 1993.

114. S. B. Alexander *et al.*, "A precompetitive consortium on wide-band all-optical networks," *J. Lightwave Technol.*, Vol. 11, No. 5/6, pp. 714-732, May/June, 1993.

115. R. M. Jopson and T. E. Darcie, "Semiconductor laser amplifiers in high-bit rate and wavelength-division multiplexed optical communication systems," in *Coherence, Amplification and Quantum Effects in Semiconductor Lasers*, Y. Yamamoto, Ed., New York: Wiley, 1990, Ch. 8, pp. 323-336.

116. E. Desurvire, *Erbium-Doped Fiber Amplifiers: Principles and Applications*, New York: Wiley, 1994.

117. N. L. Olsson, "Lightwave system with optical amplifiers," *J. Lightwave Technol.*, Vol. 7, No. 7, pp. 1071-1082, July 1989.

118. G. R. Giles and E. Desurvire, "Propagation of signal and noise in concatenated erbium-doped fiber optical amplifiers," *J. Lightwave Technol.*, Vol. 9, pp. 147-154, Feb. 1991.

119. P. A. Roshen and A. R. Hunwicks, "The analysis of crosstalk in multichannel wavelength division multiplexed optical transmission systems and its impact on multiplexer design," *IEEE J. Select. Areas Commun.*, Vol. 8, pp. 1108-1114, Aug. 1990.

120. C. Saxtoft and P. Chidgey, "Error rate degradation due to switch crosstalk in large modular switched optical networks," *IEEE Photon. Technol. Lett.*, Vol. 5, pp. 828-831, July 1993.

121. J. Zhou, M. J. O'Mahony, and S. D. Walker, "Analysis of optical croostalk effects in multi-wavelength switched networks," *IEEE Photon. Technol. Lett.*, Vol. 6, pp. 302-305, Feb. 1994.

122. P. J. Legg *et al.*, "Inter-channel crosstalk phenomena in optical time-division multiplexed switching networks," *IEEE Photon. Technol. Lett.*, Vol. 6, pp. 661-663, May 1994.

123. J. L. Gimlett and N. K. Cheung, "Effects of phase to intensity noise conversion by multiple reflection on gigabit-per-second DFB laser transmission systems," *J. Lightwave Technol.*, Vol. 7, No. 6, pp. 888-895, June 1989.

124. A. D. Whalen, *Detection of Signals in Noise*, New York: Academic Press, 1971.

125. E. L. Goldstein, L. Eskildsen, and A. F. Elrefaie, "Performance implications of component crosstalk in transparent lightwave networks," *IEEE Photon. Technol. Lett.*, Vol. 6, No. 5, pp. 557-660, May 1994.

126. E. L. Goldstein and L. Eskildson, "Scaling limitations in transparent optical networks due to low-level crosstalk," *IEEE Photon. Technol. Lett.*, Vol. 7, No. 1, pp. 93-94, Jan. 1995.

127. E. L. Goldstein, L. Eskildson, C. Lin, and A. Silberberg, "Polarization statistics of crosstalk-induced noise in transparent lightwave networks," *IEEE Photon. Technol. Lett.*, Vol. 7, No. 11, pp. 1345-1347, Nov. 1995.

128. K. Inoue *et al.*, "Crosstalk and power penalty due to fiber four-wave mixing in multichannel transmissions," *J. Lightwave Technol.*, Vol. 12, No. 8, pp. 1423-1438, Aug. 1994.

129. H. Takahashi, K. Oda, and H. Toba, "Impact of crosstalk in an arrayed-waveguide multiplexer on $N \times N$ optical interconnection," *J. Lightwave Technol.*, Vol. 14, No. 6, pp. 1097-1105, June 1996.

130. C-S. Lin and F. Tong, "Crosstalk interference penalty in all-optical networks using static wavelength routers," *J. Lightwave Technol.*, Vol. 14, No. 6, pp. 1120-1126, June 1996.

131. Y. Hamazumi, M. Koga, and K. Sata, "Beat induced crosstalk reduction against wavelength difference between signal and four-wave mixing lights in unequal channel spacing WDM transmission," *IEEE Photon. Technol. Lett.*, Vol. 8, No. 5, pp. 718-720, May 1996.

132. A. Elrefaie, S. Tu, and M. Romeser, "Performance degradation of 2.4 Gb/s NRZ/RZ lightwave systems due to reflection-induced phase-to-intensity noise conversion," *IEEE photon. Technol. Lett.*, Vol. 1, No. 7, pp. 173-175, July, 1989.

133. P. J. Blumenthal, P. Granestrand, and L. Thylen, "A comparison of coherent crosstalk induced BER floors in four types of $N \times N$ space photonic switches," *Tech. Digest of Photonics in Switching '95*, Salt Lake City, Uath, March 1995, paper PFA2-1.

134. J. J. O'Reilly and C. J. Appleton, "System performance implications of homodyne beat noise effects in optical fiber networks," *IEE Proc. - Optoelectron.*, Vol. 142, No. 3, pp. 143-148, June 1995.

135. A. Popoulis, *Probability, Random Variable and stochastic Process*, New York: McGraw-Hill, 1994.

136. G. Einarsson, *Principles of Lightwave Communications*, Chichester: John Wiley & Sons, 1996.

137. C. W. Helstrom, "Approximate evaluation of detection probability in radar and optical communications," *IEEE Trans. Aerospace and Electron. Sys.*, Vol. ASE-14, No. 4, pp. 630-639, July 1978.

138. H. Besbes, M. S. Nakhla, and Q-J. Zhang, "Performance evaluation of optical fiber system in the presence of intersymbol interference using the saddle point approximation method," *Tech. Digest of TRIO Retreat*, 1992.

139. G. P. Agrawal and N. K. Dutta, *Semiconductor Lasers*, 2nd ed. New York: van Nostrand Reinhold, 1993.

140. J. Zhou *et al.*, "Crosstalk in multiwavelength optical cross-connect networks," *J. Lightwave Technol.*, Vol. 14, No. 6, pp. 1423-1435, June 1996.

141. P. J. Legg, M. Tur, and I. Andonovic, "Solution paths to limit interferometric noise induced performance degradation in ASK/direct detection lightwave networks," *J. Lightwave Technol.*, Vol. 14, No. 9, pp. 1943-1953, Sept. 1996.

142. L. F. Tiemeijer, "High performance MQW laser amplifiers for transmission system in the 1310 nm window at bit rates of 10 Gbit/s and beyond," *Proc. ECOC'95*, Brussels, 1995.

143. I. D. Henning, M. J. Adams, and J. V. Collins, "Performance predictions from a new optical amplifier model," *IEEE J. Quantum Electron.*, Vol. QE-21, No. 6, June 1985.

144. M. J. O'Mahony, "Semiconductor laser optical amplifier for use in future fiber systems," *J. Lightwave Technol.*, vol. 6, No. 4, pp. 531-544, April 1988.

145. L. Gillner *et al.*, "Semiconductor laser amplifier optimization: an analytical and experimental study," *IEEE J. Quantum Electron.*, Vol. 25, No. 8, pp. 1822-1827, Aug. 1989.

146. L. Gillner *et al.*, "Dynamic effects in integrated 4×4 InGaAsP/InP semiconductor optical gate amplifier switch matrices," *Tech. Digest of Opt. Amplifiers and Their Applications*, Davos, Switzerland, June 1995.

147. G. P. Agrawal, "Semiconductor laser amplifiers," *Semiconductor Lasers: Past, Present, and Future*, Ed. by G. P. Agrawal, Woodbury: AIP Press, 1995. Ch. 8, pp. 243-283.

148. T. Taitoh and T. Mukai, "1.5 μm GaInAsP traveling wave semiconductor laser amplifier," *IEEE J. Quantum Electron.*, Vol. QE-23, No. 6, pp. 1010-1020, June 1987.

149. K. Magari and O, Mikami, "Semiconductor laser amplifiers - design and fabrication techniques," *Optical Amplifiers and Their Applications*, Ed. by S. Shimada and H. Ishio, Chichester: John Wiley & Sons, 1994, Ch. 4.

150. L. F. Tiemeijer *et al.*, "Polarization insensitive multiple quantum well laser amplifiers for the 1300 nm windows," *Appl. Phys. Lett.*, Vol. 62, pp. 826-828, Feb. 1993.

151. Y. Yamamoto, "Noise and error rate performance of semiconductor laser amplifier in PCM-IM optical transmission systems," IEEE J. Quantum Electron., Vol. QE-16, No. 10, pp. 1073-1081, Oct. 1980.

152. T. Mukai, Y. Yamamoto, and T. Kimura, "S/N and error rate performance in AlGaAs semiconductor laser preamplifier and linear repeater systems," *IEEE J. Quantum Electron.*, Vol. QE-18, No. 10, pp. 1560-1568, Oct. 1982.

153. J. Yao and M. J. O'Mahony, "Experimental study of semiconductor laser amplifiers for photonic time and space switching applications," *Int'l J. Optoelectron.*, Vol. 9, No. 3, pp. 219-226, 1994.

154. A. Saleh and I. Habbab, "Effects of semiconductor-optical-amplifier nonlinearity on the performance of high-speed intensity-modulation lightwave systems," *IEEE Trans. Commun.*, Vol. 38, No. 6, pp. 839-846, June 1990.

155. J. Yao and M. O'Mahony, "Impact of input signals on the bit error rate performance of semiconductor laser-amplifier-based switch systems," *Proc. IEE-Optoelectron*, Vol. 141, No. 4, pp. 265-270, Aug. 1994.

156. L. Gillner, "Properties of optical switching networks with passive or active space switches," *Proc. IEE, part-J*, Vol. 140, No. 5, pp. 309-315, Oct. 1993.

157. C. Tai and W. I. Way, "Dynamic range and switching speed limitations of an $N \times N$ optical packet switch based on low-gain semiconductor optical amplifiers," *J. Lightwave Technol.*, Vol. 14, No. 4, pp. 525-533, April 1996.

158. L. Gillner, "Analysis of input power dynamic ranges in two types of extended semiconductor optical amplifier gate switch arrays," *IEEE Photon. Technol. Lett.*, Vol. 8, No. 4, pp. 536-538, April 1996.

159. K. Inoue, "Suppression of signal fluctuation induced by crosstalk light in gain saturated laser diode amplifier," *IEEE Photon. Technol. Lett.*, Vol. 8, No. 3, pp. 458-460, Mar. 1996.

160. T. Durhuus, B Mikkelsen, and K. E. Stubkjaer, "Detailed dynamic model for semiconductor optical amplifiers and their crosstalk and intermodualtion distortion," *J. Lightwave Technol.*, Vol. 10, No. 8, Aug. 1992.

161. *ITU-T Recommendation G.957*, "Optical interface for equipments and systems relating to the synchronous digital hierarchy,"

162. *Lightwave Test and Measurement Catalog*, Hewlett-Packard Co., 1996.

163. T. P. Krauss, L. Shure, and J. N. Little, *Signal Processing Toolbox User's Guide*, MathWorks, Inc., 1993.

164. J. Haugen, F. Freeman, and J. Conradi, "Bidirectional transmission at 622 Mb/s utilizing erbium-doped fiber amplifiers," *IEEE Photon. Technol. Lett.*, Vol. 4, No. 8, pp. 913-916, Aug. 1992.

165. K. Kannan and S. Frisken, "Unrepeatered bidirectional transmission system over a single fiber using optical fiber amplifiers," *IEEE Photon. Technol. Lett.*, Vol. 5, No. 1, pp. 76-79, Jan. 1993.

166. R. J. Orazi and M. N. McLandrich, "Bidirectional transmission at 1.55 microns using fused fiber narrow channel wavelength division multiplexers and erbium-doped fiber amplifiers," *IEEE Photon. Technol. Lett.*, Vol. 6, No. 4, pp. 571-574, April 1994.

167. S. Seikai and K. Kusunoki, and S. Shimokado, "Experimental studies on wavelength division bidirectional optical amplifiers using an Er^{3+}-doped fiber," *J. Lightwave Technol.*, Vol. 12, No. 5, pp. 849-854, May 1994.

168. C. W. Barnard, J. Chrostowski, and M. Kavehrad, "Bidirectional fiber amplifiers," *IEEE Photon. Technol. Lett.*, Vol. 4, No. 8, pp. 911-913, Aug. 1992.

169. A. J. Boot and M. O. van Deventer, "Rayleigh backscattering of four-wave mixing in bidirectional optical communication systems," *IEEE Photon. Technol. Lett.*, Vol. 8, No. 1, pp. 142-144, Jan. 1996.

170. H. de Waardt, L. F. Tiemeijer, and B. H. Verbeek, "2 10 Gb/s WDM 1310-nm optical transmission over 63.5-km standard single mode fiber using optical preamplifiers," *IEEE Photon. Technol. Lett.*, Vol. 7, No. 1, Jan. 1995.

171. M. Abramowitz and I. A. Stegun, *Handbook of Mathematical Functions with formulas, Graphs, and Mathematical Tables, Applied Mathematics Series Vol. 55*, National Bureau of Standards, Second Printing, May 1968.

172. P. E. Green, Jr., "Optical networking update," *IEEE J. Select. Areas Commun.*, Vol. 14, No. 5, pp. 764-779, June 1996.

TEST TARGET (QA-3)

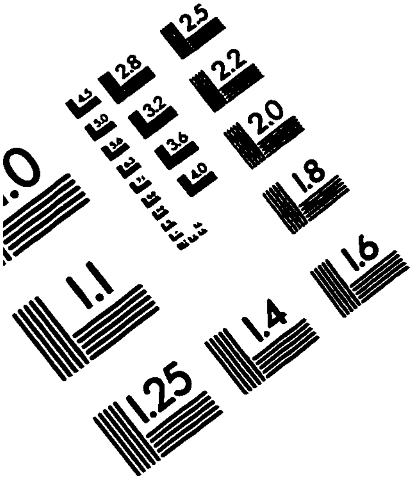

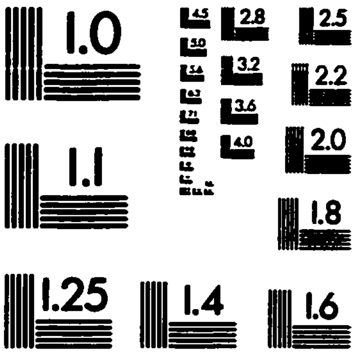

150mm

6″

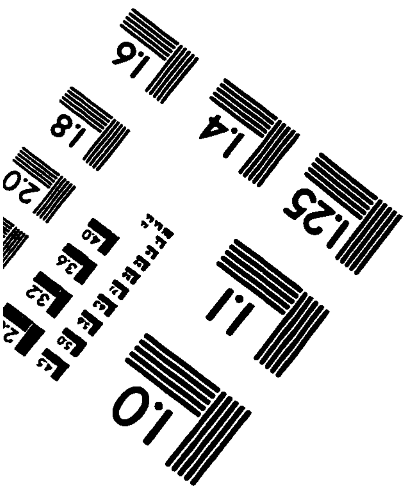

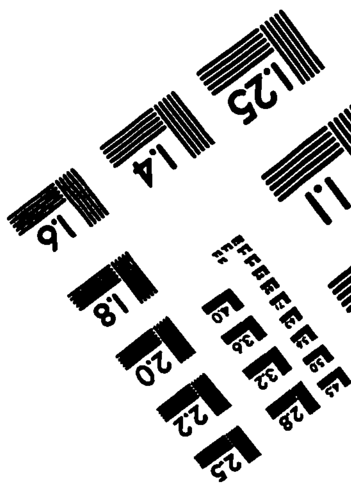

APPLIED IMAGE, Inc
1653 East Main Street
Rochester, NY 14609 USA
Phone: 716/482-0300
Fax: 716/288-5989